# Erosion of Sand at High Flow Velocities

An Experimental Study

# Erosion of Sand at High Flow Velocities

An Experimental Study

## Proefschrift

ter verkrijging van de graad van doctor
aan de Technische Universiteit Delft,
op gezag van de Rector Magnificus prof. dr. ir. T. H. J. J. van der Hagen,
voorzitter van het College voor Promoties,
in het openbaar te verdedigen op dinsdag 9 januari 2018 om 15:00 uur

door

**Frederik BISSCHOP**

mijnbouwkundig ingenieur
geboren te Heerde, Nederland.

Dit proefschrift is goedgekeurd door de:

promotor Prof. dr. ir. C. van Rhee
copromotor: Dr. ir. S. A. Miedema
copromoter: Dr. ir. P. J. Visser

Samenstelling promotiecommissie:

| | |
|---|---|
| Rector Magnificus, | voorzitter |
| Prof. dr. ir. C. van Rhee | Technische Universiteit Delft, promotor |
| Dr. ir. S. A. Miedema | Technische Universiteit Delft, copromotor |
| Dr. ir. P. J. Visser | Technische Universiteit Delft, copromotor |
| | |
| *Onafhankelijke leden:* | |
| Prof. dr. ir. L. C. van Rijn | Universiteit Utrecht |
| Prof. dr. ir. A. Bezuijen | Universiteit Gent |
| Prof. dr. S. J. M. H. Hulscher | Universiteit Twente |
| Prof. dr. ir. W. S. J. Uijttewaal, | Technische Universiteit Delft |
| Prof. dr. ir. M. L. Kaminski, | Technische Universiteit Delft, reservelid |

The studies described in this thesis have been financed by the SSB (Stichting Speurwerk Baggertechniek which includes Royal Boskalis Westminster Dredging BV and Van Oord Dredging and Marine Contractors BV), IHC Merwede, the Dr. Ir. Lely Foundation (Rijkswaterstaat) and Arcadis.





*Keywords:* Erosion, Sand, Pick-up Flux, Breaching, Dredging

*Printed by:* Ridderprint

*Front & Back:* Flow behavior during erosion of sand.



ISBN 978-94-6186-868-8

An electronic version of this dissertation is available at
http://repository.tudelft.nl/.

*To Rini, Femke and Tomas*

# Summary

The safety level of a dike is expressed in terms of risk. Risk is defined as the product of the probability of inundation of a polder (after failure of a dike) and the expected damage (casualties, economic damage and damage to the infrastructure) caused by inundation. The rate of inundation determines the amount of casualties and depends heavily on the flow velocity through the breach and breach development in time. The flow velocity in a breach can become larger than 5 m/s. Due to these large flow velocities, the application of conventional sediment pick-up functions in breach growth models, leads to a significant overestimation of the breach growth and thus the rate of inundation.

The same difference is encountered in dredging practice. Trailing suction hopper dredgers extract sand from the bottom of the sea for reclamation purposes. A suction head is trailed over the sea bed, using water jets to erode sand. Typical jet flow velocities are around 30 to 60 m/s. As in the dike breaching process, conventional pick-up functions significantly overestimate the erosion velocity during jetting.

Pick-up of grains starts when the flow conditions exceed the critical Shields parameter. When this criterion is met, grains start to move and are transported over the top of the sand bed. At a higher value of the Shields parameter grains are eroded from the sand bed: the top of the sand bed moves down. The amount of grains (weight) eroded from the sand bed per unit of time and area is defined as the pick-up flux. Present pick-up functions are mainly based on the erosion of single grains (grain by grain pick-up) and are applicable for low flow velocities (up to 1 m/s) and lag some physical understanding.

However, at flow velocities of more than 1 m/s these functions overestimate the pick-up flux. Empirical models describing the erosion of sand at higher flow velocities (up to 3 m/s) explain that this difference is caused by the behavior of the sand bed during erosion. It is assumed that the pick-up flux is influenced by the shearing of layers of sand at the top of the sand bed. The resulting dilative behavior causes an inward hydraulic gradient into the sand, hence reducing erosion (dilatancy reduced erosion). As a result bulk properties, such as porosity and permeability, start to influence the pick-up flux.

The amount of data and range of flow velocities of existing experimental studies is too limited for a proper validation of the dilatancy reduced erosion regime. Existing experimental studies show the influence of bulk properties like permeability and porosity, but the flow velocity during these experiments was limited to 1.5 m/s. Some other studies have presented data for flow velocities up to 3 m/s. However, these data are too limited for a proper validation of the erosion process at flow velocities of more than 1 m/s.

In order to study the erosion process at higher flow velocities and to gather experimental data for this process, erosion experiments were carried out at flow

velocities of 2 to 6 m/s with varying bulk properties of the sand bed. The results of these experiments show the influence of turbulent bursts, consisting of vortices traveling close to the top of the sand bed. The downward flow velocity of the sweeps of these vortices hit the top of the sand bed, causing shearing of lumps of sand. These lumps disintegrate and are transported (partly) to the main flow by the upward flow velocity of ejections. However, not all grains reach the main flow. Part of the eroded grains are re-sedimented by sweeps of the next vortices.

The shearing of lumps of sand is comparable with the description of the resistance of a sand bed to a normal stress. Shearing of these lumps leads to dilatancy, resulting in decreased pore water pressures and thus increasing the resistance to shear. The analysis of the results of the experiments shows that the porosity (determining the resistance to shear and effect on pore water under pressures) and the permeability (effect on pore water under pressures) influence the pick-up flux. The results of the experiments underline the influence of these bulk properties of the sand bed on the pick-up flux.

A semi-empirical pick-up function has been derived on the basis of the results of the experiments and visual observations during the experiments. This function is based on the shearing of lumps of sand as a result of turbulent normal wall stresses. The normal wall stress is determined by the vertical velocity in the sweeps. The depth-averaged flow velocity is used as a measure for this vertical velocity. The shearing of lumps of sand is modeled according to the resistance of a sand bed to a normal stress, including the effect of dilatancy and resulting decreased pore water stresses. This approach gives a good description of the effect of the porosity, angle of internal friction and permeability on the pick-up flux and matches well with the data of the erosion experiments.

The influence of liquefaction of the sand bed, as observed during the experiments, is absent in the present developed pick-up function. Liquefaction is caused by consecutive turbulent bursts hitting the top of the sand bed. Depending on the porosity and permeability of the sand bed, sweeps cause temporarily excess pore water stresses. The rate of decrease of these excess pore water stresses in time and thus the intensity of liquefaction depends on the time between the bursts and the permeability of the sand bed. The experiments show that fine sand is more sensitive for liquefaction than coarse sand, which can be explained by the lower permeability of fine sand in comparison with coarse sand. Visual observations during the experiments on the coarsest sand type ($d_{50} = 562$ $\mu$m) showed temporarily a small liquefied zone. Due to the high permeability of this type of sand, the generated excess pore water stresses fully decreased, before the next turbulent burst hit the top of the sand bed. Further study is necessary to improve the developed pick-up function for the influence of liquefaction.

The present experimental study has resulted in a description of the erosion process, an experimental data set and a semi-empirical model for the pick-up flux at depth-averaged flow velocities between 2 and 6 m/s including the effect of the porosity and permeability of the sand bed. This makes it possible to improve the calculation of the growth of a breach in a sand dike and to improve the dredging of sand with a trailing suction hopper dredger.

# Samenvatting

Het veiligheidsniveau van een dijk wordt uitgedrukt in termen van risico's. De grootte van het risico is afhankelijk van het product van de kans op het optreden van een dijkdoorbraak en de gevolgen hiervan, de schade. Hierbij gaat het niet alleen om economische schade of schade aan infrastructurele objecten, maar ook om aantallen slachtoffers als gevolg van de overstroming. De snelheid waarmee de overstroming optreedt, bepaalt het aantal slachtoffers en hangt sterk af van de stroomsnelheid van het water door de bres in de dijk en de groei van de grootte van deze bres. De stroomsnelheid in de bres kan oplopen tot meer dan 5 m/s. Als gevolg van deze relatief hoge stroomsnelheid, leidt het gebruik van conventionele erosie-functies in bresgroei-modellen tot een overschatting van de bresgroei en daarmee de snelheid waarmee de polder inundeert na het bezwijken van een dijk.

Hetzelfde is geconstateerd bij het baggeren van zand met sleephopperzuigers. Deze schepen winnen zand op zee voor opspuitwerkzaamheden ten behoeve van landaanwinning. Door middel van een sleepkop, die over de bodem van de zee wordt getrokken, wordt met behulp van waterjets zand geërodeerd. De stroomsnelheid in deze waterjets is tussen de 30 tot 60 m/s. Ook in deze situatie, geven de conventionele erosie-functies een overschatting van de erosiesnelheid tijdens het jetten.

Zandkorrels beginnen te bewegen wanneer de kritische Shields-parameter wordt overschreden. De korrels worden over het zandbed getransporteerd. Bij hogere waarden van de Shields-parameter vindt erosie plaats: de top van het zandbed beweegt naar beneden. De hoeveelheid korrels (gewicht) die eroderen per eenheid van tijd en oppervlak is gedefinieerd als de erosie-flux. De huidige modellen voor het bepalen van de erosie-flux zijn gebaseerd op het eroderen van separate korrels (korrel per korrel erosieregime), zijn toepasbaar voor lage stroomsnelheden (tot ongeveer 1 m/s) en er ontbreekt een zekere fysische onderbouwing.

Echter, boven stroomsnelheden van 1 m/s overschatten de huidige modellen de erosie-flux. Empirische modellen, die het gedrag bij hogere stroomsnelheden beschrijven (tot 3 m/s), verklaren dit verschil door het effect van het gedrag van het zandbed tijdens erosie. Deze modellen gaan ervan uit dat de erosie wordt beïnvloed door het afschuiven van lagen zand in het bovenste gedeelte van het zandbed. Het resulterende dilatante gedrag, veroorzaakt een hydraulische gradient in het zandbed, waardoor de erosie wordt beperkt (dilatantantie gereduceerd erosieregime). Het gevolg is dat bulkeigenschappen van het zand, zoals porositeit en doorlatendheid, de erosie-flux gaan beïnvloeden.

De hoeveelheid beschikbare gegevens en het bereik van de stroomsnelheid van bestaande experimentele studies is te beperkt voor een goede validatie van modellen in het dilatantie gereduceerd erosieregime. Bestaande experimentele studies laten de invloed van bulkeigenschappen als porositeit en doorlatendheid zien, maar de

stroomsnelheid tijdens de uitgevoerde proeven was maximaal 1.5 m/s. Sommige andere experimentele studies zijn uitgevoerd bij stroomsnelheden tot 3 m/s. Echter de hoeveelheid beschikbare gegevens was te beperkt voor een goede validatie van erosie bij stroomsnelheden van meer dan 1 m/s.

Om het erosie-proces te bestuderen bij hogere stroomsnelheden en voor het verkrijgen van experimentele gegevens, zijn in het onderhavige onderzoek erosie-experimenten uitgevoerd bij stroomsnelheden van 2 tot 6 m/s, waarbij de bulkeigenschappen van het zandbed zijn gevarieerd. De resultaten van deze experimenten laten de invloed zien van turbulente wervels dichtbij het oppervlak van het zandbed. De stroomsnelheid in de neergaande beweging van de wervel veroorzaakt het bezwijken van zandbrokken. Deze brokkken vallen uit elkaar en worden (gedeeltelijk) getransporteerd naar de hoofdstroming door de opwaartse stroming in de wervel. Echter, niet alle korrels bereiken de hoofdstroming. Een gedeelte van de korrels sedimenteert door de neergaande stroming van de volgende wervel.

Het afschuiven van brokken zand is vergelijkbaar met de weerstand van een zandbed tegen afschuiving als gevolg van een normaalspanning. Afschuiving leidt tot dilatantie, hetgeen resulteert in verlaagde waterspanningen in de poriën, waarmee de weerstand tegen afschuiving toeneemt. Dit laat zien dat de porositeit (bepalend voor de weerstand tegen afschuiving en het effect op de waterspanningen in de poriën) en de doorlatendheid (bepalend voor de grootte van de waterspanningen in de poriën) van invloed zijn op de erosieflux. De resultaten van de proeven onderschrijven de invloed van deze bulkeigenschappen van het zandbed op de erosieflux.

Een semi-empirische erosiefunctie voor de erosieflux is afgeleid op basis van de resultaten van de experimenten en visuele observaties tijdens deze experimenten. Deze functie is gebaseerd op het afschuiven van brokken zand als gevolg van een normaalspanning. De normaalspanning is gebaseerd op de verticale stroomsnelheid in de wervels dichtbij het zandbed. Deze functie gebruikt de diepte-gemiddelde horizontale stroomsnelheid als maat voor deze verticale stroomsnelheid. Het afschuiven van brokken zand is gemodelleerd op basis van het bezwijken van zand als gevolg van een normaalspanning, inclusief het effect van dilatantie en het effect daarvan op de waterspanning en effectieve spanning. Deze aanpak geeft een goede beschrijving van het effect van de porositeit, hoek van inwendige wrijving en de doorlatendheid op de erosieflux. Het model komt goed overeen met de resultaten van de erosie-experimenten.

De invloed van verweking van het zandbed, zoals deze optrad tijdens de experimenten, is niet meegenomen in de ontwikkelde erosie-functie. Verweking wordt veroorzaakt door opeenvolgende wervels die de top van het zandbed belasten. Afhankelijk van de porositeit en de doorlatendheid, veroorzaakt de normaalspanning als gevolg van de neerwaartse stroming in de wervels tijdelijke wateroverspanningen. De tijd tussen opeenvolgende wervels en de doorlatendheid van het zandbed, bepalen de afname van de wateroverspanningen en daardoor de grootte en tijdsduur van de verweking. De experimenten laten zien dat fijn zand gevoeliger is voor verweking dan grover zand. Dit kan verklaard worden door de lagere doorlatendheid van het fijne zand in vergelijking met die van het grovere zand. Het grove zand vertoonde tijdens de experimenten een relatief kleine en tijdelijk aanwezige verweekte zone. Als

gevolg van de hoge doorlatendheid waren de wateroverspanningen nagenoeg volledig afgenomen op het moment dat de volgende wervel de top van het zandbed raakte. Verdere ontwikkeling van het model is noodzakelijk om het bestaande model uit te breiden voor het effect van verweking.

De huidige experimentele studie heeft inzicht gegeven in de fysica van het erosieproces. Met behulp van deze kennis en de meetdata is een semi-empirische functie afgeleid en gevalideerd voor het bepalen van de erosieflux bij diepte-gemiddelde stroomsnelheden tussen de 2 en 6 m/s inclusief de invloed van het effect van de porositeit en de doorlatendheid van het zandbed. Dit maakt het mogelijk de groei van een bres in een zanddijk beter te voorspellen en het productieproces bij het baggeren van zand met een sleephopperzuiger te verbeteren.

# Contents

# List of Symbols

| Roman symbol | Description | Unit |
|---|---|---|
| $A$ | surface area | [$m^2$] |
| $A_b$ | bed associated flow area | [$m^2$] |
| $A_c$ | activity | [-] |
| $A_g$ | surface area grain | [$m^2$] |
| $A_s$ | specific surface area | [$m^2$] |
| $A_{sw}$ | surface area sweep | [$m^2$] |
| $A_{tot}$ | total flow area | [$m^2$] |
| $A_w$ | wall associated flow area | [$m^2$] |
| $a$ | distance of vortex from the wall | [m] |
| $B$ | width | [m] |
| $b$ | factor for the distance between the center of spheres | [m] |
| $C$ | Chézy coefficient | [$\sqrt{m}$/s] |
| $C_d$ | drag coefficient | [-] |
| $C_k$ | coefficient depending on the grain size distribution and angularity of the grains | [-] |
| $C_L$ | lift coefficient | [-] |
| $C_m$ | added mass coefficient | [-] |
| $C_u$ | coefficient of uniformity | [-] |
| $C^{'}$ | constant of compressibility | [-] |
| $c$ | cohesion | [Pa] |
| $c$ | concentration | [-] |
| $c_a$ | reference concentration | [-] |
| $c_{av}$ | depth-averaged concentration | [-] |
| $c_b$ | bed concentration | [-] |
| $c_i$ | isotropic consolidation coefficient | [$m^2$/s] |
| $c_{nb}$ | near-bed concentration | [-] |
| $c_m$ | measured concentration | [-] |
| $c_{max}$ | maximum concentration | [-] |
| $c_1$ | empirical constant | [-] |
| $c_2$ | empirical constant | [-] |
| $c$ | cohesion | [Pa] |
| $D_h$ | hydraulic diameter | [m] |
| $D_{hb}$ | bed associated hydraulic diameter | [m] |
| $D_{hw}$ | wall associated hydraulic diameter | [m] |
| $D_*$ | dimensionless grain diameter | [-] |
| $d$ | diameter | [m] |
| $d_{10}$ | size at which 10% of the grains is smaller | [m] |

| Roman symbol | Description | Unit |
|---|---|---|
| $d_{15}$ | size at which 15% of the grains is smaller | [m] |
| $d_{50}$ | size at which 50% of the grains is smaller/average grain size | [m] |
| $d_{60}$ | size at which 60% of the grains is smaller | [m] |
| $d_{90}$ | size at which 90% of the grains is smaller | [m] |
| $d_l$ | longest axis of a grain | [m] |
| $d_m$ | intermediate axis of a grain | [m] |
| $d_s$ | erosion depth | [m] |
| $d'_s$ | adapted erosion depth | [m] |
| $d_o$ | shortest axis of a grain | [m] |
| $du/dz$ | velocity gradient | [1/s] |
| $E$ | pick-up flux | [kg/m$^2$·s] |
| $E_h$ | pick-up flux including effect of hindered erosion | [kg/m$^2$·s] |
| $E_{oed}$ | oedometer loading stiffness | [Pa] |
| $e$ | void ratio | [-] |
| $e_i$ | in-situ void ratio | [-] |
| $e_{max}$ | maximum void ratio | [-] |
| $e_{min}$ | minimum void ratio | [-] |
| $F$ | force | [N] |
| $F_{acc}$ | resisting force as a result of inertia | [N] |
| $F_b$ | horizontal force exerted by a flow | [N] |
| $F_c$ | centrifugal force | [N] |
| $F_d$ | drag force | [N] |
| $F_L$ | lift force | [N] |
| $F_m$ | Magnus force | [N] |
| $F_s$ | Saffman force | [N] |
| $F_w$ | resisting force a a result of shear | [N] |
| $f$ | Darcy-Weisbach coeffient | [-] |
| $f_i$ | interface Darcy-Weisbach friction coeffient | [-] |
| $f_b$ | Darcy-Weisbach bed friction coeffient | [-] |
| $f_L$ | angularity factor of Loudon | [-] |
| $f_w$ | wall Darcy-Weisbach friction coeffient | [-] |
| $f_{w,i}$ | wall Darcy-Weisbach friction coeffient in case no sand bed is present | [-] |
| $g$ | acceleration of gravity | [m/s$^2$] |
| $H$ | thickness shear layer | [m] |
| $h$ | depth below surface sand bed | [m] |
| $h_f$ | flow/water depth | [m] |
| $h_s$ | thickness sheared layer/depth shear plane | [m] |
| $i$ | hydraulic gradient | [-] |
| $i_c$ | hydraulic gradient at which submerged weight grain is zero | [-] |
| $j$ | empirical coefficient shape grains | [-] |
| $K_0$ | lateral earth pressure coefficient | [N] |

| Roman symbol | Description | Unit |
|---|---|---|
| $k$ | permeability | [m/s] |
| $k_i$ | in-situ permeability | [m/s] |
| $k_{max}$ | permeability at maximum porosity | [m/s] |
| $k_e$ | turbulent kinetic energy | [$m^2/s^2$] |
| $k_o$ | Kozeny-Carman constant | [-] |
| $k_s$ | Nikuradse roughness | [m] |
| $l$ | length | [m] |
| $l_a$ | adaptation length | [m] |
| $L_c$ | length of sand bed | [m] |
| $L_H$ | horizontal length scale turbulence | [m] |
| $L_m$ | Bakhmetev mixing scale | [m] |
| $m_v$ | coefficient of volume compressibility | [$m^2$/N] |
| $N$ | Bagnold number | [-] |
| $N$ | number of grains per unit bed area | [$1/m^2$] |
| $N_{mass}$ | mass number | [-] |
| $N_\gamma$ | bearing capacity factor | [-] |
| $N_\phi$ | bearing capacity factor | [-] |
| $n$ | empirical constant Richardson and Zaki | [-] |
| $n$ | porosity | [-] |
| $n_{avg}$ | average porosity | [-] |
| $n_{crit}$ | critical porosity | [-] |
| $n_i$ | in-situ porosity | [-] |
| $n_l$ | porosity sheared layer | [-] |
| $n_{max}$ | maximum porosity | [-] |
| $n_{min}$ | minimum porosity | [-] |
| $n_s$ | porosity at top level of erosion depth | [-] |
| $n'_s$ | porosity at top level of adapted erosion depth | [-] |
| $O$ | perimeter cross section/flow area | [m] |
| $P$ | empirical coefficient shape grains | [-] |
| $Pe_w$ | Péclet number | [-] |
| $PI$ | plasticity index | [%] |
| $p'$ | turbulent normal wall stress | [Pa] |
| $Q$ | discharge capacity | [$m^3/s$] |
| $Q_{av}$ | average discharge | [$m^3/s$] |
| $Q_t$ | transport capacity | [$m^3/s$] |
| $Q_{t,40}$ | transport capacity at bed length of 40 m | [$m^3/s$] |
| $Q_{t,max}$ | maximum transport capacity | [$m^3/s$] |
| $q$ | specific discharge | [m/s] |
| $R$ | empirical coefficient shape grains | [-] |
| $R_e$ | relative density based on the void ratio | [-] |
| $R_h$ | hydraulic radius | [m] |
| $R_n$ | relative density based on the porosity | [-] |
| $Re$ | Reynolds number | [-] |
| $Re_A$ | bed area associated Reynolds number | [-] |

| Roman symbol | Description | Unit |
|---|---|---|
| $Re_b$ | bed associated Reynolds number | [-] |
| $Re_p$ | particle Reynolds number | [-] |
| $Re_w$ | wall associated Reynolds number | [-] |
| $Re_x$ | Reynolds number as function of x | [-] |
| $Re_{x,crit}$ | critical Reynolds number | [-] |
| $Re_\delta$ | boundary layer Reynolds number | [-] |
| $Re_*$ | roughness Reynolds number | [-] |
| $Re_{*p}$ | boundary particle Reynolds number | [-] |
| $r$ | radius of a grains | [m] |
| $S$ | sedimentation flux | [kg/m$^2$·s] |
| $S_{rel}$ | relative sedimentation flux | [kg/m$^2$·s] |
| $S_a$ | degree of saturation | [-] |
| $S_f$ | (Corey) shape factor | [-] |
| $S_v$ | specific grain surface | [m$^2$/m$^3$] |
| $S_{max}$ | maximum sedimentation flux | [kg/m$^2$·s] |
| $s$ | specific grain density | [-] |
| $s_p$ | distance between spheres | [m] |
| $t$ | time | [s] |
| $t_s$ | shear band thickness | [m] |
| $T$ | dimensionless shear stress | [-] |
| $T_e$ | temperature | [°] |
| $T_B$ | time scale turbulent bursts | [s] |
| $T_B^+$ | non-dimensional bursting period | [-] |
| $U$ | depth-averaged horizontal flow velocity | [m/s] |
| $U_0$ | uniform depth-averaged horizontal flow velocity | [m/s] |
| $U_c$ | convection rate vortex | [m/s] |
| $U_w$ | average flow velocity wall associated flow area | [m/s] |
| $u$ | time-averaged local horizontal flow velocity | [m/s] |
| $u\,(z)$ | time-averaged horizontal flow velocity at a level z | [m/s] |
| $u_H$ | horizontal flow velocity at top shear layer | [m/s] |
| $u_{max}$ | time-averaged maximum outer horizontal flow velocity | [m/s] |
| $u'$ | deviation of the horizontal flow velocity | [m/s] |
| $\hat{u}$ | instantaneous horizontal flow velocity | [m/s] |
| $\hat{u}_b$ | near-bed instantaneous horizontal flow velocity | [m/s] |
| $u_*$ | shear velocity | [m/s] |
| $u_{*c}$ | critical shear velocity according to Shields | [m/s] |
| $u_{*cs}$ | critical shear velocity including effect of injection | [m/s] |
| $V_g$ | volume of one grain | [m$^3$] |
| $V_s$ | volume of grains | [m$^3$] |
| $V_t$ | total volume | [m$^3$] |
| $V_v$ | volume of voids | [m$^3$] |
| $V_w$ | volume of water | [m$^3$] |
| $W$ | width wedge shear plane | [m] |

| Roman symbol | Description | Unit |
|---|---|---|
| $v$ | time-averaged local transverse flow velocity | [m/s] |
| $v_e$ | erosion velocity | [m/s] |
| $v_{e-av}$ | average erosion velocity | [m/s] |
| $v_s$ | suction/injection velocity | [m/s] |
| $v_{sc}$ | critical velocity at which submerged weight grain is zero | [m/s] |
| $v_{sed}$ | sedimentation velocity | [m/s] |
| $v'$ | deviation of the transverse flow velocity | [m/s] |
| $\hat{v}$ | instantaneous transverse flow velocity | [m/s] |
| $v_g$ | relative velocity grain | [m/s] |
| $w$ | time-averaged local vertical flow velocity | [m/s] |
| $w_m$ | width measurement section | [m] |
| $w_s$ | settling velocity | [m/s] |
| $w_{hs}$ | hindered settling velocity | [m/s] |
| $w'$ | deviation of the vertical flow velocity | [m/s] |
| $\hat{w}$ | instantaneous vertical flow velocity (in sweep) | [m/s] |
| $x$ | coordinate in horizontal direction | [m] |
| $y$ | coordinate in transverse direction | [m] |
| $z$ | coordinate in vertical direction | [m] |
| $z_a$ | reference level | [m] |
| $z_0$ | level at which the flow velocity is zero | [m] |

| Greek symbol | Description | Unit |
|---|---|---|
| $\alpha$ | (empirical) constant | [-] |
| $\alpha$ | calibration factor for the estimate of the temporal maximum of the local horizontal flow velocity | [-] |
| $\alpha_s$ | Saffman lift coefficient | [-] |
| $\alpha_u$ | empirical factor for the standard deviation of the horizontal flow velocity | [-] |
| $\alpha_v$ | empirical factor for the standard deviation of the transverse flow velocity | [-] |
| $\alpha_w$ | empirical factor for the standard deviation of the vertical flow velocity | [-] |
| $\beta$ | respond function | [-] |
| $\Delta$ | relative grain density | [-] |
| $\Delta V_w$ | potential difference water | [Volt] |
| $\Delta V_m$ | potential difference at measured concentration | [Volt] |
| $\Delta V_{max}$ | potential difference at maximum concentration | [Volt] |
| $\Delta F_b$ | force loss along rough wall/sand bed | [N] |
| $\Delta F_{tot}$ | total force loss | [N] |
| $\Delta F_w$ | force loss along smooth wall/wall measurement section | [N] |
| $\Delta p$ | pressure difference | [Pa] |
| $\Delta p_b$ | pressure loss along rough wall/sand bed | [Pa] |

| Greek symbol | Description | Unit |
|---|---|---|
| $\Delta p_w$ | pressure loss along smooth wall/wall measurement section | [Pa] |
| $\delta$ | thickness boundary layer | [m] |
| $\delta_s$ | sheet flow layer thickness | [m] |
| $\epsilon_s$ | sediment diffusivity | [$m^2/s$] |
| $\eta$ | dynamic viscosity | [Pa · s] |
| $\eta_{sus}$ | dynamic viscosity suspension | [Pa · s] |
| $\eta_w$ | dynamic viscosity water | [Pa · s] |
| $\phi$ | internal friction angle | [°] |
| $\gamma_0$ | empirical constant | [-] |
| $\kappa$ | constant of von Karman | [-] |
| $\xi$ | constant | [-] |
| $\lambda$ | linear concentration | [-] |
| $\lambda_b$ | area of bursts per unit of bed area | [-] |
| $\lambda_s$ | area of sweeps per unit of bed area | [-] |
| $\lambda_z$ | spanwise spacing between turbulent structures | [m] |
| $\nu$ | kinematic viscosity | [$m^2/s$] |
| $\nu_w$ | kinematic viscosity water | [$m^2/s$] |
| $\nu_t$ | turbulent viscosity | [$m^2/s$] |
| $\omega$ | strength of vortex | [$m^2/s$] |
| $\omega_g$ | angular velocity grain | [m/s] |
| $\psi$ | pivot angle | [°] |
| $\rho$ | density | [$kg/m^3$] |
| $\rho_{d,max}$ | maximum dry density | [$kg/m^3$] |
| $\rho_{d,min}$ | minimum dry density | [$kg/m^3$] |
| $\rho_{er-av}$ | average density eroding flow | [$kg/m^3$] |
| $\rho_i$ | in-situ density | [$kg/m^3$] |
| $\rho_{in}$ | density in flow measurement section | [$kg/m^3$] |
| $\rho_s$ | grain density | [$kg/m^3$] |
| $\rho_{sb-av}$ | average density sand bed | [$kg/m^3$] |
| $\rho_w$ | density water | [$kg/m^3$] |
| $\sigma_{u,v,w}$ | standard deviation of velocity distribution around the time averaged (mean) flow velocity | |
| $\sigma_p$ | failure stress due to a normal load | [Pa] |
| $\sigma_u$ | pore water stress | [Pa] |
| $\sigma_z$ | total vertical stress | [Pa] |
| $\sigma'_{max}$ | maximum effective stress | [Pa] |
| $\sigma'_{min}$ | minimum effective stress | [Pa] |
| $\sigma'_x$ | effective horizontal stress | [Pa] |
| $\sigma'_z$ | effective vertical stress | [Pa] |
| $\tau$ | shear stress | [Pa] |
| $\tau_b$ | bed or boundary shear stress | [Pa] |
| $\tau_{b,cr}$ | critical bed shear stress according to Shields | [Pa] |
| $\tau_{dil}$ | shear stress as a result of a hydraulic gradient | [Pa] |

| Greek symbol | Description | Unit |
|---|---|---|
| $\tau_i$ | saverage interface shear stress | [Pa] |
| $\tau_s$ | static shear stress | [Pa] |
| $\tau_{tot}$ | shear resistance grain dispersion | [Pa] |
| $\tau_w$ | wall shear stress | [Pa] |
| $\tau'$ | dynamic shear stress | [Pa] |
| $\tau'_g$ | shear stress grain-inertia regime | [Pa] |
| $\tau_r$ | resisting shear stress | [Pa] |
| $\tau'_v$ | shear stress viscous regime | [Pa] |
| $\phi$ | angle of internal friction | [°] |
| $\omega$ | angular velocity | [rad/s] |
| $\omega_g$ | angular velocity grain | [rad/s] |
| $\theta_b$ | Shields parameter | [-] |
| $\theta'_b$ | adapted Shields parameter | [-] |
| $\theta_{cr}$ | critical Shields parameter | [-] |
| $\theta'_{cr}$ | adapted critical Shields parameter | [-] |

| Abbreviation | Description |
|---|---|
| CEC | Cation Exchange Capacity |
| DNS | Direct Numerical Simulations |
| LEM | Large Eddy Simulations |

# 1

# Introduction

## 1.1. Background

In the Netherlands the safety level of a dike is expressed in terms of risk. Risk is defined as the product of the probability of inundation of a polder (after failure of the dike) and the expected damage caused by the inundation (Visser, 1998). It is necessary to model the inundation process of the polder (Figure 1.1) in order to be able to estimate this damage (casualties, damage infrastructure, economic damage, etc.). The process of polder inundation depends heavily on the flow velocity through the breach and breach development in time. The flow velocity in a breach can become larger than 5 m/s. Due to these large flow velocities, the application of conventional empirical sediment pick-up functions, like that of van Rijn (1984a), in breach growth models leads to a significant overestimation of the breach growth (Bisschop et al., 2010).

Figure 1.1: Dike breaching during storm of 1953 in the Netherlands

The same difference is encountered in dredging practice. Trailing suction hopper dredgers extract sand from the bottom of the sea for reclamation purposes (Figure 1.2). A suction head is trailed over the sea bed, using water jets to erode sand. Typical jet flow velocities are around 30 to 60 m/s (van Rhee, 2010). As in the breaching process, conventional pick-up functions significantly overestimate the erosion velocity during jetting (van Rhee, 2010).

Figure 1.2: Trailing suction hopper dredger rainbowing

Pick-up of grains starts when the flow conditions exceed the critical Shields parameter (Shields, 1936). When this criterion is met, grains start to move and are transported over the top of the sand bed. At a higher Shields parameter, grains are eroded from the sand bed: the top of the sand moves down. The amount of grains (weight) eroded from the sand bed per unit of time and area is defined as the pick-up flux. Functions, describing the pick-up flux, are mainly based on the erosion of single grains (grain by grain pick-up) and are applicable for relative low values of the Shields parameter ($< 0.5$ till 1.0). Within the scope of this study, sand with a grain size of 50 to 500 $\mu$m, this condition agrees with flow velocities of less than 1.0 till 1.5 m/s. Grain movement occurs when the instantaneous fluid force on a grain exceeds the instantaneous resisting force related to the submerged weight, friction force or embedding of the grain in the sand bed. One of the most well-known pick-up functions is the empirical equation of van Rijn (1984a). However, at flow velocities of more than 1 m/s the model of van Rijn (1984a) overestimates the pick-up flux.

Winterwerp et al. (1992), Mastbergen and van den Berg (2003), Mastbergen (2006) and van Rhee (2010) published empirical models regarding the erosion of sand at higher flow velocities (up to 3 m/s). These models give a better prediction of the pick-up flux at these flow velocities than the equation of van Rijn (1984a). Mastbergen and van den Berg (2003) and van Rhee (2010) explain that this difference is caused by the behavior of the sand bed during erosion. It is assumed that the pick-up flux is influenced by the shearing of layers of sand at the top of the sand

bed. Shearing was also observed by Gao (2008) at corresponding flow conditions with a Shields parameter ($\theta_b$) of more than 0.5.

The resulting dilative behavior results in an inward hydraulic gradient into the sand bed, hence reducing erosion (dilatancy reduced erosion). As a result bulk properties such as porosity and permeability start to influence the pick-up flux. van Rhee (2010) developed an adapted pick-up function for flow velocities of more than 1 m/s incorporating this effect via bulk properties like permeability and porosity in an adapted critical Shields parameter. This function agrees well with data of erosion experiments of Bisschop (1993) and Roberts et al. (1998). van Rhee (2010) showed also that the occurrence of the dilatancy reduced erosion regime only partly depends on the flow velocity, but is mainly determined by the value of the quotient of the erosion velocity and permeability ($v_e/k$).

van Rhee (2010) introduced the term hindered pick-up for this regime. Bisschop et al. (2016) changed the name of this regime into dilatancy reduced erosion to avoid confusion with the influence of the concentration of the eroding fluid on the erosion process. This last process is considered as the reduction of the pick-up flux as a result of grains, present at relatively high concentrations in the eroding fluid just above the eroding bed, hindering eroding grains moving upwards. This effect is described as hindered pick-up (Winterwerp et al., 1992).

## 1.2. Problem definition

The amount of data and range of flow velocities of existing experimental studies is too limited for a proper validation of the dilatancy reduced erosion regime. Bisschop (1993) and Roberts et al. (1998) investigated in their experiments thoroughly the influence of bulk properties, like permeability and porosity of the sand, although the flow velocity during these experiments was limited to 1 and 1.5 m/s. These experiments just met the conditions for dilatancy reduced erosion. Winterwerp et al. (1992) and Mastbergen and van den Berg (2003) present data at higher values of the Shields parameter (up to 30) and flow velocity (up to 3 m/s). However, these data are too limited for a proper validation of the erosion process of more than 1 m/s.

## 1.3. Research objective

The goal of this research program is:

- to observe and to get understanding of the process of erosion of sand at flow velocities of 2 to 6 m/s and to gather experimental data of the erosion process with varying bulk properties of the sand bed;
- to develop a pick-up flux function applicable at these flow velocities.

The erosion experiments were executed in an adapted closed flume of the slurry circuit of the Dredging Research Laboratory of Delft University of Technology. Different erosion experiments were carried out, with varying hydraulic conditions like flow velocity and density of the eroding sand-water mixture. Grain size and density

of the sand bed were varied. The description of the erosion process and the results of the different experiments have been used to describe the erosion process and to develop an analytical pick-up function.

## 1.4. Outline of this thesis

The road map of this PhD thesis is presented in Figure 1.3. The research program started with a literature survey regarding the behavior of single (sand) grains and their bulk behavior (Section 2), followed by a literature survey regarding the behavior of a flow over a sand bed and resulting energy loss or hydraulic gradient (Section 3). Section 4 describes existing empirical and partly theoretical pick-up functions. This survey shows that some empirical models exist, but the experimental data are limited to flow velocities up to 3 m/s. Due to the lack of results of erosion experiments at flow velocities above 3 m/s and the lack of knowledge regarding the effective bed shear stress at these flow velocities, erosion experiments were carried out in an adapted slurry circuit of the Dredging Technology Research Laboratory of the TU Delft (Section 5). In 2010 a first series of 17 experiments were executed on two types of sand. The results of these tests were used to improve the test set-up and experimental procedures. This resulted in a test program consisting of 65 experiments on 4 sand types with varying density of the sand bed, flow velocity and density of the eroding flow. Section 6 describes the results of the experiments including the derivation of the pick-up flux and effective bed shear stress and concludes with an experimental error analysis. All empirical functions need an estimate of the effective bed shear stress at flow velocities of more than 1 m/s. Section 7 presents an analysis, leading to a direct empirical function in order to determine the bed shear stress at these flow conditions. This is an improvement because available empirical functions are based on an implicit function relating the bed shear stress to a fictitious bed roughness, having no physical meaning. Section 8 gives a physical description of the erosion process. This has led to the improvement of the derivation of the pick-up flux from the experiments. The influence of the flow conditions and properties of the sand bed on the pick-up flux are described in this Section. The physical description and the relation with several parameters form the basis for the development of a semi-empirical pick-up function. This Section finishes with a description of the practical application of the developed knowledge of the erosion process in case of breaching of dikes and embankments and jetting of sand in dredging practice. Conclusions and recommendations are presented in Section 9.

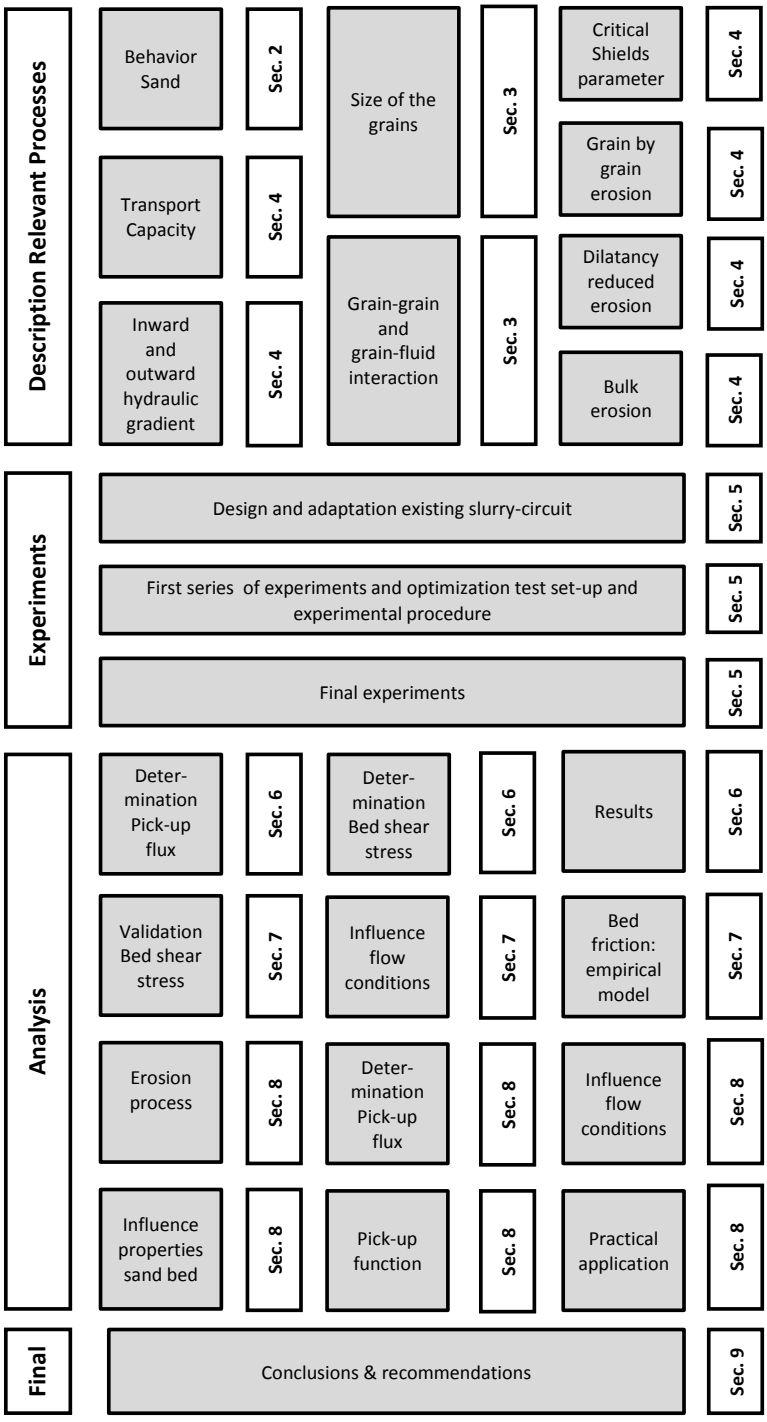


Figure 1.3: Road map of this PhD-thesis

# 2

# Behavior of sand

## 2.1. Introduction

Previous experimental studies of erosion, like Mastbergen and van den Berg (2003) and van Rhee (2010) showed that at flow velocities of more than 1 m/s erosion is influenced by the behavior of the sand bed and thus its bulk properties. Understanding the behavior of sand and its bulk behavior and properties is necessary to study the erosion process of sand at high flow velocities. The behavior of sand is not only determined by the properties of single grains (Section 2.2), like grain size, grain size distribution, roundness and sphericity, density of the grains and mineral content. The properties of single grains as well as the assemblage of the grains determine the bulk behavior and properties of a sand bed (Section 2.3). Typical bulk properties of a sand bed are porosity (density), permeability and shear resistance (angle of internal friction). For the description of the shear resistance of sand distinction is made between the shear-strain and shear-strain rate behavior. Section 2.4 describes the main findings regarding the behavior of sand, distinguishing the behavior of single grains and the bulk behavior of sand.

## 2.2. Properties of grains

The most important property of a sand grain is the size. Other properties are: roundness, sphericity, density of the grains and mineral content.

### 2.2.1. Grain size

The grain size and grain size distribution have a large influence on the behavior of the bulk properties of a sand bed. The Dutch design code (NEN, 2016), regarding the classification of soils, distinguishes four types on the basis of the grain size (Figure 2.1).

- gravel: grain size larger than 2 mm;
- sand: grain size between 2 mm and 63 $\mu$m;

- silt: grain size between 63 $\mu$m and 2 $\mu$m;
- clay: grains smaller than 2 $\mu$m.



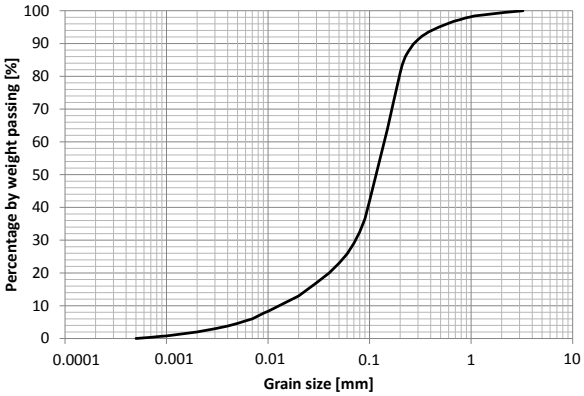


Figure 2.1: Example of grain size distribution

It should be noted that other codes classify soils on other values for the grain size. These differences are just a matter of definition, they do not represent any physical limit. The main differences are found for the limiting value of the grain size for clay and the boundary between silt and sand. The American Geophysical Union and the American Society for Testing and Material (ASTM) use for the grain size at the boundary between clay and silt: 4 $\mu$m and 5 $\mu$m instead of 2 $\mu$m. The ASTM and British Standards (BS) have defined the boundary between silt and sand at a grain size of 75 $\mu$m and 60 $\mu$m instead of 63 $\mu$m (Winterwerp and van Kesteren, 2004).

Natural sediments do not consist of grains of a separate size, but exhibit a certain grain size distribution. Figure 2.1 shows an example. Often sediments are characterized by the $d_{50}$ (size at which 50% of the grains is smaller), which is often denoted as the average grain size. Other size parameters as the $d_{10}$ and $d_{60}$ are defined as the size at which 10% respectively 60% of the grains is smaller. The grain size distribution has a large influence on the bulk behavior of granular sediments. On the basis of the grain size distribution and mineralogical composition a distinction can be made between granular and cohesive behavior. Granular behavior occurs when the behavior of the sand bed is dominated by inert (quartz) grains, without any electro-chemical interaction. The interaction consists of inter granular shear resistance (angle of internal friction), depending on the density, sphericity and roughness of the separate grains.

Cohesive behavior occurs when the behavior is dominated by grains, exhibiting electro-chemical interaction (Bisschop, 2009). Examples of clay minerals are kaolinite, smectite, montmorillonite, illite and chlorite (Winterwerp and van Kesteren, 2004). These minerals have a varying capacity of binding water, hence influencing

the behavior of clay. The fraction having a size of less than 2$\mu$m to 20 $\mu$m consists mainly of clay minerals. According to the Dutch design code (NEN, 2016) granular sediments are defined as sand (Lubking, 2004) when the sand fraction is more than 50%, the clay fraction is less than 8% and the material does not possess any cohesion (Figure 2.2). At a clay fraction of more than 8% the amount of clay influences the behavior of the sediment significantly. Properties like permeability and shear resistance, change significantly, in comparison with sediments being described as sand.

However, the value of the clay fraction determining the behavior of sediments (granular of cohesive) is not fixed. Besides the amount of clay, the behavior of a sediment depends on the electro-chemical interaction of the clay fraction, which depends on the mineralogical composition of the clay. The electro-chemical interaction influences the capacity in binding water. A sediment, comprising clay with a relative high capacity in binding water (highly active clays), will show cohesive behavior at clay fractions (weight percentage) of even less than 8%, see also Section 2.2.4. The value of 8% can be considered as representative for Dutch clay types.

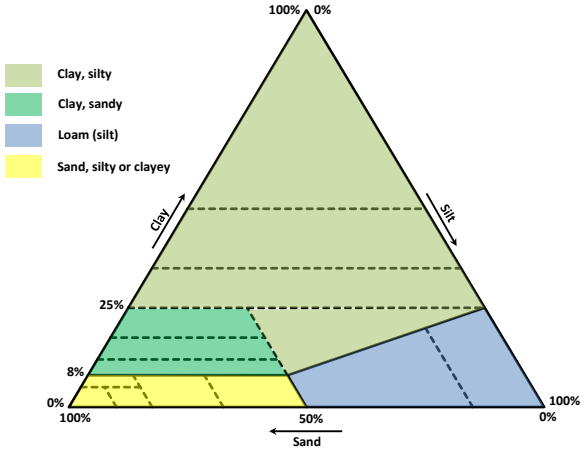


Figure 2.2: Sand-silt-clay triangle (Bisschop, 2009)

### 2.2.2. Roundness and sphericity

Natural sand grains have a certain roundness and sphericity. The roundness of a grain is determined by the shape of the corners. If the grain shape is very irregular the grains are very angular (Figure 2.3), while well rounded means that the shape of the grains is very smooth. The sphericity is a number for the overall shape of the grains. A grain with a flat shape has a low sphericity, while a high sphericity means that the grains are round. The amount of roundness and sphericity can be numbered according to Figure 2.3. Another method to determine the sphericity of a grain is the Corey shape factor ($S_f$). This factor is determined on the basis of the length of the longest ($d_l$), intermediate ($d_m$) and shortest axis ($d_o$) of a grain:

$$S_f = d_o / \sqrt{d_l \cdot d_m} \tag{2.1}$$

This factor is zero for a two-dimensional plate and unity for a sphere (Swamee and Ojha, 1991). The shape of the grains influences bulk properties like failure behavior, porosity, density and to a lesser extent permeability. Minor features of the surface of a grain, independent of size, sphericity or degree of roundness, are termed "surface texture" of a grain. Some terms to describe surface texture are dull or polished, smooth or rough, frosted, etched or pitted (Lambe and Whitman, 1969).

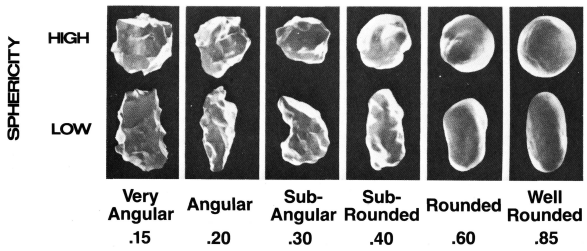


Figure 2.3: Roundness/sphericity chart (Powers, 1953)

### 2.2.3. Grain density

The grain density ($\rho_s$) depends on the type of solids of which the grains consist. In case of quartz grains, being dominant in natural sediments, the grain density is approximately 2,650 kg/m$^3$. Carbonate sand grains have a density of 2,720 kg/m$^3$. The density of other natural solids varies between 2,200 and 2,900 kg/m$^3$ (Lambe and Whitman, 1969), depending on the mineralogical composition of the solids.

### 2.2.4. Mineral content

The individual grains of the silt and sand fraction (grain size >2 $\mu$m and <63 $\mu$m) of a sediment consists mainly of quartz, feldspar and carbonates, although clay minerals still could be present. In the sand fraction (grain size >63 $\mu$m) the main mineral constituents are quartz and feldspar. However, in the Near and Middle East sand could be also of carbonate origin.

Clay minerals are to a large extent responsible for cohesion (Winterwerp and van Kesteren, 2004). This is mainly because of the size and flat shape of the minerals, yielding a very high specific surface area and the electro-chemical interaction between these minerals. Clay minerals consist largely of two-dimensional silica tetrahedra with aluminium-hydroxide octahedra (gibbsite) or magnesium-hydroxide octahedra (brucite). These sheets of silica tetrahedral and gibbsite or brucite exist in different compositions forming different clay minerals. The specific surface area ($A_s$) and cation exchange capacity ($CEC$) are parameters determining the behavior of the clay minerals. Kaolinite is known as a non- or almost non-swelling clay mineral with a low specific surface area and low CEC. Water molecules are hardly able

to enter between the clay minerals, leading to a relative large amount of free water in relation to the amount of bounded water. Other clay minerals like montmorillonite have a higher surface area and CEC. This enables water molecules to enter between the clay minerals resulting in significant swelling. This mineral has a relative large amount of bounded water in relation to free water.

A useful index to characterize the bounding capacity of water and resulting assemblage of clay particles are the Atterberg limits. The Atterberg limits are related to the amount of water that is attracted to the surface of the clay minerals and therefore they are a measure for the total volume of the clay particles and capacity to bound water (activity). Based on this knowledge Skempton (Lambe and Whitman, 1969) has defined a quantity called activity ($A_c$) based on the plasticity index ($PI$) and percentage of clay-size particles (<2 $\mu$m):

$$A_c = \frac{PI}{\% \leq 2\mu m} \tag{2.2}$$

The activity of a clay is strongly related to the type of minerals. Together with the amount of clay fraction it determines the behavior of a sediment: granular of cohesive.

## 2.3. Bulk properties

The bulk properties of granular material depend strongly on the properties of the separate grains. Besides this the bulk properties are influenced by the sedimentary environment (hydraulic circumstances) in which they are formed and the present depth (effective stress) of the sediments. This section describes the bulk behavior and bulk properties as density and/or porosity, permeability and failure behavior (static as well as dynamic).

### 2.3.1. Density

The in-situ density of a sand bed ($\rho_i$) depends on the density of the grains ($\rho_s$), density water ($\rho_w$), porosity ($n$) and degree of saturation ($S_a$):

$$\rho_i = S_a \cdot n \cdot \rho_w + (1 - n) \cdot \rho_s \tag{2.3}$$

The density of the grains depends on the mineralogical composition (Section 2.2). The degree of saturation ($S$) is defined as the volume of water ($V_w$) divided by the volume of the voids ($V_v$). The porosity and void ratio are a measure for the amount of voids. The porosity is defined as the volume of the voids ($V_v$), which can be filled with water or air, divided by the total volume ($V_t$) of the sand bed. The void ratio ($e$) is defined as the quotient of the volume of voids and the volume of the grains. The porosity of an arrangement of uniform spheres has a minimum (dense state) and maximum (loose state). The minimum porosity for uniform spheres is 0.26 and the maximum porosity is in this case 0.476 (Lambe and Whitman, 1969). The minimum porosity for natural sediments varies between 0.30 and 0.45 with a maximum porosity varying between 0.40 and 0.55. The minimum and maximum porosity depend mainly on the grain size distribution (coefficient of

uniformity: $C_u = d_{60}/d_{10}$) and angularity of the grains. A large grading leads to a low minimum porosity, because the voids between the larger grains are filled with smaller grains. The more angular and smaller the grains the lower the minimum porosity.



The relative density ($R_e$ as well as $R_n$) of sand gives the relation of the in-situ void ratio ($e_i$) to the maximum void ratio ($e_{max}$) and minimum void ratio ($e_{min}$) as well as the in-situ porosity ($n_i$) to the maximum porosity ($n_{max}$) and minimum porosity ($n_{min}$). Because the void ratio and porosity are related to the dry density of the material, $S = 0$ in Equation (2.3), the relative density can also be related to the minimum dry density ($\rho_{d,min}$) and the maximum dry density ($\rho_{d,max}$). The relative densities, $R_e$ and $R_n$, are defined as:

$$R_e = \frac{e_{max} - e_i}{e_{max} - e_{min}} = \frac{n_{max} - n_i}{n_{max} - n_{min}} \cdot \frac{1 - n_{min}}{1 - n_i} \cdot 100\% \tag{2.4}$$

$$R_n = \frac{n_{max} - n_i}{n_{max} - n_{min}} = \frac{e_{min} - e_i}{e_{max} - e_{min}} \cdot \frac{1 + e_{min}}{1 + e_i} \cdot 100\% \tag{2.5}$$

### 2.3.2. Permeability

The law of Darcy describes the relation between the specific discharge of water through a sand bed ($q$), the permeability of the sand bed ($k$) and hydraulic gradient ($i$) by:

$$q = -k \cdot i \tag{2.6}$$

The permeability of a sand bed is mainly influenced by the following three characteristics (Lambe and Whitman, 1969):

- grain size (distribution);
- porosity or void ratio;
- clay content and composition (mineralogy).

#### Grain size

The size of sand grains highly influences the permeability, because small grains exhibit small voids between the grains. These voids form the flow channels through the sand and thus the smaller the voids, the higher the flow-resistance and the lower the permeability. Based on experimental data it is proven that the smallest grains in a soil have the largest influence on permeability. These grains determine the dimensions of the size of the voids in between the larger sand grains. The size of the voids determine the size of the flow channels between the grains and therefore highly influence the permeability. The Hazen-equation, an empirical relation, is a good example for this fact, because this equation relates the size ($d_{10}$) of the smallest grains to the permeability (Carrier, 2003):

$$k = 11,570 \cdot d_{10}^2 \tag{2.7}$$

Although Equation (2.7) was developed for the design of sand filters for water purification purposes (loose, clean sands with a coefficient of uniformity: $d_{60}/d_{10}$ of less than about 2), this equation is frequently used to estimate the permeability of in-situ sands (Carrier, 2003). Wide ranges of the empirical constant (11,570) have been reported in several geotechnical textbooks (Carrier, 2003). The published constants range between 100 and 100,000, meaning that Equation (2.7) should be used with great care. This relation assumes that the distribution of particle sizes is spread enough to prevent the smallest particles from moving under the seepage force of the flowing water. If the flow washes out the fines the permeability increases with duration of the flow.

### Porosity or void ratio

Another factor, influencing permeability, is the porosity or void ratio. A mainly theoretical expression describing the permeability of porous media is the Kozeny-Carman equation. Including the effect of the angularity of grains, this equation reads (Lubking, 2004):

$$k = \frac{\rho_w \cdot g}{\eta_w} \cdot \frac{e^3}{1+e} \cdot \frac{1}{k_0 \cdot S_v^2 \cdot f_L} \tag{2.8}$$

in which $\eta_w$ is the dynamic viscosity of water, $g$ is the acceleration of gravity and $S_v$ is the specific grain surface. The Kozeny-Carman constant ($k_0$) is 5 and the angularity factor of Loudon ($f_L$) is between 1.1 and 1.4. Bear (1972) and Batu (1998) developed an adapted Kozeny-Carman equation relating the effect of the specific grain surface to the size of the smallest grains ($d_{10}$):

$$k = C_k \cdot \frac{g}{\nu_w} \cdot d_{10}^2 \cdot \frac{n^3}{(1-n)^2} \tag{2.9}$$

in which $C_k$ is a coefficient mainly depending on the grain size distribution and the angularity of the grains and $\nu_w$ is the kinematic viscosity. Kim and Parizek (1999) presents an approach based on the same assumption, relating the specific grain surface inversely proportional to the average grain size:

$$k = \frac{\rho_w \cdot g}{\eta_w} \cdot \frac{e^3}{1+e} \cdot \frac{d_{50}^2}{180} \tag{2.10}$$

Carrier (2003) has presented an empirical equation, developed by Amer and Awad (1999), which is partly related to the Kozeny-Carman equation:

$$k = (d_{60})^{0.60} \cdot (d_{10})^{1.73} \cdot \frac{e^3}{1+e} \tag{2.11}$$

Another empirical equation to which is often referred in Dutch engineering is an empirical equation proposed by den Adel (see van Rhee (2010)):

$$k = \frac{g}{160 \cdot \nu_w} \cdot d_{15}^2 \cdot \frac{n^3}{(1-n)^2} \tag{2.12}$$

in which $d_{15}$ is the size at which 15% of the grains is smaller. Equation (2.12) is not well known outside the Netherlands, but gives a rather accurate prediction of the permeability as function of the grain size of the smallest grains and porosity (van Rhee, 2010). The factor introducing the influence of the porosity is similar to the theoretical Kozeny-Carman equation as given in Equation 2.8. Experimental data has shown that the permeability is directly related to the factor $e^3/(1+e)$ (Lambe and Whitman, 1969), indicating that an increase of the void ratio is related to an increase of the permeability. The permeability of a rather loosely packed granular material is approximately 3 times higher than of a densely packed granular material. This shows that Equation 2.7 should be used with great care, because the effect of the porosity is not included in this equation.

#### Clay content

The permeability of sand is highly influenced by the clay content and composition of the clay particles (grain size <2 $\mu$m), also when the clay content is less than 8%. Smaller grains in between larger grains decrease the effective porosity and therefore the permeability. If clay particles are present between sand grains the permeability decreases significant. This is the result of the ability of clay particles to bind water. Due to their capacity in binding water the clay particles increase in size and fill a relative large volume in relation to (inert) quartz grains of similar size.

Foortse (2016) determined the permeability of two types of sand, mixed with different amounts of bentonite. Bentonite is a clay with a high swelling capacity, reducing the permeability when mixed with sand. Figure 2.4 shows the influence of bentonite on the permeability of sand with an average grain size ($d_{50}$) of 125 $\mu$m and 256 $\mu$m. The permeability of sand is highly reduced by the presence of bentonite, while the mixture of sand and bentonite is still behaving as a loose grained (non-cohesive) material. Direct shear tests revealed that up to 10% of added bentonite the friction characteristics of the sand types did not change in comparison with sand without bentonite. This shows that the typical behavior for sand (drained behavior) was maintained. The friction angle of 150 $\mu$m sand varied between 38° and 43° and for the sand with a $d_{50}$ of 256 $\mu$m values between 34 and 37° were measured.

The influence of clay on the permeability shows that Equations (2.7), (2.10), (2.11) and (2.12) should not be used in case a clay fraction is present in the sand. In case of the presence of clay the permeability is related to the clay content and activity of the clay, besides grain size and porosity of the sand grains. No specific empirical or theoretical relations exist in this case. Another situation appears when the voids between the sand grains are totally filled with clay. In this case the permeability reduces to the permeability of the clay itself.

### 2.3.3. Shearing: shear-strain behavior

The physical behavior of sand, subjected to shear and saturated with water, depends on its porosity. During shearing, but also during compression, the arrangement of the grains will change to enhance horizontal and vertical deformation. If sand is loosely packed (Figure 2.5a) the porosity decreases while shearing. This is called contractant behavior and results in the generation of excess pore water pressures at

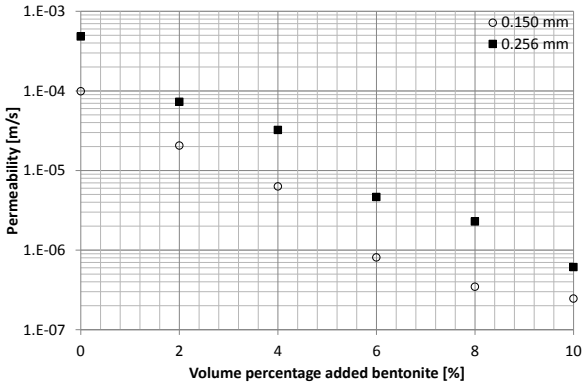


Figure 2.4: Permeability of sand mixed with different volume percentages of bentonite (Foortse, 2016)

high shear rates. Normally sand is densely packed as shown in Figure 2.5b. During shearing the grains have to move up in order to enhance horizontal displacements: the porosity increases. The increase in volume leads to a decrease of the pore water pressure in the sheared zone, introducing an inward hydraulic gradient and flow of water into the sand bed. It should be noted that the failure mode of sand, can be a combination of compression and shearing, resulting in contractant behavior and dilatancy.

In case of a sand bed saturated with water, these volume changes introduce the influence of the permeability on the shearing resistance. This was experienced during the cutting of dense packed sand under water. These experiments have revealed the effect of shear induced dilatancy (van Os, 1977) and (van Os and van Leussen, 1987), causing positive volumetric strains and pore water under pressures. These pore water under pressures increase the effective stress and thus the resisting strength of sand during shearing. The resulting pore water pressure depends on the deformation rate and permeability, showing the influence of the permeability on the strength of sand.

### Mohr Coulomb-model

The most common model to describe the failure behavior of granular and cohesive material is the Mohr Coulomb-model (Figure 2.6). The shear stress ($\tau$) at which failure occurs (Mohr Coulomb-criterion) depends on the cohesion ($C$), effective vertical stress ($\sigma'_z$) and angle of internal friction ($\phi$):

$$\tau = C + \sigma'_z \cdot tan\phi \tag{2.13}$$

in which the effective vertical stress is defined as the difference between the total vertical stress ($\sigma_z$) and pore water stress ($\sigma_u$):

$$\sigma'_z = \sigma_z - \sigma_u \tag{2.14}$$

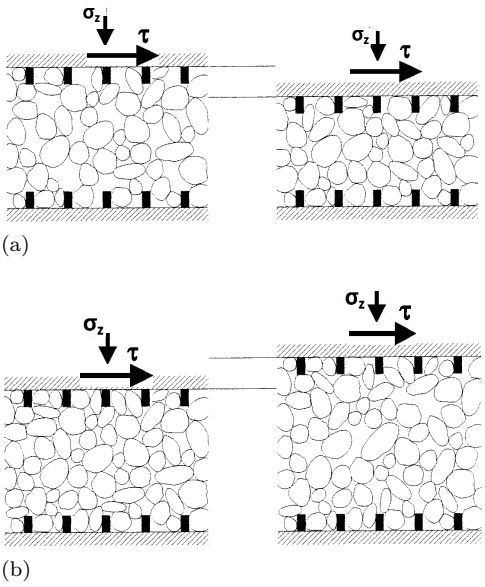


Figure 2.5: Decrease of porosity during shearing of loosely packed sand: contractant behavior (a) and increase of porosity during shearing of densely packed sand: dilatant behavior (b) (Lubking, 2004).

As long as the shear stress is below the failure criterion it is assumed elastic deformations occur. Failure occurs when the Mohr-Coulomb envelope is exceeded. This is possible with different kind of stress combinations. When failure takes place, the deformations are considered to be plastic. Increase of the vertical effective stress ($\sigma'_z$), while the horizontal effective stress ($\sigma'_x$) remains constant, results in a larger Mohr-circle. When the Mohr-circle (Figure 2.6) reaches the Mohr-Coulomb envelope failure takes place.

In case of a horizontal sand bed, the effective vertical stress is the maximum stress ($\sigma'_{max}$) in the Mohr Coulomb failure diagram (Figure 2.6), while the minimum stress ($\sigma'_{min}$) is the effective stress in horizontal direction. In case of a normally consolidated and horizontal sand bed the stress in horizontal direction is:

$$\sigma'_x = K_0 \cdot \sigma'_z = (1 - sin\phi) \cdot \sigma'_z \tag{2.15}$$

For loose sand a value for $K_0$ (lateral earth pressure coefficient) is used of 0.6 ($\phi$ = 25°), while for dense sand a value of 0.4 ($\phi$ = 35°) can be used (Lubking, 2004). The combination of Equation 2.14 and 2.13 can be used to show the influence of excess or pore water under pressures. In case the pore water pressure decreases, due to for instance dilatancy during shearing, the effective stress increases, resulting in a higher resisting shear stress at failure. Excess pore water pressures will result in a lower effective stress, hence reducing the resisting shear stress.

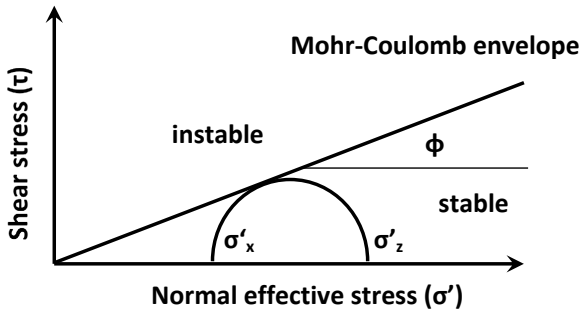


Figure 2.6: Mohr-circle determining the stable and instable stress regions

### Angle of internal friction

For granular material (sand) the cohesion is practically 0 and the angle of internal friction ranges between 25° (loose fine sand) and 45° (very dense coarse sand). Numerous empirical relations exist to determine the angle of internal friction of sand. In these relations the angle of internal friction depends mainly on the relative density. Other grain properties influencing the angle of internal friction are grain size, coefficient of uniformity and angularity. The relative density influences the effective angle of internal friction between the grains because the closer the grains are packed the higher the effective friction between the grains. Lubking (2004) has presented a relation between the angle of internal friction, relative density and coefficient of uniformity:

$$\phi = 33 - \frac{3}{C_u} + \left(15 - \frac{4}{C_u}\right) \cdot R_e \tag{2.16}$$

### Resistance to a shear stress

The effect of a horizontal shear stress on a horizontal sand bed can be determined on the basis of Equation 2.13. Due to this load a layer of thickness $h_s$ will be sheared (Figure 2.7). The thickness of the sheared layer ($h_s$) depends on the effective vertical stress increasing as function of the depth ($h$) below the surface of the sand bed:

$$\sigma'_z = h \cdot (\rho_i - \rho_w) \cdot g \tag{2.17}$$

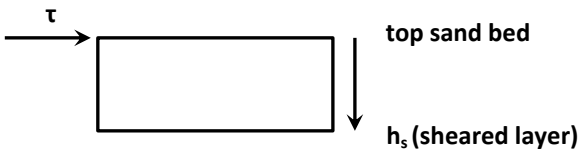


Figure 2.7: Definition sheared layer

in which $\rho_i$ is the in-situ density of the sand bed. Combining Equation (2.13) and (2.17) reveals a solution for $h_s$, assuming $c = 0$:

$$h_s = \frac{\tau}{(\rho_i - \rho_w) \cdot g \cdot tan\phi} \tag{2.18}$$

2

Resistance to a normal stress

The resistance to failure as a result of a normal stress exerted on a flat sand bed was described by Rankine (Lambe and Whitman, 1969). It is assumed that the failure zone is made up of two separate wedges (Figure 2.8a):

- active wedge I, which is pushed downward and outward;
- passive wedge II, which is pushed outward and upward.

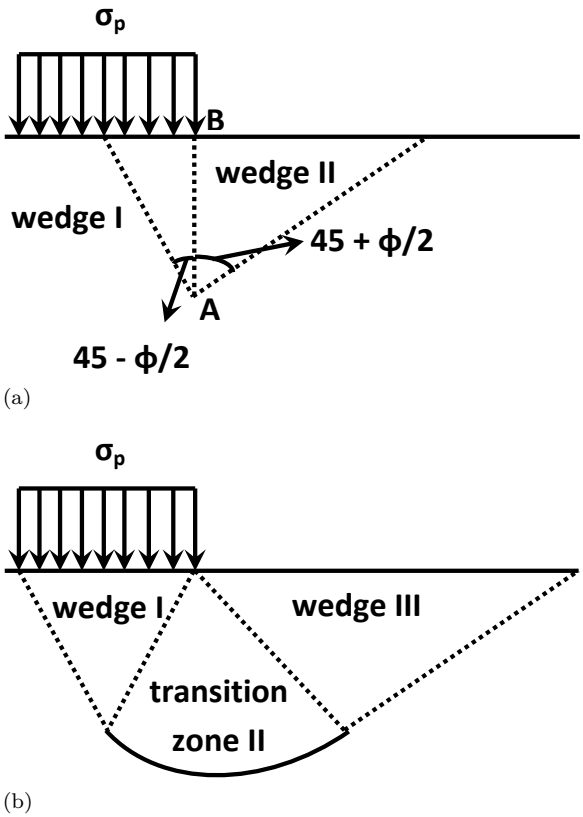


Figure 2.8: Solution of Rankine (a) and Prandtl (b)

The solution of Rankine (Figure 2.8a) underestimates the maximum resistance to a vertical strip load because the actual failure zone is curved instead of bounded by two straight lines and the shear stress along the line AB is neglected. Prandtl (1921)

developed a solution to overcome mentioned shortcomings based on two wedges (I and III) bounded with straight lines and one transition wedge (II) bounded by a logarithmic spiral (Figure 2.8b). As long as the cohesion is neglected the maximum stress at failure ($\sigma_p$) due to a normal load, with width $B$, is (Terzaghi and Peck, 1964):

$$\sigma_p = 0.5 \cdot g \cdot \rho_i \cdot B \cdot N_\gamma \tag{2.19}$$

For the solution of Rankine $N_\gamma$, bearing capacity factor, is defined as (Terzaghi and Peck, 1964):

$$N_\gamma = \frac{1}{2} \cdot \left( N_\phi^{5/2} - N_\phi^{1/2} \right) \tag{2.20}$$

in which $N_\phi$ is:

$$N_\phi = \frac{1 + sin\phi}{1 - sin\phi} \tag{2.21}$$

Verruijt (2001) gives a rather accurate approximation for $N_\gamma$ in case of spiral shaped wedges (Prandtl):

$$N_\gamma = 1.5 \cdot \left( \frac{1 + sin\phi}{1 - sin\phi} \cdot e^{\pi \cdot tan\phi} - 1 \right) \cdot tan\phi \tag{2.22}$$

The constant (0.5) in Equation 2.19 is valid for a vertical strip load. In case of a circular load this constant is 0.3, while $B$ is in this case the diameter. For a square load a value of 0.425 should be be applied (Lambe and Whitman, 1969). In this case $B$ is the width of the square load.

### 2.3.4. Shearing: stress-strain rate behavior

Besides the stress-strain behavior, sand exhibits a stress-strain rate behavior at different concentrations and strain-rates. Widely known are the experiments of Bagnold (1954) who determined the shear stress of a gravity free dispersion with grains in a Newtonian fluid. During these experiments solid spherical grains were sheared in a Newtonian fluid of varying viscosity. Segregation was avoided by balancing the density of the grains against the density of the fluid. The concentration ($c$) ranged between 0.13 and 0.62. The maximum concentration was close to the maximum concentration of a dispersion of grains in water. The dispersion was sheared in the annular space between two concentric drums. Despite the fact that Hunt et al. (2002) have doubted the validity of the results of the experiments, the experiments of Bagnold (1954) have been cited extensively. Hunt et al. (2002) have stated that the measurements of Bagnold (1954) were influenced by the design of the experimental apparatus, causing vortices influencing the measured shear stress.

Bagnold (1956) has defined the shear resistance ($\tau_{tot}$) of a sheared grain dispersion as the sum of the static shear stress ($\tau_s$) and the dynamic shear stress ($\tau'$):

$$\tau_{tot} = \tau_s + \tau' \tag{2.23}$$

The static shear stress can be calculated on the basis of the effective stress concept and Mohr-Coulomb model (Section 2.3.3). The dynamic shear stress depends on the type of regime by which the grains increase the effective viscosity of the mixture (Bagnold, 1956):

- viscous regime: as a result of presence of a velocity gradient ($du/dz$) water must be pressed through the openings between the grains;
- grain-inertia: at high concentrations and shear rates the shear stress arises from the diffusion of tangential and normal components of grain momenta created at the collisions.

The results of the experiments of Bagnold (1954) have revealed that the shear and normal stress of a grain dispersion of different volume concentrations ($c$) and velocity gradients ($du/dz$) are related to the mentioned regimes. The shear and normal stress are related to the linear concentration ($\lambda$). Bagnold (1954) has supposed a mass of rigid spheres of uniform diameter ($d$) dispersed uniformly so that the distance between the centers is $b \cdot d$. With a resulting distance between the spheres ($s_p$) this leads to:

$$b \cdot d = s_p + d \tag{2.24}$$

This can be simplified to:

$$b = \frac{s}{d} + 1 = \frac{1}{\lambda} + 1 \tag{2.25}$$

in which the linear concentration ($\lambda$) is defined as the quotient of the average distance between rigid spheres of uniform diameter and the diameter of these spheres. Rewriting Equation (2.25) shows that the linear concentration approaches infinity in case the distance between the centers of the spheres is equal to $1 \cdot d$, representing a mass of closely packed rigid spheres comparable to the maximum concentration of a suspension ($c_{max}$):

$$\lambda = \frac{1}{b - 1} \tag{2.26}$$

In case the distance between the center of the spheres approaches infinity, the concentration approaches zero and the linear concentration is equal to 0. The linear concentration can be related to the volume concentration of the suspension and maximum possible volume concentration as well as the minimum porosity and in-situ porosity by:

$$\lambda = \frac{1}{\sqrt[3]{\frac{c_{max}}{c}} - 1} = \frac{1}{\sqrt[3]{\frac{1-n_{min}}{1-n}} - 1} \tag{2.27}$$

The maximum possible volume concentration ($c_{max}$) for perfectly piled uniform spheres is 0.74.

### VISCOUS REGIME

In the viscous regime the effects of the fluid viscosity dominate, including the influence of the grains on the viscosity. For this region Bagnold (1954) derived two empirical equations for the shear stress in the viscous regime ($\tau_v^{'}$):

$$\tau_v^{'} = 2.25 \cdot \lambda^{\frac{3}{2}} \cdot \eta_w \cdot \frac{du}{dz} \tag{2.28}$$

$$\tau_v^{'} = (1+\lambda) \cdot \left(1 + \frac{1}{2} \cdot \lambda\right) \cdot \eta_w \cdot \frac{du}{dz} \tag{2.29}$$

in which $\eta_w$ is the dynamic viscosity of water. The difference between both equations is negligible within the range of values for $\lambda$ (1.3 to 17) at which the shear tests were executed by Bagnold (1954). These values correspond to a density of a dispersion of water and sand between approximately 1200 and 1900 kg/m$^3$. This means that Equations (2.28) and (2.29) can be used for a concentration of between approximately 0.1 and 0.6 (assuming a $c_{max}$ of 0.7), the last being approximately 20% of the maximum concentration. The maximum difference between both equations is 20%. Bagnold (1954) has considered Equation (2.29) as the most accurate, also because this equation reduces to $\eta_w \cdot du/dz$ when $\lambda$ is 0 (grainless fluid):

$$\tau_v^{'} = \eta_w \cdot \frac{du}{dz} \tag{2.30}$$

### GRAIN-INERTIA REGIME

In the grain-inertia regime the failure behavior of the dispersion depends on the velocity gradient and collisions of the grains. The shear stress in the grain-inertia regime arises from the diffusion of tangential and normal components of grain momenta created at the collisions. For this region Bagnold (1954) found the following empirical relation for the shear stress in the grain-inertia regime ($\tau_g^{'}$):

$$\tau_g^{'} = 0.013 \cdot \rho_s \cdot (\lambda \cdot d)^2 \cdot \left(\frac{du}{dz}\right)^2 \tag{2.31}$$

It should be noted that at high concentrations ($\lambda$ approaches to $\infty$) the resulting shear stress, when using Equation (2.31), approaches to $\infty$. However, this shear stress is limited by the maximum shear stress at which a layer starts shearing, see Equation (2.18).

### TRANSITION

The transition between the viscous and grain-inertia regime is based on the ratio between the grain-inertia and viscous stresses. This is defined as the Bagnold number $N$ (Bagnold, 1954):

$$N = \frac{\text{inertia stress}}{\text{viscous stress}} = \frac{\rho_s \cdot (\lambda \cdot d)^2 \cdot \left(\frac{du}{dz}\right)^2}{\lambda^{\frac{3}{2}} \cdot \eta_w \cdot \frac{du}{dz}} = \frac{\sqrt{\lambda} \cdot \rho_s \cdot d^2 \cdot \frac{du}{dz}}{\eta_w} \tag{2.32}$$

Bagnold (1954) has considered that the transition from grain-inertia to viscous conditions in terms of N ranges from approximately 40 to 450. Below N = 40 the shear stress is dominated by the viscous shear stress, while at values of N of more than 450 the shear stress is dominated by the grain-inertia forces. Equation (2.32) shows that the transition is determined by the concentration and/or porosity and grain size of the sand as well as the strain rate.

### Comparison models of apparent viscosity

Bagnold (1954) has considered Equation (2.29) as the most accurate for the calculation of the dynamic viscosity of concentrated suspensions ($\eta_{sus}$) of (spherical) grains. However, Equation (2.28) as well as (2.29) differ considerably from other empirical models relating the relative viscosity ($\eta_{sus}/\eta_w$) to the concentration, as the model of Einstein (Einstein, 1906) and (Einstein, 1911):

$$\frac{\eta_{sus}}{\eta_w} = 1 + 2.5 \cdot c \tag{2.33}$$

and other developed empirical relations of Thomas (1965) and Ishii and Mishima (1984). The empirical relation of Thomas (1965) reads:

$$\frac{\eta_{sus}}{\eta_w} = 1 + 2.5 \cdot c + 10.05 \cdot c^2 + 0.00273 \cdot e^{16.6 \cdot c} \tag{2.34}$$

while Ishii and Mishima (1984) has determined the following empirical relation:

$$\frac{\eta_{sus}}{\eta_w} = \left(1 - \frac{c}{0.62}\right)^{-1.55} \tag{2.35}$$

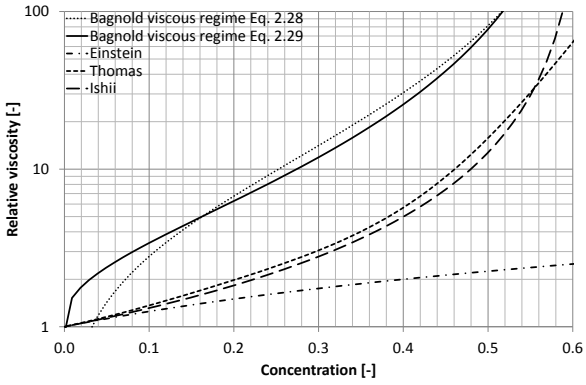


Figure 2.9: Relative viscosity of suspension of particles in a fluid in case of the viscous regime as determined by Bagnold (1954): Equation (2.28) and (2.29) compared with Equation (2.33), (2.34) and (2.35), with $c_{max} = 0.65$

Normal stress

Bagnold (1954) measured also the normal stress. The normal stress ($\sigma_n$) reaches values of about $1.3 \cdot \tau'$ in the viscous regime, while in the transition to the grain-inertia region this value increases to $3 \cdot \tau'$, which is also valid for the grain-inertia region. The validity of these results could be questioned because this means that the effective friction angle at low concentrations (viscous regime) is higher than in the grain-inertia regime (37° versus 18°).

## 2.4. Conclusions

The behavior of a sand bed is determined by the properties of single grains and bulk properties of the assemblage of the grains. A bulk property, permeability, is highly influenced by the size of the grains. The resistance of a sand bed to shear or/and a vertical load is influenced by the angle of internal friction. This bulk property is influenced by the grain size distribution and angularity of the grains, but is also highly affected by a bulk property: the density. The density does not only affects the angle of internal friction. The behavior during shearing, at constant shear rate, is also influenced by the density of the sand bed. Shearing and/or compression introduces volume changes, influencing the effective stress between the grains and the resistance to shear or compression. In case of a sand bed, which is saturated with water, this introduces the effect of the permeability and density on the resistance to shear or compression. Little knowledge exists regarding the shear-strain rate behavior of concentrated suspensions.

Widely known are the experiments of Bagnold (1954). Based on these experiments two shearing regimes are distinguished. At low concentrations of the suspension and low shear-strain rates, the shear stress is dominated by viscous shear stresses, while at higher concentrations and shear-strain rates the shear stress is considered to be dominated by grain-inertia forces. However, comparison of the empirical relations for the shear stresses in the viscous regime, as derived on the basis of the experiments of Bagnold (1954), with empirical relations for the apparent viscosity of concentrated suspension show a considerable difference (see Figure 2.9).

Besides, the conclusion that the normal stress reaches values of about $1.3 \cdot \tau'$ in the viscous regime, while in the grain-inertia regime this value increases to $3 \cdot \tau'$, is questionable. This should mean that the effective friction in the viscous regime is higher than in the grain-inertia regime, while in the viscous regime the concentration is lower than in the grain-inertia regime. Also the effective friction angle in the viscous regime is very high: 37°. This value is comparable to dense compacted sand, which is not the case in the viscous regime. The results of the 1954 suspension experiments of Bagnold (1954) have been questioned by Hunt et al. (2002). They have concluded that these experiments were influenced by some secondary circulation and arching at high concentrations, having a significant effect on the torque measurements.

# 3

# Behavior flow over sand bed

## 3.1. Introduction

The behavior of sand is determined by the behavior of single grains and their bulk properties, as described in the previous Section. Not only the bulk properties of sand and the properties of its single grains influence the erosion process, but also the behavior of the flow over a sand bed. The first step in the comprehension of the behavior of a flow over a sand bed is the description of the behavior of a flow along and close to a smooth and rough surface (Section 3.2). At flow velocities of more than 1.0 m/s the Reynolds number ($Re$) is in case of hydraulic engineering much larger than 2300, meaning that the flow conditions are determined by the turbulent behavior of the flow. Turbulence influences the forces along a rough surface consisting of (eroding) grains. The shear stress along the surface and parallel to the flow is determined by the behavior of the flow (Reynolds number), velocity distribution and the properties (roughness) of the surface.

The effective bed shear stress, exerted by a flow over a sand bed, varies in time and direction as a result of the turbulent behavior of a flow (Section 3.3). Turbulence exhibits specific flow patterns (structure) influencing the flow velocity and normal stress exerted on the top of the bed. Turbulent eddies cause large scale turbulent wall stress fluctuations acting in perpendicular direction to the flow on the bed.

In case of hardly any pick-up the effective bed roughness or friction is related to the drag and lift forces a flow exerts on single grains with varying protrusion out of the sand bed (Section 3.4). Assuming a logarithmic velocity profile, the bed shear stress is related to the effective bed roughness, which is assumed to be related to the largest size of the grains in the bed. At mobile-bed conditions, approximately at a flow velocity of more than 1 m/s, roughness physically does not exist. The friction along the bed is determined by the flow velocity or Reynolds number and energy dissipation as a result of grain-grain and grain-fluid interactions. The bed shear stress is not determined by the roughness of the bottom (size of the grains).

This effect has been intensively investigated during sheet flow conditions (Section 3.5). Dohmen-Janssen (1999) stated that during sheet flow conditions the average

bed shear stress is a measure for the energy dissipation close to the sand bed, due to grain-grain and grain-fluid interaction. Beside this effect on the bed shear stress, the shear stress is influenced by the changing flow velocity profile close to the bed: from logarithmic to linear. Explicit equations for the determination of the bed shear stress during these flow conditions do not exist. These equations are based on a apparent bed roughness having no physical meaning.

Section 3.6 discusses the main findings regarding the (effective) bed roughness, forces on separate grains, effect of turbulence and sheet flow.



## 3.2. Boundary layer

The concept of the boundary layer implies that a flow with a high Reynolds number ($Re > 2300$) can be divided into two unequally large regions (Schlichting and Gersten, 1999). In the bulk of the flow region, the viscosity can be neglected and the flow is not influenced by friction: the inviscid outer flow. The second region is the very thin boundary layer ($\delta$) at the wall where the viscosity must be taken into account. As a result the flow velocities decrease close to the bottom (van Rijn, 2008). Within the boundary layer the flow can be viscous and/or turbulent.

### 3.2.1. Development boundary layer

Generally, the thickness of the boundary layer is defined as the distance from the boundary surface to the point where $u\,(z) = 0.99 \cdot u_{max}$, with $u(z)$ = time-averaged horizontal flow velocity at a level $z$ above the surface and $u_{max}$ = time-averaged maximum outer flow velocity. The generation of a boundary layer can be demonstrated by considering a flow along a flat smooth plane of finite length. Large shear stresses are generated at the plate surface, when the fluid reaches the beginning of the plate. The fluid velocity at the plate surface is zero and the velocity of the fluid above is retarded because of the action of viscous shear in the fluid. For some longitudinal distance, the flow within the boundary layer is laminar due to the dominating viscous shear stresses (viscous layer). Downstream of the viscous layer, the flow will become unstable and eventually will become turbulent (Figure 3.1). At this location the viscous boundary layer starts decreasing in thickness.

The boundary layer thickness increases in the flow direction along a surface. The transition from laminar to turbulent flow depends on the roughness of the surface and the velocity and turbulence level of the approaching flow. The boundary layer is laminar close to the leading edge and becomes turbulent further downstream. The thickness of the viscous boundary layer depends on the length of the flow along a flat plate, maximum flow velocity and kinematic viscosity (Schlichting and Gersten, 1999):

$$\delta\,(x) = 5 \cdot \sqrt{\frac{\nu_w \cdot x}{u_{max}}} \tag{3.1}$$

The dimensionless viscous boundary layer thickness related to the total length ($l$) along the surface is:

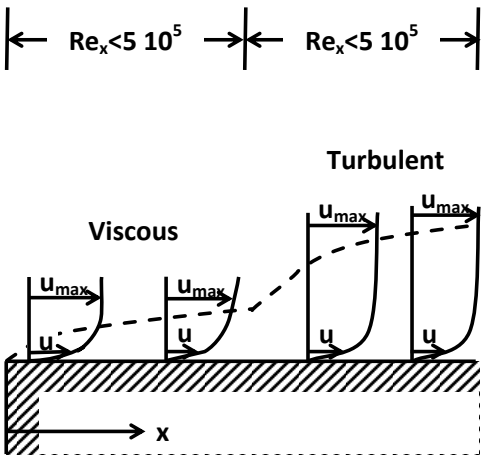


Figure 3.1: Generation of a boundary layer with $u_e$ is $u_{max}$ (van Rijn, 2008)

$$\frac{\delta(x)}{l} = \frac{5}{\sqrt{Re}} \cdot \sqrt{\frac{x}{l}} \tag{3.2}$$

in which $Re = u_{max} \cdot l/\nu_w$ is the Reynolds number related to length $l$. A larger Reynolds number leads to a smaller thickness of the viscous boundary layer. In the limiting case, $Re \to \infty$, the viscous boundary layer vanishes. After a certain distance the boundary layer becomes turbulent. The transition from viscous to turbulent flow is most noticeable by a large increase in the boundary layer thickness (Figure 3.1) and wall shear stress. The critical Reynolds number ($Re_{x,crit}$) related to the distance of the transition point is about:

$$Re_{x,crit} = \left(\frac{u \cdot x}{\nu_w}\right)_{crit} = 5 \cdot 10^5 \tag{3.3}$$

Below a value of $Re_{x,crit}$ of $2 \cdot 10^5$ to $5 \cdot 10^5$ the flow in the boundary layer is laminar (Figure 3.2). The thickness of the turbulent boundary layer is (Schlichting and Gersten, 1999):

$$\frac{\delta \cdot u_{max}}{\nu_w} = 0.14 \cdot \frac{Re_x}{lnRe_x} \cdot G(lnRe_x) \tag{3.4}$$

in which $Re_x$ is the Reynolds number as function of $x$. The function G(ln $Re_x$) depends weakly on ln ($Re_x$). It has a limiting value of 1 for ln $Re_x \to \infty$. In the region of $10^5 < Re_x < 10^6$ G $\approx 1.5$. The turbulent boundary layer thickness decreases at a given x with increasing Reynolds number. Figure 3.2 shows the transition between the viscous and turbulent boundary layer and gives a graphic presentation of Equations (3.2) to (3.4).

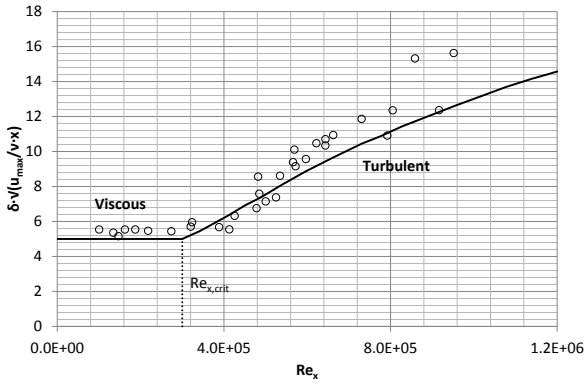


Figure 3.2: Dependence of the boundary layer thickness on the distance along a surface at zero incidence (Schlichting and Gersten, 1999)

### 3.2.2. Viscous or turbulent boundary layer

In viscous boundary layers, the boundary layer is the region in the flow field affected by the viscosity (Schlichting and Gersten, 1999). The flow is laminar and the friction is determined by the viscosity. Above this layer the turbulent logarithmic boundary layer exists. The friction in this layer is determined by the turbulent fluctuating motion and is unaffected by the viscosity of the fluid. These layers are separated by a transition layer (Figure 3.3).

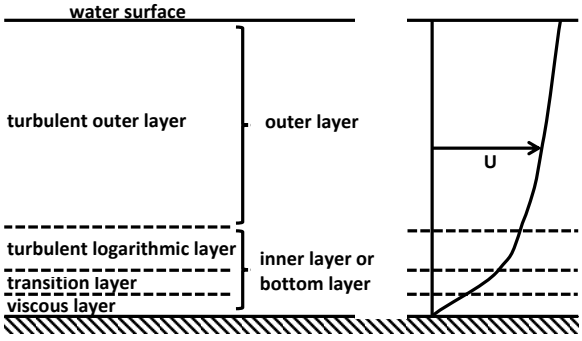


Figure 3.3: Viscous and turbulent boundary layers for a smooth bottom with $u_\infty = u_{max}$ (van Rijn, 2008)

A sand bed can be considered as a rough bottom of which the roughness elements (sand grains) influence the velocity distribution close to the bottom, because the roughness elements generate eddies with a size of the order of the height of the roughness elements affecting the turbulent structure and hence the velocities close to the bottom. The type of flow regime depends on the ratio of the Nikuradse roughness ($k_s$) and the length scale of the viscous boundary layer ($\nu_w/u_*$) according

to (van Rijn, 2008):

- hydraulically smooth flow, for $u_* \cdot k_s/\nu_w \leq 5$ the roughness elements are much smaller than the thickness of the viscous boundary layer. The velocity distribution is determined by the viscous boundary layer;
- hydraulically transitional flow, for $5 < u_* \cdot k_s/\nu_w < 70$ the velocity distribution is affected by the viscosity as well as by the bottom roughness;
- hydraulically rough flow, for $u_* \cdot k_s/\nu_w \geq 70$ the roughness elements have larger dimensions than the thickness of the viscous boundary layer and therefore determine the velocity distribution.



in which the bed shear velocity ($u_*$) is defined as:

$$u_* = \sqrt{\frac{\tau_b}{\rho_w}} \tag{3.5}$$

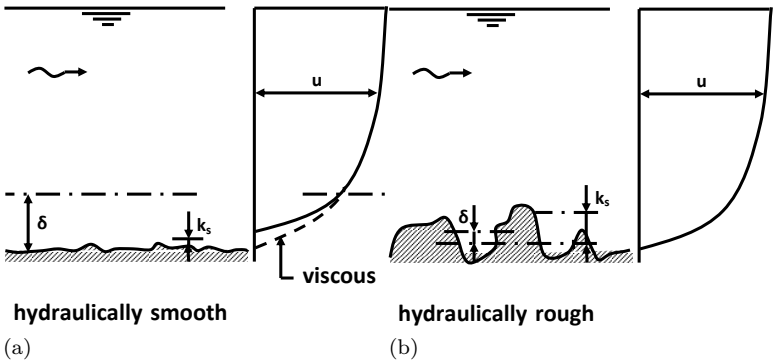


Figure 3.4: Hydraulically smooth (a) and rough (b) flow (van Rijn, 2008)

in which $\tau_b$ is the bed or boundary shear stress.

### Hydraulically smooth flow

As long as the flow is considered as a hydraulically smooth flow the velocity distribution at the bottom is determined by the viscous boundary layer (Figure 3.4). The velocity distribution is linear and this distribution intersects the logarithmic velocity distribution at $u_* \cdot z/\nu_w = 11.6$. The thickness of the fully viscous sublayer is defined at the level where the velocity distributions starts to deviate from the linear velocity distribution: $5 \cdot \nu_w/u_*$ (Figure 3.5). The level at which the flow velocity is zero ($z_0$) is defined as: $0.11 \cdot \nu_w/u_*$.

### Hydraulically rough flow

Within the scope of this thesis the roughness elements are larger than the thickness of the viscous boundary layer. The flow can be defined as a hydraulic rough flow. In this case the velocity distribution in the turbulent boundary layer is determined by the turbulent logarithmic layer. The velocity distribution is logarithmic in this layer. The logarithmic velocity distribution is valid from values of $u_* \cdot z/\nu_w > 30$ (approximately $150 \cdot z_0$) and valid up to $z \approx 0.2 \cdot h$ and yields for hydraulically rough flow:

$$\frac{u(z)}{u_*} = \frac{1}{\kappa} \cdot ln\left(\frac{z}{k_s}\right) + 8.5 = \frac{1}{\kappa} \cdot ln\left(\frac{30 \cdot z}{k_s}\right) \tag{3.6}$$

in which $\kappa$ = constant of von Karman (0.4). Above $z \approx 0.2 \cdot h_f$ ($h_f$ is flow depth) the logarithmic distribution can be used as an approach for the velocity distribution.

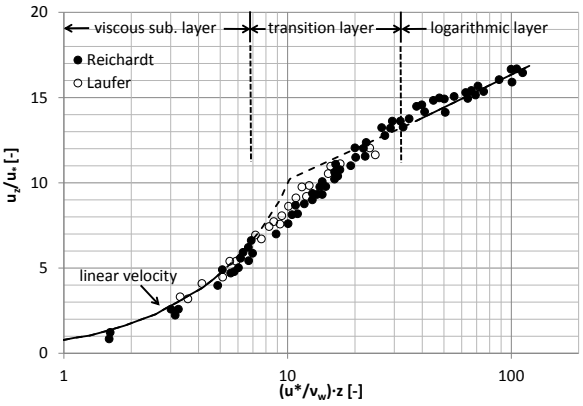


Figure 3.5: Velocity distribution in a steady uniform flow over a smooth bottom (van Rijn, 2008)

The level at which the velocity is zero ($z_0$) depends in the hydraulically rough regime on the Nikuradse roughness (Figure 3.6):

$$z_0 = 0.033 \cdot k_s \quad for \quad \frac{u_* \cdot k_s}{\nu_w} \leq 70 \tag{3.7}$$

Equation (3.7) is based on measurements of a flow over sand grains glued to a flat bed, while for a bed with randomly placed stones, the value can increase up to a value of $z_0 \approx k_s/10$. This zero-velocity level is a computational parameter without any physical meaning and can be determined by smoothing out the roughness elements (spheres with diameter $d$). This delivers a plane at a level of $0.74 \cdot d$ above the bottom of the spheres. The zero-velocity level can also be determined by plotting the values of $(z - z_0)/z_0$ on semi-logarithmic scale and vary $z_0$ until the best fit is obtained. This method yields for $z_0$ (below the top of the grains) values of $\approx 0.25 \cdot d$ for grains of sand and gravel size. Hofland (2005) has concluded that this theoretical

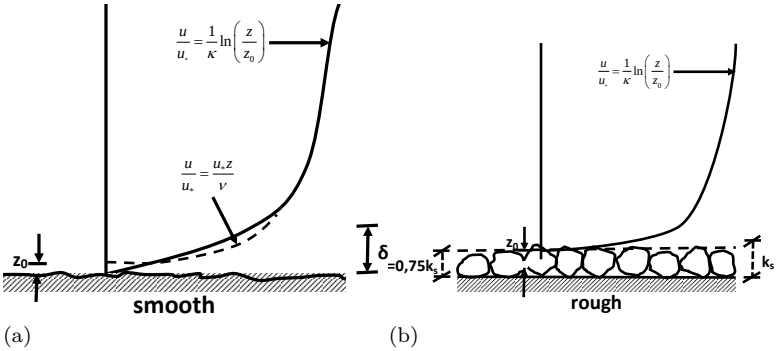


Figure 3.6: Velocity distribution and level of zero-velocity in hydraulically smooth (a) and rough (b) flow (van Rijn, 2008)

level varies from $0.35 \cdot d$ to $0.15 \cdot d$ under the top of the roughness elements (Figure 3.7).

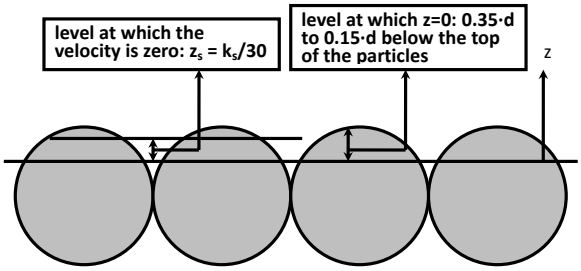


Figure 3.7: Definition of zero-velocity level and level at which $z = 0$

## 3.3. TURBULENCE

Flow velocities fluctuating in all directions characterize turbulence (Section 3.3.1). It exhibits specific flow patterns (structures) influencing the flow velocity and normal stress, exerted by the flow on the top of the bed or surface (Section 3.3.2). This flow pattern leads to fluctuations of the normal stress on the bed, which are caused by turbulent eddies (Section 3.3.3), with a length scale as described in Section 3.3.4.

### 3.3.1. CHARACTERISTICS

A typical phenomenon of a turbulent flow is the fluctuating character of the velocity at a location (Figure 3.8). Reynolds has proposed to represent the instantaneous velocities $\hat{u}$, $\hat{v}$ and $\hat{w}$ as (van Rijn, 2008):

$$\begin{aligned} \hat{u} &= u + u' \\ \hat{v} &= v + v' \\ \hat{w} &= w + w' \end{aligned} \tag{3.8}$$

in which $u$, $v$ and $w$ are respectively the time-averaged local horizontal, transverse and vertical flow velocity, while $u'$, $v'$ and $w'$ are respectively the deviation of the horizontal, transverse and vertical flow velocity from the time-averaged flow velocity as function of time.



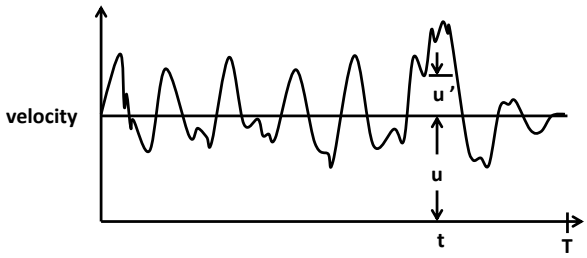


Figure 3.8: Variation of instantaneous velocity in time (van Rijn, 2008)

The turbulence intensity in a point is a measure of the strength or intensity of the velocity fluctuations in that point and is defined as the root-mean-square (rms) value of the velocity fluctuations. Applying this definition, the turbulence intensity is the standard deviation ($\sigma_{u,v,w}$) of the velocity distribution around the time-averaged (mean) flow velocity:

$$\sigma_{u,v,w} = \sqrt{\frac{\int u', v', w' dt}{t}} \tag{3.9}$$

in which $t$ is the time. Nezu and Nakagawa (1993) have given an expression for the turbulent kinetic energy ($k_e$) at a location:

$$k_e = 0.5 \cdot \left[\sigma_u^2 + \sigma_v^2 + \sigma_w^2\right] \tag{3.10}$$

The standard deviation of the velocity components is (Hofland, 2005):

$$\frac{\sigma\left(u_i\right)}{u_*} \approx \alpha_i \cdot e^{-z/h_f} \tag{3.11}$$

The values for the empirical factor $\alpha_i$ are: $\alpha_u = 2.30$, $\alpha_v = 1.27$ and $\alpha_w = 1.67$. The flow near a rough bed is more isotropic than close to a smooth bed (Hofland, 2005). The peak value of $\sigma\left(u\right)/u_*$ is about 2.8 for a smooth bed compared to 2.0 for a rough bed. Outside the boundary sublayer most turbulence statistics are rather similar for smooth and rough beds (wall similarity).

### 3.3.2. Structure

Whether the flow is turbulent or laminar depends on the magnitude of the Reynolds number (Schlichting and Gersten, 1999). The Reynolds number is, in essence, a ratio between the inertial and viscous forces. When the Reynolds number is low, the viscous forces will dampen out instabilities introduced into the laminar sublayer and the flow will remain laminar. At high Reynolds numbers the effects of the viscous forces are negligible to the effects of the inertial forces. The viscous forces can no longer dampen the effects of the instability in the viscous sublayer. The inertial forces therefore overcome the viscous forces and the viscous sublayer becomes unstable.



Turbulent flows are highly variable and chaotic. However, certain similar flow patterns can be observed repeatedly, the so-called coherent structures (Kline et al., 1967). Figure 3.9 shows the process in which turbulence and fluctuating normal stresses are generated at the boundary due to instabilities in the viscous sublayer (Annandale, 2006). Starting with a stable laminar sublayer (1), instabilities will occur in the viscous sublayer forming an undulating sublayer surface (2). When the Reynolds number is low the viscous forces will dampen the instabilities. If the Reynolds number is high enough the instabilities will grow due to the greater inertial forces leading to the formation of hairpin vortices (3).

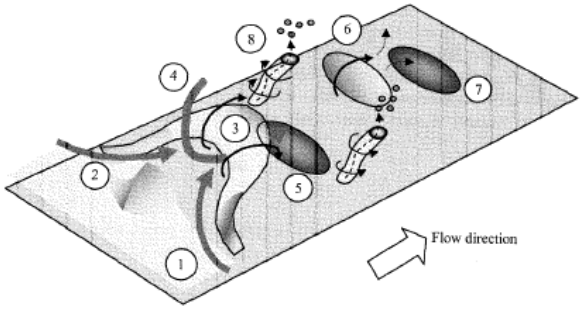


Figure 3.9: Description of turbulence along a boundary (Annandale, 2006)

The apex of the hairpin vortices are lifted upwards, creating a space between them and the boundary. As a result water will flow in from behind and above, which happens at large velocities: high velocity sweeps (4). These high velocity sweeps cause impact zones with high normal stresses on the boundary (5). As the hairpin vortex develops further, the central apex breaks loose (6). This results in eddies moving in all directions. If an eddy collides with the boundary, it results in zones with a low normal stress (7).

Between the legs of the hairpin, which forms two smaller counter-rotating, stream wise vortices near the wall, elongated low momentum streaks (low-velocity streaks) are formed (8), with a typical spanwise spacing for a smooth wall of $\lambda_z \approx 100 \cdot \nu_w / u_*$ (Hofland, 2005). This process has a smaller scale than for a rough bed consisting of sand. If parts of the viscous sublayer still exist, their downstream ends will attach

to the top of that layer. These vortices are characterized by low normal stresses due to the suction within the vortices, moving sediment from the bed and spew it out into the flow above. These effects lead to relative strong fluctuations of the normal stress on the boundary.

Yue et al. (2007) used a quadrant analysis to describe the different events during turbulence (Figure 3.10). The events in quadrant 2 and 4 are usually called ejections and sweeps and both are involved in turbulence near-wall bursting. Sweeps, having a downward flow velocity, are seen to be the largest contributor to the Reynolds stress near rough walls (Hofland, 2005).

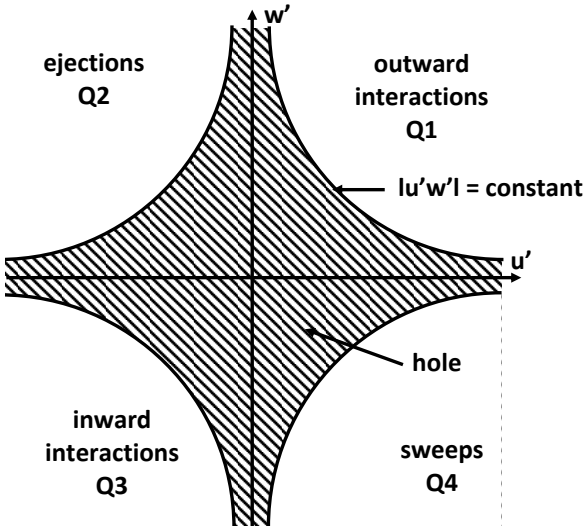


Figure 3.10: Quadrant events (Yue et al., 2007)

Figure 3.11 shows hairpin vortices, originating from the bed, along straight lines forming hairpin vortex packages. These structures were measured in gravel-bed rivers with Reynolds numbers of approximately 140.000. The large scale wedge like flow structures with either increased or decreased velocity were present over most of the depth, with a front tilted in stream wise direction with an average angle of 15° near the bed and 40° towards the surface (Buffin-Bélanger et al., 2000).

Tomkins (2001) measured hairpin vortex packages over a rough wall with boundary particle Reynolds numbers ($Re_p = (u_* \cdot d)/\nu_w$) between 200 and 400. The packages had upstream slopes of approximately 10 to 20°. The maximum length scale in the stream wise correlation was $0.6 \cdot \delta$. Grass and Mansour-Tehrani (1996) concluded that the spanwise spacing of these structures near rough walls is $\lambda_z \approx 100 \cdot \nu_t/u_*$ in which $\nu_t$ represents the turbulent viscosity.

### 3.3.3. Turbulent normal wall stress

Stress fluctuations caused by turbulent vortices can contribute considerably to the forces that initiate the motion of grains. These are known as turbulent normal wall

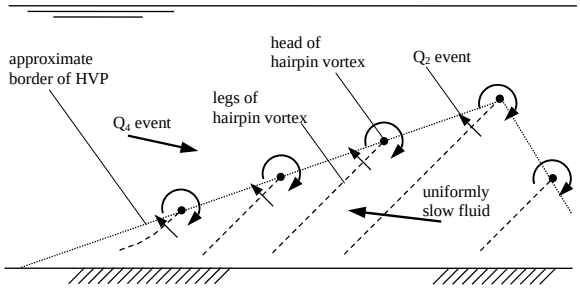


Figure 3.11: Model of hairpin vortex package (Hofland, 2005)

stresses. According to Hofland (2005) only one author presented measurements of turbulent wall stresses on a rough wall: Blake (1970). The scaling and shape of the spectrum appeared to be similar for smooth and rough walls. However, the length scale of the high frequency part of the rough wall spectrum is the roughness height instead of the viscous length scale ($\nu/u_*$).

Doligalski et al. (1994) have illustrated the turbulent wall stresses by a rectilinear model vortex in a uniform potential flow over a surface (Figure 3.12), which can be seen as a rough approximation of a vortex in a turbulent flow. Doligalski et al. (1994) have placed a point vortex with strength (circulation) $\omega$ in a uniform flow with velocity $U_0$, inducing a velocity $\omega/r$ at distance $r$ from the vortex. The convection rate ($U_c$) of the vortex is $U_0 - \omega/(2 \cdot a)$, in which $a$ is the distance of the vortex from the wall. In a frame of reference moving with the vortex, the resulting flow is stationary, and the normal wall stress can be determined using Bernoulli's law, $p' = 1/2 \cdot \rho_w \cdot \hat{w}^2$, yielding:

$$p' = \rho_w \cdot \frac{\kappa^2}{a^2} \cdot \frac{X^2 - 1}{(X^2 + 1)^2} \tag{3.12}$$

in which $\hat{w}$ is the flow velocity in vertical direction close to the wall, $x$ is the distance along the wall and $X = x/a$. The resulting stress gradient creates a net force on a stone placed in a bed. Hofland (2005) has shown that the stress between the dashed lines is higher on the upstream side (left) than on the downstream side, creating an increased horizontal force component in relation to the drag forces as a result of the average flow velocity (Figure 3.12).

However, according to Blake (1970) the turbulent normal wall stress ($p'$) for both smooth and rough walls are related to the wall shear stress ($\tau_w$). The root mean square stress is approximately:

$$\sqrt{p'^2} = 3.4 \cdot \tau_w \tag{3.13}$$

Farabee and Casaralla (1991) investigated the turbulent normal wall stress beneath a turbulent boundary layer in a wind tunnel. For boundary layer Reynolds numbers ($Re_\delta$) of less than 333 the normal wall stress can be determined according to:

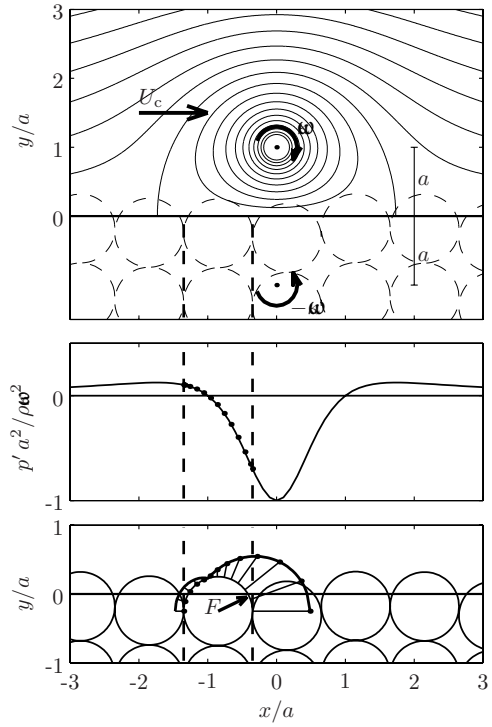


Figure 3.12: Streamlines, turbulent normal wall stress and stress field on bottom (Doligalski et al., 1994), as illustrated by (Hofland, 2005)

$$\sigma\left(\frac{p'^2}{\tau_w^2}\right) = 6.5 \tag{3.14}$$

and for a boundary layer Reynolds number of more than 333 the turbulent normal wall stress depends on this Reynolds number:

$$\sigma\left(\frac{p'^2}{\tau_w^2}\right) = 6.5 + 1.86 \cdot ln\left(Re_\delta/333\right) \tag{3.15}$$

in which $Re_\delta$ is defined as: $\frac{\delta \cdot u_*}{\nu_w}$. For boundary layer Reynolds numbers of less than 333 the ratio between the turbulent wall stress and wall shear stress is about 2 (Figure 3.13).

It should be considered that turbulence does not appear in one specific wave length and frequency. It appears in a spectrum. The maximum fluctuation of the turbulent wall stress is three to five times the standard deviation (Hofland, 2005).

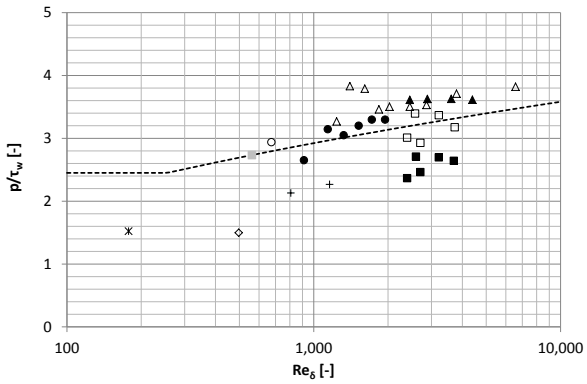


Figure 3.13: Variation of the turbulent normal wall stress (RMS) as function of boundary layer Reynolds number (Farabee and Casaralla, 1991)



### 3.3.4. Length scale of turbulence

Besides the value of the turbulent normal wall stress the horizontal length scale of the turbulence will influence the forces on a flat bed. Figure 3.14 shows a simplified flow structure according to Hofland (2005). This was used to obtain a relation between the computed parameters at a certain elevation and the (extreme) velocities that are subsequently caused near the bed.

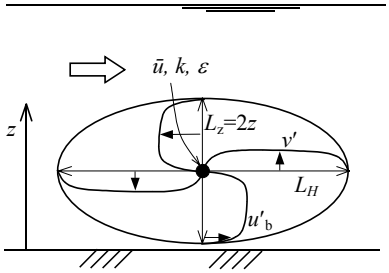


Figure 3.14: Model of large scale vortice (Hofland, 2005)

The model of large scale vortices is based on the assumption of large scale vertical velocity fluctuations at height ($z$) above the bed which are proportional to $\sqrt{k}$ ($k$ = turbulent kinetic energy) with a horizontal length scale $L_H$. The rolling structure is assumed to have a vertical size equal to $2 \cdot z$. The conservation of mass ($z \cdot \hat{u}'_b \approx 0.5 \cdot L_H \cdot \hat{w}$) leads to the following approximate relation for the near-bed horizontal flow velocity ($\hat{u}_b$):

$$\hat{u}_b \propto \frac{L_H}{z} \cdot \sqrt{k} \tag{3.16}$$

As the structure also transports the mean momentum to the bed, Hofland (2005)

has posed that the following velocity estimate can be used:

$$\hat{u}_b \propto \frac{L_H}{z} \cdot \left(u + \alpha \cdot \sqrt{k}\right) \tag{3.17}$$

in which $u+\alpha \cdot \sqrt{k}$ is an estimate of the temporal maximum of the local velocity, consisting of the mean velocity plus a few times the standard deviation, as expressed in the term $\alpha \cdot \sqrt{k}$, in which $\alpha$ is a calibration factor. Jongeling et al. (2003) found for $\alpha$ a value of 6.



A measure for the length scale of the turbulence ($L_H$) is the mixing scale $L_m$ according to the Bakhmetev distribution. This scale is not dependent on the calculated turbulence field and is derived for a uniform open-channel flow assuming a logarithmic velocity profile and a linear shear stress distribution. The Bakhmetev scale is defined as:

$$L_m = \kappa \cdot z \cdot \sqrt{\frac{h_f - z}{h_f}} \tag{3.18}$$

It is expected that the Reynolds number will be of influence on the horizontal length scale of the turbulent vortices, giving an indication that Equation (3.18) is a large simplification of the real turbulent behavior (Hofland, 2005). However, no direct equations are available giving a better understanding and view on the turbulent behavior of turbulent flows.

Xie and Castro (2008) calculated length scales of turbulent vortices (Large Eddy Simulations: LES) with direct numerical simulations (DNS) based on the Navier-Stokes equation including the normal logarithmic average velocity distribution. The results of these simulations are presented in Figure 3.15. Xie and Castro (2008) has considered $h_f$ as half the total flow height, because their is based on calculations applicable for pipeflow. The results of these numerical simulations are shown in Figure 3.15, in which $h_f$ is considered as the total flow height. The dots in the figure show that the horizontal length scale depends on the direction of the velocity it is representing. The length scale in horizontal direction is twice the length scale related to the vertical and transversal length scale. The results of these LES simulations differ from Equation (3.18). At the bottom and top of the flow the Bakhmetev length scale is zero. However, the calculated length scale according to Figure 3.15 is close to the length as determined by the numerical simulations of Xie and Castro (2008).

## 3.4. Shear stress along a granular bed

In fact the bed shear stress represents the surface- and time-averaged forces exerted/experienced by a flow over a granular bed. Due to turbulence this force varies in time and space, while different properties of the bed affect the actual force: protrusion of the grains above the bed, size and shape of the grains, while the roughness of the surface plays also a major role. As a result separate grains experience forces in two directions: parallel to the direction of the flow (drag force) and perpendicular

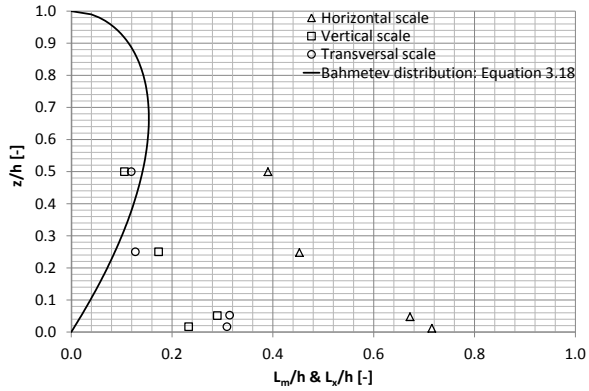


Figure 3.15: Integral length scales (Xie and Castro, 2008)

to the direction of the flow (lift force). The forces acting on single grains (lift and drag forces) are described in Section 3.4.1.

In case of a hydraulically rough flow the relation between the energy gradient and/or hydraulic head and the resulting flow velocity (distribution) and bed shear stress is determined by the flow resistance of the granular bottom. The calculation of the flow resistance is based on empirical expressions which give a more or less theoretical value of the resistance of the flow along a granular bed. There is no direct theoretical approach for the determination of the flow resistance. The flow resistance or bed shear stress depends on the depth-averaged flow velocity ($U$), hydraulic radius ($R_h$) and roughness of a granular bed ($k_s$) and are assumed to act in a direction parallel to the wall or sand bed. An example of a model with which the time-averaged horizontal bed shear stress along a granular bed can be calculated is the Chézy coefficient. The Chézy coefficient is based on an effective bed roughness and is a measure for the average friction of a flow along the bed. This approach is valid as long as there is hardly any erosion (Section 3.4.2), while the effective friction in case of a moving or eroding sand bed is considered to be related to a fictitious bed roughness. A widely used approach is described in Section 3.4.4.

### 3.4.1. Forces on single grains

The drag coefficient for spheres depends on the particle Reynolds number. However, due to the surface roughness and angularity of grains this coefficient changes for natural grains. Besides this an accelerating grain causes acceleration of the flow around the grain. This effect is known as the added mass force. Besides forces in the direction of the flow, the grains experience a lift force in vertical direction.

#### Drag force on spheres

The drag force ($F_D$) on a grain is expressed as :

$$F_D = \frac{1}{2} \cdot C_D \cdot \rho_w \cdot A_g \cdot U^2 \tag{3.19}$$

in which $A_g$ is the surface area of a grain. The drag coefficient ($C_D$) on a sphere depends on the particle Reynolds number ($Re_p = U \cdot d/\nu_w$) (Schlichting and Gersten, 1999). At low particle Reynolds numbers ($Re_p$) the inertial forces are negligible compared to viscous forces. The flow around a grain is laminar and is the resistance is dominated by viscous stresses (Stokes regime). At particle Reynolds numbers of more than 1000 the viscous forces are negligible to the inertial forces. The flow around a sphere is turbulent (Newton regime). In between the Stokes and Newton regime a transition regime is present (Figure 3.16). At a particle Reynolds number of more than 250.000 the drag coefficient decreases due to flow separation and/or vortex shedding (drag crisis).



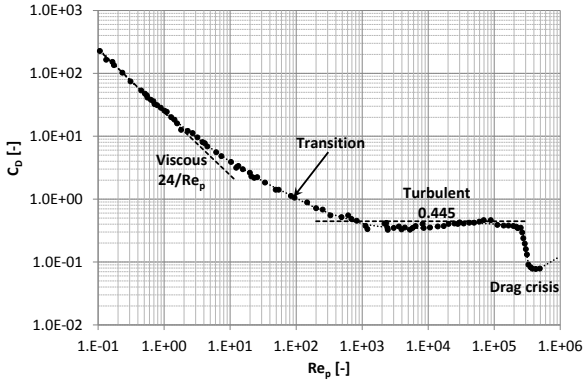


Figure 3.16: Drag coefficient ($C_D$) for a sphere as a function of the particle Reynolds number Schlichting and Gersten (1999)

### Drag force on natural grains

The drag coefficient of natural grains deviates from that of spheres. The grain shape and surface roughness affect the drag coefficient (Wu and Wang, 2006). Based on several (semi)-empirical relations the drag coefficient can be approximated by (Figure 3.17):

$$C_D = \left[ \left( \frac{P}{Re_p} \right)^{1/n} + R^{1/j} \right]^j \tag{3.20}$$

in which $P$, $R$ and $j$ are empirical coefficients which are slightly different based on research of different authors and depend on the shape of the grains. Figure 3.17 shows the influence of the shape of grains on the drag coefficient. This is factor can be described by the so-called Corey shape factor, see Equation (2.1).

The shape factor ($S_f$) of natural sediments/grains is considered to be approximately 0.7. For grains with a shape factor of 0.7 the following values are found for the empirical coefficients of Equation (3.20): $P = 33.9$, $R = 0.98$ and $j = 1.33$. The relationship between $C_D$ and the particle Reynolds number according to Equation

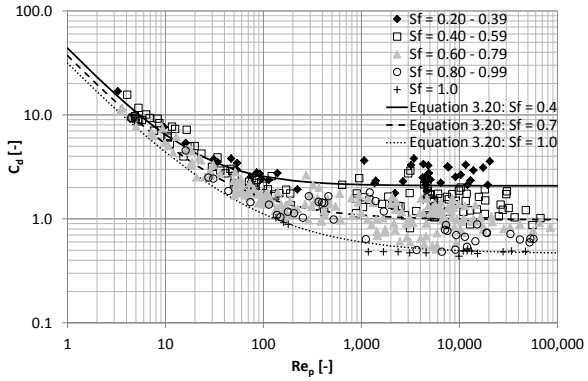


Figure 3.17: Drag coefficient as function of the particle Reynolds number and shape of the grains (Wu and Wang, 2006)

(3.20) including the mentioned empirical coefficients for natural grains is presented in Figure 3.18.

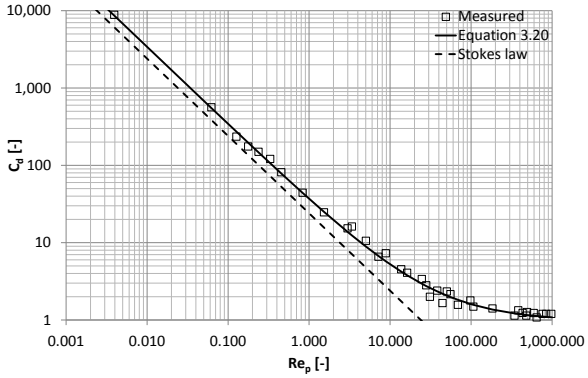


Figure 3.18: Drag coefficient as function of the particle Reynolds number for natural grains as based on Equation (3.20) according to Wu and Wang (2006)

For a shape factor of 1.0 Equation 3.20 describes a relation between the drag coefficient and particle Reynolds number deviating slightly from the relation of spheres as presented in Figure 3.16. The reason is that naturally worn grains with a Corey shape factor of 1.0 may not be spheres and the angles and surface roughness also affect the drag coefficient.

### Dynamic drag

An accelerating grain, relative to the flow, results in acceleration in some amount of the fluid surrounding the grain. This causes an extra resisting force on the grain (Hofland, 2005), besides the effect of drag as describe above. This phenomena is

modeled as an imaginary volume of fluid moving with the grain: the added mass. This effect is expressed with the added mass coefficient ($C_m$). The added mass is incorporated in the equation for the total force on a grain with a volume ($V_g$) by considering a fictitious mass consisting of the mass and the added mass, including the effect of the velocity of the grain itself ($v_g$):

$$F = \rho_w \cdot V_g \cdot \frac{Du}{Dt} + \rho_w \cdot V_g \cdot C_m \cdot \left( \frac{Du}{Dt} - \frac{dv_g}{dt} \right) \tag{3.21}$$



$D\hat{u}/Dt$ is defined as the material derivative moving along with the fluid (Lagrangian). This derivative is defined as:

$$\frac{Du}{Dt} = \frac{d\hat{u}}{dt} + u \cdot \frac{\partial \hat{u}}{\partial x} + v \cdot \frac{\partial \hat{v}}{\partial y} + w \cdot \frac{\partial \hat{w}}{\partial z} \tag{3.22}$$

Lift force on a grain

When a sphere is surrounded by a flow with a velocity gradient normal to the flow direction, the velocity difference over the spheres results in a lift force (Hofland, 2005). Besides the effect of a vertical velocity gradient, vortex shedding from an object in free shear flow can also give rise to large lift force fluctuations. The exact interaction of these two mechanisms, the influence of a wall and the importance for non-spherical particles on a bed however is not yet understood. The equation for the lift force ($F_L$) has the same form as Equation (3.19) for the drag force:

$$F_L = \frac{1}{2} \cdot C_L \cdot \rho_w \cdot A_g \cdot U^2 \tag{3.23}$$

Marsh et al. (2004) has given an overview of different measurements of the lift coefficient (Figure 3.19). The scatter of the data is considered to be the result of the grain configuration (exposure level of the grain) and force measuring techniques during the different experiments. Vollmer and Kleinhans (2007) has given an approximation of the lift coefficient ($C_L$) as function of the roughness Reynolds number ($Re_* = u_* \cdot k_s/\nu_w$), which was based on the data of Coleman (1967):

$$\begin{aligned} C_L &= \frac{-10.5}{Re_*} && Re_* < 5 \\ C_L &= \frac{-24}{Re_*} + \frac{4}{Re_*^{0.7}} + \frac{2.3}{Re_*^{0.3}} && 5 < Re_* < 200 \\ C_L &= 0.45 && Re_* > 200 \end{aligned} \tag{3.24}$$

This function is based on uniform spheres fully exposed to an approaching flow for plane beds and time averaged values of the flow velocity. It should be noted that the data of the presented experiments does not match well with Equation (3.24). This difference possibly could be explained by the fact that Vollmer and Kleinhans (2007) use Equation (3.24) to determine the criterion for incipient motion. This criterion should not be based on the average value but on the maximum possible value of the lift coefficient. Figure (3.24) shows that the lift force is negative (exerting a downward force on the particles) for roughness Reynolds numbers of less than

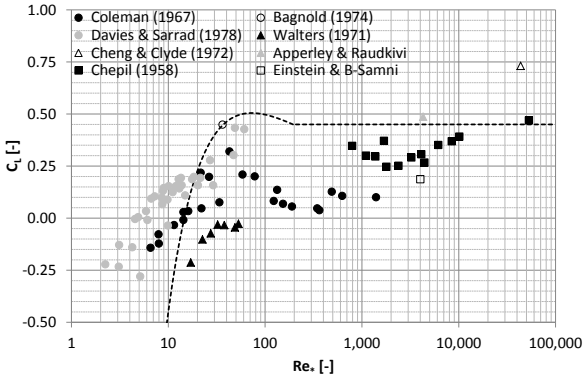


Figure 3.19: Measured lift coefficient as function of the boundary Reynolds number (Marsh et al., 2004) in comparison with Equation 3.24 of Vollmer and Kleinhans (2007)

approximately 15. This transition can be explained by the presence of a viscous boundary layer at these roughness Reynolds numbers (Miedema, 2010). At higher Reynolds numbers the boundary layer is turbulent and the lift coefficient is positive. However for grains with a size of for instance 100 $\mu$m ($k_s$ is approximately 200 $\mu$m) this effect appears at flow velocities of less than 1 m/s which is not relevant in case of the erosion at high flow velocities.

Ling (1995) has described the lift force as the sum of the Saffman force or shear lift ($F_s$), the Magnus force or spin lift ($F_m$) and the centrifugal force ($F_c$) in which:

$$F_s = \alpha_s \cdot \rho_s \cdot \nu_w^{0.5} \cdot d^2 \cdot v_g \cdot \left(\frac{du}{dz}\right)^{0.5} \tag{3.25}$$

$$F_m = \pi \cdot r^3 \cdot \rho_w \cdot \omega_g \cdot v_g \tag{3.26}$$

$$F_c = m_g \cdot \frac{(r \cdot \omega_g)^2}{2 \cdot r} \cdot \cos\lambda \tag{3.27}$$

in which $\alpha_s$ is the Saffman lift coefficient (= 1.615), $v_g$ relative velocity between fluid and grains, $r$ radius of a grain, $\omega_g$ angular velocity of the sphere, $m_g$mass of a grain and $\lambda$ angle between normal force and gravity. The Saffman lift force is a result of the velocity gradient over a particle (shear effect). The Magnus force describes the effect of the spinning motion of a grain on the lift force. At incipient motion $F_m$ and $F_c$ can be neglected because the angular velocity ($\omega_g$) will be zero at this moment. This means that the lift force solely is determined by the Saffman force ($F_s$). The relative velocity of the fluid in relation to the velocity of the grain equalizes the flow velocity in this case.

### 3.4.2. Friction

The flow resistance determines the relation between the energy gradient and/or hydraulic head of the flow and the resulting flow velocity. This relation depends

on the dimensions of the cross-section of the channel or pipe and the roughness of the bottom and/or conditions along the bottom like the sediment flux across the top of a sand bed. Based on empirical data for turbulent flow, Chézy proposed the following formula (van Rijn, 2008) relating the discharge capacity ($Q$) and hydraulic gradient:

$$Q = C \cdot A \cdot \sqrt{R_h \cdot i} \quad or \quad U = C \cdot \sqrt{R_h \cdot i} \tag{3.28}$$



The Chézy coefficient ($C$) can be related to the Darcy-Weisbach coefficient ($f$) with:

$$C^2 = \frac{8 \cdot g}{f} \tag{3.29}$$

The bed shear stress ($\tau_b$) is given by:

$$\tau_b = \rho_w \cdot g \cdot \frac{U^2}{C^2} = \frac{f}{8} \cdot \rho_w \cdot U^2 \tag{3.30}$$

It should be noted that the Chézy coefficient increases for a decreasing $k_s$-value, meaning that the Chézy coefficient is a "smoothness" coefficient. In this way the Darcy-Weisbach coefficient is more logic. In case of fully rough flow the influence of the Reynolds number vanishes. Integrating Equation (3.6) to obtain the average flow velocity in case of pipe flow yields (White, 2009):

$$\frac{U}{u_*} = 2.44 \cdot ln \frac{D_h}{k_s} + 3.2 \tag{3.31}$$

Combining Equation (3.5) and (3.30) with Equation (3.31) gives a solution for the Darcy-Weisbach coefficient in case of fully rough flow:

$$\frac{1}{\sqrt{f}} = -2.0 \cdot log \frac{k_s}{3.7 \cdot D_h} \tag{3.32}$$

Equation (3.32) forms part of the well-known Colebrook-equation (Colebrook, 1939) valid for turbulent smooth and rough flow, valid for Reynolds numbers $>$ 4000:

$$\frac{1}{\sqrt{f}} = -2.0 \cdot log \left( \frac{k_s}{3.7 \cdot D_h} + \frac{2.51}{Re \cdot \sqrt{f}} \right) \tag{3.33}$$

in which $D_h$ is the hydraulic diameter. Equation (3.33) was developed for pipe flow, in which the roughness is determined by the roughness of the material of the pipe. However this equation could also be used in case of pipe flow in which a none or almost non eroding sand bed is present. Another assumption of this equation is that the velocity distribution of the sand bed is logarithmic.

### 3.4.3. Bed friction dependent of grain size

Nikuradse introduced the concept of an equivalent sand roughness height ($k_s$) to simulate the roughness of arbitrary roughness elements of the bottom boundary. The effective bed roughness consists of grain and form roughness. The grain roughness is generated by skin friction forces, while form roughness is generated by normal forces acting on the bed forms (van Rijn, 1993). The grain roughness is the roughness of individual moving or non-moving sediment grains as present in the top layers of a movable or non-movable natural plane bed. In case of a none or hardly eroding sand bed, the total flow resistance is related to the time-averaged horizontal force on all the sand grains at the top of the sand bed. The dimensions and protrusion of the grains are a measure for the roughness height, which is mainly related to the size of the largest grains ($d_{90}$) at the top layer of the bed:



$$k_s = c_1 \cdot d_{90} \tag{3.34}$$

in which $d_{90}$ is the size at which 90% of the grains is smaller. van Rijn (1993) has proposed for $c_1$ a value of 3, although his analysis of 120 sets of data showed a range of 1 to 10 for $c_1$ ($d_{50}$ between 130 and 5,000 $\mu$m).

### 3.4.4. Friction independent of grain size

Equation (3.34) is valid during flow conditions with hardly any erosion: Shields parameter ($\theta_b = \frac{\tau_b}{d_{50} \cdot g \cdot (\rho_s - \rho_w)}$) $< 0.5$ to 1.0. Measurements at higher values of $\theta_b$ ($>$ 0.5 to 1.0) show that Equation (3.34) is not valid anymore during these flow conditions. Dohmen-Janssen (1999) made an extensive literature overview of different expressions, based on experiments during sheet flow conditions, to determine the roughness height. These expressions all look like:

$$\frac{k_s}{d_{50}} = c_2 \cdot \theta_b \tag{3.35}$$

Equation (3.35) is an implicit empirical relation, because the roughness height ($k_s$) determines the friction and thus is directly related to the bed shear stress. According to Dohmen-Janssen (1999) the constant ($c_2$) in Equation (3.36) ranges between 3 and 430. The most well-known expression is that of Wilson (1989) assuming $c_2 = 5$. Equation (3.36) shows that at relative high flow velocities the roughness height is independent of the grain size and is determined by the flow conditions, represented by the bed shear stress (Figure 3.20):

$$k_s = c_2 \cdot \frac{\tau_b}{(\rho_s - \rho_w) \cdot g} \tag{3.36}$$

Miedema and Ramsdell (2016) and Camenen and Larson (2013) have concluded that Equation 3.35 have to be solved by iteration, because the Shields parameter depends on the relative roughness through the Darcy-Weisbach friction coefficient. Equation can be solved also numerically and has theoretically three solutions or one solution. However, one solution ($k_s > 14.8 \cdot R_h$) is physically incorrect (Miedema and Ramsdell, 2016). This means that two or no solutions are left, thus the use of 3.35 is questionable. An direct explicit equation is necessary.

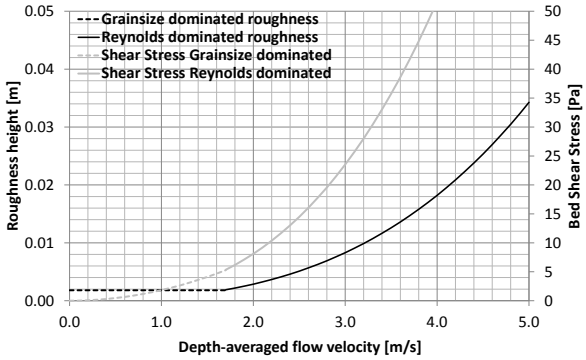


Figure 3.20: Grain and Reynolds dominated roughness height and shear stress for a breach width of 20 m and water depth in the breach of 2 m

Equation (3.36) should be used also with care, because in some occasions the calculated roughness height is larger than the dimensions of the test equipment. This means that the roughness height has no physical meaning in case of a flow over an eroding or moving sand bed. The bed roughness should not be considered as a measure for the thickness of the disturbed bed or sheet flow layer. The bed roughness is only a measure for the energy dissipation close to the eroding bed, due to grain-grain and grain-fluid interaction (Dohmen-Janssen, 1999). Besides this Equation (3.32) is only applicable in a flow field with a logarithmic velocity profile, while the velocity profile in the sheet flow layer (high density slurry) close the stationary bed can be considered as linear (Pugh and Wilson, 1999).

A more specific explanation for the effect of suspended grains on fictitious roughness height is given by van Rijn (1993). High concentrations and high flow velocities cause interaction of the flow with the grains in the near-bed region. The grain velocities are greatly suppressed by collisions with the bed and with each other. This results in a relatively large difference between the overall fluid velocity and grain velocity (slip). The associated fluid drag forces are the driving forces of grain motions. Conversely, these drag forces are reducing the fluid velocity, which can be interpreted as a shear effect additional to the fluid shear. This effect on shear has been investigated by Bagnold (1954) and resulted in the definition of a viscous and grain-inertia regime (see Section 2.3.4).

Equation (3.35) and Figure 3.20 show that the effective Darcy-Weisbach friction factor in case of sheet flow or a highly eroding sand bed increases as function of the depth-averaged flow velocity. Due to a larger flow velocity more grains are suspended in the flow close to the bottom leading to higher energy losses and effective friction as a result of grain-grain and grain-fluid interaction. In case of a non-eroding or almost non-eroding sand bed the friction decreases as the depth-averaged flow velocity increases (increasing Reynolds number). However, this does not result in a lower bed shear because the relative increase of the squared value of the depth-averaged flow velocity is larger than the decrease of the friction at an increasing flow

velocity.

## 3.5. Sheet flow

Sheet flow is considered as the transport of sand in thin layers close to the bed in which the sediment concentration is very high (Dohmen-Janssen, 1999). Sheet flow conditions occur during pipe flow but also during storms when wave conditions cause strong near-bed oscillating flows, such that ripples are washed out and sand is transported in a thin layers close to the bed. The transport of sand during sheet flow is assumed to occur at a Shields parameter ($\theta_b$) of more than 0.5 to 1. For sand with a grain size of between 50 and 500 $\mu$m this is comparable to the flow regime during flow velocities of more than 1 m/s.



An overall description of the physical processes during sheet flow is given in Section 3.5.1. In the description of sheet flow the thickness of the layer comprising sand grains at the maximum shear stress or Shields parameter is an important parameter in the description of the sediment transport process. Different definitions exist for this layer (Section 3.5.2). The concentration and/or porosity profile of this layer is described in Section 3.5.3. It should be considered that the flow conditions in this layer differ from a logarithmic velocity profile (Section 3.5.4). During sheet flow conditions the effective bed friction cannot bed determined on the basis of the equation valid in the regime with $\theta_b < 1$. Dohmen-Janssen (1999) reviewed different studies regarding the bed friction during sheet flow conditions. In these studies the bed roughness is considered to be representative for the thickness of the disturbed layer of sand, just above the non-moving bed (Section 3.5.5). Based on these findings it is proposed to distinguish five different regimes, varying in concentration and/or porosity profile and shear stress model (Section 3.5.6).

### 3.5.1. Description physical process sheet flow

Gao (2008) has distinghuished two regimes occurring during sheet flow: the saltation and sheet flow regime. Fig. 3.21(a) shows that in the saltation regime only a few grains are entrained into the flow. The top layer is partially mobile. As $\theta_b$ increases more grains are transported as bed load. At a certain critical value of $\theta_b$ all grains in this layer move as bed load (Figure 3.21(b)). In other words the surface layer of the bed changes from being partially mobile to being fully mobile. At higher values of $\theta_b$ multiple layers of grains will be fully mobile (Figure 3.21(c)). Figure 3.22(d) and (e) show the existence of a laminated layer at values of $\theta_b$ of more than 0.5. This layer consists of multiple layers shearing over each other: the sheet flow regime. The saltation regime (pick-up zone) is still applicable at the top of this layer. More grains will be available for pick-up because the porosity in the top layer increases, due to the effect of dilatancy, leading to a lower friction resistance of the grains.

Sheet flow during oscillating flow conditions differs from pipe flow. During pipe flow, sheet flow occurs at a constant velocity and the layer of sand is transported with a constant thickness in horizontal direction. However, during an oscillating flow the flow velocity is increasing and decreasing and changes in direction. During an increasing flow velocity grains start shearing and move in upward direction, leading

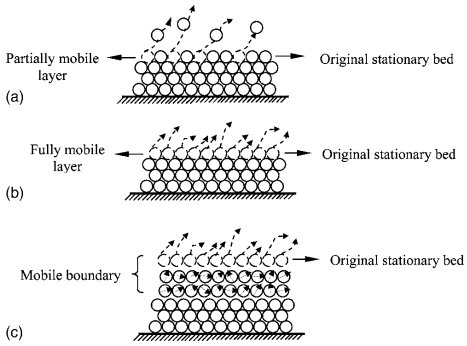


Figure 3.21: Diagram showing bed conditions: (a) saltation regime; (b) onset of sheet flow regime and (c) sheet flow regime (Gao, 2008).

to saltation as well as sheet flow as described by Gao (2008). From a Shields parameter of more than 0.5 a laminated zone develops (Figure 3.22), showing the presence of sheet flow at this flow condition. These sheet flow layer move in the direction of the flow.

The pick-up flux is higher than the sedimentation flux, causing a decrease of the height of the stationary bed. The system is dominated by pick-up (erosion). When the flow starts decreasing the sedimentation flux increases while the pick-up decreases. At the moment the sedimentation flux exceeds the pick-up flux, the sand bed starts to grow in upward direction (settling phase). The behavior of the system is dominated by the settling velocity of the grains (including hindered settling) and consolidation of the resulting sand bed after settling. The same cycle occurs when the flow velocity changes in direction, causing also a change in the direction of transport of the sheet flow layer.

As described above, sheet flow is considered as the transport of sand in thin layers close the bed. The thickness of and concentration of grains in this layer depend on the effective bed shear stress. However, it should be noted that the thickness and concentration influences the bed shear stress, because the shear stress-strain rate behavior is highly influenced by the thickness of and concentration in this layer (see Section 2.3.4). Dohmen-Janssen (1999) has assumed that sheet flow occurs from a Shields parameter ($\theta_b$) of approximately 1. Experimental results (Gao, 2008) suggest however, that the sheet flow regime starts at lower values for $\theta_b$ ($\approx 0.5$). This shows that there is no exact criterion when sheet flow occurs.

### 3.5.2. Sheet flow layers

Different definitions exist for the thickness of the layer in which grains are transported during sheet flow conditions: the erosion depth, the sheet flow and shear layer (see Fig. 3.23). The erosion depth ($d_s$) is defined as the distance between the bed level at zero velocity and the level of the stationary bed at the highest flow velocity. The level of the stationary bed is the boundary between the layer exhibiting

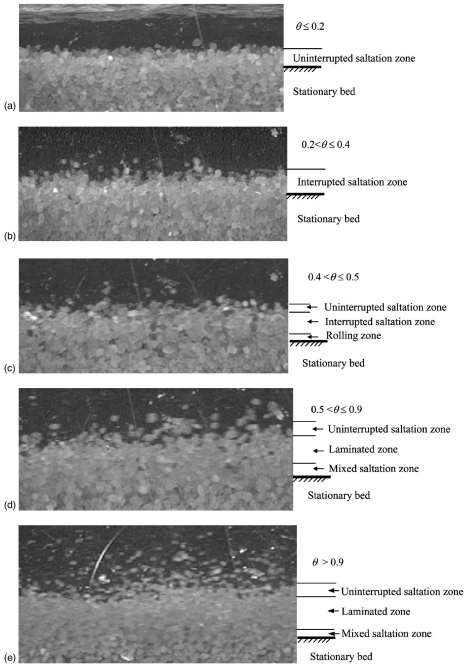


Figure 3.22: Images showing behaviour of bed of sand during different values of $\theta$ (Gao, 2008).

sheet flow conditions and the stationary bed.

The sheet flow layer thickness ($\delta_s$) is defined as the distance between the stationary bed and the level where the concentration becomes (almost) zero. Dohmen-Janssen (1999) defines the upper limit of the sheet flow layer thickness as the level where the time-averaged volume concentration is equal to 8%. Pugh and Wilson (1999) defined the level of top of the shear layer ($H$) as the intercept of the slope of the concentration profile ($dc/dz$) with the vertical coordinate (Figure 3.24: $c = 0$ axis). This level corresponds with a concentration of 0.05 (porosity 0.95) and shows that the definition for the sheet flow and shear layer thickness are based on comparable conditions. However, it should be noted that no exact definition exists for the top of this layer. A definition for this layer could be the transition between the grain-inertia and viscous regime. This transition is based on the Bagnold number (see Section 2.3.4).

The stationary bed is defined as that part of the bed that is not eroded or transported in horizontal direction at the maximum shear stress during an oscillating flow (Figure 3.24). The porosity of the layer above the stationary bed increases and decreases. The porosity of the stationary bed below the influence of the maximum shear stress will not change and is equal to the in-situ porosity of the sand bed.

The level up to which the sand bed moves, is defined by the effective bed shear stress of the flow and the resisting force of the sand bed. This resisting stress is

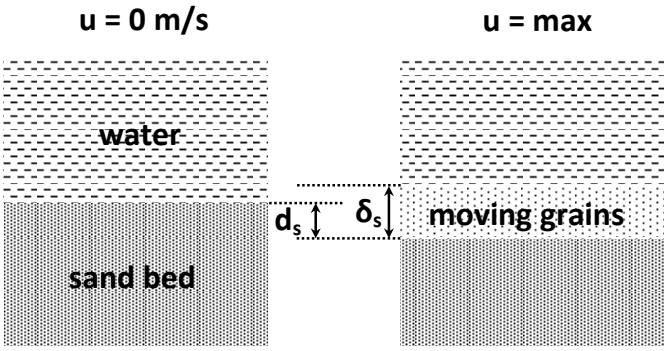


Figure 3.23: Definition of erosion depth ($d_s$) and sheet flow layer thickness ($\delta_s$) according Dohmen-Janssen (1999)

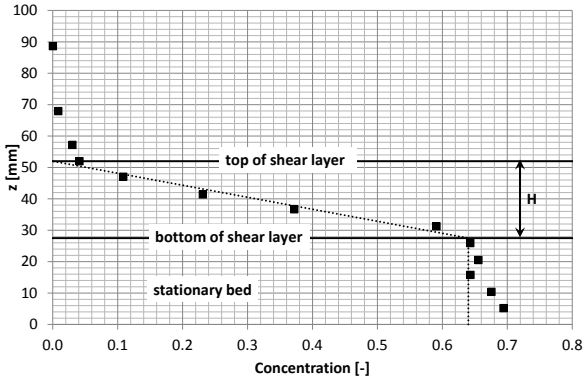


Figure 3.24: Definition of shear layer ($H$) according to Wilson (2005)

determined by the effective vertical stress, depending on the submerged density of the layer above the failure zone. The effective stress concept (Equation 2.14) is still valid in this layer, because the grains are still in contact with each other. The most common model to describe the failure behavior is the Mohr Coulomb-model, see Equation (2.13). Using both equations, an expression for the erosion depth can be found:

$$d_s = \frac{\tau_b}{(1 - n_i) \cdot (\rho_s - \rho_w) \cdot g \cdot \tan(\phi)} \tag{3.37}$$

Figure 3.25 presents lines of equal porosity as function of the actual bed shear stress under sheet flow conditions and the height above or below the bed level at zero velocity according to the Mohr-Coulomb criterion as described by Equation (3.37). The line at an equal porosity of 0.5 presents the transition between the stationary bed and the moving (eroded) bed. This represents the erosion depth as function of the bed shear stress. Equation (3.37) gives a good prediction of the actual erosion

depth when the effective angle of internal friction is assumed to be 20°. This value is comparable to the effective angle of internal friction in the grain-inertia regime (Bagnold, 1954): 18° (see Section 2.3.4). However, it should be noted that the experiments of Bagnold (1954) were executed with spheres instead of grains. This will have underestimated the friction in comparison with natural grains.



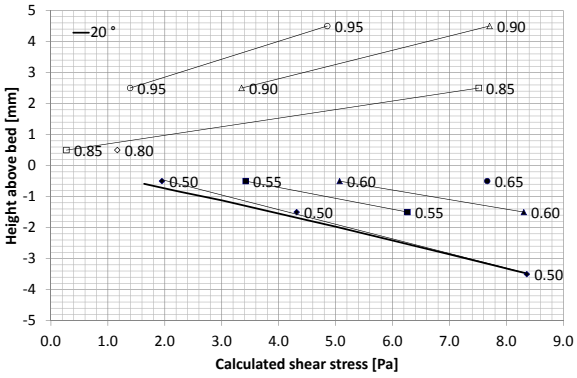


Figure 3.25: Porosity at different levels below and above the original bed level during an oscillatory flow. The porosity is presented as function of shear stress ($d_{50} = 210$ $\mu$m) based on data of Dohmen-Janssen (1999) and the height above or below the bed level at zero velocity according to Equation (3.37) in case of an effective angle of internal friction of 20°

Sand at its maximum porosity normally has a minimum angle of internal friction of 25 tot 35°, depending on the angularity, grain size and coefficient of uniformity of the material. This is higher than the effective angle of internal friction as found above. The value of 20° could also be interpreted as a fictitious angle of internal friction, due to excess pore water pressures. While settling and forming a bed above the stationary bed, the weight of the grains can be temporarily supported by water, leading to excess pore water pressures. This reduces the effective and resisting shear stress, which could be interpreted as a lower fictitious angle of internal friction. Figure 3.26 shows the excess pore water pressures in case of an angle of internal friction of 30°. The excess pore pressure increases with the depth below the zero velocity level, which is caused by the increasing total weight of the sheet flow layer at increasing depth. The actual excess pore pressure depends on the density of the settling column, settling velocity of the grains, permeability and angle of internal friction of the sand bed and the time between consecutive cycles of settling and erosion (wave period). This means that the fictitious angle of internal friction, 20°, represents not a fixed value but depends on the properties of the sand bed and wave period of the oscillating flow.

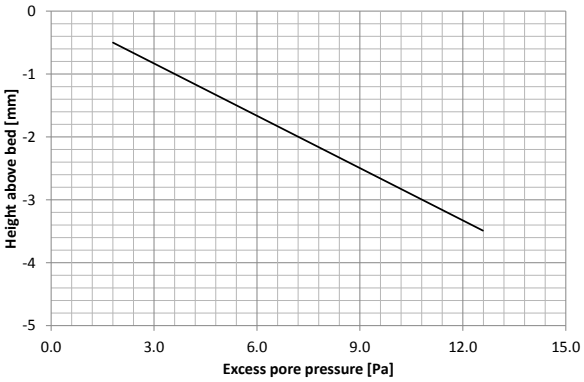


Figure 3.26: Excess pore water pressure assuming an angle of internal friction of 30° as function of the height below the bed level at zero velocity

### 3.5.3. Concentration and/or porosity profile sheet flow layer

During sheet flow the layer above the stationary bed exhibits an increase in porosity (Figure 3.25) as a result of shearing. This layer is known as the sheet flow layer. Shearing is localized in a specific thin shear plane. The thickness of the plane will be limited to a few layers of grains. Due to the oscillating flow the porosity at the bottom of this layer is approximately equal to the maximum porosity ($n_{max} = 0.5$), because the initial porosity of the sand bed is disturbed after the first oscillation during which the level of the stationary bed moves down. At the moment the depth-averaged velocity is decreasing and the settling flux starts to exceed the erosion flux, the sand grains will start to rearrange at a porosity equal to the maximum porosity. The increasing and decreasing porosity of the shearing sand layer shows that the dilatant behavior plays a role in this layer and water has to flow in and out this layer. This shows that sheet flow is a cyclic process of grains moving in upward and downward direction and water flowing in the opposite direction.

Figure 3.25 shows that the porosity in the sheet flow layer, at a level just below the level of the sand bed at zero velocity (initial bed level), increases at increasing shear stress to a value (0.65) above the theoretical maximum porosity. This means that the upward movement of the grains is supported by the turbulent character of the flow and by grain-grain interactions (collisions).

The maximum porosity in the sheet flow layer at different levels below the top of the initial bed is a function of the Shields parameter (Figure 3.28a). The porosity in this layer (measured at a depth of 0.5 and 1.5 mm below the initial stationary bed) is directly related to the Shields parameter or bed shear stress. The linear increase of the porosity for the lower part of the sheet flow layer (or decrease of the concentration) as function of the Shields parameter has also been recognized by several researchers as published by Wang and Yu (2007) and Wilson (2005):

$$n(z) = n_{max} + (n_s - n_{max}) \cdot \frac{z}{d_s} \tag{3.38}$$

in which $n_s$ = porosity at top level of erosion depth and $z$ = the vertical coordinate related to the erosion depth $d_s$ (Figure 3.27). This zone can be considered as part of the sheet flow layer in which the behavior of the grains is dominated by collisions.

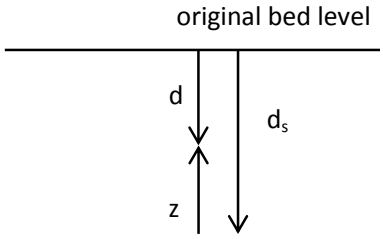


Figure 3.27: Definition of vertical coordinate $z$ and depth $d$ relative to the erosion depth $d_s$

At a certain level the vertical porosity or concentration profile changes from a linear to a curved profile. Figure 3.28b shows that the porosity at the transition between both profiles stays at the initial bed level with a constant porosity of approximately 0.75. This porosity is independent of the bed shear stress. This is in accordance with the findings of Wang and Yu (2007). Based on the data of Dohmen-Janssen and Hanes (2002), Wang and Yu (2007) concluded that the transition between the linear and the curved profile is at a porosity of 0.7 (Figure 3.29). This is in accordance with the mass number ($N_{mass}$), which evaluates the ratio of solid mass to fluid mass per unit volume (Iverson and Vallance, 2001):

$$N_{mass} = \frac{\rho_s \cdot (1 - n)}{\rho_w \cdot n} \tag{3.39}$$

A mass number of $> 1$ implies that momentum transport may be dominated by solid grains. According to Equation (3.39) this effect appears at a porosity of less than 0.73, coinciding with the transition between the linear and curved profile of Figure 3.28b.

Figure 3.30 shows the measured porosity below and above the original bed level for different values of the Shields parameter. The top level of the erosion depth is defined as the level of the original bed. Due to the effect of dilatancy (increase of the porosity) the top level will raise. This means that the adapted top level of the erosion depth ($d_s'$) can be approximated by (neglecting the effect of erosion and the increase of the porosity above the original bed):

$$d_s' = d_s \cdot \frac{1 - n_{max}}{1 - n_{avg}} \tag{3.40}$$

in which $n_{avg} = (n_{max} + n_s)/2$. The porosity at the top level of the adapted erosion depth can be determined with the help of Equation (3.40). The top level of

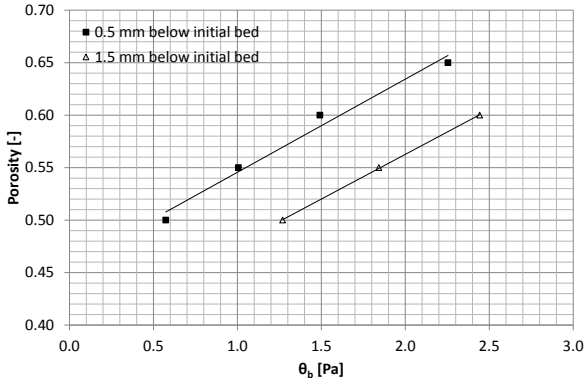


(a)

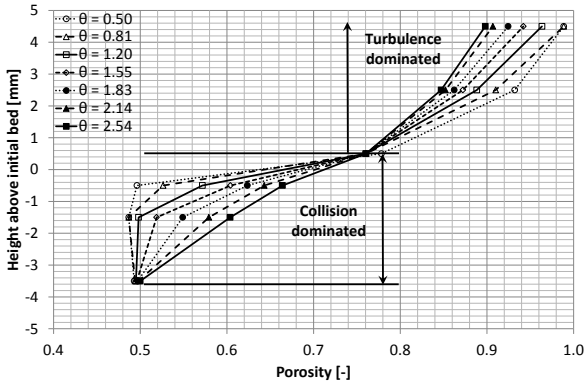


(b)

Figure 3.28: Porosity at a depth of 0.5 and 1.5 milllimeter below the initial stationary bedlevel as function of the Shields parameter (a) and porosity profile as function of the Shields parameter (b)

the adapted erosion depth and the porosity at this level ($n'_s$) were used as reference level ($z_a$) and reference concentration ($c_a$) for the calculation of the concentration profile according to Rouse (1937).

Rouse (1937) has defined an expression for the time-averaged suspended sediment concentration over a plane bed by assuming that the sediment diffusivity ($\epsilon_s$) is constant in time and increases linearly with height ($\epsilon_s = \kappa \cdot u_* \cdot z$). This sediment diffusivity represents the effect of vertical motions of fluid transporting grains in vertical direction. The so-called Rouse profile meets the advection-diffusion approach:

$$w_s \cdot c + \epsilon_s \cdot \frac{\partial c}{\partial z} = 0 \tag{3.41}$$

in $w_s$ is the settling velocity of a grain. This results in a power law distribution of the time-averaged concentration ($c\,(z)$) corresponding to a straight line on a log-log scale:

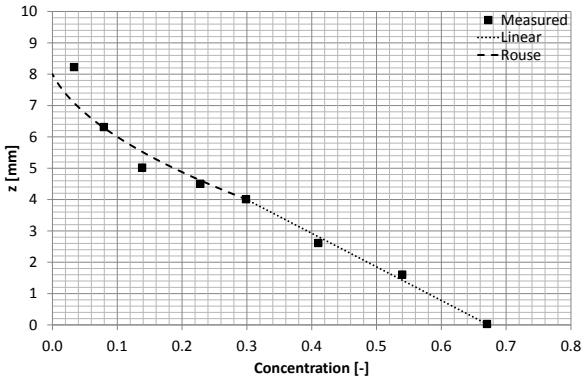


Figure 3.29: Concentration profile at wave peak phase within and above the sheet flow layer (Wang and Yu, 2007)

$$c(z) = c_a \cdot \left[\frac{(h-z)\cdot z_a}{z\cdot(h-z_a)}\right]^{\frac{w_s}{\beta\cdot\kappa\cdot u_*}} \tag{3.42}$$

Normally the respond function ($\beta$) is supposed to be equal to 1 based on the assumption that the sediment mass-transfer mechanism is the same as the fluid momentum-transfer mechanism. van Rijn (1984b) has assumed that $\beta$ is a measure for the quotient of the sediment diffusivity and the fluid momentum diffusivity. $\beta$ approaches to 1 in case of grains smaller than the size of the turbulent eddies, which will follow the behavior of turbulent eddies.

Greimann and Holly (2001) have derived a general two-phase flow equation in order to determine the concentration profile including the effect of sediment diffusivity, Reynold stresses in the particle phase, forces between the grains and the fluid including added mass and collision between the grains. Their approach has proved that when neglecting the effect of the inertia of grains the solution of this two-phase flow equation equals Equation (3.42). As mentioned before the effect of the inertia of the grains has been incorporated by van Rijn (1984b) with the factor $\beta$ in Equation (3.42). van Rijn (1984b) has derived the following empirical relation for the value of $\beta$:

$$\beta = 1 + 2\cdot\left(\frac{w_s}{u_*}\right)^2 \tag{3.43}$$

Equation (3.42) needs an estimate for the reference concentration at a reference level. Smith and McLean (1977) have proposed for the reference concentration and level of the reference concentration:

$$c_a = \frac{c_b\cdot\gamma_0\cdot T}{1+\gamma_0\cdot T} \tag{3.44}$$

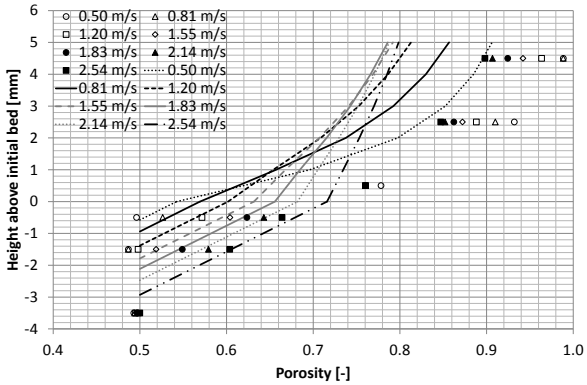


Figure 3.30: Measured porosity below and above the original bed level (presented as dots) in relation to the calculated porosity profile (presented as lines) at different depth averaged flow velocities based on the reference concentration at the top of the dilated bed based on data of Dohmen-Janssen (1999)

$$z_a = \frac{26.3 \cdot \tau_{cr} \cdot T}{\rho_w \cdot g \cdot (s-1)} + \frac{d_{50}}{12} \tag{3.45}$$

in which $\gamma_0$ = constant (0.001 - 0.005); $T$ = dimensionless shear stress $(\tau_b - \tau_{b,cr})/\tau_{b,cr}$; $c_b$ = bed concentration; $\tau_b$ = bed shear stress and $\tau_{b,cr}$ = critical bed shear stress according to Shields.

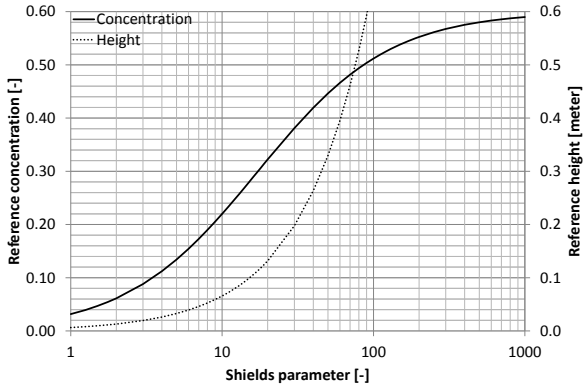


Figure 3.31: Reference concentration and reference height as function of the Shields parameter according to Equation (3.44) and (3.45) for sand with a grain size of 250 $\mu$m, $\gamma_0$ is 0.0025 and $c_b$ is 0.025

Figure 3.31 shows that the reference concentration above the initial bed at the beginning of sheet flow is approximately 0.025. At higher values of $\theta_b$ (> 100) the reference concentration is limited to the bed concentration. Smith and McLean

(1977) uses for the level of the reference concentration $z_a$ the saltation height of the grain above the initial bed (Equation 3.45). However Equation (3.45) seems to be limited to values of $\theta_b$ of approximately 1. At higher values of $\theta_b$ the level rises to values which can be considered as unrealistic. In this case it seems more convenient to chose for the level of the reference concentration a value of: $0.05 \cdot h_f$, as confirmed by numerous authors (Miedema and Ramsdell, 2016). However, Equation (3.42) and (3.43) can be used to determine the concentration profile, considering the above mentioned assumptions, the necessary reference concentration and level at which this reference concentration is valid need more support.



Figure 3.30 shows that the resulting concentration profile overestimates the measured concentration of the suspension above the original bed. This is the result of the fact that the Rouse profile represents a time averaged concentration profile at constant bed shear stress. The concentration in the suspension is in equilibrium with the bed concentration. The pick-up flux equals the sedimentation flux. During sheet flow however the shear stress is not constant and the suspension needs time to balance with the bed concentration. The eroding grains need time to fill the suspension, leading to a less dense concentration profile in relation to a Rouse profile. The pick-up flux and sedimentation flux do not balance each other.

### 3.5.4. Velocity profile

Pugh and Wilson (1999) measured the velocity gradient in the shear layer and flow velocity at the top of this layer (Figure 3.32). The thickness ($H$) of the shear layer is comparable to the sheet flow layer thickness defined as $\delta_c$. The concentration profile during these experiments was mainly linear, corresponding with the findings as described in Section 3.5.3. The horizontal flow velocity at the top of the shear layer: $u(z = H)$, is found to be proportional to the shear velocity:

$$u_{z=H} = 9.4 \cdot u_* \tag{3.46}$$

Figure 3.32 shows the measured velocity gradient in the shear layer during pipe flow (Pugh and Wilson, 1999). The velocity gradient is linear above a depth of $0.25 \cdot H$. Below this depth the velocity distribution is unknown. This linear relation was also recognized in the measurements of the velocity gradient in a sheet flow layer during an oscillating flow by Dohmen-Janssen and Hanes (2002), despite the difference in flow conditions during pipe flow and sheet flow. During pipe flow sedimentation and pick-up can be considered to be in equilibrium, while in oscillating sheet flow conditions these fluxes are not in equilibrium. The velocity distribution in the shear layer as derived from Figure 3.32 is ($u$ represents the horizontal flow velocity at level $z$):

$$\frac{u}{u(z = H)} = 0.6 \cdot \frac{z}{H} + 0.4 \tag{3.47}$$

The velocity gradient is:

$$\frac{du}{dz} = 0.6 \cdot \frac{u(z = H)}{H} \tag{3.48}$$

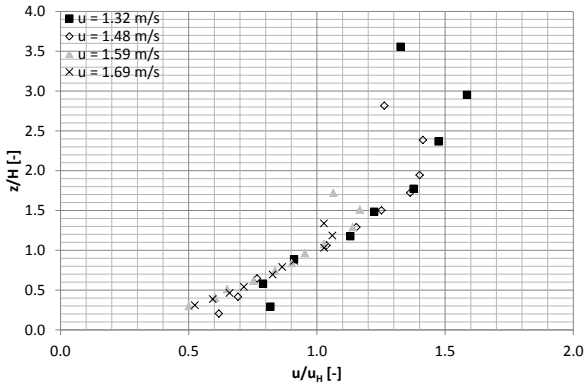


Figure 3.32: Measured velocity gradient in pipeline for 300 $\mu m$ sand (Pugh and Wilson, 1999).

The deviation from the logarithmic velocity profile was confirmed by the results of closed-flume experiments on plastic circular and elliptic cylinders with an equivalent size of approximately 3 mm (Sumer et al., 1996) at $\theta_b$ of more than 0.5. The velocity profile measured in the sheet flow layer, however, did not exhibit a linear profile, but a power form. However, the experiments of Sumer et al. (1996) were executed on material, with characteristics which differed considerable from the properties of natural sand: size 3 mm and density between 1,140 and 1,270 kg/m$^3$. This will have influenced the velocity profile in comparison with natural sand.

### 3.5.5. Shear stress during sheet flow

Bagnold (1954) derived models to determine the shear stress of relative dense mixtures of fluid and grains (see Section 2.3.4) considering different regimes. In the viscous regime the shear stress is linearly related to the velocity gradient ($du/dz$), while in the grain-inertia regime the shear stress is related to the squared value of the velocity gradient $(du/dz)^2$. An expression for the shear stress can also be derived by rewriting Equation (3.48), using Equation (3.46):

$$\frac{du}{dz} = 5.64 \cdot \frac{u_*}{H} \tag{3.49}$$

and with $u_* = \sqrt{\frac{\tau_b}{\rho_w}}$ follows for $du/dz$:

$$\frac{du}{dz} = 5.64 \cdot \frac{\sqrt{\frac{\tau_b}{\rho_w}}}{H} \tag{3.50}$$

This leads to the following expression for $\tau_b$:

$$\tau_b = 0.031 \cdot \rho_w \cdot H^2 \cdot (du/dz)^2 \tag{3.51}$$

This equation has the same form as the shear stress according to Bagnold (1954) in the grain-inertia regime:

$$\tau_g^{'} = 0.013 \cdot \rho_s \cdot (\lambda \cdot d)^2 \cdot \left(\frac{du}{dz}\right)^2 \tag{3.52}$$

This gives an indication that the squared value of the velocity gradient and the concentration of the grains in the layer just above the stationary bed are a good indication of the energy losses due to grain-fluid and grain-grain interactions at this level. Comparison of Equation (3.51) with Equation (3.52) shows further that the thickness of the shear layer seems to be related to the linear concentration ($\lambda$) and the grain size ($d$). This is however questionable because both bed shear stress and concentration (or porosity of the sand bed) determine the thickness of the shear layer (Wilson, 2005).



### 3.5.6. Distinguished zones

Five different zones can be distinguished during sheet flow. All five zones have differences in the failure process, porosity and/or concentration profile, flow and resulting shear stress regime. The level of the stationary bed is defined as that part of the bed that does not deform at the actual shear stress. The Coulomb zone describes the level at which the shear stress at the top of the bed equals the resisting force of the sand due to friction and the effective stress at that level. Above these zones the grain-inertia and viscous zone exist. The suspension zone forms the top level of the sheet flow layer. Figure 3.33 presents the five distinguished zones with their assumed characteristics showing the different zones during sheet flow:

1. Stationary zone: the bed does not deform at the exerted shear stress;
2. Coulomb zone: zone at which deformations start to appear due to static failure which can be described by the Mohr-Coulomb failure criterion. Dilatation of sand will take place;
3. Grain-inertia zone: the shear stress in the sand bed above the Coulomb regime depends on the velocity gradient and collisions of the grains. Further dilation takes place;
4. Viscous zone: the shear stress is dominated by the fluid viscosity, including the influence of the grains on the fluid viscosity, and velocity gradient. In the upper part of this zone the grains are picked-up by the flow. During sheet flow the pick-up zone is situated approximately at the original bed level;
5. Suspension zone: the behavior is determined by the settling velocity of the grains and turbulent energy of the flow.

The stationary zone consists of the undeformed sand bed and has a porosity of $n_i$ and forms the bottom of the layer in the Coulomb zone. The level of the bottom of the Coulomb zone depends on the effective shear stress of the flow at the bottom of the grain-inertia zone and the resisting shear stress of the sand bed. The resisting shear stress depends on the effective vertical stress at this level and angle of friction of the sand bed. The Coulomb zone will be limited to a relative small shear

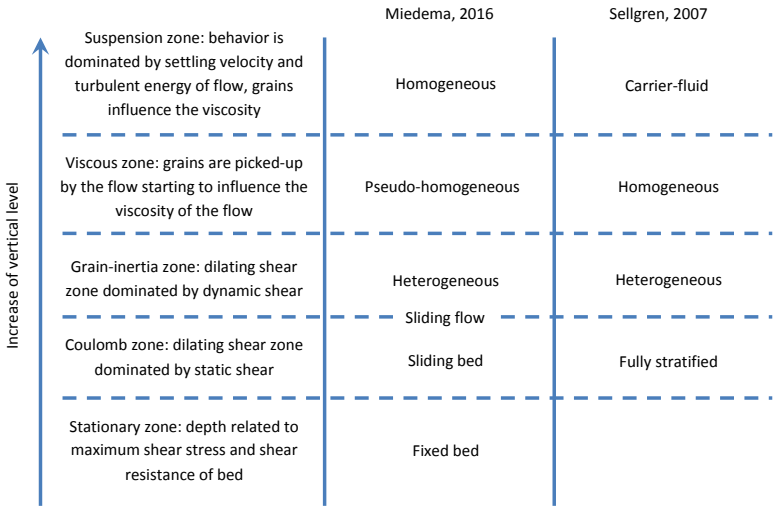


Figure 3.33: Description of zones with different type of behavior compared to the regimes and components as described by Miedema and Ramsdell (2016) and Sellgren and Wilson (2007)

zone as for instance investigated by Alshibli and Sture (1999). They investigated the sand shear band thickness of sand with a grain size of 220 to 1,600 $\mu$m under plane strain conditions in a triaxial apparatus. The experiments showed that failure was characterized by bifurcation and spontaneous localization of deformations into rupture zones called "shear bands" that have certain thicknesses and patterns. For fine sand (220 $\mu$m) the ratio between the shear band thickness and average grain size ($d_{50}$) was approximately 13 to 14, while in the case of medium-grained (550 $\mu$m) and coarse-grained sand (1,600 $\mu$m) this ratio decreased to a value between 11 and 12 (Figure 3.34). The effect of the density and confining stress is negligible (Alshibli and Sture, 1999). The measured ratios by (Alshibli and Sture, 1999) coincide with the theory that sand can be described by its bulk properties at a layer thickness of at least 10 times the average grain size.

In the grain-inertia zone the failure behavior and resulting shear stress depends on the velocity gradient and collisions of the grains. The shear stress in the grain-inertia zone arises from the diffusion of tangential and normal components of grain momenta created by the collisions. In the viscous zone the effect of the fluid viscosity dominates, including the influence of the grains on the viscosity. According to Bagnold (1954) the transition between the grain-inertia and viscous zone is based on the ratio between the grain-inertia and viscous stress. This is defined as the Bagnold number $N$. Below $N = 40$ the shear stress is dominated by viscous stresses, while at values of more than 450 grain-inertia is considered to dominate the stress stress (Section 2.3.4). Between these values the flow behavior changes from viscous to grain-inertia dominated. The vertical concentration profile and velocity gradient in the grain-inertia and viscous zone will be linear. The top of both zones will be

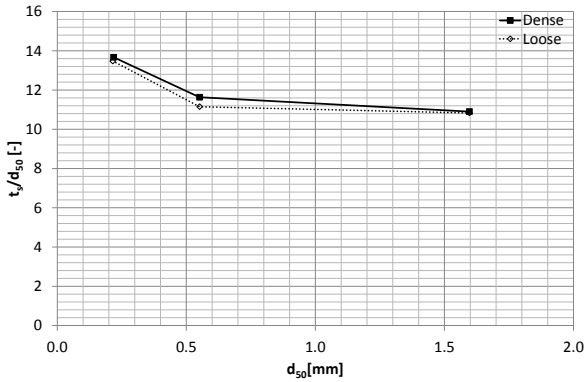


Figure 3.34: Measured shear band thickness ($t_s$) at a confining stress of 15 kPa (Alshibli and Sture, 1999)

limited at the vertical coordinate where the velocity gradient start to deviate from the linear behavior. From this level the suspension zone dominates the behavior of the grains and is determined by the settling velocity of the grains and the turbulent energy of the flow. In both the viscous and suspension zone the grains influence the effective viscosity of the carrier fluid.

It is assumed that the grains present in the Coulomb and grain-inertia will move mainly in horizontal direction, while the grains in the viscous and suspension zone will move predominantly in vertical direction. The grains are picked-up by the flow in the viscous and suspension zone. The exact transition between this difference in behavior is unclear. However, this transition zone could be defined by the level at which the concentration profile and velocity gradient change from linear to curved.

Sellgren and Wilson (2007) and Miedema and Ramsdell (2016) have described different flow components and flow regimes, which can be distinguished during pipe flow (Figure 3.33). The difference between the components and regimes is based on the effect they have on the friction loss. In these flow components or regimes one of the zones as described above is considered to dominate the friction losses in slurry transport. Other zones disappear or do not dominate the friction loss. The conditions at which these regimes were identified depend mainly on the flow velocity, grain size and/or Shields parameter.

In the flow regime consisting of a fixed bed without suspension, as distinguished by Miedema and Ramsdell (2016), the stationary zone is dominating the flow regime. The Shields parameter in this regime is below the critical Shields parameter for sheet flow: no sheet flow occurs, while only a low amount of grains is in suspension. The bed shear stress is dominated by the size of the grains.

The flow regime changes to the sliding bed regime at a Shields parameter just above the critical Shields parameter for sheet flow. During this regime a sheet flow layer starts to develop above the stationary bed. A small amount of grains could be partly in suspension (Miedema and Ramsdell, 2016). The lower part of the sheet flow layer can be considered as the Coulomb zone. This regime can be compared

to the component fully-stratified load as defined by Sellgren and Wilson (2007). In this component the friction loss is determined by grains, traveling along the top of the stationary bed.

At a higher Shields parameter the flow regime changes to heterogeneous flow. During these flow conditions the stationary bed disappears. However, the turbulent forces interacting with the grains, are not strong enough to create a uniform distribution of the grains throughout the cross-section of the pipe (Miedema and Ramsdell, 2016). Part of the grains are carried by sliding contacts and partly by turbulent suspension (Sellgren and Wilson, 2007). Depending on the value of the Bagnold number the shear stress is dominated by the grain-inertia or viscous zone. The sliding flow regime is considered as the transition regime between the sliding bed and heterogeneous regime.



The (pseudo)-homogeneous regime is considered as the regime at which the spatial concentration starts to meet the transport concentration (at a very high Shields parameter). The friction is determined by the influence of the grains on the viscosity and density of the carrier fluid.

## 3.6. Discussion

Numerous researchers published data and empirical models regarding the (effective) bed roughness of a flow over a non-eroding and eroding sand bed. Their results are discussed in this Section 3.6.1. At low velocities the forces on single grains play a major role (Section 3.6.2). At flow velocities of more than 1 m/s is in case of hydraulic engineering much larger than 2300, meaning that turbulence plays a major role during the flow conditions (Section 3.6.3). Especially the structure of vortices influence the stress on the wall and behavior of grains in the flow. Section 3.6.4 gives a short discussion regarding relevant processes during sheet flow.

### 3.6.1. Bed roughness

It is mainly considered that a horizontal flow over a flat bed exerts an average horizontal shear stress over the top of the bed. This shear stress depends on the flow velocity and the roughness of the bed. This roughness is determined by the size of the grains when the flow can be considered as a hydraulically rough flow. In this case the dimensions of the bottom roughness are larger than the thickness of the viscous sublayer. The roughness elements (sand grains) influence the velocity distribution close to the bottom, because the roughness elements generate eddies with a size of the order of the roughness elements affecting the turbulence structure and hence the velocities close to the bottom. Only in the case of a hydraulically smooth flow the shear stress is determined by the viscous forces of the flow, because the roughness elements are much smaller than the thickness of the viscous sublayer.

In case of sand grains the effective bed roughness is considered to be related to the largest grains of the top layer of the bed (grain roughness) and the bed forms (form roughness). The grain roughness is generated by skin friction, while form roughness is generated by normal stresses acting on bed forms. The effective bed roughness in the lower flow regime is considered to be related to the largest grains.

The physical meaning of the equation for the effective bed roughness ($k_s = 3 \cdot d_{90}$) is however unknown. The effective bed roughness will be influenced by the protrusion of grains at the top of a sand bed. On average the exposure level of grains above a bed is approximately $0.5 \cdot d$. Assuming that the largest grains determine the effective roughness, the effective bed roughness should have been in the order of $0.5 \cdot d_{90}$ to have a real physical meaning. Considering $d_{90} \approx 2 \cdot d_{50}$ the effective roughness should be in the order of the $d_{50}$. This is much less than is proposed by for instance van Rijn (1993) for the value of the effective bed roughness.

At higher flow velocities and/or Shields parameter ($\theta_b > 1$) the effective bed roughness is related to the value of the bed shear stress. This means that the effective bed roughness increases as function of the flow velocity. It should be noted that the effective bed roughness under these conditions is a fictitious parameter and is a result of increasing sediment concentrations at higher flow velocities causing interaction of the flow with grains in the near-bed region. The resulting energy loss along a sand bed is not only determined by the interaction of the fluid and the grains but also by collisions of grains with the bed and with each other.



### 3.6.2. Forces on separate grains

The forces of a flow on separate grains can be divided in a drag and lift force. The models to calculate the effective force on a grain are related directly to the grain size. The drag force is based on a drag coefficient, which relates the fluid velocity to the forces on a sphere or grain. Natural sediments have at a particle Reynolds number of more than 1000 a drag coefficient of 1.0, which is higher than the drag coefficient of spheres (0.445). This difference can be explained by the effect of the shape and roughness of the grains increasing the drag coefficient. Besides the drag force as a result of friction along a grain, a pressure gradient also gives a net force on a grain. Due to the acceleration of fluid surrounding a grain an extra force is exerted on the sphere. This phenomenon is modeled as some volume of fluid is moving with the grains: the added mass.

A velocity gradient normal to the flow direction results also in a lift force on the grain, while vortex shedding can also give rise to large lift force fluctuations. The effect of the velocity gradient over the grain is known as the shear lift or Saffman force. Spinning of a grain leads to an extra spin lift and centrifugal forces.

### 3.6.3. Effect of turbulence

A typical phenomenon of turbulent flows is the fluctuating character of the velocity in a point in all three axis of direction. The structure of turbulent flows is highly variable and chaotic. If the Reynolds number is high enough the instabilities will grow leading to the formation of hairpin vortices. The apex of the hairpin vortices are lifted upwards, creating a space between them and the boundary. As a result water will flow in from behind and above, which happens at large flow velocities (high velocity sweeps). These sweeps cause impact zones with a high normal stress on the boundary. Between the legs of the hairpin, forming two smaller counter-rotating, streamwise vortices near the wall, elongated low momentum streaks are formed. These vortices result in low normal stresses due to the suction within the vortices,

moving sediment from the bed and spew it out into the flow above. These effects lead to relative strong fluctuations of the normal stress on the boundary, varying between negative and positive stresses. In a quadrant analysis the sweeps are characterized by a positive horizontal velocity and a negative vertical (downwards) velocity. The ejections, which are thought to move sediment vertical from the bed, show negative horizontal velocities and positive (upward) vertical velocities.

It is believed that fluctuations of the normal stress caused by turbulent vortices could contribute considerably to the forces that initiate the motion of bed particles. These normal stresses are known as turbulent wall stresses. The fluctuations of the normal stress on the wall reach approximately 2.5 to 3.5 times the average wall shear stress.



### 3.6.4. Sheet flow

Sheet flow can occur during oscillating flows, as a result of severe wave conditions, but also in pipe-flow conditions. During wave conditions the flow velocity increases and decreases and changes in direction with a positive or negative offset following a sinusoidal shape. This results in changing flow regimes with repetitive erosive and settling cycles. During the pipe-flow the flow conditions are mainly constant. The dominating flow regime does not change. Due to the relative high shear stresses ($\theta_b > 0.5$ to 1) multiple layers of sand grains are mobile. Sheet flow deviates from a flow over a sand bed at lower Shields parameters ($\theta_b < 0.5$ to 1). The concentration profile close to the bed is considered to be linear and changes at a certain height in a curved profile. This profile deviates from the well-known Rouse profile. Another difference is the velocity gradient close to the bed. Normal the velocity gradient is logarithmic, while during sheet flow conditions part of the velocity profile is linear. Both deviations influence the third difference: the effective roughness. The effective roughness during sheet flow conditions is not related to the size of the grains but is implicitly related to the bed shear stress. It means that the effective roughness is a measure for the energy dissipation close to the stationary bed, due to grain-grain and grain-fluid interaction, instead of a value for the real roughness.

# 4

# Erosion of sand

## 4.1. Introduction

Chapter 3 shows that the behavior of the flow influences the behavior of the sand bed. At low flow velocities and Shields parameter ($\theta_b$) smaller than 0.5 to 1.0, the size of the grains influences the energy loss of a flow over a sand bed. At higher values of the Shields parameter the behavior of the sand bed changes and start to influence the energy loss. This behavior influences the erosion process. This knowledge forms the basis for the description of known erosion regimes and related pick-up functions. The type of regime depends on the flow velocity, related bed shear stress and the behavior of single grains and bulk properties of the sand bed. The pick-up of grains starts to occur when the instantaneous fluid force on a grain exceeds the instantaneous resisting force related to the submerged weight, angle of internal friction and embedding of the grain in the sand bed. The critical Shields parameter ($\theta_{b,cr}$), a non-dimensional number defined by the bed shear stress and grain diameter, defines the criterion at which erosion of grains is initiated (Section 4.2).

As a result of the pick-up the concentration of the eroding flow increases, simultaneously introducing a sedimentation flux. Net erosion takes places as long as the pick-up flux exceeds the sedimentation flux. When the concentration of the eroding flow meets the maximum transport capacity of the flow (Section 4.3) pick-up and sedimentation are in equilibrium. The amount of grains picked up by the flow as function of time depends on several parameters and conditions. Bisschop et al. (2016) distinguishes two erosion regimes: the grain by grain and the dilatancy reduced erosion regime.

Pick-up functions for low flow velocities ($< 1.5$ m/s) and Shields parameter ($\theta_b <$ 0.5 to 1.0) are based on the erosion of single grains (grain by grain erosion regime: Section 4.4). One of the most well-known sediment pick-up functions for this regime is the empirical equation of van Rijn (1984a).

At flow velocities of more than 1 to 2 m/s the model of van Rijn (1984a) overestimates the pick-up flux (Bisschop et al., 2010). At these flow velocities, it is assumed

that the pick-up flux is influenced by pore water under pressures, due to dilatancy effects, as described by Mastbergen and van den Berg (2003) and van Rhee (2010). The resulting dilative behavior causes inflow of water into the sand bed increasing the effective stress and hence reducing erosion (dilatancy reduced erosion). As a result bulk properties of the sand bed, such as porosity and permeability, are assumed to influence the pick-up flux (see Section 4.5). This shearing process of layers of grains was also observed by Gao (2008) during sheet flow at a corresponding Shields parameter ($\theta_b > 0.5$).

Instead of the shearing of layers turbulence could also lead to bulk erosion as described in Section 4.6. In this case lumps of sand are eroded by turbulent bursts. This regime will not only be determined by the dimensions of the turbulent eddies and related turbulent wall stresses but also by the failure mechanism of the lumps of sand.



Erosion is considered not to be influenced solely by the flow velocity and properties of grains and bulk properties of the sand bed, but the transport capacity of the flow influences the pick-up of grains as well (Section 4.8). This is considered as the reduction of the pick-up flux as a result of grains, being present at relatively high concentrations in the eroding fluid just above the eroding bed, hindering eroding grains moving upwards. This effect is described as hindered pick-up (Winterwerp et al., 1992). The applicability of the various pick-up functions and the existence of the distinct erosion regimes are discussed in Section 4.9.

## 4.2. Critical Shields parameter

Pick-up starts to occur when the instantaneous fluid force on a grain is just larger than the instantaneous resisting force (van Rijn, 1993). The instantaneous fluid force on a grain is determined by the fluctuation of the velocity and direction of flow of the fluid just above a sand bed. These fluctuations are the result of the behavior of a turbulent flow, while the resulting force on the grains is determined by the effect of protrusion, submerged weight and internal angle of friction of the grains. This causes an average lift and drag force on the grain. Depending on the position of the grain relative to the bed, this results in sliding or rolling. Pure lifting will take place if the lift force is equal to the gravity force (Miedema, 2010).

### 4.2.1. Shields

The most widely known criterion for grain movement is the Shields curve (Shields, 1936). This curve (Figure 4.1) presents the relation between the dimensionless Shields parameter ($\theta_b$) and boundary particle Reynolds number. Disadvantage of this implicit relation is that the grain size and shear velocity are present on both axes. The critical bed shear stress can only be obtained by iteration. Shields determined the critical shear stress by measuring transport rates at bed shear stresses just larger than the critical bed shear stress. The critical bed shear was defined as the value of the bed shear stress at which the extrapolated transport rate was zero (van Rijn, 1993). In the same period Hjulström (1935) and Hjulström (1939) have published the famous Hjulström-diagram. This diagram shows a direct relation between the

critical threshold velocity and grain size.

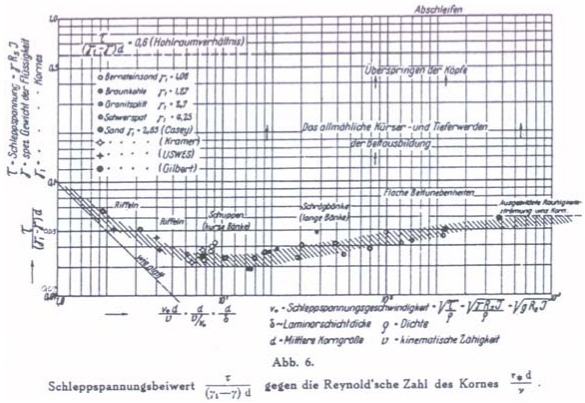


Figure 4.1: Original Shields curve (Shields, 1936)

van Rijn (1993) has presented an explicit equation representing the Shields curve in terms of the critical Shields parameter and the dimensionless grain diameter ($D_*$):

$$\begin{aligned}
\theta_{cr} &= 0.24 \cdot D_*^{-1.00} && 1 < D_* < 4.5 \\
\theta_{cr} &= 0.14 \cdot D_*^{-0.64} && 4.5 \leq D_* < 10.2 \\
\theta_{cr} &= 0.04 \cdot D_*^{-0.10} && 10.2 \leq D_* < 17.9 \\
\theta_{cr} &= 0.013 \cdot D_*^{0.29} && 17.9 \leq D_* < 145 \\
\theta_{cr} &= 0.055 && D_* \geq 145
\end{aligned} \tag{4.1}$$

in which $D_*$ is defined as:

$$D_* = d_{50} \cdot \sqrt[3]{\frac{(s-1) \cdot g}{\nu_w^2}} \tag{4.2}$$

in which $s$ is $\rho_s/\rho w$. Soulsby and Whitehouse (1997) have presented an algebraic expression that represents the total Shields curve closely, including the effect that critical Shields parameter can not exceed 0.3 for small grains:

$$\theta_{cr} = \frac{0.30}{1 + 1.2 \cdot D_*} + 0.055 \cdot \left(1 - e^{-0.020 \cdot D_*}\right) \tag{4.3}$$

### 4.2.2. Recent research

Miedema (2010) has given an overview of other empirical equations for the relation between the critical Shields parameter and the dimensionless grain diameter. Research of Miedema (2012a) has shown that many researchers use different definitions for incipient motion: is it when one grain starts moving, or many and then how many. In general each of the existing models lacks specific phenomena and/or aspects. The modeling usually stops, if a model has sufficient correlation with data of

many researchers and with the original Shields curve. Miedema (2012a) developed a full theoretical model to match the Shields curve and measurements from literature (Figure 4.2). This model distinguishes rolling, sliding or lifting as mechanism of entrainment and includes the effect of:

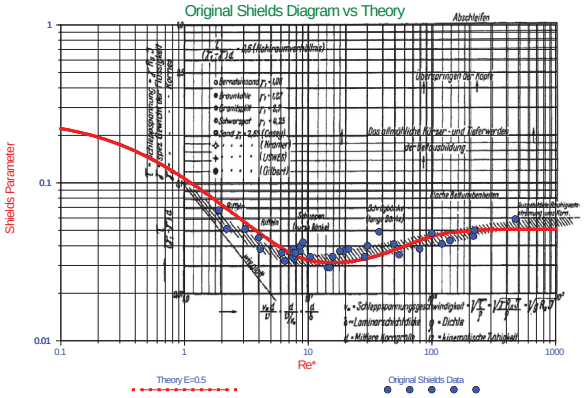


Figure 4.2: Theoretical Shields curve (Miedema, 2012a) compared to the original Shields curve

- protrusion level of the grains above the bed, which is chosen as $0.5 \cdot d$. The value for the protrusion level is fitted on the actual Shields curve. The value of $0.5 \cdot d$ results in a protrusion level of $0.3 \cdot d$, because the virtual bed (zero-velocity level) is chosen to be situated at a level of $0.2 \cdot d$ below the top of the bed;

- drag and lift induces sliding and/or rolling: in case of sliding an internal friction angle of 30° is chosen. For rolling a pivot angle ($\psi$) of 59° is used, matching a protrusion level of $0.3 \cdot d$, based on Luckner (2002);

- flow velocity profile: the velocity profile depends on the roughness of the bed surface and the thickness of the viscous sublayer. Full laminar flow is considered up to a boundary layer/roughness Reynolds number of 5 and full turbulent flow above 70, with a transition zone in between these numbers based on a logarithmic interpolation;

- drag coefficient is based on the relation between this coefficient and particle Reynolds number ($Re_p$), corresponding to a drag coefficient of grains with a grain shape factor of 0.7. For grains with a size smaller than 40 $\mu$m this means that the Shields parameter depends directly on the particle Reynolds number ($C_D = 24/Re_p$, in which $Re_p = (w_s \cdot d)/\nu_w$). Sand grains larger than 40 $\mu$m exhibit a larger drag coefficient than spheres of a corresponding size. This leads to a lower critical Shields parameter for sand in comparison with spheres of a size of $>$ 40 $\mu$m;

- lift is neglected below a boundary Reynolds number of 5: above a boundary Reynolds number of 70 the lift coefficient ($C_L$) is chosen as 0.423. This is a relative high value for $C_L$ in comparison with Equation (3.24), which gives an estimate of the average lift coefficient ($\approx 0.2$). It should be noted that the initiation of motion of grains is determined by the incidental maximum value of $C_L$;
- velocity fluctuations as a result of turbulence are taken into account: Miedema (2012a) assumes that the maximum flow velocity in the vortices is a factor 3 higher than the average flow velocity.

It should be noted that natural sand does not fit exactly the Shields curve as presented in Figure 4.2. Due to variations in grain size, angle of friction of separate grains, exposure level and turbulence intensity, grains will move before the criterion for incipient motion is reached. Several studies are available regarding the amount of grains or transport conditions as function of the Shields parameter. These studies show indeed that the Shields curve does not represent the criterion for incipient motion of the first grains moving. Figure 4.3 shows the theoretical Shields curve (Miedema, 2012a) in comparison with data describing the amount of grains moving along a sand bed (Delft Hydraulics, 1972). These data show that the Shields curve matches with general transport and permanent grain movement at all locations. Graf and Pazis (1977) determined the amount of grains per unit area ($m^2$) being entrained in the flow as function of the Shields parameter. These experiments have revealed that the Shields curve matches with a value of 100 to 1000 grains per $m^2$ (Figure 4.3).

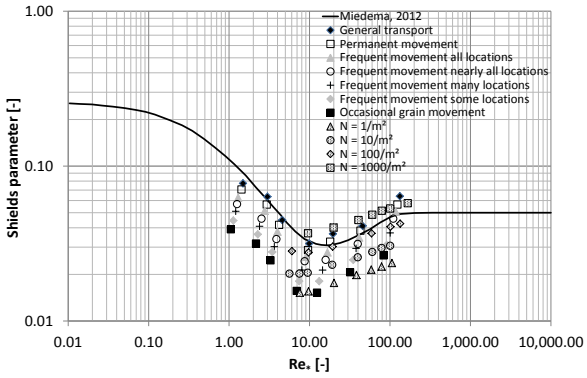


Figure 4.3: Theoretical Shields curve compared to the amount of grains eroding from the bed (Miedema, 2012b)

### 4.2.3. Effect of injection and suction

Outward (injection) and inward seepage (suction) of water out or into the sand bed influences the critical Shields parameter due to their effect on the flow velocity

distribution and on the hydraulic gradient which is exerted by the outward or inward flow into the sand bed. Experiments of Brink and Oldenziel (1974) have shown that as a result of suction the velocity profile close to the bottom changed. During their experiments the local flow velocity close to the bed increased, while injection decreased the local flow velocity (Figure 4.4).

As a result of the increase of the local flow velocity close to the bed the local velocity gradient increases. This causes an increase of the shear stress close to the bed because $\tau_b = \eta \cdot du/dz$, hence enabling the initiation of motion of grains. This means that suction increases the forces on the grains, while injection causes a decrease of the forces on the grains. The effect of suction on the near-bed flow field have been confirmed by numerical CFD-simulations (Cao and Chiew, 2013). Similar changes of the near-bed flow field have also been confirmed by other studies, like Chen and Chiew (2004). Experiments of Rao and Sitaram (1999) confirm the effect of the changing local velocity gradient on the critical Shields parameter. During their experiments suction reduced the stability of grains, while injection caused the opposite effect. Due to the changing flow field grains are subjected, in case of suction, to larger hydronamic forces, resulting in a reduction of the critical Shields parameter during these experiments.

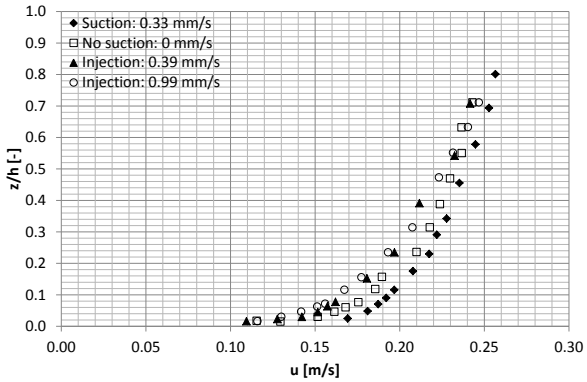


Figure 4.4: Influence of injection and seepage on flow velocity distribution (Brink and Oldenziel, 1974)

Experiments executed by Cheng and Chiew (1999), Cao and Chiew (2013) and Liu and Chiew (2012) show an opposite effect of suction and injection on the critical Shields parameter. Brink and Oldenziel (1974) related the effect of the suction and injection discharge to the hydraulic gradient ($i$) on the sand bed, using Darcy's law. As a result of this inward (suction) or outward gradient (injection) fine sand experiences in comparison with coarse sand, a larger inward or outward hydraulic gradient at a corresponding injection or suction velocity. This is caused by the effect of the permeability. Fine sand has a smaller permeability than course sand, leading to a higher hydraulic gradient, in comparison to coarse sand. In case of suction this leads to an extra downward force on the grains, hence increasing the resisting forces before motion of the grains occurs.

Cheng and Chiew (1999) executed experiments to examine the effect of injection of water from the sand bed in the flow on the incipient motion of grains with a grain size of 630, 1,020 and 1,950 $\mu$m. These experiments show a reduction of the critical shear velocity caused by injection (Figure 4.5). The outward oriented hydraulic gradient reduces the resisting forces of the grains, before motion occurs. These results show that the outward hydraulic gradient prevails over the effect of the changing velocity distribution. The effect of the changing velocity gradient during suction and injection and the influence of the resulting hydraulic gradient on the critical Shields parameter are presented in Figure 4.7.

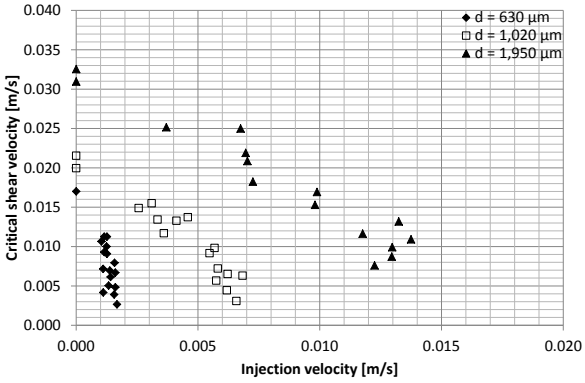


Figure 4.5: Influence of injection on the critical shear velocity (Cheng and Chiew, 1999)

Liu and Chiew (2012) executed experiments showing a comparable influence of suction as Cheng and Chiew (1999). They compared their results to the experiments of Cheng and Chiew (1999) and Kavcar and Wright (2009), by plotting the quotient of the critical shear velocity ($u_{*cs}$) including injection and the critical shear velocity ($u_{*c}$) according to Shields (1936) versus the quotient of the suction or injection velocity ($v_s$) and injection velocity at which the submerged weight of the grains reaches zero (quick condition: $v_{sc}$): Figure 4.6. At this condition the resulting upward hydraulic gradient ($i_c$) is in equilibrium with the submerged weight of the grains for a certain sand type. Liu and Chiew (2012) present for this case a curve representing the critical shear velocity ($u_{*cs}$) as a result of the injection velocity:

$$\left(\frac{u_{*cs}}{u_{*c}}\right)^2 = 1 - \frac{v_s}{v_{sc}} = 1 - \frac{k \cdot i}{k \cdot i_c} \tag{4.4}$$

Equation (4.4) shows that the critical shear velocity strongly depends on the hydraulic gradient. This indicates that the effect of the inward or outward gradient prevails over the effect of the changing flow velocity gradient close to the bottom. Figure 4.7 summarizes the effect of changing velocity gradient close the the sand bed and the effect of the hydraulic gradient in the sand bed during suction and injection on the critical Shields parameter. Depending on the discharge during injection or

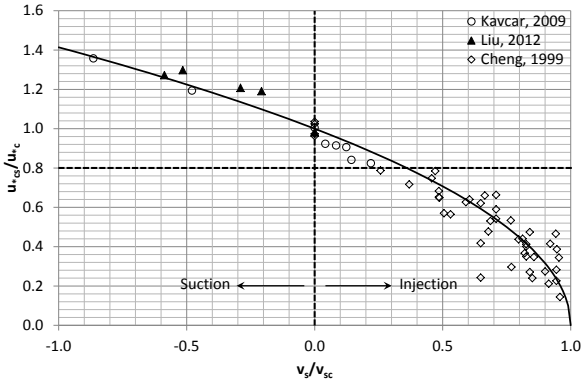


Figure 4.6: Influence of suction and injection on the critical shear velocity (Liu and Chiew, 2012)

suction and the permeability of the sand bed one of both of these effects on the critical Shields parameter prevails.

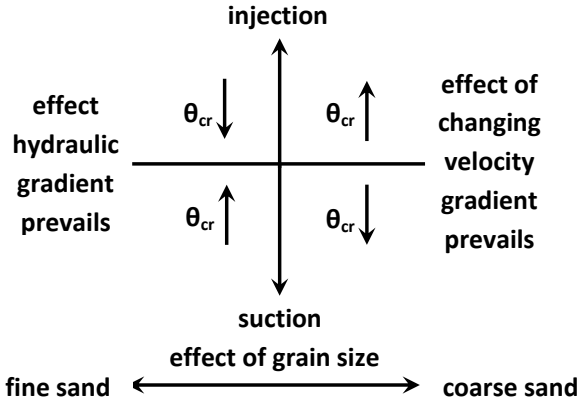


Figure 4.7: Effect of velocity and hydraulic gradient, suction and injection and grain size of the critical Shields parameter

## 4.3. Erosion, sedimentation and transport

Section 4.3.1 describes the definition of the pick-up flux from a sand bed. As a result of pick-up the transport of grains in the eroding fluid increases. This transport capacity is limited (see Section 4.3.2).

### 4.3.1. Erosion and sedimentation

Pick-up of grains is initiated when the flow conditions exceed the critical Shields parameter. The pick-up flux increases with increasing flow velocity. The net erosion

velocity is determined by the flux of sediment passing a moving interface between an eroding sand bed and eroding flow. The interface between these two zones is the surface of the sand bed and moves downwards with a vertical erosion velocity: $v_e$ (Figure 4.8). Net erosion takes place when the pick-up flux exceeds the sedimentation flux ($v_e > 0$). The erosion velocity is negative in case the sedimentation flux is exceeding the pick-up flux: settling takes place leading to an increase of the bed height. The eroding sand bed has a porosity $n_i$, while the eroding flow is considered to have a concentration $c$.

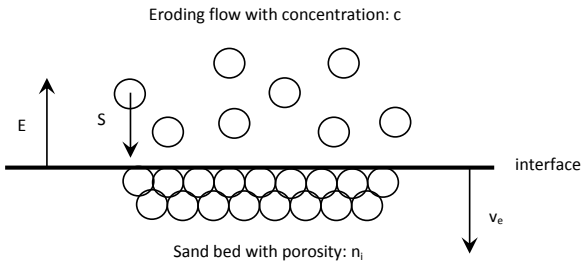


Figure 4.8: Volume of grains moving along moving interface

The flux of grains moving through the interface depends on the pick-up ($E$) and sedimentation flux relative ($S_{rel}$) to the interface. The relative sedimentation flux is defined as:

$$S_{rel} = \rho_s \cdot c \cdot (w_{hs} - v_e) \tag{4.5}$$

in which $w_{sh}$ is the settling velocity of single grains including the effect of hindered settling. The flux of grains moving through a downward moving interface is equal to the eroding flux of grains eroding from the sand bed:

$$E - S_{rel} = E - \rho_s \cdot c \cdot (w_{hs} - v_e) = \rho_s \cdot v_e \cdot (1 - n_i) \tag{4.6}$$

Equation (4.6) can be used to determine the erosion velocity:

$$v_e = \frac{E - S}{\rho_s \cdot (1 - n_i - c)} \tag{4.7}$$

It is questionable which value for the concentration ($c$) should be used in Equation 4.7. It influences the sedimentation flux as well as the effective settling velocity of grains including the effect of hindered settling. This concentration should be representing the concentration of the flow close to the top of the sand bed: the near-bed concentration ($c_{nb}$). However, the level at or height over which this near-bed concentration should be determined is unknown.

The value of the near-bed concentration was also addressed by Miedema and Ramsdell (2016) in case of heterogeneous slurry transport. Instead of using the formulation for the hindered settling velocity of grains: $w_{hs} = w_s \cdot (1 - c)^n$ (Richardson

and Zaki, 1954), in order to determine the concentration profile of a sand-water mixture, Miedema and Ramsdell (2016) developed an adapted equation for the hindered settling velocity incorporating the effect of the concentration gradient influencing the hydraulic pressure loss in case of heterogeneous slurry transport:

$$w_{hs} = w_s \cdot \left(1 - \frac{c}{0.175 \cdot (1+n)}\right)^n \tag{4.8}$$

As a result of the concentration gradient, the concentration close to the bottom of the pipe (near-bed concentration) will be higher than the average concentration. The factor $c/0.175 \cdot (1+n)$ is a measure for the quotient between the near-bed concentration ($c_{nb}$) and the average concentration of the flow ($c$). For small grains ($d_{50}$ < 70 $\mu$m) $n$ approaches to 4.65 giving for the factor $\frac{c}{0.175 \cdot (1+n)} \approx 1.05 \cdot c$. The near-bed concentration approaches the average concentration. This is in accordance with the concentration profile of sand-water mixtures consisting of relative small grains. For larger grains ($d_{50}$ > 1.5 mm) $n$ approaches to 2.39 and the near-bed concentration ($c_{nb}$) approaches to $1.69 \cdot c$. This means that the near-bed concentration is approximately 1.7 times the average concentration. At high average concentrations, this approach can not be valid, because the near-bed concentration can not exceed the bed concentration.

Besides, it should be noted that the near-bed concentration is also influenced by the shear velocity or bed shear stress, which is not taken into account in this approach. This approach is developed for heterogeneous slurry transport in case pick-up and sedimentation are in equilibrium. This is not the case during erosion as long as pick-up and sedimentation are not in equilibrium. In this case the near-bed concentration will be higher than during heterogeneous slurry transport and will be influenced by the shear velocity or bed shear stress.

### 4.3.2. Influence of transport capacity

When the pick-up exceeds the sedimentation flux the average concentration of the flow increases along the eroding sand bed. The concentration of the flow increases until the maximum transport rate ($Q_{t,max}$) of the flow is reached. In this situation the pick-up and sedimentation flux are in equilibrium (Figure 4.9). The length at which the maximum transport capacity is reached is defined as the adaptation length ($l_a$), see Section 4.7.

Experiments and mathematical modeling by Voogt et al. (1991) show this effect. In a flume with a length of 110 meter (length of test section 60 meter) erosion tests were carried out with sand with a grain size ($d_{50}$) ranging between 205 and 230 $\mu$m. The depth-averaged flow velocity during these tests ranged between 1.0 and 2.8 m/s. The water depth ($h$) during the test was 1.15 meter. The depth-integrated transport capacity was determined at two locations in the flume, showing an increase of the transport rate along the eroding sand bed. Figure 4.10 shows the results of a test with sand with a $d_{50}$ of 220 $\mu$m. The figure presents the measured relative transport rate ($Q_t/Q_{t,40}$: in which $Q_{t,40}$ represents the transport capacity at a distance of 40 m from the beginning of the sand bed in the flume) as function of the position of the sand bed in the test section ($x/h_f$). The calculated transport capacity, as shown in

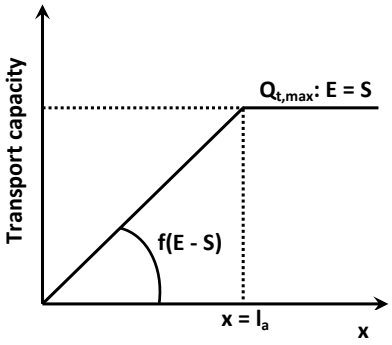


Figure 4.9: Transport capacity as function of the distance along the sand bed ($x/h_f$)



Figure 4.10, was based on a convection-diffusion equation (Voogt et al., 1991).

After calibration of the model with the measured transport capacity, the model was used to calculate the equilibrium or maximum transport capacity, which was assumed to be reached at coordinate $x/h_f = 200$. The increase of the transport capacity ($dQ_t/dx$) is directly related to the difference between the pick-up and sedimentation flux (Figure 4.10):

$$\frac{dQ_t}{dx} = E - S \tag{4.9}$$

Figure 4.10 shows that the transport capacity increases linearly with the distance to the beginning of the sand bed until $x/h_f = 30$. The sedimentation flux was negligible in this first section, because the concentration of sand in the eroding flow in this part was too low to cause any significant sedimentation flux. The erosion velocity ($v_e$) is directly related to the pick-up flux ($E$). After $x/h_f = 30$ the sedimentation flux increased significantly reducing the increase of the transport capacity as function of $x/h_f$. At $x/h_f = 200$ the pick-up flux is in equilibrium with the sedimentation flux ($E = S$: $v_e = 0$), meaning the maximum transport capacity is attained.

The effect of the transport capacity can also be determined by comparing the concentration in a situation in which the pick-up flux is developing along an eroding bed. The Rouse-profile is based on the balance between the downward-directed sedimentation flux and upward-directed turbulent diffusion of grains (Section 3.5.3). As long as the average concentration of a flow, with a pick-up flux exceeding the sedimentation flux, is smaller than the average concentration of a flow in which sedimentation and turbulent diffusion are balanced, the upward diffusion is enough to enable the increase of the average concentration (Figure 4.11). The pick-up flux can develop until sedimentation and pick-up flux are in equilibrium and the concentration profile meets the Rouse profile.

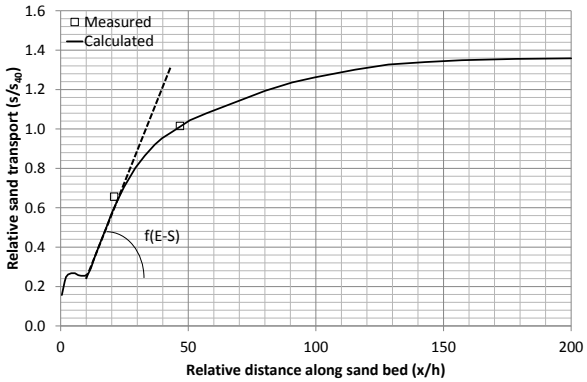


Figure 4.10: Relation between transport capacity and erosion velocity

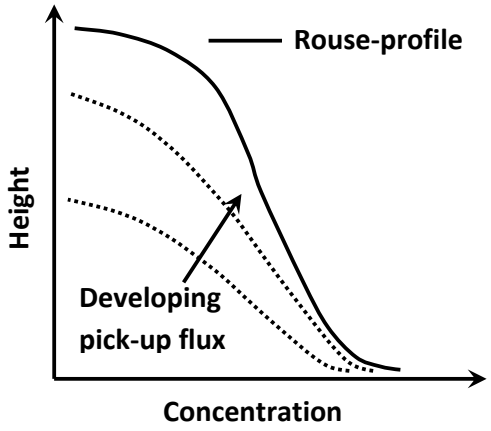


Figure 4.11: Developing concentration profile

## 4.4. Grain by grain erosion

In the grain by grain erosion regime the erosion process is dominated by the behavior (erosion) of separate grains (Bisschop et al., 2016). The most well-known pick-function in this regime is the empirical equation of van Rijn (1984a), see Equation (4.11). This equation is applicable for low flow velocities. Application of this equation at higher flow velocities gives a large overestimation of the pick-up flux as demonstrated by van Rhee (2010) and Bisschop et al. (2010). van Rijn (1984a) executed experiments to determine the pick-up rate of grains in the range of 130 $\mu$m up until 1500 $\mu$m. These tests were executed with depth-averaged flow velocities (in the center of the flume) ranging between 0.5 and 1.0 m/s. The bed shear stress varied between 0.5 and 2 Pa, corresponding to a Shields parameter ranging between 0.02 and 0.6. A Shields parameter of less than 0.6 means that the experiments were

mainly executed in the condition where erosion is defined by the pick-up of separate grains. Sheet flow conditions occur at a Shields parameter of more than about 0.5 to 1.0 indicating that the bed shear stress is too low to shear whole layers of sand (see Section 3.5).

The experimental set-up of van Rijn (1984a) was based on a flume with a vertical sediment lift, which was moved by an operator. The sediment lift was filled with different types of sand with an assumed porosity of 0.4. The bed shear stress was based on measurements of the local flow velocity close the bed. The bed shear stress was derived using:

$$u_* = \frac{u(z) \cdot \kappa}{ln\left(\frac{z}{z_0}\right)} \tag{4.10}$$



in which $\kappa$ is the constant of von Karman (= 0.4), $z$ is the vertical coordinate and $z_0$ is the zero velocity level: $0.11 \cdot (\nu_w/u_*) + 0.033 \cdot k_s$. The origin of the velocity profile ($z = 0$) was considered to be located at a distance of $0.25 \cdot d_{50}$ below the top of the grains. The effective roughness height ($k_s$) was considered to be equal to $2 \cdot d_{50}$. Analysis of the experimental data have yielded the following empirical pick-up function (van Rijn, 1984a):

$$E = 0.00033 \cdot \rho_s \cdot [\Delta \cdot g \cdot d_{50}]^{0.5} \cdot D_*^{0.3} \cdot T^{1.5} \tag{4.11}$$

in which $\Delta$ is the relative grain density: ($\rho_s$ - $\rho_w$)/$\rho_w$. Other erosion equations were developed by Nagakawa and Tsujimoto (1980):

$$E = \alpha \cdot \rho_s \cdot (\Delta \cdot g \cdot d_{50})^{0.5} \cdot \left[1 - \frac{0.035}{\theta_b}\right]^3 \cdot \theta_b \tag{4.12}$$

and Fernandez Luque (1974):

$$E = \alpha \cdot \rho_s \cdot (\Delta \cdot g \cdot d_{50})^{0.5} \cdot (\theta_b - \theta_{cr})^{1.5} \tag{4.13}$$

Equations (4.13) shows a close resemblance with the equation for the bed-load transport rate of Meyer-Peter and Müller (1948):

$$Q_t = 8 \cdot \rho_s \cdot d_{50} \cdot (\Delta \cdot g \cdot d_{50})^{0.5} \cdot (\theta_b - \theta_{cr})^{1.5} \tag{4.14}$$

Equation (4.12) and (4.13) yield the best results for grain sizes of $< 200$ $\mu$m. van Rijn (1984a) have fitted the factor $\alpha$ for the executed tests. The value of 0.02 proved to be the best fit for the results of the experiments with a grain size between 130 and 190 $\mu$m.

Figure 4.12 shows that the influence of the grain size on the pick-up flux according to Equation (4.11) (van Rijn, 1984a) is negligible, while Equations (4.12) and (4.13) show a significant influence of the grain size. The pick-up flux increases at a decreasing grain size. This is in line with the concept of grain by grain erosion. Small grains erode easier because their low resisting force to erosion, showing the dominance of the behavior of single grains in this regime.

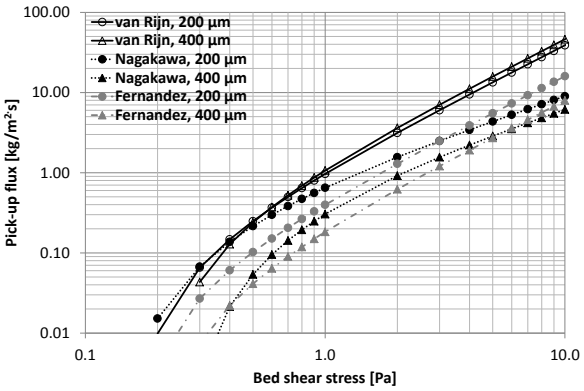




Figure 4.12: Pick-up flux according to Eqs. 4.11 (van Rijn, 1984a), 4.12 (Nagakawa and Tsujimoto, 1980) and 4.13 (Fernandez Luque, 1974) using Equation (4.1) for the critical Shields parameter

## 4.5. Dilatancy reduced erosion

The flow conditions during dilatancy reduced erosion are comparable to sheet flow. Both processes take place at a relatively high flow velocity (more than 1 m/s) and bed shear stress ($> 1.5$ Pa). For grains with a size between 100 and 500 $\mu$m this corresponds with a Shields parameter of 0.5 to 1.0. This criterion agrees approximately with the criterion for the beginning of sheet flow. Several experimental results (Gao, 2008) suggest that the sheet flow regime starts at a Shields parameter of 0.5. In this regime the bed is completely mobile resulting in sheared layers of grains (see Section 3.5). Dilatancy reduced erosion is based on the same process. At these conditions the pick-up flux is considered to be affected by the shearing of layers of sand. Depending on the in-situ porosity shearing can result in dilatancy, introducing a pore water under pressure and hence an inward hydraulic gradient into the sand bed (van Rhee, 2010). The pore water under pressure results in an increase of the effective stress and hence an increase of the resistance to shear and reduction of the pick-up flux. This effect introduces the effect of soil mass properties like dilatancy, relative density and permeability. For instance a low permeability ($k$) causes a relative high inward hydraulic gradient resulting in a relative high extra downward force on the eroding layers of grains and thus restricting the effective pick-up flux.

Similar behavior was encountered during the breaching process of a vertical wall of sand. Shearing of this vertical wall results in dilatancy, leading to pore water under pressures. As a result the effective stress increases, hence increasing the shear resistance. Breusers (1977) derived an equation for the active wall velocity (horizontal propagation velocity of a vertical wall of sand), introducing the effect of bulk properties like relative density and permeability.

### 4.5.1. Models

Winterwerp et al. (1992) are the first researchers publishing data of erosion experiments executed at a Shields parameter of more than 1 ($2 < \theta_b < 35$). The

corresponding bed shear stress is between 5 and 130 Pa. The research of Winterwerp et al. (1992) has been based on field surveys and laboratory experiments. The field surveys were executed during the construction of a sand dam close to an estuary. The erosion and sedimentation rates were observed during a sand-mixture flow (released from a pipe) between guide bunds of sand. The laboratory experiments were executed in a tilting flume. During the experiments a sand-water mixture flowed over a steep slope to establish supercritical flow. The slope was decreased up to the point where the growth of sand bars was observed. The slope just before the development of the sand bars has been used as the condition at which sedimentation and erosion were in balance (Winterwerp et al., 1992). The effective pick-up flux has been corrected for the sedimentation flux ($S$) including the effect of hindered settling [1]:



$$S = \rho_s \cdot w_s \cdot c \cdot (1-c)^n \tag{4.15}$$

Winterwerp et al. (1992) has used for $n$ a constant value of 4. The Shields parameter was calculated using:

$$\theta_b = \frac{f_b}{8} \cdot (1 + \Delta \cdot c_{av}) \cdot \left( \frac{U}{\sqrt{\Delta \cdot g \cdot d_{50}}} \right)^2 \tag{4.16}$$

in which $f_b$ is the Darcy-Weisbach friction coefficient as a result of flow along a sand bed (value based on grain size) and $c_{av}$ is the depth-averaged concentration of sand-water mixture. The near-bed concentration was assumed to be 0.35 for all experiments (Winterwerp et al., 1990). However, the exact level of the near-bed concentration was not defined. The approach of Winterwerp et al. (1992) does not incorporate the effect of the shearing of layers of sand during erosion on the effective bed roughness. Numerous publications mention the implicit relation between the bed shear stress and effective bed roughness. It is assumed that the roughness height during sheet flow conditions is influenced by the thickness of the mobile layer. The thickness of this layer is considerable larger than the size of the grains, resulting in a larger fictitious bed roughness and friction coefficient. This means that the shear stress is underestimated during these field survey and laboratory experiments. Nevertheless Winterwerp et al. (1992) have used these data to derive an empirical relation for the pick-up flux:

$$E = 0.012 \cdot \rho_s \cdot (\Delta \cdot g \cdot D_{50})^{0.5} \cdot D_*^{0.3} \cdot \left(\theta_b^{0.5} - 1.3\right) \tag{4.17}$$

The constant 1.3 limits the applicability of Equation (4.17) to the dilatancy reduced erosion regime. More recently, Mastbergen and van den Berg (2003) have

[1] It should be noted that in case the concentration ($c$) is equal to the concentration of the sand bed ($c_b$), the correction for hindered settling: $(1-c_b)^n$ should give a settling flux of 0. However, use of Equation 4.15 does not give this result. When the original approach of (Richardson and Zaki, 1954) is used, the settling flux at $c = c_b$ is not zero. Instead, a better approach for this term is proposed: $\left(1 - \frac{c}{c_b}\right)^{n_2}$. It should be noted that the coefficient $n$ should be adapted to $n_2$ in order to find the same correction for hindered settling in case the original approach is used for low concentrations.

developed an empirical equation including soil bulk properties like permeability, relative density and dilative behavior in order to describe the breaching process in fine sands. Mastbergen and van den Berg (2003) have derived an empirical pick-up function for the dilatancy reduced erosion regime, based on the data of van Rijn (1984a) and Winterwerp et al. (1992):

$$E = \rho_s \cdot (1 - n_i) \cdot \sqrt{\frac{0.018 \cdot (\theta_b - \theta_{cr})^{1.5} \cdot D_*^{0.3} \cdot k_{max} \cdot (1 - n_{max}) \cdot \sqrt{\Delta^3 \cdot g \cdot d_{50}}}{n_{max} - n_i}} \tag{4.18}$$

in which $k_{max}$ is the permeability at the maximum porosity of the sand bed. The critical Shields parameter is set on a fixed value of 0.06 and is comparable to the critical Shields parameter of sand with a grain size of approximately 150 $\mu$m. Equation (4.18) shows that the erosion rate increases as the permeability of the sand increases. Coarse sand will erode easier than fine sand because of its higher permeability. A high permeability means that the erosion of sand is less restricted by the inward flow of water into the sand bed as a result of the dilative behavior. However, at larger grain sizes ($d_{50} > 1$ mm) the effect of the inertia of the grains starts to influence the erosion process (see Figure 4.13), reducing the effective pick-up flux of coarse sand. The flow conditions and properties of the grains meet the grain by grain erosion regime, because the properties of single grains start to influence the pick-up flux.

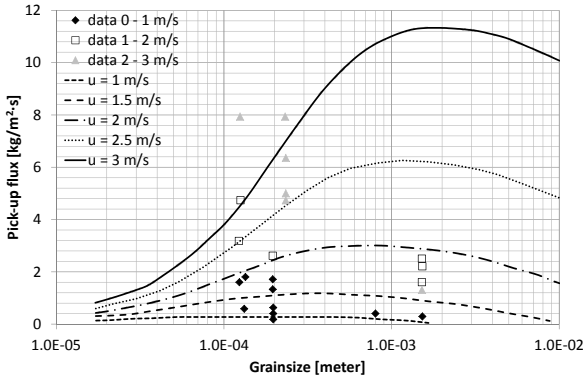


Figure 4.13: Pick-up flux as function of grain size (Mastbergen and van den Berg, 2003)

Later Mastbergen (2006) described a new empirical equation for high flow velocities:

$$E = 0.018 \cdot \rho_s \cdot \sqrt{\Delta \cdot g \cdot d_{50}} \cdot (\theta_b - 0.06)^{1.5} \cdot D_*^{0.3} \tag{4.19}$$

Equation (4.19) is not related to bulk properties as permeability and porosity. However, if Equation (4.19) is rewritten as a direct function of the grain size, this equation shows surprisingly a decreasing pick-up flux when the grain size increases

(increasing permeability). This is in contradiction with the concept of dilatancy reduced pick-up and the model published by Mastbergen and van den Berg (2003).

van Rhee (2010) has derived a model to adapt existing pick-up functions, applicable in the grain by grain erosion regime such as Equation (4.11), for high flow velocity erosion by taking into account the effect of the dilatant behavior of sand during shearing. The resulting shear stress of a flow over a sand bed causes shear of the top layer of the sand bed. The porosity of the top layer has a tendency to increase as a result of shear (dilatancy), resulting in pore water under pressures. This increases the effective stress and thus the resisting shear resistance of the sand bed. The pore water under pressure creates an inflow of water and the specific discharge into the sheared zone ($q$) as a result of the inward hydraulic gradient ($i$) as determined by the law of Darcy:



$$q = -k \cdot i \tag{4.20}$$

Equation (4.20) demonstrates that a low permeability limits the inflow rate of water and thus reducing the effective pick-up flux. van Rhee (2010) has incorporated this effect in an adapted critical Shields parameter ($\theta_{cr}^{'}$) for a flow over a horizontal bed:

$$\theta_{cr}^{'} = \theta_{cr} \cdot \left(1 + \frac{v_e}{k} \cdot \frac{n_l - n_i}{(1 - n_l) \cdot (1 - n_i) \cdot \Delta}\right) \tag{4.21}$$

in which $n_l$ is the porosity of the sheared layer. van Rhee (2010) has described that the critical porosity ($n_{cr}$) can be used as a measure for ($n_l$). The critical porosity is defined as the value of the porosity that will occur during shear after large deformations. Neither dilatation nor contraction will occur at this porosity. The critical porosity depends on the sand type and effective stress. At the top of a sand bed the effective stress is negligible. The effective stress will be mainly determined by the hydraulic gradient in the top of the sand bed. van Rhee (2010) has used $n_{max}$ as the best estimate for $n_l$. van Rhee (2010) has assumed this as reasonable, because the porosity has to increase to a porosity above the critical porosity and maybe even to a porosity above $n_{max}$, in order to make it possible for the flow to pick-up the grains. van Rhee (2010) has used Equation (4.11) to combine the concept of dilatancy reduced pick-up with the grain by grain erosion regime:

$$E = 0.00033 \cdot \rho_s \cdot (\Delta \cdot g \cdot d_{50})^{0.5} \cdot D_*^{0.3} \cdot \left(\frac{\theta_b - \theta_{cr}^{'}}{\theta_{cr}^{'}}\right)^{1.5} \tag{4.22}$$

However, other equations for the pick-up flux in the grain by grain erosion regime could also be used as long a they are related to $\theta_{cr}$). van Rhee (2010) has defined the inequality $v_e/k > 3$ as the condition at which the permeability starts to influence the erosion process (dilatancy reduced erosion regime). This criterion corresponds with a value for the Shields parameter just above the critical Shields parameter ($\approx 0.05$). This is far below the criterion for sheet flow and the bulk properties of the sand bed can not have influenced the pick-up flux. The bed shear stress at these

flow conditions is not large enough to shear multiple layers of sand. However, as a result of the upward movement of the grains, the grains are hindered by the flow of water around these grains. The resulting drag force reduces the entrainment of grains. So this criterion can be used as the condition at which dilatancy reduced erosion starts to influence the pick-up flux.

The criterion $v_e/k > 50$ to 100, for sand with a grain size between 200 and 400 $\mu$m, will represent the conditions at which multiple layers of sand are sheared. This criterion corresponds with a Shields parameter of 0.5 to 1.0. The conditions for the dilatancy reduced erosion regime are fully met.

Figure 4.14 compares the models of Winterwerp et al. (1992), Mastbergen and van den Berg (2003), Mastbergen (2006) and van Rhee (2010) for sand with a $d_{50}$ of 200 and 400 $\mu$m. This figure shows that the calculated pick-up flux according to Mastbergen (2006) significantly deviates from the other models including the opposite effect of the grain size on the pick-up flux.



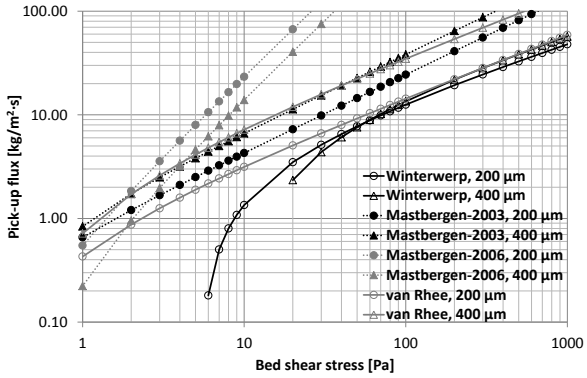


Figure 4.14: Pick-up flux according to Equation (4.17) (Winterwerp et al., 1992), (4.18) (Mastbergen and van den Berg, 2003), (4.19) (Mastbergen, 2006) and (4.22) (van Rhee, 2010)

### 4.5.2. Influence of bulk properties

The models in the dilatancy reduced erosion regime consider that in this regime bulk properties, like porosity and permeability, influence the erosion process. However, a limited amount of data is available in which the influence of these bulk properties is explicitly confirmed by experiments. Experimental results of Roberts et al. (1998) show the influence of the porosity, while the influence of the permeability is theoretically explained by van Rhee (2010) and compared to erosion experiments executed by Foortse (2016).

#### Porosity

Roberts et al. (1998) executed erosion experiments on silt and sand with an average grain size ($d_{50}$) ranging from 5.7 $\mu$m (fine silt) to 1350 $\mu$m (coarse sand). The results of these experiments show that for sand with a grain size up to 125 $\mu$m the pick-up

flux decreases as the porosity of the sand bed decreases (increasing bulk density: see Figure 4.15).

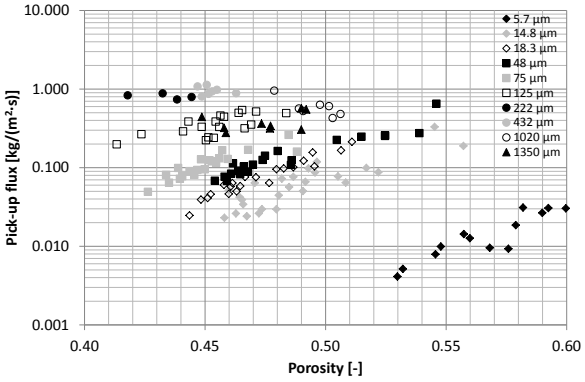


Figure 4.15: Pick-up flux as function of grain size and porosity at a bed shear stress of 1.6 Pa (Roberts et al., 1998)



However, the porosity does not influence the erosion rate for sand with a grain size of more than 125 $\mu$m. The Shields parameter during the experiments on the coarsest sand types ($d_{50} \geq 222$ $\mu$m) was less than 0.5, meaning that the condition for sheet flow was not met. This means that during these experiments erosion was determined by the behavior of single grains instead of layers of grains: grain by grain erosion regime. A bulk property as the porosity does not influence the pick-up flux in this regime.

### Permeability

The model of van Rhee (2010) theoretically explains the influence of the permeability on the pick-up flux. The results of the experiments of Roberts et al. (1998) show, implicitly, the influence of the permeability on the pick-up. Figure 4.15 shows, for a grain size of up to 222 $\mu$m, that the pick-up flux increases at increasing size of the grains. This effect can be explained by the effect of the grain size on the permeability. The permeability of sand increases at increasing grain size. In case of dilatancy reduced erosion a higher permeability results in a relative low hydraulic gradient, causing a lower reduction of the pick-up flux in comparison with sand with a lower permeability and consisting of smaller grains. It should by noted that for the finest sand types ($d_{50}$: 5.7, 14,8 and 18,3 $\mu$m) van der Waals forces can have influenced the pick-up flux. These forces cause a kind of cohesive effect and increase the critical Shields parameter for inert (quartz) silt in comparison with coarser material (Miedema, 2013). This effect could have been also (partly) responsible for the reduction of the pick-up flux.

Recently Foortse (2016) executed erosion experiments on two types of sand, mixed with different amounts of bentonite. Bentonite is a clay with a high swelling capacity, reducing the permeability when mixed with sand. Figure 2.4 shows the influence of bentonite on the permeability of sand with an average grain size ($d_{50}$) of

125 $\mu$m and 256 $\mu$m. Direct shear tests revealed that up to 10% of added bentonite the friction characteristics of the sand types did not change in comparison with sand without bentonite, meaning that the typical behavior for sand (drained behavior) was maintained during these experiments. The friction angle of 150 $\mu$m sand varied between 38° and 43° and for the sand with a $d_{50}$ of 256 $\mu$m values between 34 and 37° were measured.

Foortse (2016) executed the erosion experiments in an open flume with a width of 0.145 m. Flow velocities were varied between 1 and 2 m/s. The porosity of the sand-bentonite mixture was between 0.40 and 0.41. Figure 4.16 shows the measured pick-up flux as function of the permeability for a flow velocity of approximately 1.1 and 2.0 m/s. The results show that for sand with an average grain size of 256 $\mu$m the pick-up increases as function of the permeability at a flow velocity of 1.1 and 2.0 m/s. The sand with an average grain size of 150 $\mu$m also shows an influence of the permeability at a flow velocity of 2.0 m/s. Besides the influence of the permeability on the pick-up flux, the results show also an influence of the grain size on the pick-up flux. This could be caused by the fact that the condition for dilatancy reduced erosion of $v_e/k > 3$ was not met for all experiments.

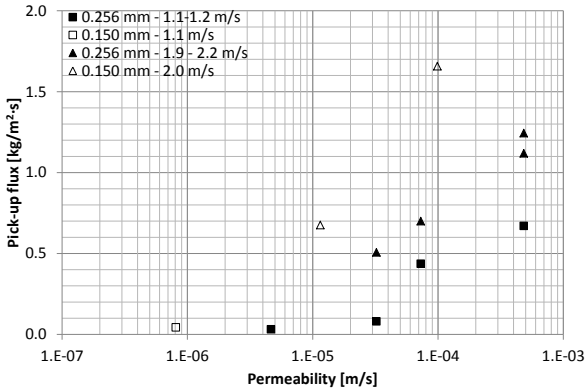


Figure 4.16: Pick-up flux as function of permeability (Foortse, 2016)

### 4.5.3. Theoretical approach dilatancy reduced erosion

Instead of the approach of van Rhee (2010), adapting an existing pick-up function with the effect of dilatancy reduced erosion, the pick-up flux can be derived directly from the theory of dilatancy reduced erosion. This model is based on a flow exerting a horizontal force ($F_b$) resulting in a sheared layer of sand, dilating with a thickness $h_s$, while the erosion front moves down with a velocity $v_e$ (erosion velocity), see Figure 4.17. The horizontal forces, as exerted by the flow over the bed, should be in balance with shear resistance caused by:

- shear resulting in a sheared layer with thickness $h_s$: the resisting force depends on the effective stress, increased by the influence of the resulting inward

hydraulic gradient into the sand bed and the angle of internal friction ($\phi$): $F_w$;

- the horizontal acceleration of the sheared layer and horizontal force required to induce a vertical acceleration: $F_{acc}$.

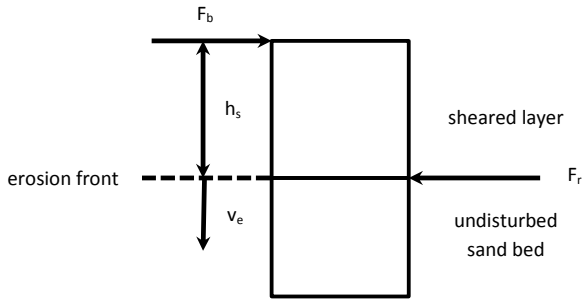


Figure 4.17: Theoretical approach dilatancy reduced erosion

Under steady-state conditions the horizontal forces exerted by the flow on the sand-bed should be in balance with the resisting horizontal forces ($F_r = F_w + F_{acc}$):

$$F_b = F_w + F_{acc} \tag{4.23}$$

Lu (2012) concluded on the basis of a comparison of the results of the erosion experiments of Bisschop (1993) and Bisschop et al. (2016) with the approach as mentioned above, that the effect of inertia can be neglected during erosion up to depth-averaged flow velocities of 5 m/s for sand with a grain size between 80 and 562 $\mu$m. Neglecting the effect of inertia, this leads to the following equilibrium:

$$F_b = F_w \tag{4.24}$$

with $F_b = \tau_b \cdot A$ and $F_r = \tau_r \cdot A$ this results in:

$$\tau_b = \tau_r \tag{4.25}$$

Effect of effective stress and friction

The resisting shear stress ($\tau_r$) is determined by the effective stress and friction of the dilated layer:

$$\tau_r = \sigma_z' \cdot tan\phi = (1 - n_i) \cdot (\rho_s - \rho_w) \cdot g \cdot h_s \cdot tan\phi \tag{4.26}$$

The porosity ($n_i$) can be assumed as the average porosity of the sheared layer. The porosity above the non-disturbed bed increases linear as function of the distance to the non-disturbed bed (see Section 3.5.3).

Effect of inward hydraulic gradient

The inward hydraulic gradient results in an increase of the effective stress resulting in an increase of the resisting shear stress ($\tau_{dil}$) of:

$$\tau_{dil} = i \cdot \rho_w \cdot g \cdot h_s \cdot tan\phi \tag{4.27}$$

The hydraulic gradient during erosion matches (van Os and van Leussen, 1987), (van Rhee, 2010):

$$i = \frac{v_e}{k} \cdot \frac{n_{max} - n_i}{1 - n_{max}} \tag{4.28}$$

Combining Equation (4.24), (4.26), (4.27) and (4.28) provides a solution for the erosion velocity:

$$v_e = \frac{k \cdot (1 - n_{max})}{n_{max} - n_i} \cdot \frac{\tau_b - (1 - n_{max}) \cdot (\rho_s - \rho_w) \cdot g \cdot h_s \cdot tan\phi}{\rho_w \cdot g \cdot h_s \cdot tan\phi} \tag{4.29}$$

The unknown in Equation (4.29) is the thickness of the sheared layer. Because this parameter depends on the effective stress including the effect of the inward gradient during the erosion, this parameter can not be determined directly.

### 4.5.4. Effect of Suction

Numerous studies are executed concerning the influence of suction and injection on the moment of incipient motion of grains (critical Shields parameter). Jacobsen and Magda (1988) are two of the few researchers who studied the effect of suction and injection on the pick-up flux of sand (Figure 4.18). The results of these experiments show that an outward gradient of water (injection of water into the flow) gives a slight reduction of the flow rate for the incipient motion of the grains. However, the curves (A and B) for the pick-up flux above incipient motion are nearly identical. Suction (flow of water into the sand bed) increases the resistance against motion and decreases the pick-up flux as function of the flow velocity (A and C). This effect is consistent with the theory of dilatancy reduced erosion.

### 4.5.5. Forced Suction and Sediment Transport

Section 4.2.3 describes the effect of suction and injection on the critical Shields parameter, being a key issue for dilatancy reduced pick-up. Studies regarding the effect of forced inflow of water in the sand bed (suction) on sediment transport and scour show different effects, comparable to the effect on the critical Shields parameter as described in Section 4.2.3. Forced suction can lead to an increase as well as a decrease of sediment transport. Suction changes the near-bed flow field (Section 4.2.3). This effect increases the driving force on sand grains, hence increasing sediment transport rates. The opposite effect is the result of the vertical flow through the sand bed leading to an extra downward drag force, hence increasing the effective weight of the grains. This reduces bed load transport (Cao and Chiew, 2013). The dominating effect depends on the flow conditions, amount of suction and bulk properties (permeability and porosity) of the sand bed.

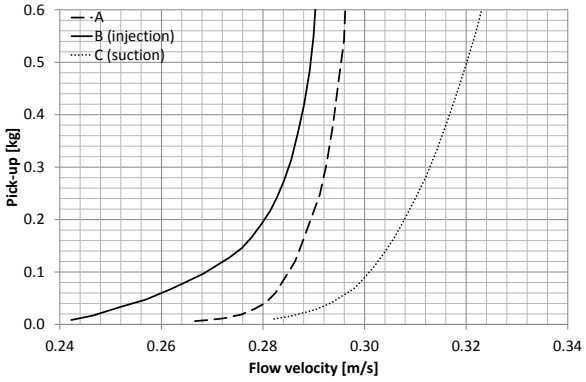




Figure 4.18: Pick-up of sand after 30 minutes as function of the flow rate: A = no pressure gradient, B = injection and C = suction (Jacobsen and Magda, 1988)

Two experimental studies as reported by Cao and Chiew (2013) show that suction increases bed load transport in closed-conduits as well as in open channel flows. The change of the near-bed flow field is considered to be dominant over the effect of the vertical flow increasing the effective weight of the grains. Other studies show an opposite effect on sand transport. In the experiments of Brink and Oldenziel (1974) suction decreases the rate of sand transport, while also an increase of the horizontal near-bed flow velocity was reported. These results show that the effect of suction on the effective weight of the grains dominated. Soltani-Gerdefaramarzi et al. (2014) show a similar effect of bed suction. Their experiments, on scouring around a circular pier, showed that suction leads to a reduction of the development of the scour depth. These different effects of suction were also noted by a summary of different studies presented by Jahan (2014).

## 4.6. Bulk erosion

Cao (1997) has presented a theoretical model including the influence of turbulence on the pick-up flux of grains. Most empirical and theoretical models assume that the driving force for erosion is determined by a an average horizontal shear stress acting on a horizontal eroding sand bed. However, turbulent flows are characterized by turbulent bursts consisting of repeatable and cyclic fluid motions referred to as ejection and sweep events (Cao, 1997). This means that under turbulent conditions the sand bed is subject to changing loads. Turbulent sweeps exert temporarily a vertical downward force on the sand bed, while during ejections the turbulent streaks move in vertical direction moving grains to upper parts of the flow (see Chapter 3).

The model of Cao (1997) was based on assumptions regarding the time and length scale of turbulent bursting and assumes one layer of grains is eroded over the area of all bursts per unit of bed area. The time scale of the turbulent bursts: $T_B$ is based a non-dimensional bursting period: $T_B^+ \approx 100$ (Luchik and Tiederman, 1987) and is expressed as:

$$T_B = \nu_w \cdot \frac{T_B^+}{u_*^2} \tag{4.30}$$

The amount of characteristic turbulent bursts per unit bed area depends on the dimensions and spacing of the bursts. In smooth wall circumstances the scale of the bursts is in axial direction of the flow about 40 $\cdot\nu_w/u_*$ and in transverse direction 25 $\cdot\nu_w/u_*$. The spacing of the burst in axial and transverse direction is 500 $\cdot\nu_w/u_*$ respectively 100 $\cdot\nu_w/u_*$ (Nezu and Nakagawa, 1993). This means for the averaged area of all bursts per unit of bed area ($\lambda_b$):

$$\lambda_b = 40 \cdot 25 / (500 \cdot 100) = 0.02 \tag{4.31}$$



Cao (1997) has assumed that the flow depth has no influence on turbulence bursting, as based on several studies and experiments on sediments entrainment in relation to flow depth. The influence of grains and associated wall roughness on the bursting process, however, is not well known. Limited data is available regarding the influence of grains on the bursting process. Besides this, Cao (1997) has discussed the influence of the size difference of the bursts and the ability to pick-up grains from the sand bed. Only sufficiently energetic bursts of enough large scale are able to o pick-up grains. However, limited information is available regarding the influence of the bed shear velocity on the ability to pick-up grains from the sand bed. Based on a theoretical study Aseada et al. (1989) have proposed that the fraction of area from which grains are picked up increases with the Shields parameter. Cao (1997) has used this assumption to quantify the influence of the bed shear stress on the pick-up flux by relating the amount of bursts per unit bed area to the bed shear velocity and critical bed shear velocity for initial motion of grains ($u_{*c}$) according to:

$$A = \lambda_b \cdot \left(u_*^2/u_{*c}^2\right) \tag{4.32}$$

The sediment pick-up flux (mass flux) is:

$$E = \frac{A \cdot N \cdot \rho_s \cdot \pi \cdot d^3}{6 \cdot T_B} \tag{4.33}$$

with $N$ as the number of grains per unit bed area: $6 \cdot (1 - n_i)/\pi \cdot d^2$. Using Equation (4.30), (4.31), (4.32) and (4.33) Cao (1997) defined the turbulent bursting based pick-up flux:

$$E = \lambda_b \cdot \frac{\left(u_*^2 - u_{*c}^2\right) \cdot u_*^2 \cdot (1 - n_i) \cdot \rho_s \cdot d}{u_{*c}^2 \cdot \nu_w \cdot T_B^+} \tag{4.34}$$

Cao (1997) has compared this model with the experimental results of van Rijn (1984a) and has concluded that for sand with a grain size between 130 and 1500 $\mu$m the model agrees well with these data. It should be noted that the flow velocity of these experiments was within the grain by grain erosion regime, making this pick-up function only applicable in the erosion regime. The model of Cao (1997) gives in the

grain by grain erosion regime comparable results as Equations (4.12) and (4.13) as shown in Figure 4.19. Remarkably the model of Cao (1997) shows that sand with a larger grain size will have a larger pick-up flux in comparison with sand with a smaller grain size. This is in contradiction with Equations (4.12) and (4.13) and the concept of grain by grain erosion, in which the pick-up flux is considered to decrease at increasing size of the grains. A possible explanation for this defect is the assumption of Cao (1997) that each burst erodes a layer of grains with a thickness equal to the grain size, neglecting the influence of the higher weight of larger grains in comparison with smaller grains.

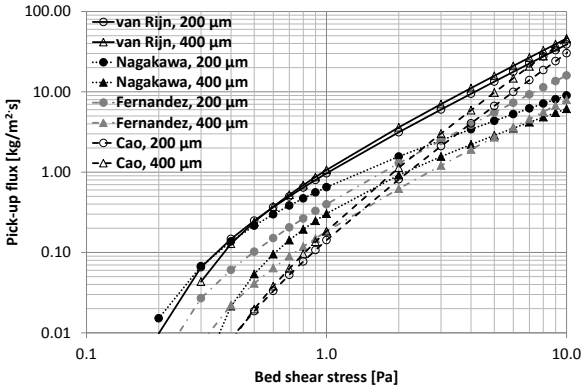


Figure 4.19: Pick-up function of Cao (1997) in comparison with pick-up functions valid in the grain by grain erosion regime

## 4.7. Adaptation length

Visser (1998) has used the adaptation length ($l_a$) to model the erosion of a breach in a dike. The adaptation length is defined as the distance a flow along an eroding sand bed needs to develop the full transport capacity ($s_{max}$) (Galappatti, 1983):

$$Q_t(x) = \left(\frac{x}{l_a}\right)^{n_1} \cdot Q_{t,max} \tag{4.35}$$

For large values of $u_*/w_s$, $n_1$ is equal to 1. The adaption length can be approximated by (Galappatti, 1983):

$$l_a = \xi \cdot \frac{U \cdot h_f}{w_s} \tag{4.36}$$

in which $\xi$ is a coefficient being about equal to 0.4 in case of a (nearly) uniform flow (Visser, 1998) and $h_f$ is the flow height. This approach differs from the results of Voogt et al. (1991). Galappatti (1983) has assumed a linear increase of the transport rate as function of the flow distance, while the experimental results as well as the results of the calculations of Voogt et al. (1991) show a decrease of

$ds/dx$ as function of the flow distance. A linear increase of the transport rate means that the sedimentation flux is neglected: $dQ_t/dx = E$ in the approach of Galappatti (1983). Neglecting $Q_t$, by combining Equations (4.9), (4.35) and (4.36) a relation between the pick-up flux, adaptation length and maximum transport rate can be derived:

$$E = \frac{w_s}{U \cdot h_f} \cdot Q_{t,max} \tag{4.37}$$

In Equation (4.37) the pick-up flux seems to decrease as function of the flow velocity, however it should be noted that the transport capacity increases as function of the flow velocity ($U^n$). Because the constant n is mainly larger than 1, the pick-up flux increases as function of the depth-averaged flow velocity.



## 4.8. Hindered erosion

Hindered erosion is defined as the influence of high concentrations of grains suspended in the flow close to the bed and turbulent eddies hindering the pick-up of grains from the bed. This effect can be explained by the effect of suspended grains close to the bed, colliding with eroding grains and ticking them back to the bed. Besides this suspended grains will suppress the effect of turbulence close to the top of the bed.

Winterwerp et al. (1992) observed that the pick-up was limited by the concentration of the sand-water mixture. At higher concentrations of the eroding sand-water mixture the maximum attainable pick-up flux is lower (Figure 4.20). In this figure the pick-up flux flux was corrected for the sedimentation flux of the grains in order to derive the effective pick-up flux ($E$). This means that the reduction of the entrainment of the eroded grains into the eroding sand-water mixture can only be affected by the influence of suspended grains on eroding grains (hindered erosion), analogous to the effect of hindered settling (Winterwerp et al., 1992). This influence of this effect was described by the following empirical equation ($E_h$: pick-up flux including the effect of hindered erosion):

$$E_h = 0.033 \cdot \rho_s \cdot \sqrt{\Delta \cdot g \cdot d} \cdot \left[ \frac{1 - n_i}{c} - 1 \right] \tag{4.38}$$

Equation (4.38) shows that erosion with clear water ($c = 0$) will affect in an infinite pick-up flux. It means that this equation can only be used for concentrations of 0.1 or more.

The effect of hindered erosion was also addressed by van Rhee and Talmon (2010). They have defined a reduction factor incorporating the effect of the near-bed concentration on the net pick-up flux:

$$E_h = E \cdot \frac{1 - n_i - c_{nb}}{1 - n_i} \tag{4.39}$$

Their approach is based on the assumption that the pick-up flux is determined by turbulent bursts (Cao, 1997). Due to these bursts grains are not only picked up.

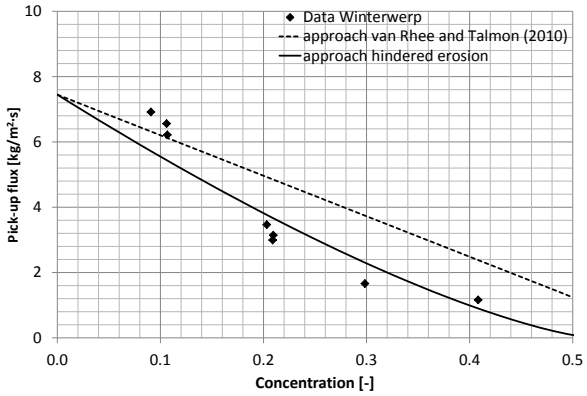




Figure 4.20: Maximum pick-up flux, corrected for the sedimentation flux, influenced by the concentration of the eroding flow (Winterwerp et al., 1992), including the concept of hindered erosion ($n = 1.38$ and $E = 7.45$ kg/(m$^2$·s))

Part of the suspended grains will be transported back to the bed surface hindering and reducing the pick-up. van Rhee and Talmon (2010) checked the validity of Equation (4.39) on the basis of the results of erosion experiments on three sand types in a rectangular measurement section. The data of these experiments, as presented in Figure 4.21, show the hindered pick-up flux ($E_h$) and net pick-up flux ($E$), using Equation (4.39). Comparison of the hindered pick-up and net pick-up flux shows that the scatter of the data of the experiments is reduced and the erosion behavior of the three sand types is more distinctive, when using Equation (4.39). This indicates that the effect of hindered erosion, can be determined according to Equation (4.39). However, this approach does not fit the data of Winterwerp et al. (1992) (Fig. 4.20).

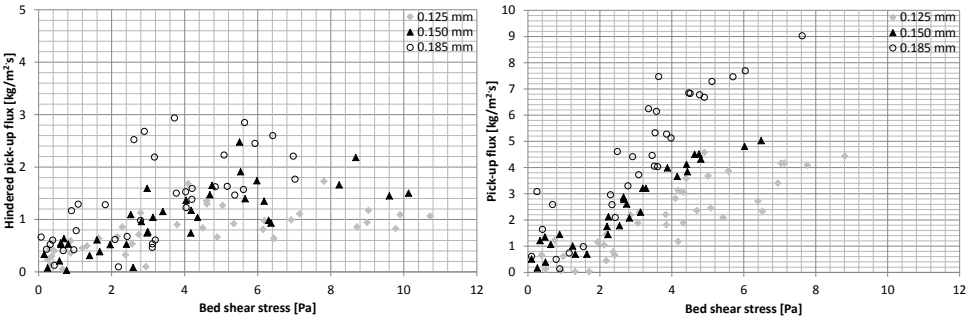


(a) (b)

Figure 4.21: Hindered pick-up ($E_h$) as function of bed shear stress (a) and net pick-up flux ($E$) as function of bed shear stress (b) for sand with a $d_{50}$ of 125, 150 and 185 $\mu$m (van Rhee and Talmon, 2010)

Another approach to incorporate the effect of the concentration of the sand-water mixture can be based on the reversed concept of hindered settling according to Richardson and Zaki (1954):

$$E_h = E \cdot \left(1 - \frac{c}{1 - c_{max}}\right)^n \tag{4.40}$$

This approach limits the concentration to the maximum concentration ($c_{max}$), which can be considered as $1 - n_{max}$. This approach coincides well with the data of Winterwerp et al. (1992) for $n = 1.38$ and $E = 7.45$ kg·m$^2$/s (Figure 4.20).

## 4.9. Discussion



Figure 4.22 shows the different erosion regimes after the flow conditions exceed the critical Shields parameter: grain by grain erosion regime and the dilatancy reduced erosion regime. The driving force could be horizontal or vertical oriented. The driving force of the main existing pick-up functions are based on a horizontal oriented bed shear stress. Both regimes are influenced by hindered erosion and the transport capacity of the eroding flow.

The so-called Shields curve gives a good indication of the flow conditions at which grains start to erode. Recently Miedema (2012a) developed a full theoretical model, using rolling or sliding as the main mechanism for the initiation of motion, to match the Shields curve and several measurements from literature. This models includes the effect of the exposure level of the grains, flow velocity profile close to the sand bed, drag and lift and the influence of the velocity fluctuations as a result of turbulence. It should be noted that the Shields curve does not predict the exact moment at which single grains start to move. Grains could start to move at a lower or higher Shields parameter due to differing exposure levels and the influence of turbulence. Miedema (2012a) showed that the Shields curve (Figure 4.1) corresponds with approximately 100 to 1000 moving grains per m$^2$ or transport conditions like the general transport of grains: almost all grains at the top of the sand bed are mobile.

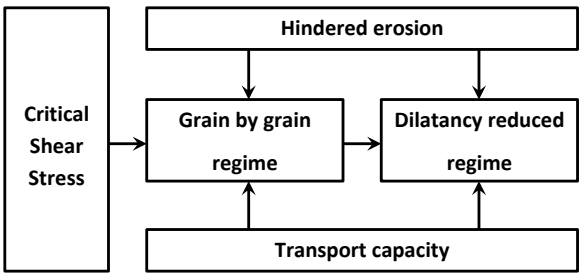


Figure 4.22: Overview different erosion regimes and processes influencing conditions

After exceeding the Shields curve the pick-up flux increases. Up to a flow velocity of approximately 1 m/s and/or Shields parameter of 0.5, the pick-up flux is

dominated by the properties of the grains, like size and density. In this regime the erosion process is assumed to be dominated by the erosion of single grains which are entrained into the eroding flow: the grain by grain erosion regime. Empirical pick-up flux models like that of van Rijn (1984a) are applicable in this regime. Theoretical models are not available, however Cao (1997) made a first attempt to include the effect of turbulent bursting in a pick-up function. However, this function showed an increasing pick-up flux for grains of larger size. This is in contradiction with the concept of grain by grain erosion. This effect was caused by the assumption that turbulent bursts erode a single layer of grains with a thickness equal to the size of the grains.

At higher flow velocities and/or Shields parameter layers of grains start to shear like in sheet flow conditions ($\theta > 0.5$ - 1.0). Winterwerp et al. (1992), Mastbergen and van den Berg (2003) and van Rhee (2010) have considered that shearing leads to the influence of the bulk properties of sand, like porosity and permeability. In case of compacted sand, shearing leads to dilatant behavior. During the shearing the volume of the voids between the grains increase, resulting in pore water under pressures. The resulting inward hydraulic gradient increases the stability of the sheared layer and stability of individual grains at the surface, reducing the pick-up flux. This is known as the dilatancy reduced erosion regime.



The same behavior is encountered during experiments, executed with forced suction of water into the sand bed. Suction causes an extra downward resisting force on the sand bed, hence reducing erosion. Suction has also an additional effect. The flow velocity directly above the top of the sand bed increases. This leads to a larger shear force on the grains, hence increasing erosion instead of reducing erosion. The inward gradient depends on suction velocity and the permeability of sand. Depending on the permeability of the sand bed, suction volume and flow conditions, the effect of the changing flow field or the effect of the downward hydraulic gradient will prevail.

The models of Winterwerp et al. (1992) and van Rhee and Talmon (2010) consider a driving force, modeled as an average shear force at the top of the bed. However, due to turbulence the size and direction of the forces on the sand will vary. Turbulent bursts lead to vertical forces on the sand bed introducing bulk erosion by single grains or lumps of sand. The dimensions and energy of these bursts determine the amount of grains entrained in the flow (Cao, 1997). In case only grains are picked up by the turbulent eddies, this process is equivalent to the grain by grain erosion regime. However, only the driving forces are defined in another way. Higher vertical stresses will lead to shear following a shear plane according to the wedge of Prandtl (Section 2.3.3). This introduces the influence of the angle of internal friction of the sand and dilatancy, leading to the influence of the permeability of sand to the shearing resistance, comparable to the dilatancy reduced erosion regime. This failure mechanism is not incorporated in the model of Cao (1997).

Other aspects influencing the pick-up are the density of the eroding flow and the size of single grains. Winterwerp et al. (1992) and van Rhee and Talmon (2010) have noticed that, despite their measurements of the pick-up flux were corrected for the sedimentation flux from the eroding flow, the pick-up flux decreases due to the

presence of grains in the eroding flow. Like hindered settling, grains in the eroding fluid hinder eroding grains: hindered erosion. However, this is out of the scope of the present study, Mastbergen and van den Berg (2003) have noticed that at flow velocities of more than 1.0 m/s for grains with a size larger than 1 mm the size of the grains still affects the pick-up flux the to the effect of inertia to accelerate grains of this size. The erosion regime changes to the grain by grain erosion regime as is also shown by the experiments of Roberts et al. (1998).

The above analysis shows that the erosion process at flow velocities of more than 1 m/s and a Shields parameter of more than 0.5 is yet not well understood. The amount of erosion experiments showing the behavior of the sand bed and pick-up of (layers of) grains is limited. The models of Winterwerp et al. (1992), Mastbergen and van den Berg (2003) and van Rhee (2010) consider that the fluid exerts an average bed shear stress acting in horizontal direction, while turbulence causes that the forces on the bed vary in direction and size as a result of turbulent sweeps and injections. This results in fluctuations of the normal stress on the bed, influencing the pick-up. Cao (1997) is the first researcher who has considered this effect. He incorporates the effect of fluctuations of the normal stress on the sand bed: like size and time scale of the turbulent sweeps. However, this model does not incorporate the effect of the stress on the sand bed and resisting force of the sand bed to shear.

# 5

# Experiments

## 5.1. Introduction

Chapter 4 shows that different erosion regimes exist and that in the dilatancy erosion regime the bulk properties of the sand bed influence erosion. In the dilatancy erosion regime it is assumed that the erosion process is determined by the shearing of layers of sand. However, another publication stresses the effect of the turbulence of the flow on the erosion process. The amount of data and range of flow velocities of existing experimental studies is too limited for a proper validation of the dilatancy reduced erosion regime and/or effect of the turbulence of the flow on the erosion process.

The effect of bulk properties of sand, as permeability and porosity, has been investigated by Bisschop (1993) and Roberts et al. (1998), although the flow velocity during these experiments was limited to 1 and 1.5 m/s. Winterwerp et al. (1992) and Mastbergen and van den Berg (2003) have presented data at higher values of the flow velocity (up to 3 m/s) and Shields parameter (up to 30). However these data were too limited for a proper validation of the erosion process of more than 1 m/s. In order to study the erosion process, check the effect of the bulk properties of sand on the erosion process and to gather more data of erosion experiments at flow velocities between 2 m/s and 6 m/s, erosion experiments were executed.

The erosion experiments were executed in an adapted closed flume of the slurry transport circuit of the Dredging Research Laboratory of Delft University of Technology (Section 5.2). The experimental set-up already has been shortly described by Bisschop et al. (2016). Specific instruments were mounted in order to measure certain parameters during the erosion process, like the discharge and pressure gradient in the measurement section. Before the execution of the experiments the conductivity probes were calibrated and the frictional characteristics of the measurement section were determined, to be able to derive the effective bed shear stress along the top of the eroding sand bed (Section 5.3). In order to determine the density of the sand and study the concentration profile during the erosion experiments, the

conductivity probes were calibrated for the influence of the temperature, type of sand and composition of the water used to execute the experiments.

Four types of sand were selected for the erosion experiments. Three of these types were selected because their grain size and behavior were comparable to sand types encountered during dredging and sand types present in dikes in the Netherlands. The fourth type of sand was selected for an extra check of the theory of dilatancy reduced erosion. This type consisted of very fine material ($d_{50}$ = 51 $\mu$m), leading to a very low permeability in comparison with the other sand types. A relative low permeability should lead to dilatancy reduced erosion at relative low flow velocities (1 m/s to 2 m/s) in comparison with the other sand types. The main mineral constituent of all four sand types was quartz, leading to a comparable physical behavior. Section 5.4 describes the properties of these four sand types.

Two series of erosion experiments were executed. The first series was executed in order to test and improve the experimental set-up. The second series consisted of 4 sets of experiments, each set was executed on a different type of sand. Per set different experiments were executed in order to investigate the influence of the flow velocity, type of sand, density of the sand bed and density of the eroding flow on the erosion process. Each experiment was executed in 5 consecutive tests in order to calibrate and check several instruments before and during each experiment. The experimental procedure and the varied operational conditions during the experiments are described in Section 5.5. Section 5.6 gives an overview of the main findings regarding the behavior and exhibits of the experimental set-up and used sand.



## 5.2. Experimental set-up

### 5.2.1. Experimental arrangement

The test arrangement consisted of a closed circuit in which a sand-water mixture was pumped through a parallel system of a measurement section and a by-pass (Figure 5.1). The measurement section was rectangular and had an internal height of 288 mm, a width of 88 mm and a length of 6.25 m. The sand was added to the circuit using a silo. The sand-water mixture was pumped through the circuit (diameter main line is 0.15 m) at a velocity, which was higher than the limit deposit velocity of the mixture. The sand bed was created by lowering the flow velocity in the measurement section by (partly) closing the valve to the measurement section (Figure 5.2a). The by-pass was kept open ensuring that the flow velocity in the whole slurry circuit stayed above the deposition velocity, preventing the circuit from being blocked by deposited sand. The valve to the measurement section (valve 1.2, Figure 5.2b) was completely closed after a sand bed with a height varying between 0.15 to 0.20 m was created. The remaining sand in the circuit was discharged to the slurry tank. Before the actual erosion experiment was executed, a slurry with the desired density for the erosion test was pumped through the whole slurry circuit via the by-pass, while the measurement section remained closed. The erosion test was started by tuning the pump at the desired rotation speed and opening the valve to the measurement section. The eroding slurry flowed over the created sand bed, starting the erosion process. The by-pass was kept open during the erosion experiments.

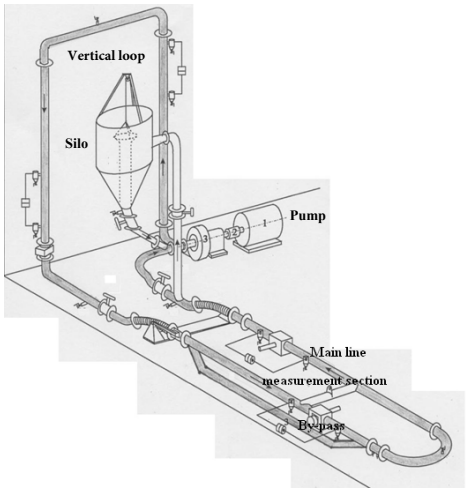




Figure 5.1: Slurry transport circuit consisting of pump, vertical loop, silo, main line, by-pass and measurement section

### 5.2.2. Instrumentation

The slurry transport circuit was equipped with the following instruments:

- radio active density meter measuring the spatial concentration in the measurement section. These measurements were also used to calibrate the conductivity probes.
- conductivity probes at different vertical levels in the measurement section: due to the difference of the electrical conductivity of water and sand the height of the level of the sand bed could be determined during the erosion experiments;
- relative pressure gauges measuring the pressure gradient in the measurement section;
- relative pressure gauges in the vertical loop to determine the density of the sand-water mixture;
- relative pressure gauges to measure pore water pressures in the sand bed;
- two electromagnetic flow meters to measure the total discharge through the slurry circuit and the discharge through the measurement section;
- two-axis electromagnetic flow meter;
- temperature sensor.

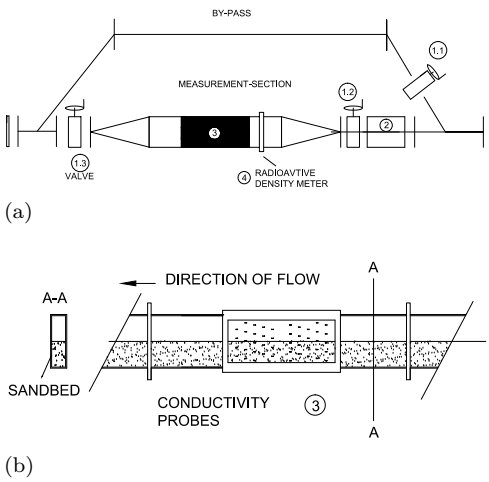


Figure 5.2: Overview and outline measurement section with: 1.1 to 1.3 = butterfly valves, 2 = electromagnetic flow meter, 3 = location conductivity probes and 4 = radio active density meter

5

The spatial concentration of density of the sand-water mixture and sand bed was determined with the radio active density meter. The vertical level of this instrument was adjustable. The measurements with this instrument were also used to calibrate the conductivity probes. The conductivity probes consisted of two transducers (diameter 3 mm) placed 8 mm from each other. Fifty six conductivity probes were mounted in a non-conducting lexan plate in a sloping matrix (see Figure 5.3a). Each conductivity probe was located in horizontal direction 50 mm and in vertical direction 5 mm from the surrounding probes, preventing that the probes influenced each other. This caused that consecutive probes in vertical direction did not have the same horizontal location (see Figure 5.3b). During the erosion experiments the potential difference over 16 probes was measured (Figure 5.4), resulting in a vertical and horizontal distance between the connected probes of 10 and 100 mm.

The pressure gradient measurements were necessary in order to determine the effective bed shear stress during the erosion experiments. The overall density of the sand-water mixture was measured in the vertical loop of the slurry circuit. This was executed by measuring the pressure gradient in the upward and downward section of the vertical loop (Figure 5.1). The pore water pressures in the sand bed before and during the erosion process were measured in the second series of experiments (see Section 5.5.2) with relative pressure gauges, mounted at a certain level above and in the sand bed. The electromagnetic flow meters were used to control the flow velocity in the slurry-circuit and to determine the flow velocity in the measurement section. The two-axis electromagnetic flow meter was mounted at 75 mm above the inner bottom of the measurement section. The data of this instrument were used to derive the flow velocity profile above an eroding sand bed. Due to the sensitivity of this instrument for the impact of grains, these measurements were only executed on the finest sand ($d_{50} = 51$ $\mu$m). The measurements with the temperature sensor were

necessary to calibrate the conductivity probes for the influence of the temperature.

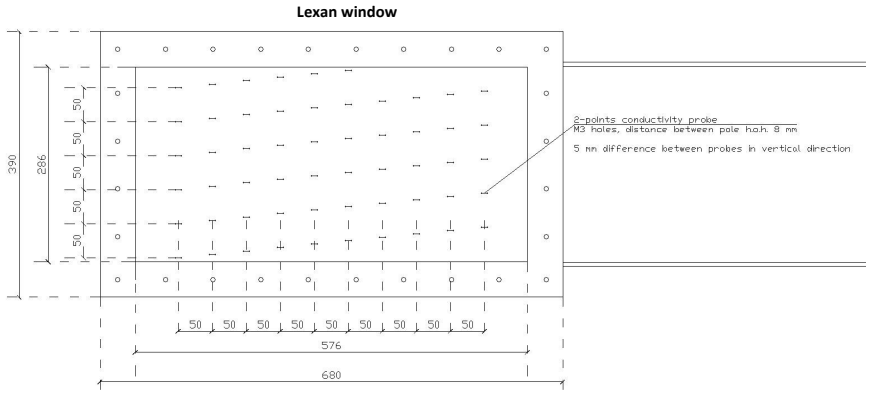


(a)

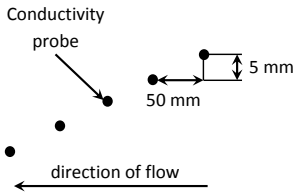


(b)

Figure 5.3: Location conductivity probes in lexan plate (a) and outline of sloping matrix of conductivity probes (b)

## 5.3. Characteristics experimental set-up

Before, during and after each set of experiments the pressure gradient in the measurement section was determined, while flowing with water (Section 5.3.1). These measurements showed that the friction between the liquid and the wall (wall friction) of the measurement section changed during the execution of the experiments. Besides this a thorough calibration procedure was developed to calibrate the measurements with the conductivity probes for the temperature and to determine the relation of the measured potential difference with the concentration/density of the slurry or sand bed in the measurement section (Section 5.3.2).

### 5.3.1. Hydraulic pressure gradient measurement section

#### Calibration procedure

Calibration of the pressure gradient measurements in the measurement section was executed before, during and after each set of experiments in both series of experiments (see Table 5.3 and 5.4). Each set consisted of a number of experiments on one type of sand, in order to determine the friction factor and effective roughness of the measurement section during this set of experiments and check the calibration of the

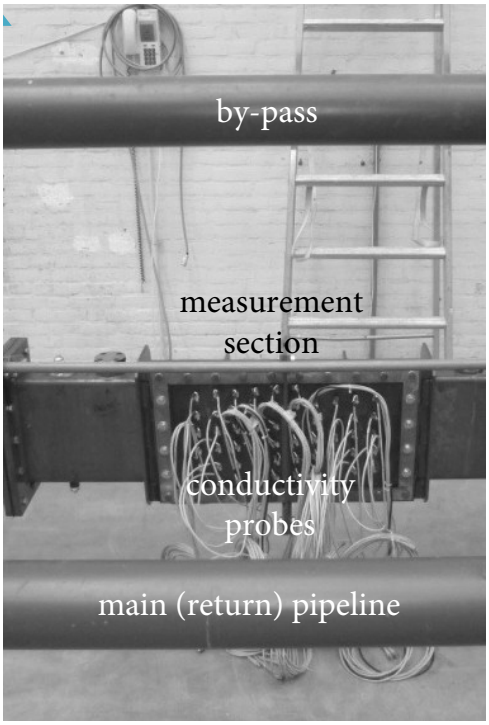


Figure 5.4: Connected conductivity probes

pressure gauges (Figure 5.5). Before and after each set of experiments the pressure loss was measured at different depth-averaged flow velocities. During each separate experiment the pressure loss was checked at a depth-averaged flow velocity of 0 m/s and approximately 4 m/s. Figure 5.6 shows the results of the calibration of the pressure gradient gauges at different depth-averaged flow velocities for clear water before and after the set of experiments on Dorsilit sand (see Figure 5.6). Figure 5.6 also shows the results of the calibration of the pressure gauges during each experiment on Dorsilit sand (Experiments 61-75 and 82-85). The results of these pressure gradient measurements show that the frictional characteristics hardly changed during these experiments and that the pressure gauges did function well.

### Determination of wall friction and roughness height

The results of the pressure gradient ($dp/dx$) measurements were used to determine the frictional characteristics and roughness height ($k_s$) of the measurement section using:

$$A \cdot \frac{dp}{dx} = \tau_w \cdot O \tag{5.1}$$

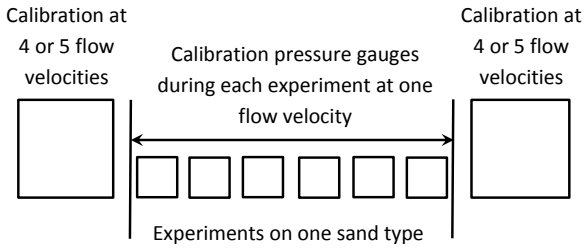


Figure 5.5: Calibration procedure pressure gradient measurements in measurement section

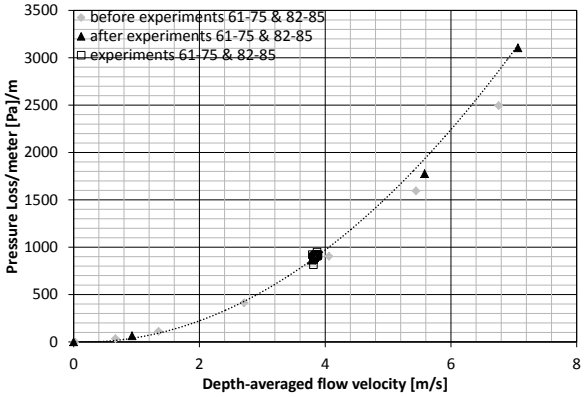


Figure 5.6: Results pressure loss measurements executed before, during and after the experiments on Dorsilit sand (Experiment 61 through 75 and 82 through 85, see Table 5.4)

in which $A$ is the area of cross section of the rectangular measurement section and $O$ the perimeter of the measurement section. The Darcy-Weisbach friction factor ($f_w$) is related to the wall shear stress and depth-averaged flow velocity:

$$\tau_w = \frac{f_w}{8} \cdot \rho_w \cdot U^2 \tag{5.2}$$

Combining Equations (5.1) and (5.2) the Darcy-Weisbach friction factor can be derived from the measured pressure gradient ($dp/dx$) in the measurement section:

$$f_w = \frac{dp}{dx} \cdot \frac{2 \cdot D_h}{\rho_w \cdot U^2} \tag{5.3}$$

in which $D_h$ is defined as the hydraulic diameter ($\frac{4 \cdot A}{O}$). In case of a circular pipe with diameter $D$ the hydraulic diameter equals $1/4 \cdot D$, while the hydraulic diameter equals the water depth in case of a river flow. In this case, with a rectangular measurement section, the hydraulic diameter was between 0.5 to 0.8 times the flow height above the sand bed. The effective roughness of the inner walls of the measurement section is derived using the following implicit relation between the

| Experiment<br>- | Roughness height<br>mm |
|---|---|
| 1 - 17 | 0.000080 |
| 25 - 37 & 39 - 42 | 0.000001 |
| 38 | 0.000053 |
| 43 | 0.000001 |
| 44 - 51 & 53 - 59 | 0.000070 |
| 52 | 0.000025 |
| 60 | 0.000027 |
| 61 - 75 & 82 - 85 | 0.000039 |
| 76, 78 - 81 & 87 - 89 | 0.000075 |
| 77 | 0.000157 |

Table 5.1: Roughness height of walls of measurement section per set of experiments



friction factor, hydraulic diameter, Reynolds number and roughness height for pipes (Colebrook, 1939):

$$\frac{1}{\sqrt{f_w}} = -2 \cdot \log_{10}\left(\frac{k_s/D_h}{3.7} + \frac{2.51}{Re \cdot \sqrt{f_w}}\right) \tag{5.4}$$

The initial estimate for the wall friction factor is based on Swamee and Jain (1976):

$$f_w = 0.25 \cdot \left[\log_{10}\left(\frac{k_s/D_h}{3.7} + \frac{5.74}{Re^{0.9}}\right)\right]^{-2} \tag{5.5}$$

Results

Because the roughness of the walls of the measurement section was not constant and the experimental arrangement was reconstructed between Augustus and November 2012, the wall friction of the measurement section was defined per set of experiments (see Table 5.1). Calibration of the pressure gauges before and after each set of experiments, made it possible to check the pressure gauges during each experiment (see Section 5.5.1). Figure 5.6 shows that the results of the pressure gradient measurements before and after the set of experiments on Dorsilit sand were comparable to the results of the calibration of the pressure gauges during each separate experiment. On the basis of these measurements the roughness height of the wall of the measurement section could be derived. For this set of experiments the roughness height was 0.039 mm. Figure 5.6 shows the calculated hydraulic pressure gradient based on this roughness height. Table 5.1 gives the representative effective roughness height for each (set of) experiment(s).

The results as presented in Table 5.1 show that the pressure gradient measurements during experiment 38, 43, 52, 60 and 77 differ from preceding and later executed experiments. These results were subject to an extra check during the analysis of the measurements (Section 7).

### 5.3.2. Calibration conductivity probes

The conductivity probes consisted of two transducers (diameter 3 mm) placed 7 mm from each other. The measured potential difference over these transducers depends on the electrical resistivity of the medium between these transducers and is a measure for the density of this medium. A relation between the electrical resistivity and the density of the medium (sand-water mixture and/or sand bed) for each conductivity probe was based on measuring the electrical resistivity at three different densities: water, a sand-water mixture (slurry) and sedimented and/or compacted sand (sand bed). The density of the sand-water mixture and sand bed at the level of the conductivity probes was measured with the radio active density meter, which was adjustable in vertical level. However, it should be noted the electrical resistivity is not only influenced by the density of the medium, but also by the temperature, the salinity of the water and the type of sand. These influences made it necessary to execute for each experiment a separate calibration procedure to determine the influence of the temperature on the electrical resistivity and the relation of the electrical resistivity with the density for each conductivity probe.



#### Temperature dependence

During all experiments the temperature dependence of the conductivity probes was determined during 3 calibration tests: with water (1), sand-water mixture (2) and sedimented and/or compacted sand: sand bed (3). The first calibration was executed by measuring the conductivity with water in the measurement section before and after the experiment. The difference between the temperature before and after the experiments was large enough to calibrate each conductivity probe for the influence of the temperature. Figure 5.7 shows the results of the first calibration test for two selected conductivity probes, mounted at 19 and 224 mm above the inner bottom of the measurement section. Both conductivity probes showed an equal temperature dependence for a set of experiments. The difference between all sets was caused by replacement of water in the system, type of sand and change of the settings of the signal amplifier.

The temperature dependence of the conductivity probes during the second calibration test, while pumping a sand-water mixture through the measurement section at a depth-averaged flow velocity above the limit deposit velocity, is presented in Figure 5.8. Before each experiment the density-height profile was measured at ten different vertical levels with a radio-active density meter. During this calibration procedure the temperature of the sand-water mixture increased, enabling the determination of a relation between the measured potential difference and temperature for each conductivity probe. Due to differences in the total density of the sand-water mixture during all experiments no overall relation for each set of experiments could be derived. However, Figure 5.8 shows that the slope of the relation between the potential difference and temperature is more or less constant for each group of experiments.

During the third calibration test for the relation of the electrical resistivity and density of the medium, executed during each experiment, the density of the sand bed was measured with the radio-active density meter at 10 different vertical levels. The

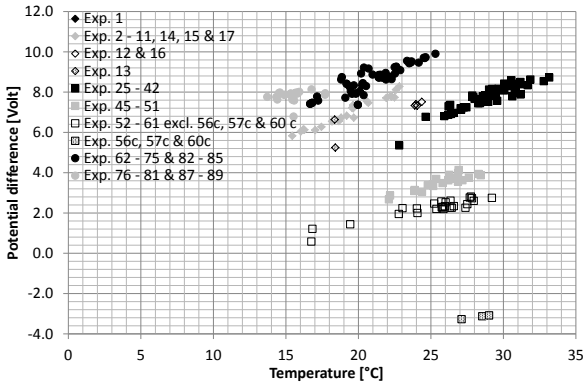


(a)

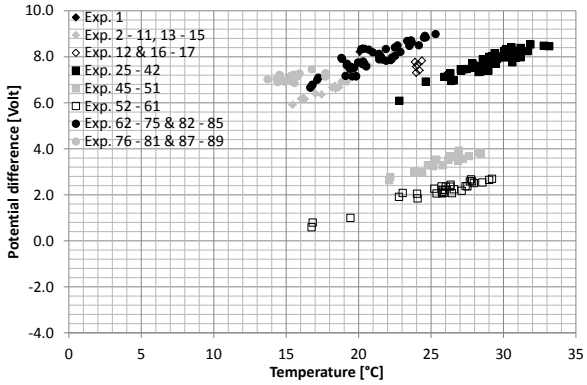


(b)

Figure 5.7: Temperature dependence of two selected conductivity probes with water in the measurement section, mounted at 19 (a) and 224 mm (b) above the inner bottom of the measurement section, during all experiments while pumping water through the measurement section

density of the sand bed between each experiment differed from each other, because during some experiments the sand bed was only sedimented and not compacted, while during other experiments the sand bed was compacted after sedimentation. Due to this variation no overall relation could be derived for the relation between the potential difference and the temperature. Again for each experiment a separate relation between the potential difference and temperature was determined (see Figure 5.9). This was possible because during this calibration test the temperature of the sand bed decreased.

In order to use the results of these calibration tests for the determination of the relation between the density and measured potential difference for each conductivity probe, the measured potential difference was corrected for the difference of the temperature between each of the calibration tests and the actual erosion test of the experiments, as if the calibration test was executed at the same temperature as the

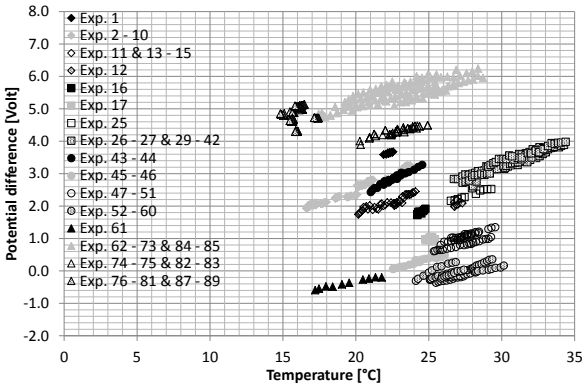


(a)

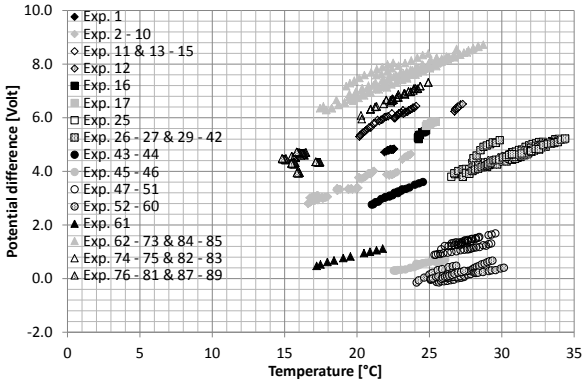


(b)

Figure 5.8: Temperature dependence of two selected conductivity probes mounted at 19 (a) and 224 mm (b) above the inner bottom of the measurement section, during pumping a sand-water mixture through the measurement section

temperature during the erosion test.

### Relation between electrical resistivity and density

The relation between the potential difference between the conductivity probes and the concentration of grains in a suspension is often assumed to be linear, however Maxwell (1881), Bruggeman (1935) and De La Rue and Tobias (1959) have showed that this relation is curved. Specific experiments with sand with an average grain size ($d_{50}$) of 562 $\mu$m were executed to determine the shape of the relation between the concentration and measured potential difference. The shape of the curve was determined by measuring the vertical density profile with the radio-active density meter and potential difference over the probes at different overall densities of the mixture:

- water: 1000 kg/m$^3$;

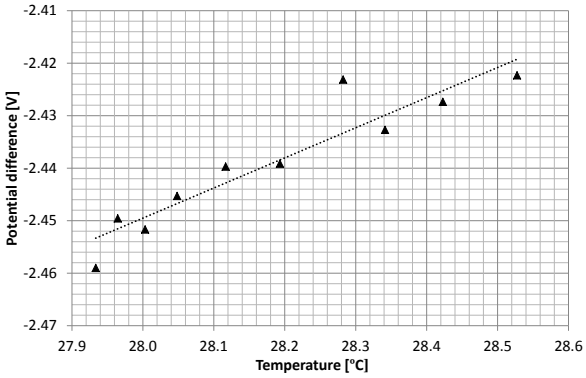


Figure 5.9: Temperature dependence of conductivity probe mounted at 19 mm above the inner bottom of the measurement section during the measurement of the density of the sand bed



- sand-water mixture pumped at an average density of approximately 1100, 1275 and 1425 kg/m$^3$ through the measurement section;
- a non-compacted and compacted sand bed (density approximately 1900 and 1975 kg/m$^3$).

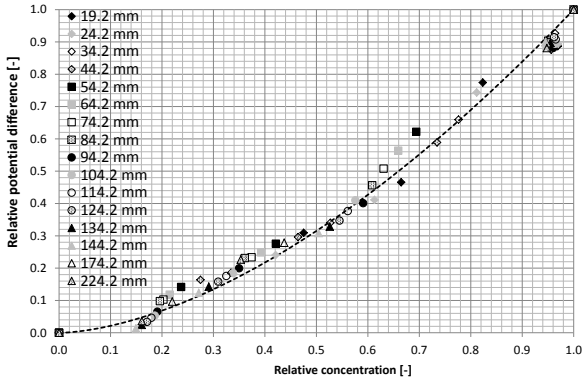


Figure 5.10: Curved shape of the relation between the relative concentration and relative potential difference for 562 $\mu$m sand

Figure 5.10 shows the relation between the relative concentration ($c_m/c_{max}$)and the relative potential difference ($(\Delta V_w - \Delta V_m) / (\Delta V_w - \Delta V_{max})$) for all connected conductivity probes and proved to be of the following form:

$$\left(\frac{c_m}{c_{max}}\right)^{\alpha} = \frac{\Delta V_w - \Delta V_m}{\Delta V_w - \Delta V_{max}} \tag{5.6}$$

in which $c_m$ is the measured concentration, $c_{max}$ is the maximum concentration of the sand bed, $\Delta V_w$ is the potential difference at the presence of water in the measurement section, $\Delta V_m$ is the measured potential difference at the measured concentration, $\Delta V_{max}$ is the potential difference at the maximum concentration of the sand bed. The curved shape, as presented in Figure 5.10, was used to calibrate all conductivity probes during all experiments. This figure gives also an indication of the maximum error of the concentration measurements. The maximum absolute error of relative concentration is approximately 0.05. This means that the maximum absolute error of the concentration measurement is 0.03.

Figure 5.11 presents the relation between the relative concentration and the relative potential difference for 4 experiments executed with different sand types ($d_{50}$ = 51, 125, 262 and 562 $\mu$m) for all conductivity probes. The curved relation between the relative concentration and potential difference could not be checked for the concentration probes which were situated above the sedimented sand bed, making it possible to calibrate these probes only in the presence of water and the sand-water mixture. For these probes a linear relation between the relative concentration and relative potential difference was assumed.

The calibration procedure showed that for the finest and coarsest sand the relation was curved, while the shape of this relation for sand of medium grain size ($d_{50}$ = 125 and 262 $\mu$m) was more or less linear. The average of the power ($\alpha$) in Equation 5.6 was between 1.05 ($d_{50}$ = 125 and 262 $\mu$m) and 1.45 ($d_{50}$ = 51 and 562 $\mu$m) (see Figure 5.11). The value of $\alpha$ in Equation 5.6 was determined for each concentration probe for each separate experiment.

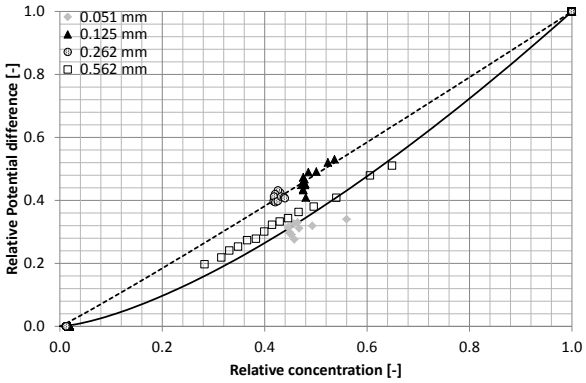


Figure 5.11: Curved and linear shape of the relation between the relative concentration and relative potential difference for all sand types and concentration probes

## 5.4. Properties sand

As described in Section 5.1 four types of sand (Zilverzand, Geba, Dorsilit and Silverbond) were used in the experimental program. Three sand types were chosen because their grain size is comparable to sand present in dikes in the Netherlands

and sand which is encountered during dredging. The finest sand (Silverbond) is chosen because of its low permeability, while it behavior is still dominated by (inert) quartz material. According to the theory of dilatancy reduced erosion the pick-up flux should be highly reduced by this low permeability.

The main properties of these types of sand are summarized in Table 5.2. These types of sand were chosen because the grain size distribution (Figure 5.12) was mainly poorly graded/well sorted: uniformity coefficient ($C_u$) = 1.45), except for Silverbond sand. This reduces the segregation of finer and coarser grains during the sedimentation process while creating a sand bed in the measurement section, during step 3 of the execution of the experiments (see Section 5.5.1). The Silverbond sand was very fine and consisted mainly of silt. The grains consisted mainly of quartz, being an inert material. This avoided the presence of cohesive behavior. Unfortunately it was not possible to select poorly graded/well sorted material with this average grain size. The uniformity coefficient of this material was 3.35.



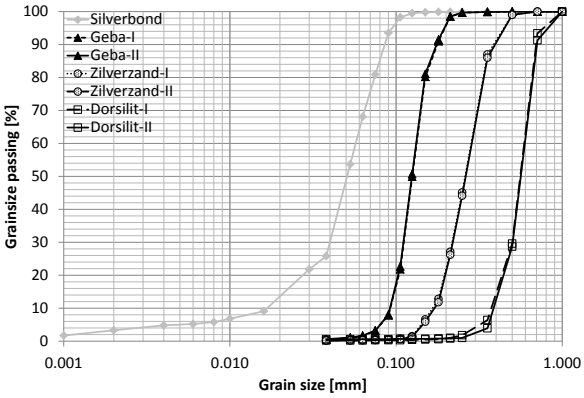


Figure 5.12: Grain size distribution Silverbond, Geba, Zilverzand and Dorsilit

The permeability of all sand types was measured at different porosities (Fig. 5.13) showing that the permeability increases as the porosity increases. A semi-empirical, semi-theoretical expression describing the permeability of porous media is the well known Kozeny-Carman equation. This equation relates the effect of the porosity, specific grain surface and angularity of the grains to the permeability. Bear (1972) and Batu (1998) have developed an adapted Kozeny-Carman equation relating the effect of the specific grain surface to the size of the smallest grains ($d_{10}$):

$$k = C_k \cdot \frac{g}{\nu_w} \cdot d_{10}^2 \cdot \frac{n_i^3}{(1-n_i)^2} \tag{5.7}$$

Figure 5.13 presents the results of the measurements of the permeability as function of the porosity for all sand types. This figure slso shows the results of the adapted Kozeny-Carman equation. The value of $C_k$ was determined by empirical correlation of the data and this equation. This constant was more or less equal for

| Name | Grain size | | | | Porosity | | Constant Kozeny-Carman |
|---|---|---|---|---|---|---|---|
| | $d_{10}$ | $d_{50}$ | $d_{60}$ | $C_u$ | $n_{max}$ | $n_{min}$ | $C_k$ |
| | $\mu$m | $\mu$m | $\mu$m | - | - | - | - |
| Silverbond | 17 | 51 | 57 | 3.35 | 0.536 | 0.385 | 0.01280 |
| Geba | 92 | 125 | 133 | 1.45 | 0.506 | 0.370 | 0.00387 |
| Zilverzand | 168 | 262 | 285 | 1.69 | 0.470 | 0.370 | 0.00465 |
| Dorsilit | 380 | 562 | 594 | 1.56 | 0.475 | 0.366 | 0.00449 |

Table 5.2: Properties sand

Geba, Zilverzand and Dorsilit sand (see Table 5.2), while the value of $C_k$ for the finest sand (Silverbond) was higher. This could be the result of the angularity of the grains. According to the scale of Powers (Powers, 1953) the roundness grade of the three coarsest sand types is sub-rounded (grade between 37 and 49), while the finest sand is sub-angular (grade between 20 and 30). This is not in accordance with the value of $C_k$ of the finest sand in comparison with the coarser sand types. More angular material, being the case for Silverbond sand in comparison with the other sand types, should show a lower value of $C_k$ in comparison with the value of $C_k$ for the other sand types. This is not the case: Silverbond sand shows a higher value of the uniformity coefficient in comparison with the other sand types. This shows that Equation (5.7) should be used with great care in case of silt. Besides this Figure 5.13 shows that Equation (5.7) gives a good indication of the effect of the porosity on the permeability, as long as the right value for $c_k$ is known.

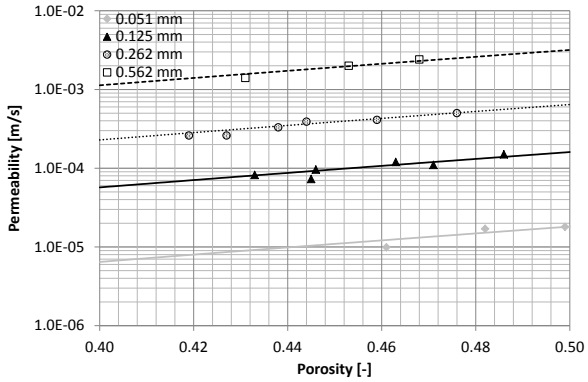


Figure 5.13: Permeability as function of the porosity for all sand types including the permeability calculated with the adapted Kozeny-Carman equation with corresponding values for $C_k$

## 5.5. Experiments

A step-wise execution of the experiments was necessary in order to calibrate the results of the measurements with the conductivity probes and to check the measurements with the pressure gauges (Section 5.5.1). In total two series of experiments were executed (Section 5.5.2).

### 5.5.1. Execution of experiments

In order to calibrate the conductivity probes and pressure gauges and to create a compacted or non-compacted sand bed, a specific experimental procedure was developed. Each erosion experiment consisted of 5 consecutive tests (Bisschop et al., 2016). During the last test the actual erosion was measured:

1. The whole slurry circuit was filled with clear water: this stage was used to check all the instruments (especially pressure gauges and conductivity probes) at a depth-averaged flow velocity of 0 m/s and approximately 4 m/s.

2. Sand was added to the slurry circuit while pumping the sand-water mixture through the whole slurry circuit at a velocity above the deposition limit of the type of sand. The density of the sand-water mixture flowing through the measurement section was measured at 10 different levels by adjusting the height of the radio-active density meter.

3. The valve to the by-pass was opened, making it possible to (partially) close the valve upstream of the measurement section (valve 1.2 in Figure 5.2), preventing sedimentation of sand in the whole slurry circuit. The resulting sedimentation in the measurement section created a sand bed with a height of approximately 0.15 m. Visual observation, through a glass window in the measurement section (approximately 0.5 m long), showed that the created sand bed was more or less horizontal.

4. After the sand bed was created, the remaining sand in the slurry circuit was discharged to the slurry tank. The density of the settled sand bed was measured at 10 different levels with the radio-active density meter.

5. The slurry circuit was filled with a sand-water mixture at the desired density, with a depth-averaged flow velocity above the critical velocity for deposition. The erosion experiment was started by tuning the pump at the desired rotation speed, in order to achieve the aimed depth-averaged flow velocity in the measurement section and opening the valve upstream to the measurement section (valve 1.1). Water or a sand-water mixture flowed over the sand bed, starting the erosion process. The erosion velocity was measured with the help of the conductivity probes. The measured hydraulic pressure gradient was used to determine the effective bed shear stress during erosion.

Tests 1, 2 and 4 were used to calibrate the conductivity of all probes with the measured density at the same height. With the help of the results of tests 1, 2 and 4 the measured conductivity was corrected for the influence of the temperature

and the relation of the potential difference with the density for each conductivity probe was determined. This calibration procedure was repeated for all experiments because of the variability of the temperature and conductivity of the used water during all tests and influence of the type of sand on the conductivity.

### 5.5.2. Experimental program

The experimental program existed of two series of experiments. The first series of the experiments was executed in November and December 2010. The results of this series of experiments were used to improve the test arrangement, optimize the calibration procedure and execution of the erosion experiments. The second series of experiments was executed in 2012. The first part of the second series of experiments was executed in July and August 2012. A mechanical break-down caused a delay in the execution of the final experiments. After reconstruction, including some final improvements, the second part of the second series of experiments were executed in November and December 2012. Each series consisted of a set of a experiments of which each set was carried on one type of sand (Figure 5.14). One experiment consisted of 5 tests (see Figure 5.14) of which the last test was the actual erosion experiment. The other tests were executed in order to calibrate the conductivity probes and the hydraulic pressure gradient measurements.



#### First series of experiments

The first series consisted of 17 experiments with Geba and Dorsilit sand. Test 1 through 10 were executed with Geba sand while experiments 11 through 17 were executed with Dorsilit sand. Nine of the first ten experiments gave reliable results (experiments 1 through 4 and 6 through 10). However, only the results of the pressure gradient measurements for experiment 1 through 4 were unreliable. Of the experiments executed on Dorsilit sand, only experiments 12, 13 and 14 gave useful results. Table 5.3 gives an overview of the operational conditions during these experiments, while Appendix A presents the operational conditions off all separate executed experiments. For the first 6 experiments (experiments 1 through 6) the depth-averaged flow velocity during the sedimentation process was between 0.5 and 1.0 m/s causing a relative high density (0.3 to 1.0) of the sand bed after sedimentation. Grains settling in a flowing slurry will only settle in the existing sand bed when the grains find a sheltered place within other grains (van Rhee, 2002). This effect results in a higher density of the sand bed compared with grains settling in a stagnant slurry. For experiment 7 through 10 the sand bed was sedimented at a lower flow velocity ($u < 0.5$ m/s). The resulting relative density of the sand bed varied between 0.2 and 0.5. The relative density during experiment 12 through 14, on Dorsilit sand, was between 0.0 and 0.2. It was the intention that all erosion experiments were executed with water. However, not all sand could be removed from the circuit with the help of the slurry tank. The experiments were executed with a density of the eroding slurry of approximately 1050 kg/m$^3$.

#### Second Series of experiments

The second series consisted of 7 experiments to check the calibration procedure and all instruments. After these experiments in total 65 experiments (experiments 25

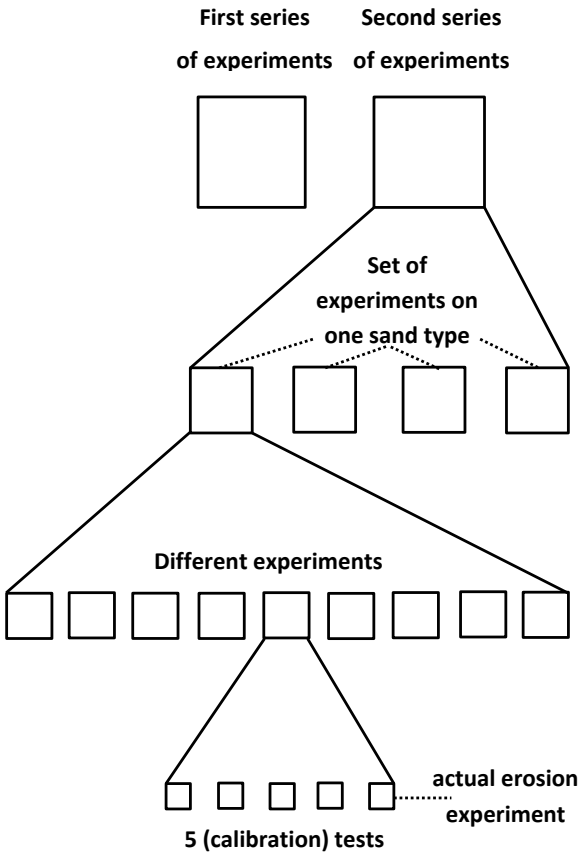


Figure 5.14: Experimental program consisting of two series, each series consisting of different sets of experiments. Each experiment consisted of 5 (calibration) tests

through 89) were executed on four types of sand (Zilverzand, Geba, Dorsilit and Silverbond). The operational conditions of the experiments are depicted in Table 5.4, while Appendix A presents the operational conditions of all separate executed experiments. The parameters varied during the experiments are: grain size (type of sand), relative density sand bed, flow velocity and density of the eroding flow. By varying the grain size and relative density the effect of the permeability of a sand bed on erosion could be studied. The relative densities during the experiments were between approximately 0.0 and 0.25 (low relative density), 0.25 and 0.50 (medium) and larger than 0.50 (high).

During some experiments on Silverbond-sand the relative density of the sand bed was smaller than 0.0. This meant that during the measurement of the density of the sand bed the consolidation process, after the sedimentation of the grain, did not occur fully. Excess pore water pressures will have been present in the sand bed, due to the low permeability of this type of sand. This effect has been reduced by

| Sand type | Grain size $d_{50}$ | Relative density $R_n$ | Depth-averaged flow velocity U | Experiment no. |
|---|---|---|---|---|
| - | $\mu$m | - | $m/s$ | - |
| Geba | 125 | High/medium | 2.0 - 6.0 | 1/2/3/4/6 |
| | | Low | 3.0 - 6.0 | 7/8/9/10 |
| Dorsilit | 562 | Low | 3.0 - 4.5 | 12/13/14 |

Table 5.3: Operational conditions test program first series of experiments

a longer period between the sedimentation process and the execution of the density measurements and actual erosion experiment. This enabled a further decrease of these excess pore water pressures and resulted in a higher relative density.

During the last set of experiments with Silverbond-sand an electromagnetic current sensor (EMS) was installed to determine the flow velocity profile during erosion. The sensor (constructed in a discus mounted at the end of a rod) of the EMS was mounted at a distance of 78 mm above the bottom of the measurement section. This sensor generates an electromagnetic field and measures the resulting potential difference as caused by the flow of water. The sensor measures the flow velocity in horizontal as well as in vertical direction. During the erosion experiments the top of the sand bed moves down, resulting in an increase of the distance between the sensor and the top of the sand. This made it possible to determine the flow velocity profile during the erosion experiments. This instrument was only used during the experiments with Silverbond-sand, because of its grain size. This instrument was considered to be very sensitive for mechanical break-down as a result of suspended grains in the flow. Due to the relative small size of grains it was expected that the electromagnetic current sensor was not damaged during the erosion experiments on this sand type.

In the second series of experiments variation of the relative density of the sand bed was achieved by variation of the flow velocity during the sedimentation process of the sand bed and additional hammering. Sedimentation of a stagnant sand-water mixture delivered a relative low density. A medium density was achieved by sedimentation with a flowing sand-water mixture. Higher densities were achieved by additional hammering of the measurement section. The intensity of the hammering process was checked by a short test program on Zilverzand (Figure 5.15).

## 5.6. Conclusions

The calibration of the hydraulic pressure gradient measurements show that the roughness of the walls of the measurement section changed during the erosion experiments. This is caused by wear due to the impact of the sand grains on the walls of the measurement section. A special calibration program was necessary to check the operation of the pressure gauges and to calibrate these measurements for the varying friction factor of the walls of the measurement section.

Using (electrical) conductivity probes needs a specific calibration procedure in

| Sand type<br>- | Grain size $d_{50}$ $\mu$m | Relative density $R_d$ - | Density inflow $\rho_{in}$ $kg/m^3$ | Depth-averaged flow velocity U $m/s$ | Experiment no.<br>- |
|---|---|---|---|---|---|
| Zilverzand | 262 | Low | 1075 | 2.5 - 4.5 | 25/26/27/28/29 |
| | | High | 1100 | 2.5 - 6.0 | 30/31/32/33 |
| | | Medium | 1100 | 2.5 - 5.0 | 34/35/36/37 |
| | | | 1250 | 3.0 - 5.0 | 38/39/40 |
| | | | 1450 | 3.5 - 5.5 | 41/42 |
| Geba | 125 | Low | 1075 | 2.0 - 5.0 | 43/44/45/46 |
| | | High | 1100 | 2.0 - 5.5 | 51/52/53/54 |
| | | Medium | 1100 | 2.0 - 5.0 | 47/48/49/50 |
| | | | 1200 | 3.0 - 5.0 | 55/56/57 |
| | | | 1350 | 3.0 - 4.5 | 58/59/60 |
| Dorsilit | 561 | Low | 1100 | 1.5 - 5.0 | 61/62/63 |
| | | High | 1100 | 4.0 - 5.0 | 67/68/69 |
| | | Medium | 1100 | 3.0 - 4.5 | 64/65/66/82 |
| | | | 1225 | 3.5 - 5.0 | 70/71/72 |
| | | | 1350 | 4.0 - 5.5 | 74/75/83/85 |
| Silverbond | 51 | Low | 1050 | 1.5 - 2.5 | 76/77/78/82 |
| | | Medium | 1075 | 1.5 - 5.0 | 79/80/81/87/88/89 |

Table 5.4: Operational conditions test program second series of experiments

order to determine the influence of the temperature, type of water and sand on the relation between the electrical resistivity and density. Special attention was necessary for the influence of the type of sand on the shape of the relation between the measured potential difference and density of the sand-water mixture or sand bed. The sand types, as used during the experiments, showed a varying relation (curved or linear) between the potential difference and density. This was incorporated in the calibration procedure of the measurements with the conductivity probes.

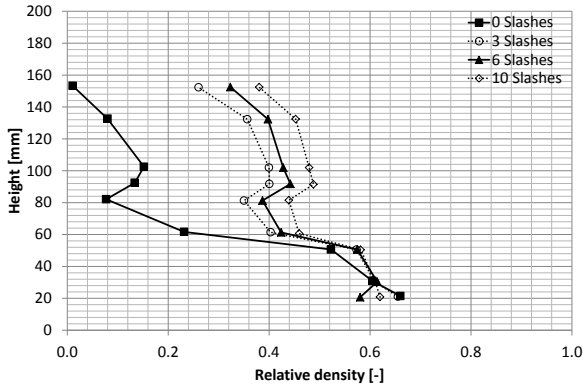


(a)

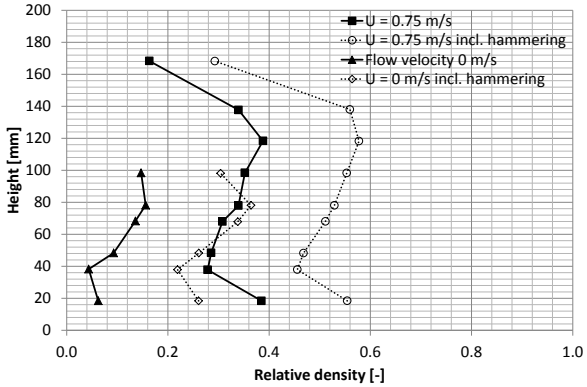


(b)

Figure 5.15: Calibration of compaction procedure on Zilverzand: influence of intensity of hammering a and comparison of compaction

# 6

# Determination of results experiments

## 6.1. Introduction

Chapter 5 describes the experimental set-up and specific characteristics of the test arrangement and instrumentation as well as the hydraulic resistance of the measurement section, behavior of the conductivity probes and used types of sand. Two series of experiments were executed. The results of the first series of experiments were used to optimize and improve the experimental and calibration procedure, design of the measurement section and location of the instruments. The results of these experiments already have been described by Bisschop et al. (2016). The results of the second series are used to determine the relation of the pick-up flux with operational parameters as the flow velocity and bed shear stress and bulk properties of the sand bed like permeability and porosity. For the analysis of these data it is necessary to derive the pick-up flux and effective bed shear stress from the results of the measurements. This chapter describes the way of determination of these parameters from the measurements with the conductivity probes and the hydraulic pressure gradient measurements and the influence of the behavior of the measurement section and instruments on the measurements of the density of the sand bed, pick-up flux, flow velocity and bed shear stress.

Specific attention is paid to the influence of the change of the dimension of the measurement section during the experiments on the measurements with the conductivity probes. This influenced the determination of the density of the sand bed and eroding sand-water mixture during the erosion experiments (Section 6.2).

The determination of the pick-up flux during the measurements is described in Section 8.6.5. The determination of the effective bed shear stress is more complicated. Different procedure(s) are available to determine the bed shear stress from pressure gradient measurements in a pressurized circuit. These are described in Section 6.4. Section 6.5 gives the results of the experimental error analysis for the first

series of experiments, giving an indication of the accuracy with which the bed shear stress and pick-up flux are derived. The results of the experiments are summarized in Section 6.6. Section 6.7 presents the main conclusions regarding the methods to derive the main parameters as density of the sand bed, pick-up flux and bed shear stress.

## 6.2. Density sand bed

The density of the sand bed was measured after sedimentation or, if executed, after the compaction procedure. These measurements were executed with the radio-active density meter at 10 different levels in the measurement section and were also used to calibrate the measurements with the conductivity probes (Section 5.3.2). In the analysis of the change of the density (just) before the moment of erosion, it should be considered that the measurements with the conductivity probes were influenced by the pressure in the slurry circuit. Before the actual erosion experiment the pump was set at the desired speed in order to execute the erosion experiment at the desired discharge. The pressure in the slurry circuit expanded the walls of the measurement section, enabling the formation of a water film between the sand bed and the lexan plate with the conductivity probes. This resulted in a lower resistivity, as measured with the conductivity probes, and resulted in a lower fictitious density of the sand bed.



This effect was enlarged at the moment when the valve to the measurement section was opened, enabling the erosion process to start, increasing the pressure in the measurement section (Figure 6.1). Figure 6.1 shows also that the conductivity probes, mounted relative high from the bottom, show a larger decrease of the fictitious density than conductivity probes mounted just above the bottom of the measurement section. The measurement section will show the largest expansion at the middle. This means that the water film between the lexan plate and sand bed is thicker, leading to a larger decrease of the density. Besides the decreasing pressure during the erosion test causes a decrease of the expansion of the measurement section during the erosion tests, leading to an increase of the measured fictitious density. This effect can be seen in Figure 6.1. The results of the measurements of the concentration probe at a level of 14.2 mm above the bottom of the measurement section show that when the pressure in the measurement section decreases, the fictitious density of the sand bed increases again.

Expansion of the measurement section was decreased by improving the construction of the reinforcing rib in the middle of the lexan plate for the first part of the second series of experiments (Experiment 25 through 60). This measure was not sufficient to reduce this effect significantly. Before the last part of the second series of the experiments (experiments 61 through 89) two extra reinforcing ribs were mounted before the lexan plate. This reduced the expansion of the measurement section and resulting decrease of the fictitious density significantly (Figure 6.2).

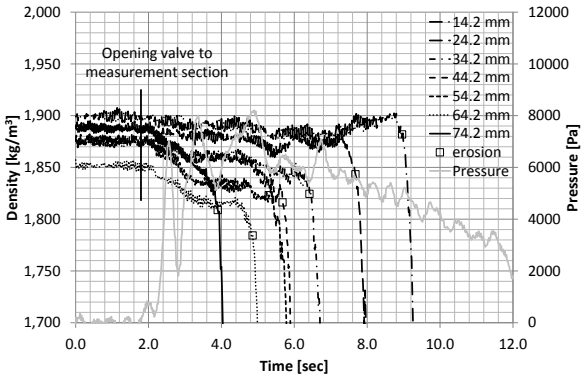


Figure 6.1: Decrease of density, measured with the conductivity probes, (just) before the actual moment of erosion (Experiment 7)

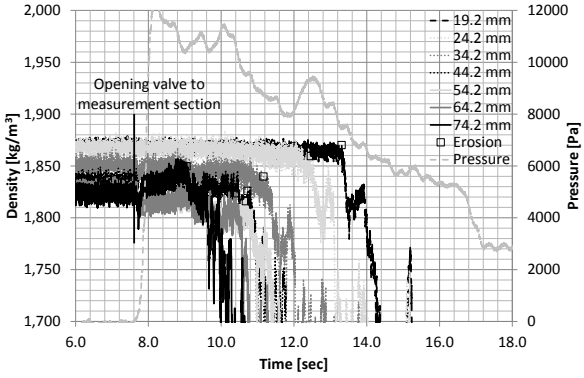


Figure 6.2: Decrease of density, measured with the conductivity probes, (just) before the actual moment of erosion showing the effect of the extra reinforcing ribs (experiment 62)

## 6.3. Determination pick-up flux

The determination of the pick-up fluxes is based on the data of the measurements with the conductivity probes. These measurements showed specific exhibits as described in Section 6.3.1. Section 6.3.2 describes the determination of the pick-up fluxes on the basis of the measurement of the conductivity probes during the erosion experiments.

### 6.3.1. Density measurements with conductivity probes

Figure 6.3 shows the change of the density at different levels above the bottom of the measurement section (measured with the conductivity probes) during experiment 7 at different levels in the measurement section. The erosion moment was manually determined and have been defined as the moment at which the density decreased

significantly and the density was close to the minimum density of the sand bed.

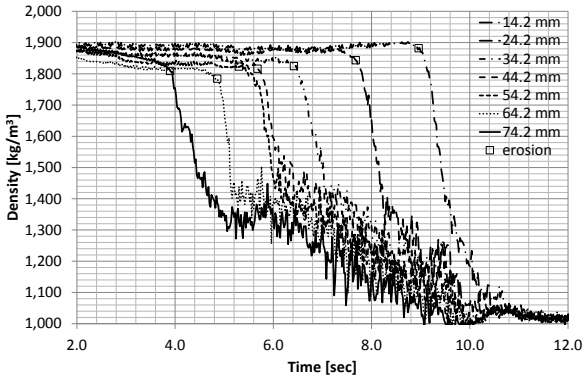


Figure 6.3: Change of density at different levels above the bottom of the measurement section during experiment 7

The observed apparent density drop before the erosion moment was caused by the dimensions of the electrical flow field around the conductivity probes. This was investigated by Liefferink (2012) who executed experiments with a specific designed apparatus. During these experiments the potential difference between two transducers, mounted at the same distance in horizontal direction from each other (7 mm), was measured at different distances of these transducers above and below the top of the sand bed. Experiments were executed with two types of sand (Geba and Zilverzand). Two experiments ('a' and 'b') were executed with Zilverzand and two experiments ('c' and 'd') with Geba sand. The vertical level of the transducers could be adjusted with the help of a wedge shaped sliding tool. Figure 6.4 shows the results of these experiments in comparison with the measurements of one conductivity probe during the first erosion experiment. The measured density during the erosion experiment shows a slight decrease of the density before erosion, while just before the moment of erosion (probe approximately 0.5 mm below the top of the sand bed) the density drop increases.

The measurements of Liefferink (2012) show that at a level of more than 2 to 3 mm below the top of the sand bed the measurements with the conductivity probes were unaffected by the presence of water (with a lower electrical resistivity) above the top of the sand bed. Closer to the sand bed the measurements with the conductivity probes were affected by the presence of water. If a probe was situated just below the top of the sand the measured potential difference was still influenced by the lower electrical resistivity of the water above the top of the sand bed. The electric current followed the way of the lowest electric resistance and did not follow the shortest way through the sand bed, as shown by arrow (1) in Figure 6.5. The electric current experiences the lowest electric resistance, following a path through the sand bed to the eroding fluid and back in the bed again: arrow (2), reducing the measured potential difference. This effect causes a lower apparent density in comparison with the real in-situ density of the sand bed. Based on these

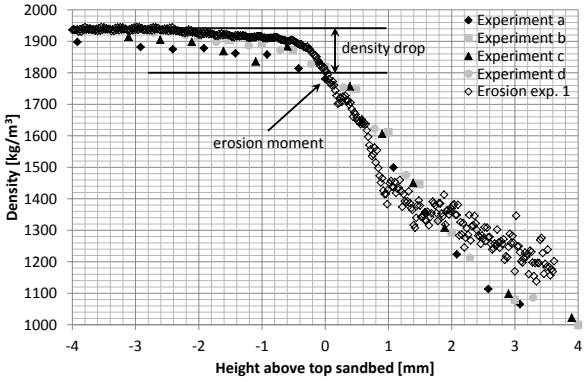


Figure 6.4: Comparison of change of density during erosion experiment 1 and apparent density as measured with the conductivity probe at different levels above and below a sand bed

measurements and substantiated by modeling the resistivity of a 2-layered system it was concluded that the eroding fluid influences the measurements of the conductivity probes, when the top of the sand bed was approximately 3 mm above the probes (Liefferink, 2012). This influenced also the determination of the moment of erosion. This was defined as the moment at which the density, after a first curved decrease, decreases along a more or less straight line as function of time.



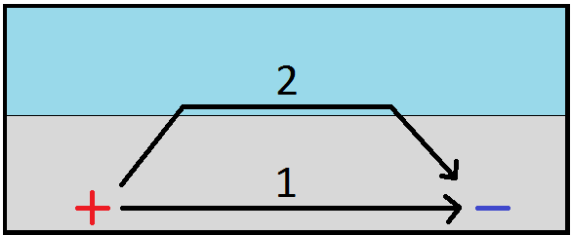


Figure 6.5: Influence of electrical flow field on measurements with conductivity probes (Liefferink, 2012)

### 6.3.2. Determination pick-up flux

Section 4.3.1 describes the definition of the pick-up flux along a downward moving erosion front with an erosion velocity $v_e$. The erosion velocity is derived from the data of the measurements by the time interval ($\Delta t$) between two erosion moments at two conductivity probes and their corresponding height difference ($\Delta z$):

$$v_e = \frac{\Delta z}{\Delta t} \tag{6.1}$$

During erosion, pick-up and sedimentation occur simultaneously. The pick-up

flux is determined according to van Rhee (2010), including the effect of the settling flux (Section 4.3.1):

$$E = v_e \cdot (1 - n_i - c_{nb}) \cdot \rho_s + S \tag{6.2}$$

In this equation the value for the near-bed concentration ($c_{nb}$) is unknown. van Rhee and Talmon (2010) use for the near-bed concentration a value of 15%. However, the level, at which this near-bed concentration is defined, is not specified. The level at the which the value for the near-bed concentration should be specified is further investigated in Section 8.3. The sedimentation flux ($S$) is determined according to Equation (4.15) as function of the settling velocity of the grains and the average concentration of the eroding flow. The settling velocity of a single grain is corrected for the effect of hindered settling according to Richardson and Zaki (1954): $w_{hs} = w_s \cdot (1 - c)^n$. The power $n$ in this equation is given as:

$$\begin{aligned} n &= 4.65 && Re_p < 0.2 \\ n &= 4.35 \cdot Re_p^{-0.03} && 0.2 \leq Re_p < 1 \\ n &= 4.45 \cdot Re_p^{-0.1} && 1 \leq Re_p < 200 \\ n &= 2.39 && Re_p \geq 200 \end{aligned} \tag{6.3}$$



It should be noted that Equation (6.3) does not represent a continuous function (Miedema and Ramsdell, 2016). A continuous function is created when the limit for $Re_p$ of 0.2 is changed in 0.1 and the limit of 200 is changed in 400. Still Equation (6.3) was used, because the resulting difference in the value for the hindered settling velocity was negligible. The settling velocity of a single grain ($w_s$) is estimated with (Zanke, 1977):

$$w_s = \frac{10 \cdot \nu_w}{d_{50}} \cdot \left[ \sqrt{1 + \frac{0.01 \cdot \Delta \cdot g \cdot d_{50}^3}{\nu_w^2}} - 1 \right] \tag{6.4}$$

According to Miedema and Ramsdell (2016) Equation 6.4 is valid for grains with a size between 10 $\mu$m and 10 mm. The influence of the temperature on the kinematic viscosity ($\nu_w$) of water is taken into account using the following correction (van Rijn, 1993):

$$\nu_w = \left[ 1.14 - 0.031 \cdot (T_e - 15) + 0.00068 \cdot (T_e - 15)^2 \right] \cdot 10^{-6} \tag{6.5}$$

in which $T_e$ is the temperature of the water during the erosion experiment in $^\circ C$.

The sedimentation flux depends mainly on the assumed value for the near-bed concentration. The near-bed concentration is not a well defined parameter because the level at which the near-bed concentration should be determined is not well defined. The actual level of the near-bed concentration depends on the concentration profile above the eroding bed and the dimensions of the turbulent eddies influencing the sedimentation flux by transporting grains from the eroding flow to the eroding sand bed. This means that the error in the determination of the actual pick-up

flux mainly depends on the assumed value of the near-bed concentration. This is influenced by the turbulent energy and settling velocity of the grains. The influence of the near-bed concentration on the actual pick-up flux during the experiments has been studied in Section 8.3.

The density of the eroding flow during the experiments is not equal to the density of the flow at the entrance of the measurement section. The density of the flow increases over the length of the measurement section as a result of pick-up. The pick-up flux is derived from the erosion velocity as based on the measurements with the conductivity probes. The average density of the eroding flow ($\rho_{er-av}$) at the location of the conductivity probes during an experiment is determined on the basis of the average density ($\rho_{in}$) and average discharge ($Q_{av}$) of the inflow in the measurement section and the erosion velocity over the length of the sand bed from the beginning of the sand bed until the location of the conductivity probes ($L_c$):

$$\rho_{er-av} = \frac{\rho_{in} \cdot Q_{av} + v_{e-av} \cdot L_c \cdot (\rho_{sb-av} - \rho_{in})}{Q_{av}} \tag{6.6}$$

in which $v_{e-av}$ is the average erosion velocity during an experiment and $\rho_{sb-av}$ is the average density of the sand bed.

## 6.4. Determination bed shear stress



The effective bed shear stress is derived from the pressure gradient measurements induced by friction in the measurement section during the erosion experiments. However, for the derivation of the effective bed shear stress it should be taken into account that the flow in the measurement section was not uniform (in x-direction) and stationary (in time) due to:

- acceleration of the flow after opening the valve to the measurement section;
- change of density of the flow in the measurement section due to the erosion process;
- difference in surface roughness between the eroding bed and the wall of the measurement section.

The results of experiment 5 through 10 have been used to check all assumptions and the validity of the different methods regarding the derivation of the effective bed shear stress. The pressure gradient in the measurement section was measured over 3 different distances (approximately 1, 2 and 3 m). The pressure gradient measured over a distance of 2.96 meter (experiments 1 through 60) and 3.08 m (experiments 61 through 89) was used in order to determine the effective bed shear stress. The pressure gradient, measured over this distance, was the most reliable because it was measured over the longest distance giving the best accuracy. During the first series of experiments these results were highly comparable to the pressure gradient measured over a distance of approximately 2 m.

### 6.4.1. Pressure gradient due to friction

The pressure gradient measured, is corrected for the mentioned effects to derive the pressure gradient as a result of friction. The pressure gradient measured in the direction of the flow during the erosion tests follows from the theoretical pressure gradient according to the depth-averaged Navier-Stokes equation:

$$-\frac{\partial p}{\partial x} = \tau_i \cdot \frac{O}{A_{tot}} + \frac{\partial}{\partial t}(\rho \cdot U) + \frac{\partial}{\partial x}\left(\rho \cdot \overline{U}^2\right) \tag{6.7}$$

in which $\tau_i$ is the average interface shear stress, $O$ is the perimeter flow area and $A_{tot}$ is the total flow area. Using Equation (6.7) the total force gradient is:

$$-\frac{\Delta p}{\Delta l} \cdot h_f \cdot w_m = \tau_i \cdot 2 \cdot (h_f + w_m) + w_m \cdot \frac{\partial}{\partial t}(\rho \cdot h_f \cdot u) + w_m \cdot \frac{\partial}{\partial x}\left(\rho \cdot h_f \cdot u^2\right) \tag{6.8}$$

in which $\Delta l$ is the length over which the pressure difference ($\Delta p$) is measured and $w_m$ is the width of the measurement section. The effective flow height is defined on the basis of the effective discharge area in the measurement section above the part of the sand bed, which was not yet eroded. Visual observation of the sand bed during erosion showed that the bed was more or less horizontal during the experiments ($\frac{\partial h_f}{\partial x} = 0$) meaning that the depth-averaged flow velocity in x-direction was constant ($\frac{\partial u}{\partial x} = 0$). The inflow of water into the sand, as a result of dilatancy reduced pick-up, did not change the discharge above the eroding bed, because water temporarily invading the sand bed, did entrain again in the flow when the sand was eroded. The pick-up flux was more or less constant during the erosion test, meaning $\frac{\partial \rho}{\partial t} = 0$. Due to the erosion process the density of the eroding flow changed in x-direction ($\frac{\partial \rho}{\partial x} \neq 0$), while the flow depth changed as function of time ($\frac{\partial h_f}{\partial t} \neq 0$). The pressure gradient as a result of the flow over the sand bed was also influenced by the acceleration of the flow during the experiments ($\frac{\partial u}{\partial t} \neq 0$). Considering influences mentioned, the total loss of momentum as a result of friction along the walls of the measurement section and top of the sand bed is:

$$-\tau_i \cdot 2 \cdot (h_f + w_m) = \frac{\Delta p}{l} \cdot h_f \cdot w_m + w_m \cdot \rho \cdot u \cdot \frac{dh_f}{dt} + w_m \cdot \rho \cdot h_f \cdot \frac{du}{dt} + w_m \cdot h_f \cdot u^2 \cdot \frac{d\rho}{dx} \tag{6.9}$$

The average interface shear stress ($\tau_i$) is defined on the basis of the average pressure loss ($\Delta p$) between two erosion moments. The interface shear stress is a function of the effective shear stress along the walls of the measurement section ($\tau_w$) and top of the eroding sand bed ($\tau_b$). The influence of the acceleration of the flow is determined for each time interval within two erosion moments. The influence of the change in height and density of the flow on the pressure loss is included on the basis of their averaged values over the whole erosion experiment ($\frac{\Delta h_f}{\Delta t} = c$ and $\frac{\Delta \rho}{\Delta x} = c$). Due to a sometimes irregular erosion process the measured increase of the height of the flow ($\frac{\Delta h_f}{\Delta t}$) and resulting local changes of the density gradient, showed temporarily large variations during an experiment, while the average increase of

the height of the flow and density over the whole experiment was more or less constant. Correcting the pressure gradient for the actual increase of the change of height and density gradient between two erosion moments, results in the derivation of a highly variable effective pressure gradient during the experiments, which was not representative for the actual friction losses. A correction based on the average $\frac{\Delta h_f}{\Delta t}$ and $\frac{\Delta \rho}{\Delta x}$ over the whole experiment give more realistic values for the effective pressure gradient as a result of friction.

### 6.4.2. Bed friction

The pressure gradient solely due to friction, as derived according to the method as described in Section 6.4.1 incorporates the effect of the friction of the exposed wall of the measurement section and the friction of the eroding bed. Different methods exist in order to determine the friction of the eroding bed, as long as the friction or roughness of the wall of the measurement section are known. Two methods are used to determine the effective bed friction: the method of Vanoni and Brooks (1957) and Pugh and Wilson (1999). Both methods consider that the total force loss as a result of friction is equal to the sum of the force loss along the top of the sand bed and the walls of the measurement section. The difference between both methods is the way in which the wall friction coefficient is determined.

#### Vanoni and Brooks (1957)

The method of Vanoni and Brooks (1957) assumes that the total force loss in a section with smooth and rough walls equals the sum of the force loss along the smooth ($F_w$) and force loss along the rough wall ($F_b$):

$$\Delta F_{tot} = \Delta F_b + \Delta F_w \tag{6.10}$$

This means that:

$$\Delta p \cdot A_{tot} = \Delta p_b \cdot A_b + \Delta p_w \cdot A_w \tag{6.11}$$

in which $\Delta p_b$ is the pressure loss along the sand bed (rough wall), $A_b$ is the bed associated area, $\Delta p_w$ is the pressure loss along the wall of the measurement section (smooth wall) and $A_w$ is the wall associated area. Equation (6.11) can be rewritten as:

$$\tau_i \cdot \Delta x \cdot 2 \cdot (h_f + w_m) = \tau_b \cdot \Delta x \cdot w_m + \tau_w \cdot \Delta x \cdot (2 \cdot h_f + w_m) \tag{6.12}$$

Assuming the depth-averaged flow velocity in both sections to be equal, Equation (6.12) can be rewritten as:

$$f_i \cdot (2 \cdot w_m + 2 \cdot h_f) = f_b \cdot w_m + f_w \cdot (w_m + 2 \cdot h_f) \tag{6.13}$$

in which $f_i$ is the interface friction coefficient as derived on the basis of the pressure gradient measured during the erosion experiments, $f_b$ is the bed friction coefficient and $f_w$ is the wall friction coefficient. Equation (6.13) needs an estimate

for the Darcy-Weisbach wall friction coefficient. This friction coefficient cannot be determined directly because the wall associated hydraulic diameter is unknown. In order to solve Equation (6.13), Vanoni and Brooks (1957) used an empirical relation between the wall friction coefficient and relative Reynolds number (quotient between wall associated Reynolds number ($Re_w$) and wall friction coefficient) in order to determine the wall friction coefficient:

$$f_w = a \cdot \left( \frac{Re_w}{f_w} \right)^b \tag{6.14}$$

Tests with water at different flow velocities revealed that this relation was also valid for the experimental set-up used for the erosion experiments (Figure 6.6). The coefficients $a$ and $b$ in Equation (6.14) are based on the check of the pressure gradient measurements before, during and after the experiments. These coefficients have comparable values for each set of experiments except for experiment 38, 43, 52, 60 and 77 (see Table 6.1). The results of the pressure gradient measurements of these experiments are validated in Section 7.2.

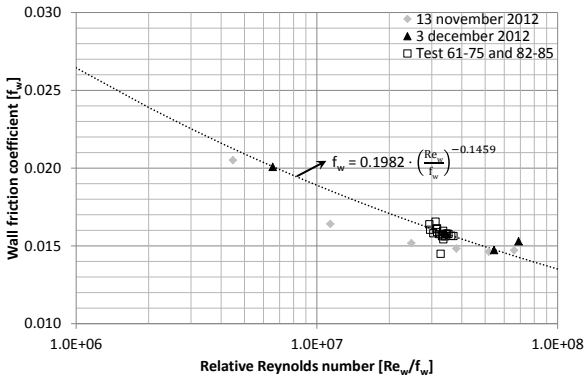


Figure 6.6: Wall friction versus relative Reynolds number measurements November and December 2012

However, Equation (6.14) needs an estimate of the wall associated Reynolds number ($Re_w$), which depends on the wall associated hydraulic diameter ($D_{hw}$). This parameter is unknown and depends on the wall friction coefficient and vice versa. This can be solved directly by combining:

$$Re_w = \frac{U_w \cdot D_{hw}}{\nu_w} \tag{6.15}$$

and:

$$Re = \frac{U \cdot D_h}{\nu_w} \tag{6.16}$$

Assuming $U_w = U$, this results in:

| Experiment | a | b |
|---|---|---|
| - | - | - |
| 1 - 17 | 0.2016 | -0.1370 |
| 25 - 37 & 39 - 42 | 0.2650 | -0.1715 |
| 38 | 0.3260 | -0.1715 |
| 43 | 0.2550 | -0.1715 |
| 44 - 51 & 53 - 59 | 0.4152 | -0.1821 |
| 52 | 0.3730 | -0.1821 |
| 60 | 0.3790 | -0.1821 |
| 61 - 75 & 82 - 85 | 0.1982 | -0.1458 |
| 76, 78 - 81 & 87 - 89 | 0.1420 | -0.1246 |
| 77 | 0.1650 | -0.1246 |

Table 6.1: Coefficients Equation (6.14)

$$\frac{Re_w}{Re} = \frac{D_{hw}}{D_h} \tag{6.17}$$

in which $D_{hw}$ is the wall associated hydraulic diameter and $D_h$ is the hydraulic diameter based on the total cross-section of the flow. Assuming $\Delta p = \Delta p_w$ Equation (6.12) leads to:

$$\frac{D_{hw}}{D_h} = \frac{f_w}{f_i} \tag{6.18}$$

Combining Equations (6.17) and (6.18) leads to:

$$\frac{Re}{f_i} = \frac{Re_w}{f_w} \tag{6.19}$$

The interface friction coefficient ($f_i$) and Reynolds number ($Re$) during the erosion tests are known: the overall friction coefficient can be derived from the (known) overall pressure loss and Reynolds number. The overall Reynolds number is based on the (known) hydraulic diameter of the total cross section of the flow. Replacing $Re_w$ and $f_w$ in Equation (6.14) by $f_i$ and $Re$ gives an explicit solution for $f_w$:

$$f_w = a \cdot \left(\frac{Re}{f_i}\right)^b \tag{6.20}$$

Pugh and Wilson (1999)

The approach of Pugh and Wilson (1999) is based on the same assumption as the method of Vanoni and Brooks (1957):

$$\Delta p \cdot A_{tot} = \Delta p_b \cdot A_b + \Delta p_w \cdot A_w \tag{6.21}$$

In order to solve Equation (6.21) Pugh and Wilson (1999) developed a method on the idea to divide the flow into two areas: the wall and bed associated area. At

the intersection between both areas, the shear stress is assumed to be zero (Figure 6.7). In case the walls of both areas have different roughnesses, the position of the dividing line shifts towards the smoother wall. The pressure gradient as well as the depth-averaged flow velocity in both areas of the flow is considered to be equal (see Figure 6.7). An unequal pressure gradient in both areas is physically impossible. In case of an unequal pressure gradient, the difference in pressure between both areas should lead to a flow perpendicular to the direction of the flow.

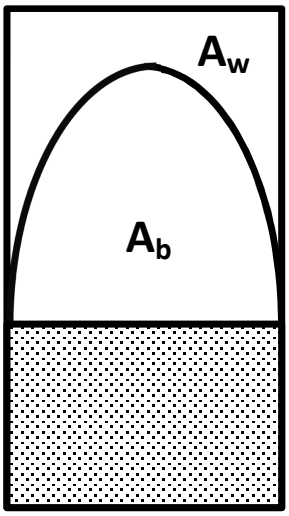


Figure 6.7: Bed and wall associated area

Including the assumption: $\Delta p = \Delta p_b = \Delta p_w$, in which $p_{tot}$ is the total pressure loss over the length of the measurement section, $l$, $p_b$ is the pressure loss along sand bed and $p_w$ is the pressure loss along the wall of the measurement section, this leads to:

$$A_{tot} = A_b + A_w \tag{6.22}$$

Equation (6.22) needs an estimate for the wall associated hydraulic diameter to define the wall associated bed area. The wall associated hydraulic diameter is determined with an iterative procedure on the basis of:

$$D_{hw} = \frac{f_w \cdot \Delta x \cdot U^2 \cdot \rho_w}{2 \cdot \Delta p} \tag{6.23}$$

$\Delta p$ can be used in Equation (6.23) because Pugh and Wilson (1999) have assumed that $\Delta p = \Delta p_w$. The first value for $f_w$ in the iterative procedure is based on the overall hydraulic diameter of the total (bed + wall associated) area above the sand bed, using Equation (3.33). Equation (5.4), however, is an implicit equation, needing a first guess for the wall friction. This first guess is based on Equation (5.5)

(Swamee and Jain, 1976) giving an accurate first guess for $f_w$, with a maximum difference between the both values, as calculated with Equation (5.5) and (5.4), of 0.5 %.

The value for the roughness height of the wall of the measurement section is determined on the basis of flow tests at different depth-averaged flow velocities and the calibrations before and after a set of erosion experiments and an one-point calibration test during the actual erosion experiment. The data of tests result in a varying wall roughness, according to Equation (5.4), as presented in Table 5.1. These results show the same trend as concluded on the basis of the results as presented in Table 6.1. Each set of experiments on the same sand type showed a corresponding roughness height.

Only the results of experiments 38, 43, 52, 60 and 77 deviated from the corresponding set of experiments (see Table 5.1). This is caused by the presence of air in the pressure gauges, for which these gauges were very sensitive. Although, these gauges were checked by deaeration of the pressures gauges for the beginning of each experiment, still some results proved to be unreliable. The results of the deviating pressure gradient measurements are validated in Section 7.2.

The wall associated hydraulic diameter is determined with Equation (6.23) according to an iterative procedure. The first guess for the wall associated hydraulic diameter is based on the flow area above the eroding sand bed. The resulting wall friction coefficient, according to Equations (5.5) and (5.4), is used to get a new value for wall associated hydraulic diameter with the help of:

$$D_{hw} = \frac{f_w}{2} \cdot U^2 \cdot \rho_w \tag{6.24}$$

Five or six iterations, according to the procedure as described, converge to a relative error of less than 0.01% for the wall friction coefficient and wall associated hydraulic diameter. Based on this wall associated hydraulic diameter the the wall and bed associated area are determined, while the bed associated hydraulic diameter is derived ($D_{hb}$), using:

$$D_{hb} = \frac{4 \cdot A_b}{O_b} \tag{6.25}$$

in which $O_b$ is the wetted bed perimeter related to surface of sand bed, in this case equal to the width $w$ of the sand bed in the measurement section. With a known bed associated hydraulic diameter and the bed friction coefficient is derived:

$$D_{hb} = \frac{f_b}{2} \cdot U^2 \cdot \rho_w \cdot \Delta x \tag{6.26}$$

### 6.4.3. Validation bed shear stress

The methods of Vanoni and Brooks (1957) and Pugh and Wilson (1999) give comparable results for the bed shear stress (Figure 6.8). The maximum difference between both methods for the results of the first test series is 8%, while on overall the difference during the first series is less than 3%. This difference is much less than the influence of the experimental errors (Section 6.5). The method of Pugh and

Wilson (1999) is used in the further analysis of the data, because this method is more widely used than the method of Vanoni and Brooks (1957), like for instance by Matousek (2007). Secondly this method is based on a bed associated area (Figure 6.7), assuming no friction between this area and the wall associated area. This is comparable with breaching and jetting (Figure 6.9). The flow through a breach is comparable to open channel flow, with no friction at the surface, while the flow as a result of a translating water jet is comparable with the situation assuming a bed and wall associated area.

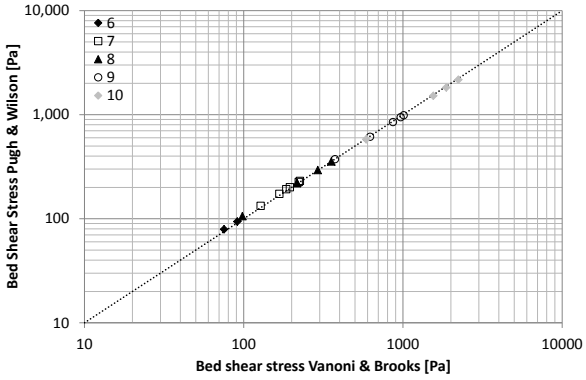




Figure 6.8: Comparison of calculated bed shear stress according to Vanoni and Brooks (1957) and Pugh and Wilson (1999)

The results of the method of Pugh and Wilson (1999) are used to validate the calculated bed shear stress with implicit relations relating the Shields parameter and the bed roughness $k_s$, because this approach is comparable to the way in which the bed shear stress is calculated during breaching of a sand dike and jetting of sand with a translating jet in horizontal direction (Figure 6.9). During breaching and water jetting part of the circumference of the flow is influenced by friction of the sand bed or sand core of the breach in the dike. The upper part of the flow is considered to be free of friction. This is comparable to the basic assumption in the determination of the bed shear stress, which is related to a bed associated area. The top of this area is also considered as free of friction.

The term apparent bed roughness is used because for $\theta_b > 1$ it is assumed that the calculated bed roughness does not represent the actual roughness of the bed. Many researchers consider that the bed roughness or bed friction at these conditions is a measure for the thickness of the disturbed bed or sheet flow layer assuming a logarithmic velocity profile. However, it should be considered that these apparent parameters are a measure for the energy dissipation close to the eroding bed, due to grain-grain and grain-fluid interaction (Dohmen-Janssen, 1999). Besides the velocity profile in the sheet flow layer (high density slurry) close the stationary bed is linear instead of logarithmic (Pugh and Wilson, 1999), see also Section 3.4.4. The apparent bed roughness ($k_b$) has been derived from the apparent bed friction ($f_b$) on the basis of the expression of Nikuradse for a hydraulic rough boundary

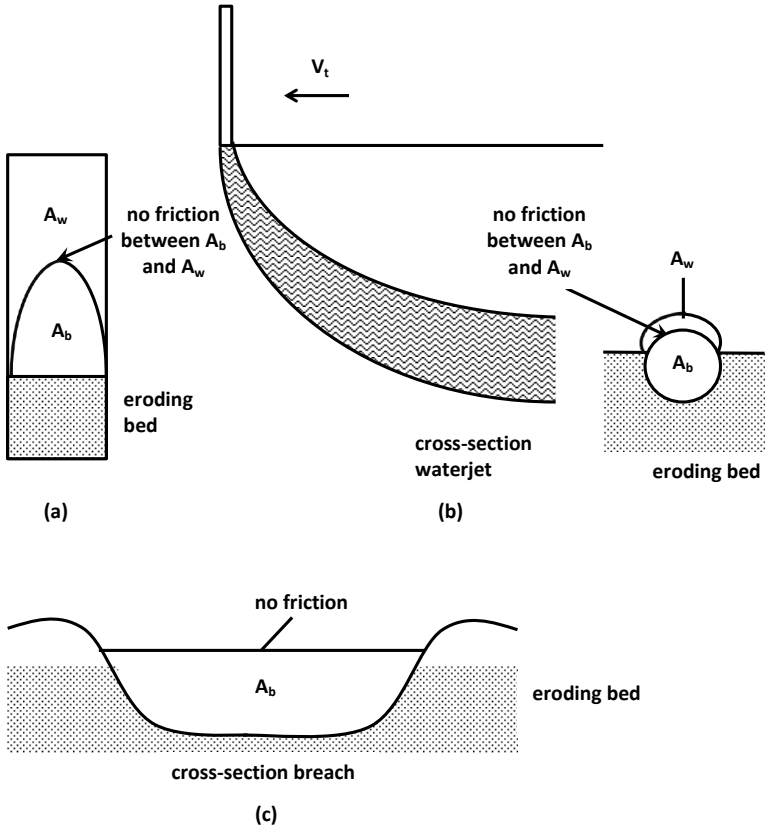


Figure 6.9: Bed friction during water jetting and breaching

(Schlichting and Gersten, 1999):

$$\sqrt{\frac{8}{f_b}} = 2.46 \cdot ln\left(\frac{3.7 \cdot D_{hb}}{k_s}\right) \tag{6.27}$$

According to Pugh and Wilson (1999) the relative apparent bed roughness ($k_s/d_{50}$) is related to the Shields parameter (see Figure 6.10) according to:

$$\frac{k_s}{d_{50}} = C \cdot \theta_b \tag{6.28}$$

The constant $C$ in Equation (6.28) is estimated to be 5, within the range of this constant in numerous existing comparable relations as summarized by Dohmen-Janssen (1999): $k_s/d_{50} = C \cdot \theta_b^{\alpha}$ in which $C$ = constant ranging between 3 and 430 and $\alpha \approx 1$. The results of experiment 6 through 10 show the same relation between the relative apparent bed roughness and Shields parameter as the results of pressurized-conduit experiments in a rectangular section of Nnadi and Wilson

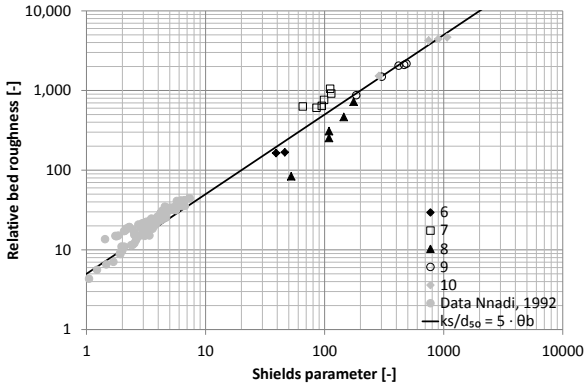


Figure 6.10: Relative apparent bed roughness ($k_s/d_{50}$) as function of the Shields parameter ($\theta_b$) based on the present experiments and data from Nnadi and Wilson (1992), which are also based on pressurized-conduit experiments in a rectangular section



(1992). Besides they coincide also well with the most well-known expression of Wilson (1989) in which the constant $C$ is estimated to be equal to 5, see Equation (6.28). It should be noted that Equation (6.28) has its limitations, because it is a implicit equation. According to Equation (6.28) the apparent bed roughness is independent of the grain size. As long as considering a linear relation between the apparent bed roughness and Shields parameters, the apparent bed roughness can be considered to depend on the bed friction coefficient and depth-averaged flow velocity and to be independent of the grain size.

The calculated apparent bed roughnesses during the first series of experiments are between 0.025 and 0.6 m. Some values are larger than the dimensions of the measurement section. This means that the apparent bed roughness, as calculated according to Equation (6.27), has no physical meaning in case of a flow over an eroding or moving sand bed. It is impossible that the apparent bed roughness is a measure for the thickness of the disturbed bed or sheet flow layer above the non-disturbed bed, substantiating the explanation of Dohmen-Janssen (1999), that the friction along an eroding or sedimenting bed is determined by the interaction of grains with each other and the surrounding fluid. However, it should be noted that the effect of inertia, as result of the acceleration of eroded grains, should be taken also into account.

### 6.4.4. Other parameters

The depth-averaged flow velocity is derived on the basis of the average discharge through the measurement section between these erosion moments and the area of the cross section above the sand bed. All other parameters are also determined on the basis of their average value between these moments.

## 6.5. Experimental errors

Figure 6.11 and 6.12 show the relation between the pick-up flux (Bisschop et al., 2016) and the bed shear stress and depth-averaged flow velocity including the experimental errors for the first test series. The relative error of the bed shear stress is between 0.05 and 0.8. However, because the bed shear stress during the experiments of the second series is mainly above 100 Pa, Figure 6.11b shows that the maximum relative error for most experiments is between 0.05 and 0.5. The main contributor to this error is the error made in the derivation of the hydraulic pressure gradient due to friction in the measurement section. This error is mainly influenced by the uncertainty in the rate of the change of the flow height ($\Delta h/\Delta t$) between two erosion moments and the uncertainty in the determination of the density of the eroding flow.

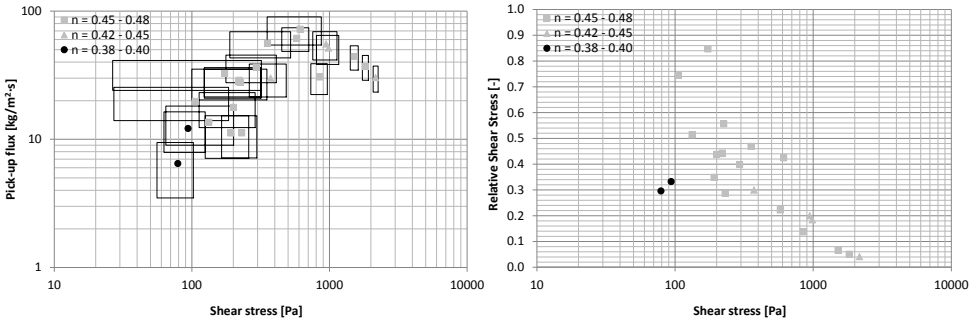


(a) (b)

Figure 6.11: Pick-up flux as function of the bed shear stress (Bisschop et al., 2016) (a) and relative error ($\Delta\tau_b/\tau_b$) as function of the bed shear stress (b)

The experimental error of the pick-up flux is less substantial. For a pick-up flux of more than 5 kg/m$^2$·s the relative experimental error ($\Delta E/E$) is between 0.2 and 0.4. Lower pick-up fluxes show an relative error increasing up to 0.7. This error is mainly caused by the fact that the erosion process is characterized by consecutive erosion and sedimentation fluxes (Section 8.2). This results in a relative irregular change of the level of the top of the eroding sand bed and fluctuating pick-up flux. Besides, this error is influenced by the fact that during the erosion process the top of the eroding sand bed was not fully horizontal and the conductivity probes were mounted in a sloping matrix. Probes, located at different vertical levels, had different horizontal coordinates. The horizontal distance between two consecutive conductivity probes in vertical direction was between 0.1 and 0.4 meter. In case the top of the eroding sand bed was not horizontal during the experiment, this has influenced the determination of the actual erosion velocity and pick-up flux. Another contributor to the error is the uncertainty of the value of the near-bed concentration (Section 8.3). Figure shows also that the relative experimental error of the depth-averaged flow velocity is negligible (0.01 to 0.02).

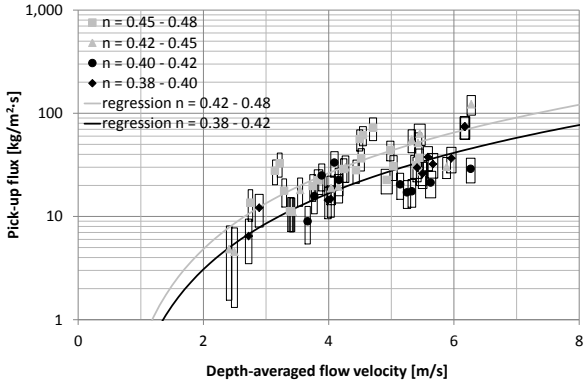


Figure 6.12: Pick-up flux as function of the depth-averaged flow velocity above the sand bed and porosity (Bisschop et al., 2016)

## 6.6. Results

The obtained results of all experiments are summarized in Appendix B, C and D. These appendices show the results of all experiments of which a reliable determination of the pick-up flux and bed shear stress is possible. During each experiment more erosion data were obtained than presented, because some of these data have been removed from the results in case of:

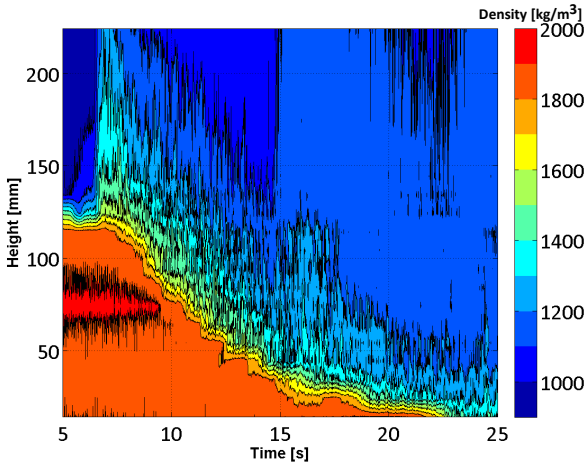


Figure 6.13: Retarding of erosion velocity during experiment 25

1. strongly increasing or decreasing erosion velocity. During some experiments the erosion velocity increased or decreased strongly at the end of the erosion experiment (data derived from the lowest mounted conductivity probes). The

increase of the erosion velocity is the result of shearing of the remaining sand bed over the bottom of the measurement section. However, other experiments (see Figure 6.13) exhibited a decreasing erosion velocity at the end of the experiment.

2. the pick-up flux is derived on the basis of the erosion velocity and is defined as the quotient of the height interval (mainly 10 mm) between two connected conductivity probes and the time interval between the erosion moments at which the erosion front passed both probes. These conductivity probes were mounted in a sloping matrix: the probes did not have the same horizontal coordinate in the lexan plate (see Figure 5.3). In order to avoid mutual influence of the electric current between the conductivity probes, these were mounted at a minimum distance of 50 mm from each other. The horizontal distance between the connected conductivity probes was 100 mm (not all mounted conductivity probes were connected to the signal amplifier). However, the second row of the sloping matrix of conductivity probes started 400 mm upstream of the row above. In case of a not completely horizontal erosion front this influenced the determination of the actual erosion velocity. Only data were used of two conductivity probes mounted at a maximum horizontal distance of each other of 100 mm and vertical distance of 10 mm;

3. accelerating depth-averaged flow velocity during the experiments. Only data were used, based on an erosion interval during which the depth-averaged flow velocity did not differ more than 10 to 15% from the minimum and maximum flow velocity in this interval. At higher accelerating depth-averaged flow velocities between two erosion moments the correction for the influence of the accelerating depth-averaged flow velocity led to the determination of unrealistic and unreliable bed shear stresses;

4. highly temporarily accelerating or retarding depth-averaged flow velocity in the time interval between two erosion moments. No reliable or realistic bed shear stress could be derived in this case;

5. maximum range of the pressure gauges was reached;

6. difference of the measurements with the pressure gauges. As long as the pressure gradient measurement over a distance of approximately 3 m differs not more than approximately 25% from the measurement of the pressure gradient over approximately 2 m, the data are used for the determination of the bed shear stress;

7. the derived bed shear stress is negative. This was mainly the case at the end of the experiment, when almost all sand was eroded from the measurement section.

These criteria were used to determine three datasets:

1. pick-up flux versus depth-averaged flow velocity;

2. bed shear stress versus depth-averaged flow velocity;

3. pick-up flux versus bed shear stress.

The data of these datasets are presented in appendix B, C and D.

## 6.7. Conclusions

The measurements with the electrical conductivity probes were influenced by the dimensions of the electrical flow field between the transducers of these probes. Analysis of the results of these measurements during the experiments, showed an apparent density drop of the density of the sand bed before the sand bed was actually eroded by the flow. This was influenced by the fact that the conductivity probes consisted of two transducers mounted in horizontal direction at a distance of 7 mm from each other. Based on some specific executed experiments it was concluded that when the top of the sand bed was less than 3 mm above the conductivity probes the measurements were influenced by the presence of water above the sand bed. In this situation the electrical resistivity between the transducers was influenced by the lower electrical resistivity of the water present above the top of the sand bed. The electric current followed the way of the lowest electric resistance, following a path through the sand bed to the eroding fluid and back in the bed again, reducing the electrical resistivity (Figure 6.5). This effect explains the apparent drop of the density before the erosion front actual reached the exact level of the conductivity probes. This means that only measured changes of the electrical conductivity, at a level of more than approximately 3 mm, represent a real physical change of the density of the sand bed.



The main uncertainty in the determination of the pick-up flux is the value for the near-bed concentration in order to determine the effective sedimentation flux during the erosion experiments. The level above the erosion front (height above the non-eroded sand bed), over which the near-bed concentration should be determined, is not well defined. This level varies and depends on the pick-up flux, turbulent energy of the flow, dimensions of the turbulent eddies and fall velocity of the grains. The near-bed concentration which is representative for the sedimentation flux is based on the analysis of the erosion process. This is described in Section 8.3.

The data of the pressure gradient measurements are corrected for pressure losses as a result of acceleration of the flow, increase of the flow height and increase of the density of the eroding flow as a result of erosion. This results in a total pressure gradient depending on the friction along the bed and wall of the measurement section. This needs a method to distinguish the effect of friction due to the wall of the measurement section and the effective friction along the eroding sand bed in order to derive the shear stress along the top of the sand bed. Different methods are available to distinguish the wall and bed shear stresses on the basis of the overall pressure gradient in the measurement section. Two different methods, as described by Vanoni and Brooks (1957) and Pugh and Wilson (1999), show highly comparable results for the determination of the bed shear stress including correction for the wall friction of the measurement section. The method of Pugh and Wilson (1999) is used

in the further analysis because the basic assumption of this method is comparable to the flow conditions during breaching and a translating water jet and this method is more widely used as for example by Matousek (2007).

The validity of these methods has been checked by comparison of the calculated effective bed roughness with existing experimental data of Nnadi and Wilson (1992) and comparison of these data with an existing empirical relation of Pugh and Wilson (1999). The difference between the bed shear stress as derived by both methods is negligible, especially in comparison with the experimental error made in the determination of the bed shear stress. The calculated effective bed roughness agrees well with the implicit empirical Equation (6.28), with $C = 5$, and shows the same trend as the experimental data of Nnadi and Wilson (1992). This substantiates the validity of the pressure gradient measurements, used correction of the influence of the non-uniform flow conditions and effect of the friction of the wall of the measurement section for the determination of the effective bed shear stress during the erosion experiments.

Pick-up fluxes of more than 5 kg/m$^2$ show a relative experimental error between 20 and 40%. However, lower pick-up fluxes show a considerable error of up to 70%. The main contributors to this error are the uncertainty of the value for the near-bed concentration, inclination of the sand bed during the erosion experiments and the fact that the conductivity probes were mounted in a sloping matrix. The relative experimental error of the bed shear stress for most of the experiments is between 5 and 50%. The main contributor is the error made in the derivation of the pressure gradient due to friction in the measurement section. The total relative experimental error in the determination of the depth-averaged flow velocity is negligible (1 to 2%).

The visual observations demonstrate the presence of excess pore water pressures and the description of the erosion process assumes the presence of pore water under pressures during erosion. However, during the erosion experiments the pressure gauges did not show significant changes of the pore water pressures during the erosion process. Improvement of the experimental set-up is necessary to measure the pore water pressures during erosion.

# 7

# Analysis bed shear stress

## 7.1. Introduction

For the determination of the bed shear stress and/or energy loss along the eroding sand bed, the measured hydraulic resistance needed correction for the acceleration of the flow during the erosion experiments, the change of density of the flow and the difference between the energy loss along the wall of the measurement section and the eroding sand bed. The effective bed roughness, as derived from these measurements, agreed well with existing implicit equations, relating the bed roughness to the bed shear stress, despite the relative error in the determination of the bed shear stress (5 to 50%). In order to gather more knowledge regarding the energy loss along an eroding sand bed, the effect of several parameters on the bed shear stress and bed friction coefficient were studied.

The effective bed shear stress during the dilatancy reduced erosion process is determined by the energy dissipation between the eroding flow and sand bed. All present pick-up functions consider the shear forces along the bed as the driving mechanism for the pick-up of grains and are widely used as input parameter for the calculation of the pick-up flux in case of dilatancy reduced erosion (Section 4.5). However, it should be noted that the pick-up flux influences also the effective bed shear stress and bed friction, meaning that the pick-up and bed shear stress influence each other. Section 7.2 gives a short validation of the data of the bed shear stress of all experiments by comparing the data with existing relations between the bed roughness and Shields parameter.

In case of a turbulent flow the relation between the roughness of the wall and wall shear stress is based on a logarithmic velocity profile. However, sheet flow experiments of Pugh and Wilson (1999) have revealed a linear velocity profile in the sheet flow layer. In order to check this assumption, in case of erosion, the velocity profile was measured with a 2-axis electromagnetic flow velocity meter. The results of these experiments are described in Section 7.3.

The followed approach for the validation of the effective bed shear stress and

bed friction as derived from the hydraulic pressure gradient measurements, gives unrealistic values for the apparent bed roughness, making it necessary to develop an alternative approach in order to determine the friction loss along an eroding sand bed. This approach is described in Section 7.4. This Section gives a description of the relation of the effective bed shear stress and Darcy-Weisbach bed friction coefficient with several operational parameters. The bed shear stress and the bed friction coefficient depend mainly on the product of the flow velocity and density of the eroding flow. Other operational parameters have less influence. Section 7.5 describes two empirical models in order to determine the bed friction relating the flow velocity to the bed shear stress. These models can also be used in case of breaching and water jetting. The results of the analysis of the measurements are discussed in Section 7.6.

## 7.2. Validation measurements

Numerous investigations, see Dohmen-Janssen (1999), have related the apparent relative bed roughness ($k_s/d_{50}$) during sheet flow conditions to the Shields parameter: Equation (3.35). However, it should be noted this is an implicit relation. Considering a linear relation between the relative apparent bed roughness and Shields parameter, the bed roughness is independent of the grain size but is directly related to the bed shear stress and as a result to the depth-averaged flow velocity. Besides the apparent bed roughness has no physical meaning. The bed friction along an highly eroding sand bed is determined by the energy dissipation due to grain-grain and grain-fluid interaction (Dohmen-Janssen, 1999).

The comparison of the experimental data with Equation (3.35) gives only an indication of the accuracy of the experimental results and necessary corrections. These corrections are necessary because of the non-uniform flow conditions during the erosion tests (Section 6.4), in order to derive the bed shear stress on the basis of the pressure loss measurements in the measurement section.

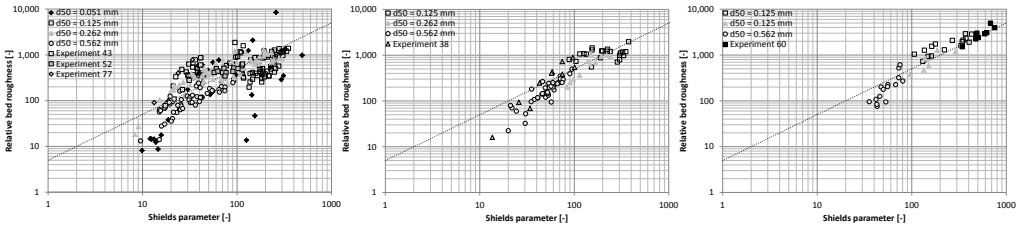


(a) (b) (c)

Figure 7.1: Derived apparent relative bed roughness ($k_s/d_{50}$) as function of the measured Shields parameter as derived from all experiments on four sand types ($d_{50}$: 0.051 mm, 0.125 mm, 0.262 mm and 0.562 mm) at a density of the eroding flow of 1070 - 1190 kg/m$^3$ (a), 1210 - 1310 kg/m$^3$ (b) and 1360 - 1470 kg/m$^3$ (c). The results of the experiments with deviating results of the calibration procedure (experiments 38, 43, 52, 60 and 77) are shown separately. These results are compared, together with the results of all other experiments, with Equation (3.35) with $C = 5$

Figure 7.1 shows that the data of the experiments follow the existing relation

between the relative bed roughness and Shields parameter according to Equation (3.35) with $C = 5$ (Wilson, 1989). This gives confidence on the way of determining the bed shear stress on the basis of the measured pressure gradient. The effect of the density of the eroding flow is negligible, which can also be derived from Figure 7.2. Above a Shields parameter of 50 the results of all experiments show a corresponding relation between the relative bed roughness and the Shields parameter. Besides, at a Shields parameter of less than 50, Equation (3.35) overestimates the bed roughness for $C = 5$.

The data show also that the apparent bed roughness ($k_s$) can not have a physical meaning at a high Shields parameter. In case of a Shields parameter of 200 the apparent relative bed roughness is between 500 and 2000, leading to an apparent bed roughness ranging between 25 mm and 0.5 meter. This last value is far beyond the height of the measurement section (0.288 meter). This endorses that the apparent bed roughness cannot be a measure for the thickness of the sheet flow layer or shear layer (Section 3.5).

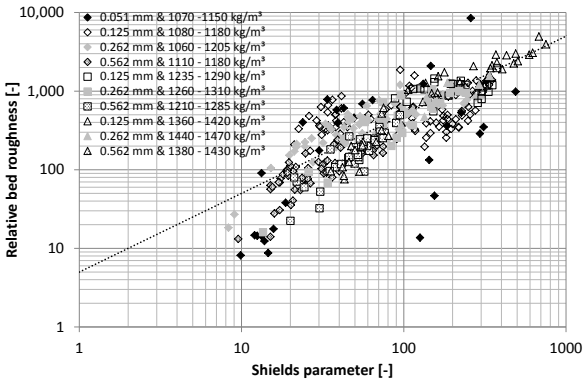


Figure 7.2: Relative bed roughness as function of the Shields parameter as derived from all experiments

Section 6.4.2 describes the results of the calibration tests of the pressure gauges. During some experiments (experiments 38, 43, 52, 60 and 77) the results of the calibration procedure of the differential pressure gauges in the measurement section deviated from the other experiments. The pressure measurements during these experiments have been corrected for this specific deviation. Figure 7.1 shows that the results of these experiments do not deviate significantly from the results of the other experiments.

The data have been further validated on the basis of the relation between the wall and bed friction coefficient, as determined according to section 6.4.2. Figure 7.3 shows that the results of experiments 38, 43, 52, 60 and 77 deviate significantly from the results of the other experiments, due to the difference in the results of the calibration of pressure gauges (see Section 6.4.2). On the basis of the relation between the bed friction coefficient and the wall friction coefficient the results of the deviating experiments have been excluded from the analysis of the bed friction and

bed shear stress.

This means that Equation (3.35) should be used with great care because it is an implicit equation and this equation has more than one solution (see Section 3.4.4). This introduces the effect that deviating experimental results, due to for instance measurement errors, still fulfill Equation (3.35). The implicit character of this relation causes that deviating results in for instance the Shields parameter are corrected by the same deviation in the related relative bed roughness.

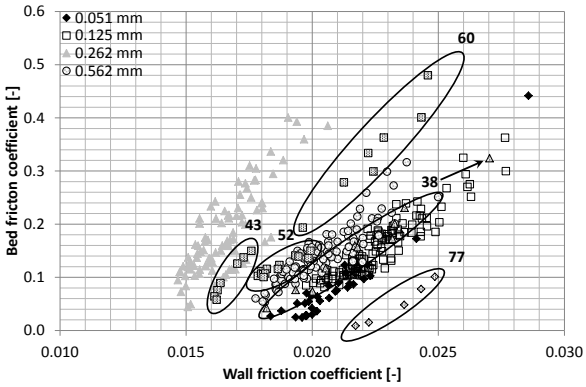


Figure 7.3: Bed friction as function of the wall friction as derived from the results of the experiments: validation of the results of experiments 38, 43, 52, 60 and 77

7

## 7.3. Results velocity profile measurements

The velocity profile was measured with a 2-axis electromagnetic flow velocity meter (EMS) mounted at a distance of 78 mm above the bottom of the measurement section. Due to the sensitivity of this instrument for the impact of grains and maximum range of the flow velocity of the EMS ($< 3$ m/s) only measurements were executed during the experiments with Silverbond sand. According to Pugh and Wilson (1999) (Section 3.5.4) the velocity profile during sheet flow is constant above a water depth of $0.25 \cdot h_s$ ($h_s$ = thickness shear layer). At the beginning of the erosion experiment the flow velocity meter was located in the sand bed, because during sedimentation a sand bed was created of which the top was above the location of the flow velocity meter. Due to erosion the top of the sand bed moved downwards until the top of the sand bed reached the level of the flow velocity meter. From this moment the flow velocity meter could measure the flow velocity at an increasing height above the top of the sand bed. The vertical distance between the electromagnetic flow velocity meter and the non-eroded sand bed was determined on the basis of the average erosion velocity of the sand bed below a depth of 78 mm in the measurement section. The results of these measurements are presented in Figure 7.4.

Instead of a linear profile, as measured by Pugh and Wilson (1999), the results of these measurements seem to correspond more with a traditional logarithmic profile.

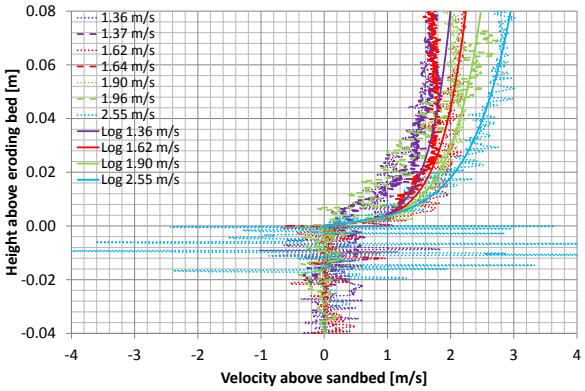


Figure 7.4: Measured velocity profile above the eroding sand bed during the experiments on Silverbond sand at different depth-averaged flow velocities compared to the traditional logarithmic velocity profile

This can be explained by the fact that the pick-up flux during these experiments was relative low, causing a relative steep concentration gradient directly above the eroding sand bed (Figure 7.5). The concentration of grains was relative low, resulting in a limited influence of the grains on the velocity profile. Comparison of these data with the logarithmic profile needs a value for the bed roughness ($k_s$) in Equation (3.6). This was determined on the basis of a specific empirical relation between the apparent bed roughness and Shields parameter for Silverbond sand, deviating slightly from the overall relation $\frac{k_s}{d_{50}} = 5 \cdot \theta_b$ as derived by Wilson (1989):

$$\frac{k_s}{d_{50}} = 5.804 \cdot \theta_b \tag{7.1}$$

With $\theta_b = \frac{\tau_b}{(\rho_s - \rho_w) \cdot g \cdot d_{50}}$ Equation (7.1) can be rewritten as:

$$k_s = 5.804 \cdot \frac{\tau_b}{(\rho_s - \rho_w) \cdot g} \tag{7.2}$$

Equation (7.2) needs an estimate for the bed shear stress during these experiments. This was determined on the basis of an empirical relation between the bed shear stress and the Darcy-Weisbach friction coefficient: Using:

$$\tau_b = \frac{f_b}{8} \cdot \rho_w \cdot U^2 \tag{7.3}$$

On the basis of the results of the experiments on Silverbond sand (7.6a) an empirical value for the Darcy-Weisbach friction factor ($f_b = 0.079$) was determined. The theoretically velocity profile was calculated using Equation (3.6) in which $k_s$ was determined using Equation (7.2) and Equation (7.3). This gives a good comparison of the theoretical and measured velocity profile, emphasizing that the effective bed roughness or energy loss along the eroding bed increases strongly due to the effect of grain-grain and grain-fluid interactions in comparison with a non eroding sand

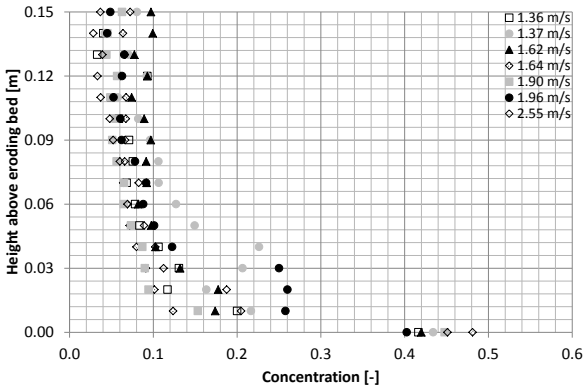


Figure 7.5: Average concentration profile at different depth-averaged flow velocities

bed at which the energy loss is determined by the roughness of the grains. This can be substantiated by determining the apparent bed roughness, using Equation (7.2). Between a depth-averaged flow velocity of 1.3 and 2.5 m/s the apparent bed roughness varies between 0.009 and 0.023 m. As described in Section 3.4.2 the bed roughness of a non or almost non-eroding bed is approximately $3 \cdot d_{90}$. The $d_{90}$ of the used Silverbond sand is 0.000087 m. This means that the bed roughness is approximately 0.00026 m. This is a factor 35 to 90 smaller in comparison with the apparent roughness during erosion. This supports the assumption that the apparent bed roughness at these flow velocities does not represent the actual roughness. The apparent bed roughness or bed friction is a measure for the energy loss as a result of grain-grain and grain-fluid interaction.

## 7.4. Bed shear stress and bed friction

The bed shear stress and bed friction are determined by the density of the eroding flow and the depth-averaged flow velocity and are influenced by the effect of the erosion process. Section 7.4.1 gives an analysis of the influence of the density of the eroding flow and the depth-averaged flow velocity on the bed shear stress and bed friction. The concentration gradient just above the eroding bed, which is influenced and/or determined by the pick-up and sedimentation flux, influences the bed friction (Section 7.4.2), where the bed associated area is also related to the bed friction (Section 7.4.3).

### 7.4.1. Influence of density eroding flow and flow velocity

Operational parameters influencing the bed shear stress are the density of the flow and the depth-averaged flow velocity. The bed shear stress is related to the product of the density of the flow and the squared value of the depth-averaged flow velocity: the dynamic pressure (Figures 7.6a, 7.6d, 7.6g and 7.6j). However, these figures show also a striking difference between the experiments with Geba sand, Zilverzand

and Dorsilit sand. Geba sand ($d_{50}$ = 125 $\mu$m) shows an influence of the density of the eroding flow on the relation between the bed shear stress and the squared value of the depth-averaged flow velocity. The effective bed friction increases as the density of the eroding flow increases. The experiments on coarser sand (Zilverzand and Dorsilit) do not exhibit any influence of the density of the eroding flow on the relation between the bed shear stress and squared value of the depth-averaged flow velocity. All four sand types show more or less the same (implicit) relation between the bed friction and bed shear stress. This is in accordance with the assumption that the fictitious bed roughness under these flow conditions, to be determined according to Equation (3.35), is independent of the grain size.

Figure 7.7 shows a clear relation between the bed shear stress and the product of the density of the eroding flow and the squared value of the depth-averaged flow velocity, especially for the experiments at which the density of the eroding flow is approximately 1100 kg/$m^3$. The three sand types with the largest grain diameter show a more or less coinciding relation of the bed shear stress with the squared value of the depth-averaged flow velocity, while the experiments with the finest sand type (Silverbond: $d_{50}$ = 51 $\mu$m) show a lower stress at corresponding density and depth-averaged flow velocity. At a higher density of the eroding flow the relation between the bed shear stress and the squared value of the depth-averaged flow velocity is less clear and some sand types show a deviating behavior of the overall view: Zilverzand $d_{50}$ = 262 $\mu$m at a density of the eroding flow of approximately 1300 kg/m$^3$ and Dorsilit at a density of the eroding flow of approximately 1450 kg/m$^3$.

### 7.4.2. Influence of concentration gradient



Another parameter considered to influence the effective bed friction is the near bed concentration gradient, because the effective bed friction is influenced by grain-grain and grain-fluid interaction. Figure 7.8 shows for all sand types the influence of the instantaneous concentration gradient above the eroding sand bed over a distance of 0.01 m and 0.02 m above the eroding sand bed on the effective bed friction. The concentration gradient is defined as the difference between the concentration of the sand bed and concentration of the eroding fluid, as measured by the concentration probes, divided by the distance of the probes situated 0.01 and 0.02 m above the eroded sand bed. A high concentration gradient means that the concentration of the eroding flow just above the eroding sand bed is relative low in comparison with a low erosion gradient.

It should be noted that the instantaneous concentration gradient is influenced by the highly irregular character of the erosion process as a result of the irregular presence of turbulent vortices, causing a variable concentration gradient above the eroding sand bed. Figure 7.8 shows that there is a certain envelope determining the bed friction as function of the concentration gradient. The bed friction is relative low at a high concentration gradient, because of the relative low concentration of grains just above the eroding bed, while the bed friction at a low concentration gradient is higher due to the effect of a higher concentration of grains. The existence of an envelope can be explained by the fact that there is a minimum concentration just above the eroding bed at certain flow conditions, while the maximum concentration

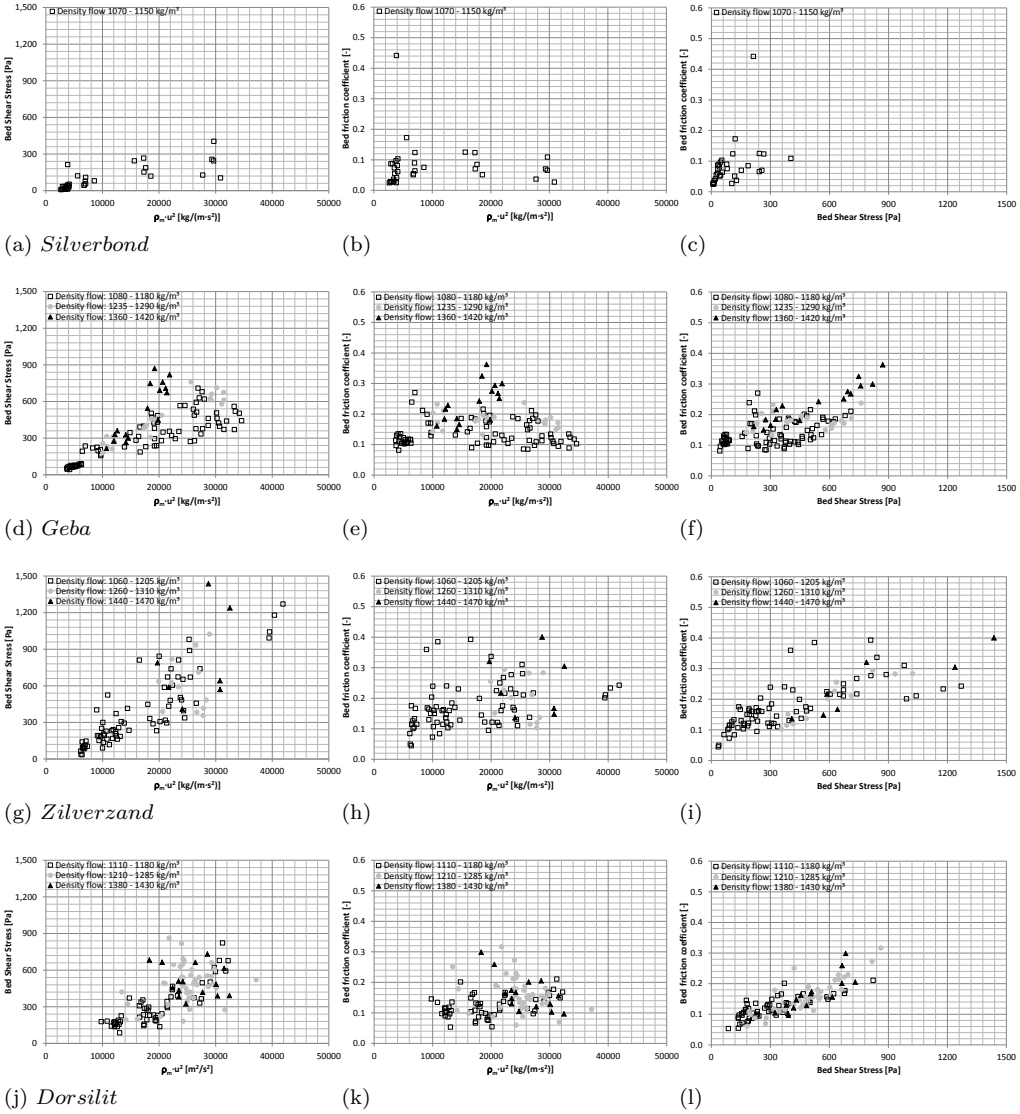


(a) *Silverbond* (b) (c)

(d) *Geba* (e) (f)

(g) *Zilverzand* (h) (i)

(j) *Dorsilit* (k) (l)

Figure 7.6: Bed shear stress and bed friction as derived from the measured pressure gradient versus the product of the density of the eroding flow and the squared value of the depth-averaged flow velocity ($U^2$) and bed friction versus shear stress for all sand types

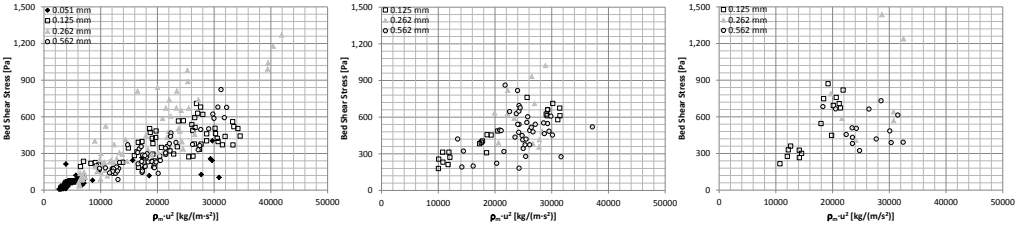


Figure 7.7: Bed shear stress as derived form the measured pressure gradient as function of the squared value of the depth-averaged flow velocity at a density of the eroding flow of 1060 - 1190 kg/m$^3$ (a), 1210 - 1310 kg/m$^3$ (b) and 1360 - 1470 kg/m$^3$ (c) for all sand types

(matching with a low concentration gradient) at these flow conditions is influenced by the highly variable character of the erosion process resulting in large temporary variations of the concentration above the sand bed.

### 7.4.3. Relation with bed associated area and hydraulic diameter

Pugh and Wilson (1999) have assumed that the pressure gradient in the bed and wall associated area (Figure 6.7) is equal. The relative energy loss along the rough (sand bed) and relative smooth, but still rough, walls of the measurement section determines the extent of the bed associated area in relation to the wall associated area. These areas are a measure for the extent of the area influenced by the effective friction along the sand bed and walls of the measurement section. The wall associated area has been derived on the basis of the wall associated diameter which has been derived on the basis of the pressure gradient measurements and wall friction coefficient determined according to Equation (3.33). The results of this analysis show that an increasing bed friction leads to an increasing bed associated hydraulic diameter and area (Figure 7.9). The assumption of Pugh and Wilson (1999) means that an increase of the bed friction in relation to the wall friction leads to a larger bed associated area. In other words: a larger bed friction influences a larger part of the total cross section of the flow.

Figure 7.10 shows that the bed friction leads and the wall friction are related to each other. An increase of the bed friction leads to an increase of the wall friction because an increasing bed friction leads to an increase of the (relative) bed associated area. As a result the wall associated area and corresponding wall associated hydraulic diameter decrease. Using Equation (3.33) a decreasing wall associated hydraulic diameter leads to an increase of the wall friction.

The grain size seems to influence the relation between the bed and wall friction (Figure 7.10a). However, this difference is caused by the difference in roughness of the wall of the measurement section during the experiments. The data of the calibration tests for the experiments on sand with a grain size of 51 and 125 $\mu$m have shown a corresponding roughness (70 to 75 $\mu$m) of the walls of the measurements

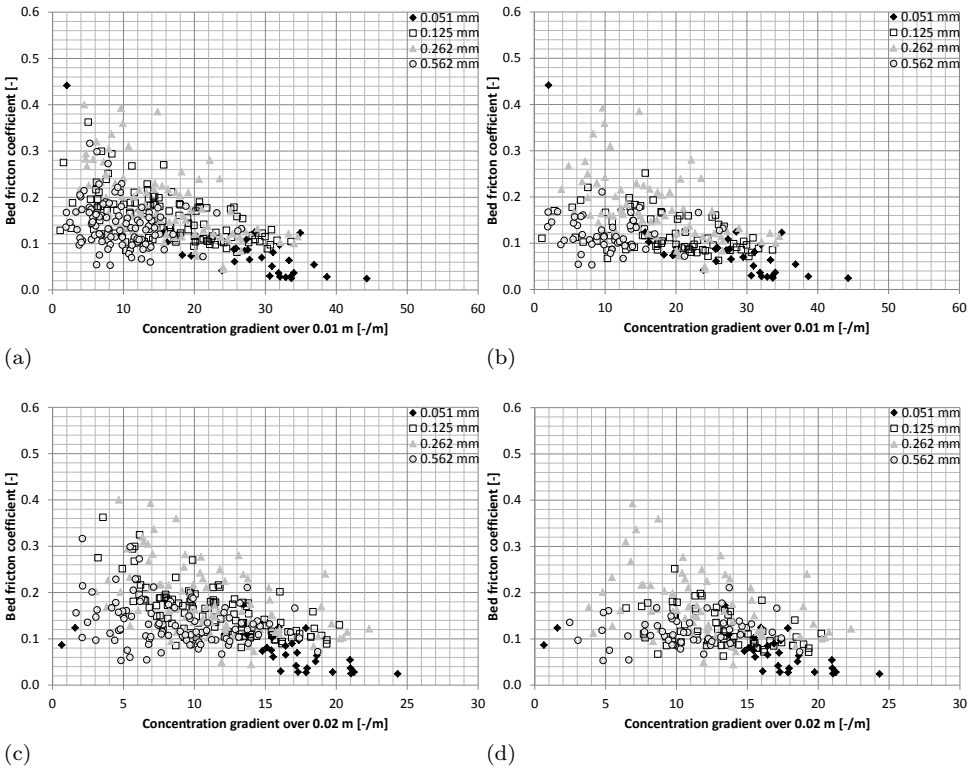


Figure 7.8: Bed friction coefficient as derived from the measured pressure gradient as function of the instantaneous concentration gradient during an experiment over a distance of 0.01 m above the level of the eroding sand bed for all sand types: (a) all experiments & (b) density eroding flow $< 1190$ kg/m$^3$) and over a distance of 0.02 m above the level of the eroding sand bed for all sand types: (c) all experiments & (d) density eroding flow $< 1190$ kg/m$^3$). Note: negative values for the concentration gradient are not shown and the maximum concentration gradient at the x-axes in both figures is not equal

section, leading to a corresponding relation between bed and wall friction. The roughness of the walls of the measurement section during the experiments with the coarser sand types (262 $\mu$m and 562 $\mu$m) were lower: 1 $\mu$m for 262 $\mu$m sand and 39 $\mu$m for 562 $\mu$m sand. The smaller effective roughness of the wall and corresponding lower wall friction coefficient ($f_w$), led to a higher bed friction coefficient. In order to reduce the effect of the wall friction on the bed friction, the bed friction is corrected for the wall friction of the measurement section in case no sand bed was present ($f_{w,i}$): $f_b - f_{w,i}$. This relative bed friction is compared to the relative wall friction, defined as:

$$\frac{f_w - f_{w,i}}{f_{w,i}} \tag{7.4}$$

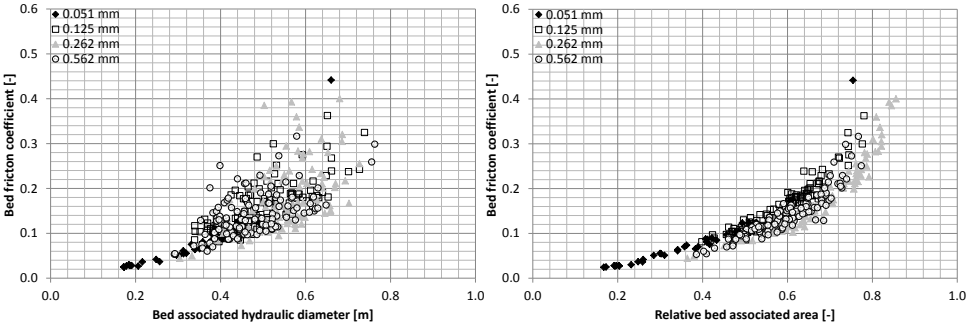


(a) (b)

Figure 7.9: Bed friction as derived from the measured pressure gradient for all sand types as function of the bed associated hydraulic diameter (a) and relative bed associated area: $A_b/A_{tot}$ (b)

in which $f_w$ is defined as the wall friction during the erosion experiment. Figure 7.10b shows the relation between the relative bed friction and relative wall friction, excluding the influence of the wall friction during the experiments on the bed friction. As a result of an increasing bed friction coefficient, the part of the area influenced by the energy-loss along the top of the sand bed increases. The result of this correction shows also that the effect of the grain size on the bed friction can be neglected, being the case at sheet flow conditions.



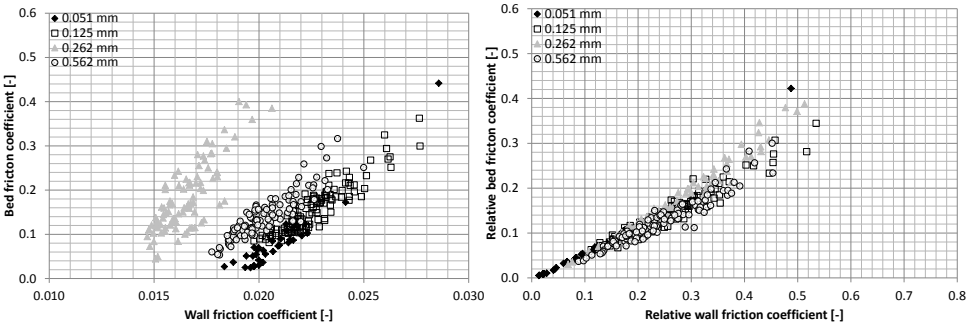


(a) (b)

Figure 7.10: Bed friction as derived from the measured pressure gradient versus wall friction (a) and relative bed friction versus relative wall friction: $A_b/A_{tot}$ (b)

Figure 7.11 presents the relation between the bed associated area and the flow velocity. These results show that the relative bed associated area is more or less constant at depth-averaged flow velocities of more than 2.5 m/s. This is more or less in accordance with data of van Rhee and Talmon (2010). However, it should be noted that the maximum flow velocity during these experiments was 2 m/s.

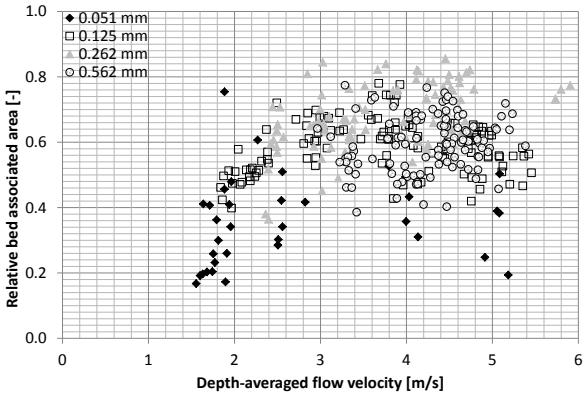


Figure 7.11: Relative bed associated area as derived from the measured pressure gradient as function of the flow velocity for the data of all experiments

## 7.5. Predicting bed friction and bed shear stress

The present models for the determination of the effective bed friction during erosion and sheet flow conditions are based on an apparent bed roughness. As already explained, the apparent bed roughness has no physical meaning in these flow conditions. Besides this, the widely used relation ($\frac{k_s}{d_{50}} = C \cdot \theta$) is an implicit relation and cannot be solved directly, because it has more than one solution (Miedema and Matousek, 2014). These are reasons to derive an explicit relation between the bed friction and relevant operational parameters. A direct relation between the relative bed friction coefficient and the bed associated Reynolds number ($Re_b = U \cdot D_{hb}/\nu_w$) can be derived comparing the relative bed friction to a bed adapted Shields parameter ($\theta^*$, see Figure 7.12), which is defined as:

$$\theta_b^* = \frac{\tau_b \cdot D_{hb}^2}{\rho_w \cdot \nu_w^2} \tag{7.5}$$

on the basis of:

$$f_b - f_{w,i} = a \cdot (\theta^*)^b \tag{7.6}$$

in which $a = 7.721 \cdot 10^{-6}$ and $b = 0.384$, using the results of all experiments. The influence of the density of the eroding flow on this empirical relation is negligible, because the data of the experiments of which the density of the eroding flow is below 1190 kg/m$^3$ give for $a = 8.008 \cdot 10^{-6}$ and for $b = 0.386$. These empirical constants are highly comparable to the empirical constants as derived for all experiments.

Using the results of all experiments and considering $f_{w,i} = 0$ and $\tau_b = \frac{f_b}{8} \cdot \rho_w \cdot U^2$, this leads to the following explicit relation between the bed friction coefficient and bed associated Reynolds number:

$$f_b = 1.373 \cdot 10^{-9} \cdot Re_b^{1.247} \tag{7.7}$$

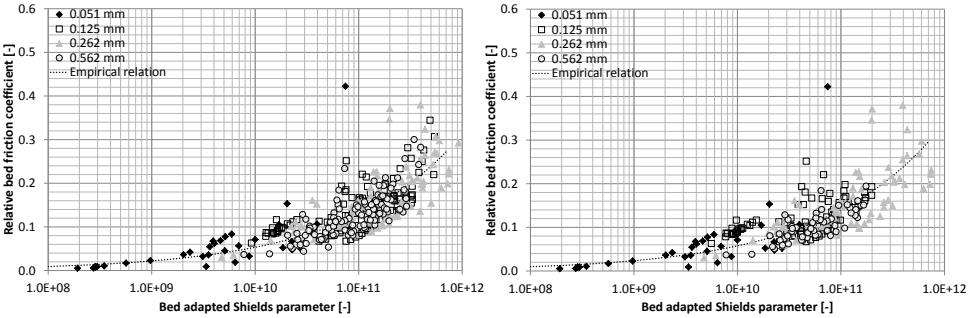


(a) (b)

Figure 7.12: Relative bed friction versus bed adapted Shields parameter as derived from the measured pressure gradient for all data (a) and data with a density of the eroding flow of $< 1190$ kg/m$^3$) (b)

As stated above the influence of the density of the eroding flow is negligible, because the data of the experiments of which the density of the eroding flow is below 1190 kg/m$^3$ give a highly comparable relation:

$$f_b = 1.355 \cdot 10^{-9} \cdot Re_b^{1.257} \tag{7.8}$$

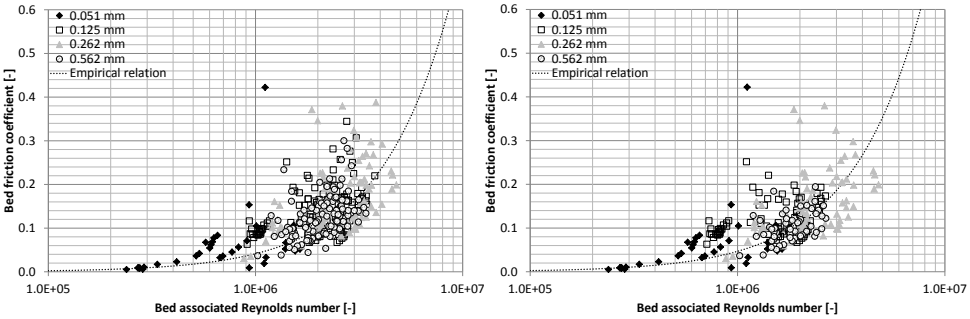


(a) (b)

Figure 7.13: Relative bed friction versus bed associated Reynolds number as derived form the measured pressure gradient for all data (a) and data with a density of the eroding flow of $< 1190$ kg/m$^3$) (b)

Assuming $f_{w,i} = 0$, means that Equations (7.7) and (7.8) can be used in case of jetting and breaching. Figure 6.9 shows that the apparent boundary between the bed and wall associated area during the experiments is comparable to the frictionless surface during water jetting and breaching. In this case the bed hydraulic diameter is equal to the total hydraulic diameter of the flow. However, these equations should be used with great care, because of the specific dimensions of the measurement section. During these experiments the bed associated area is relative large in comparison with

the circumference of the bed (bed width: 0.088 m), leading to a relative large bed associated hydraulic diameter, which is far beyond the height of the measurement section. In order to avoid this restriction an empirical relation can be derived on the basis of a bed area adapted Shields parameter instead of the bed adapted Shields parameter:

$$\theta_b^* = \frac{\tau_b \cdot A_b}{\rho_w \cdot \nu_w^2} \tag{7.9}$$

Using the data from all experiments and considering $f_{w,i} = 0$ and $\tau_b = \frac{f_b}{8} \cdot \rho_w \cdot U^2$, the following relation is found:

$$f_b = 1.026 \cdot 10^{-10} \cdot Re_A^{1.591} \tag{7.10}$$

in which the bed area Reynolds number ($Re_A$) is defined as:

$$Re_A = \frac{U \cdot \sqrt{A_b}}{\nu_w} \tag{7.11}$$

However, Figure 7.14 shows that this approach leads to a less accurate prediction of the bed friction coefficient in comparison with Equations (7.7) and (7.8), as depticted in Figure 7.13.



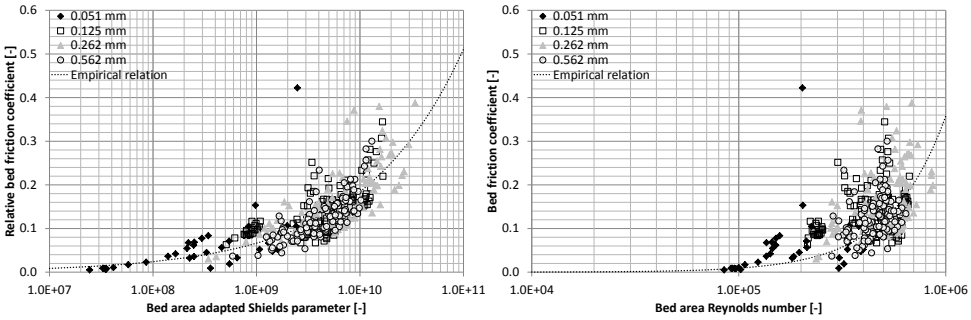


(a) (b)

Figure 7.14: Relative bed friction versus bed area associated Reynolds number (a) and bed friction versus bed associated Reynolds number (b) as derived from the measured pressure gradient of the data of all experiments

Recently Miedema and Ramsdell (2016) developed an explicit equation for the bed friction factor in case of sheet flow during pipeline transport. However, in this case the flow conditions differ from the erosion of sand. If a layer of moving grains or sand bed is present at the bottom of a pipeline (sheet flow conditions), the pick-up and sedimentation flux will be in equilibrium. In case of erosion, the pick-up is larger than the sedimentation flux. Miedema and Ramsdell (2016) have found a corresponding influence of the wall friction in case no sand bed is present and their analysis supported the hypothesis of Wilson (1988) that head loss and as a result the bed friction, does not depend on grain size. However, there is also a difference

in the dependence of the depth-averaged flow velocity. The analysis by Miedema and Ramsdell (2016) shows that the bed friction depends on approximately $U^{2.5}$, while this study shows a relation of the bed friction with $U^{1.25}$ and $U^{1.59}$.

Another difference is the relation with the hydraulic diameter. In the empirical relation of Miedema and Ramsdell (2016) the bed friction depends on the reciprocal value of the hydraulic diameter, while this study shows that the bed friction increases as the bed associated hydraulic diameter increases. The reason for this difference can be explained by the fact that Miedema and Ramsdell (2016) have related the bed friction to the hydraulic diameter based on the total cross section of the flow, while this study relates the bed friction to the hydraulic diameter based on part of the flow: the bed associated hydraulic diameter. The first mentioned hydraulic diameter is defined by the dimensions of the total cross-section of the flow, while the bed associated hydraulic diameter can develop in size at increasing bed friction (see Figure 7.9b).

Miedema and Ramsdell (2016) have presented also an empirical explicit equation, to determine the bed friction coefficient, based on the idea that the energy loss in a sheet flow layer is influenced by the mass of the grains. The mass of a grain is directly related to $d^3$, meaning that the grain size should influence the bed friction coefficient. The empirical equation of Miedema and Ramsdell (2016) relates the bed friction coefficient to $d^{0.28}$. Therefore, this influence is not very strong and the present analysis of the measurements (see Figures 7.13 and 7.14b) as well as Equation (6.28) (Pugh and Wilson, 1999) do not endorse the influence of the size of the grains on the bed friction coefficient. However, this is in contradiction with Figure 7.8 showing the relation between the bed friction coefficient and concentration gradient. The concentration gradient depends on the pick-up and sedimentation flux and especially the sedimentation flux depends on the settling velocity of the grains and hence depends on the grain size.



## 7.6. Discussion

The flow conditions during sheet flow can be considered to be comparable with the flow conditions during the erosion of sand. Present studies relate the bed friction during these conditions, in case of a hydraulic rough flow, via for instance the Colebrook equation (pipe flow) or Chézy equation (open channel flow) to a relation between the relative bed roughness ($k_s/d_{50}$) and the Shields parameter.

This is not the case at low flow velocities and low Shields parameter ($\theta < 0.5$ to 1), being the case during a none or almost non-eroding sand bed. In this case the Colebrook equation is based on the presence of fixed wall roughness elements. The size of the fixed roughness elements determines the friction along the wall and depends on the grain size. Numerous studies show that the effective roughness depends on the size of the largest grains ($d_{90}$). The roughness was mainly found to be in the range of 1 to 10 $\cdot$ $d_{90}$ of the bed material (van Rijn, 1993). Increase of the size of the roughness elements leads to a larger friction coefficient, because large grains will have a larger effect on the retardation of the flow velocity close to the wall or bed than small grains, increasing the effective friction along the bed.

At high flow velocities ($U > 1$ m/s) and/or Shields parameter ($\theta > 0.5$ to 1)

grains simultaneously entrain into the flow and settle down on the eroding sand bed. During these conditions it is considered that the effective roughness is much larger than the grain size of the grains and the relative bed roughness is related to the Shields parameter according to Equation (3.35). The implicit character of this relation apparently improves the accuracy of the equation in relation the experimental data, while the bed roughness during these flow conditions has no physical meaning. Using Equation (3.35) can lead to physical unrealistic dimensions of the effective roughness: effective roughness larger than the diameter in case of pipe flow or larger than the water depth in case of breaching. This emphasizes the fact that the effective roughness has no physical meaning, but is just a measure for the energy loss along on eroding sand bed or in sheet flow conditions.

The results of the present experiments confirm the existing relation between the relative bed roughness and Shields parameter, however the data confirm that implicit relations should be used with great care (Section 7.2). Deviating experimental results, due to for instance measurement errors, still fulfill Equation (3.35) because these deviating experimental results cause deviation of the relative bed roughness as well as the Shields parameter. This was proven by the fact that the results of five experiments fulfilled Equation (3.35), but their results where highly questionable because of deviations during the final calibration of the pressure gauges and comparison of the bed friction with the wall friction in the measurement section.

The need for an explicit empirical relation is emphasized by the fact that Equation 3.35 is an implicit relation and has in most cases more than one solution (see Section 3.4.4). The experiments show that the bed shear stress is directly related to the product of the density of the eroding flow and the squared value of the depth-averaged flow velocity. The effect of the grain size is more or less negligible for the three largest grain sizes ($> 125$ $\mu$m). The experiments show the influence of the concentration of grains directly above the non-eroded part of the sand bed by comparing the concentration gradient over a distance of 0.01 and 0.02 m above the top of the non-eroded part of the sand bed with the bed friction (Figure 7.8). A large concentration gradient (large decrease of the concentration above the top of the sand bed) means that the concentration just above the bed is relative low. This comparison shows that there is a certain envelope determining the maximum bed friction as function of the instantaneous concentration gradient. The maximum bed friction is relative low at a high concentration gradient, because of the low concentration just above the top of the sand bed. A lower concentration gradient, in case higher concentration just above the sand bed, leads to a higher bed friction. The existence of an envelope can be explained by the highly variable character of the erosion process. As a result of turbulent bursts lumps of sand are eroded, leading to a temporarily relative high concentration and low concentration gradients, which are not representative for the average concentration and thus average bed friction.

In case of erosion the pick-up flux is larger than the settling flux. During an oscillating sheet flow the pick-up flux or sedimentation flux consecutively dominate. Because the pick-up and sedimentation process are determined by the grain size (and off course flow velocity) it is expected that the grain size influences the effective bed friction during erosion or sheet flow. However, Equation (3.35) assumes a linear

relation between the relative bed roughness and Shields parameter, considering that the effective bed friction is independent of the grain size and depends solely on the depth-averaged flow velocity and density of the flow. This is confirmed by the results of this study, showing that the bed friction is independent of the grain size. However, this is still questionable because the results of the erosion experiments show that the bed friction coefficient is related to the concentration gradient, which is influenced by the sedimentation and pick-up flux and hence the size of the grains.

The bed friction coefficient depends on the concentration gradient (and concentration) just above the eroding sand bed, not on the average density of the eroding flow. The energy loss is determined by the energy losses as a result of grain-fluid and grain-grain interaction close to the top of the eroding sand bed. However, the concentration is not a useful parameter in order to derive an explicit expression for the determination of the bed friction coefficient. The concentration can only be determined on the basis of experimental results. Considering the negligible influence of the grain size the (implicit) relation between the bed friction and bed shear stress was used to derive a direct relation for the bed friction, which could also be used in case of jetting and breaching. This comparison showed that the bed friction was directly related the bed associated Reynolds number ($Re_b = U \cdot D_{hb}/\nu_w$). The effect of the concentration close to the eroding sand bed is implicitly incorporated in this relation. This can be explained by the influence of the depth-averaged flow velocity. At increasing flow velocity the pick-up of grains will increase leading to a lower concentration gradient and hence a higher concentration just above the non-eroded part of the sand bed. This effect causes an increase of the bed friction during the erosion of sand and shows that the bed friction is directly related to the depth-averaged flow velocity.

Summarizing the analysis of the experimental results shows that the hydraulic pressure gradient along an eroding sand bed and thus the bed shear stress and bed friction depend on concentration gradient close to the eroding sand bed. This concentration gradient depends on the pick-up and sedimentation flux. This means that the hydraulic pressure gradient and thus the bed shear stress and bed friction depend on the pick-up and sedimentation flux. As further explained in Section 8 the shear force along an eroding sand bed, at a Shields parameter of more than 0.5 to 1.0, can not be considered as the driving force for the pick-up of grains. It is an apparent parameter representing the hydraulic pressure gradient along an eroding sand bed, as a result of the pick-up and sedimentation flux. More specific the hydraulic pressure gradient is influenced by:

1. the energy necessary for the acceleration of the grains which are picked-up by the flow;

2. the influence of the concentration of the grains, just above the top of the sand bed, introducing an increase of the effective viscosity of the sand-water mixture;

3. energy losses as a result of collisions between the grains just above the top of the sand bed;

4. turbulence of the flow, which is determined by the depth-averaged flow velocity and bed associated hydraulic diameter. An increase of the depth-averaged flow velocity and bed associated hydraulic diameter causes an increase of turbulence.

# 8

# Analysis pick-up flux

## 8.1. Introduction

The literature survey shows that at flow velocities of more than 1 m/s the bulk properties of the sand bed are assumed to influence the erosion process, as described in Section 4.5. The pick-up flux is reduced as a result of dilatancy during shearing of the sand bed. However, the amount of experimental data was too limited to check this hypothesis and study the erosion process at flow velocities of more than 1 m/s. To gather more experimental data, erosion experiments were carried out in an adapted slurry transport circuit of the Dredging Research Laboratory of Delft University of Technology (see Section 5.2). The results of these experiments are described in Chapter 6. This chapter comprises the analysis of the experiments in order to describe the physical process during the erosion of sand at flow velocities of more than 1 m/s and to develop an analytical pick-up function, in order to fulfill the goal of this experimental study.

The characteristics of the erosion process are described in Section 8.2. This Section describes the influence of the turbulence of the flow and behavior of the sand bed on the pick-up flux. The pick-up flux cannot be measured directly during the experiments. The effective pick-up flux is determined on the basis of the erosion velocity, as based on the measurements with the conductivity probes, and estimation of the sedimentation flux during the experiments. The sedimentation flux depends on the settling velocity of the grains and the concentration close to the top of the sand bed representative for the sedimentation flux. Section 8.3 describes the influence of the assumption for the bed concentration and sedimentation process on the estimation of the sedimentation flux and resulting derived pick-up flux. On the basis of this analysis the way of the estimation of the sedimentation flux is determined.

Section 8.4 shows the influence of the flow conditions (depth-averaged flow velocity and density eroding flow) on the erosion velocity and pick-up flux on the basis of the results of the experiments. The effect of the permeability and the relative

density of the sand bed on the measured pick-up flux is shown in Section 8.5.

Recently van Rhee and Bisschop (2015) compared the results of the first series of experiments (Bisschop et al., 2016) with the results of calculations with a CFD-model. In this model the Reynolds Averaged Navier-Stokes equation is solved with a k-$\epsilon$ turbulence closure. The pick-up is modeled with the pick-up function according to Equation (4.22) as described by van Rhee (2010). The results of these calculation agree well with the results of the first series of the erosion experiments. However the description of the erosion process as described by van Rhee (2010) differs from the visual observations of the high-speed films made during the second series of the experiments. Because of this difference a new semi-empirical analytical function was derived for the determination of the pick-up flux as function of the depth-averaged flow velocity (Section 8.6) on the basis of the description of the physics of the erosion process and the results of the experiments.

This function is based on the physics of the erosion process, that has close resemblance with the model of Gao (2008). This section describes also the basic assumptions for this function, while this function is further calibrated and improved on the basis of a comparison with the results of the experiments. The practical application of the improved knowledge of the erosion of sand in case of breaching is described in Section 8.6.7. Finally the validity and physics of the function are discussed in Section 8.7.

## 8.2. Characteristics erosion process

This section describes the influence of the turbulent behavior of a flow, represented by ejections and sweeps, on the erosion process (Section 8.2.1). The resulting behavior of the sand bed during erosion is described in Section 8.2.2. Section 8.2.3 describes the influence of the concentration of the eroding flow on the erosion process. The erosion regime during the executed experiments is analyzed, described and discussed in Section 8.2.4.



### 8.2.1. Effect of turbulence

Videos made of the experiments with a high speed camera show that the erosion process is influenced by vortices consisting of ejections and sweeps as a result of the turbulent behavior of the flow (as depicted in Figures 3.9 and 3.10). A sequence of ejections and sweeps hitting the bottom is usually called 'bursting' or are known as 'turbulent bursts' (Nezu and Nakagawa, 1993). An ejection is characterized by a local upward flow velocity and a local horizontal velocity lower than the depth-averaged flow velocity. The flow of a sweep is characterized by a local horizontal velocity larger than the depth-averaged flow velocity and a downward local vertical velocity.

As depicted in Figure 3.11 these vortices move upwards from the bottom of the flow into the main flow, while later moving back to the bottom. According to Nezu and Nakagawa (1993) the spacing between these bursts is related to the water depth (between $1.4 \cdot h_w$ and $2.7 \cdot h_w$). However, Figure 8.1 shows that neighboring bursts do not have any spacing in between. Bursts hit the top of the sand consecutively,

without any spacing in between. This difference could be caused by the presence of grains close to the bottom of the flow, because the description of bursting is based on a turbulent flow without any grains. The presence of grains will dampen the kinetic energy of the vortices, resulting in vortices staying close to the bottom. Figure 8.1 shows that the length of the bursts responsible for pick-up and sedimentation is 0.05 to 0.10 m. The ejections and sweeps, influencing pick-up and re-sedimentation close to the top of the sand bed, both cover approximately a length of 0.03 to 0.05 m of the bottom, while in vertical direction they extend over a height of 0.02 to 0.03 m. The ejections and sweeps influencing the erosion process form a layer with a thickness of 0.02 to 0.03 m above the top of the sand bed. Above this layer of bursts vortices exist, forming a layer in which the grains are kept into suspension. It should be noted that the observed dimensions of the vortices are valid for the dimensions of the experimental set-up and depth-averaged flow velocities during the experiments. Other flow conditions will affect the dimensions of the vortices.

Figure 8.1 shows the typical characteristics determining the erosion process. Ejections transport the grains, which have been released from the sand bed by sweeps, into the main flow, see Figure 8.2. This can be compared with the saltation of grains, studied by for instance Lee and Hsu (1994). Part of the grains is kept in suspension by the turbulent energy of the flow, while some ejections change in sweeps causing re-sedimentation of the grains. This process results in a net pick-up flux. In the ejections the concentration is determined by the bed concentration, while the resulting sedimentation flux of grains by the sweeps is determined by the near-bed concentration and the downward velocity of the grains in the sweeps and ejections. This velocity is not determined by the settling velocity of the grains and thus the bulk of the grains, but is influenced by the flow velocity of the sweeps in the vortices. Considering the ejections and sweeps in the vortices exhibit the same angular flow velocity, the difference between the bed concentration and the near-bed concentration results in a pick-up flux exceeding the sedimentation flux (see Figure 8.3).



These ejections and sweeps follow the main flow direction, sometimes interspersed with smaller vortices, rotating with a relative high angular velocity in clockwise direction as depicted in Figure 8.1d through 8.1h. The resulting centrifugal forces on the grains decrease the concentration of grains in the center of these vortices to almost zero. These rotating vortices follow the direction of the main flow, while moving slightly downwards to the top of the sand bed. Close to the sand bed, some of these vortices lose their kinetic energy, which is (partly) replaced by potential energy, necessary to pick-up grains. As a result they (partly) extinguish close to the bottom (Figure 8.1i and 8.1j).

The successive cycles of pick-up and partly re-sedimentation also can be recognized clearly during experiment 28 from the density measurements with the conductivity probes. This experiment was executed with Zilverzand ($d_{50}$ = 262 $\mu$m). The depth-averaged flow velocity during this experiment was approximately 4 m/s and the relative density of the sand bed was between 0.0 and 0.2. Figure 8.4 shows the density as measured with selected conductivity probes at different levels in the measurement section. This figure shows the results of the measurements of the con-

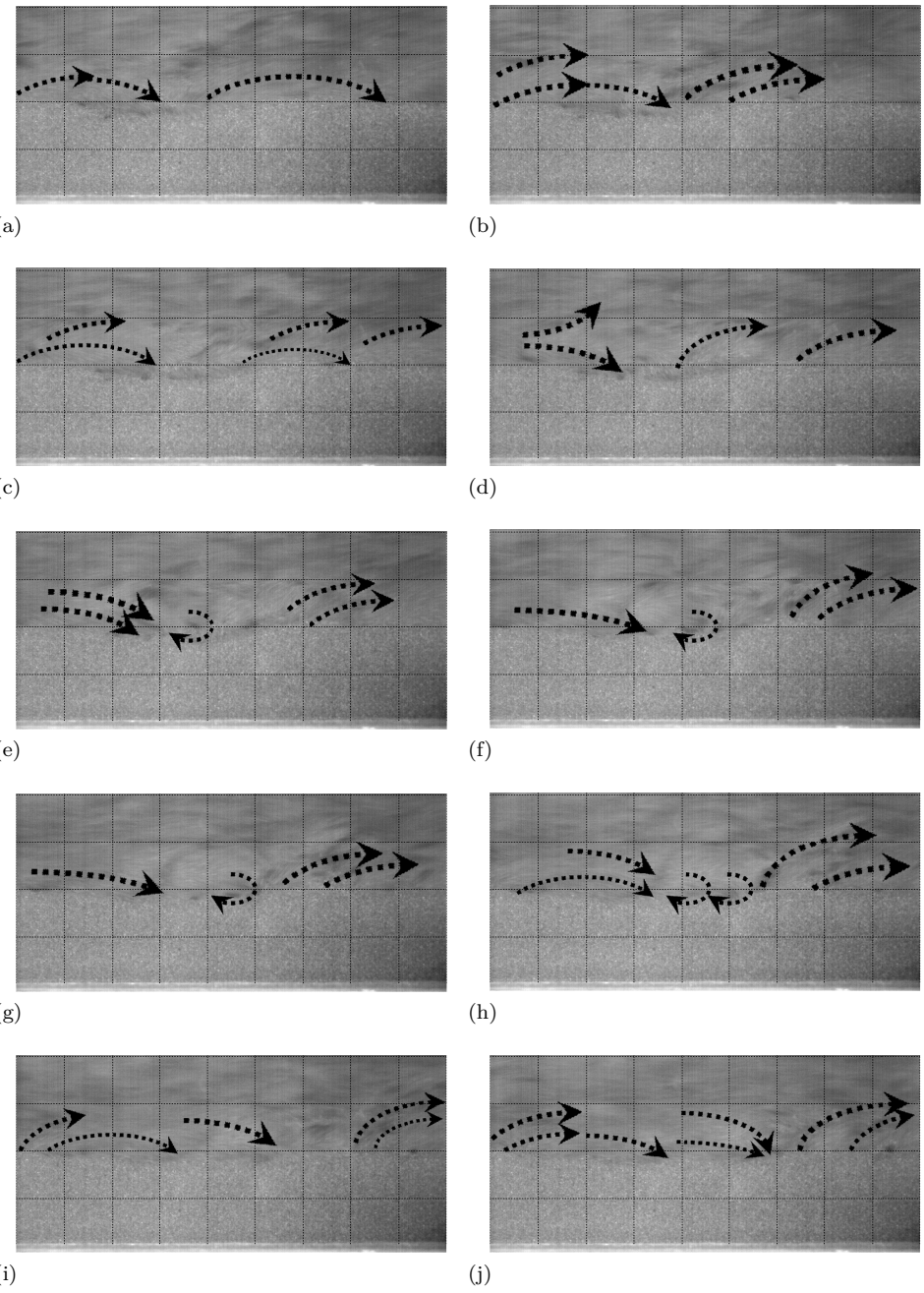


Figure 8.1: Erosion during experiment 33: flow direction is to the right. Operational conditions: $d_{50} = 262$ $\mu$m, $R_n = 0.66$ - $0.70$, $h_f = 0.12$ m, $v_s = 5.6$ - $6.0$ m/s, $\rho_m = 1200$ kg/m$^3$. The time interval between each frame is 0.004 seconds, while the distance between the grid lines is 0.02 m in horizontal as well as vertical direction

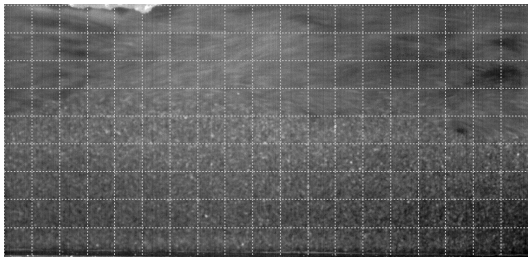

Figure 8.2: Ejection during experiment 69: flow direction is to the right. Operational conditions: $d_{50}$ = 562 $\mu$m, $R_n$ = 0.6 - 0.9, $h_w$ = 0.2 m, $v_s$ = 4.7 - 5.2 m/s, $\rho_m$ = 1090 kg/m$^3$

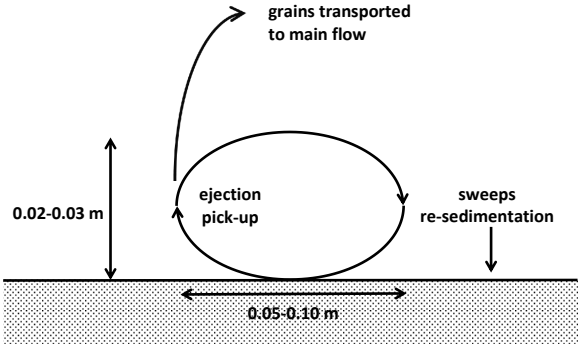


Figure 8.3: Erosion process as influenced by vortices, consisting of sweeps and ejections, hitting the bottom (turbulent bursts)

ductivity probes at a vertical distance of 0.02 m from each other. The effect of the sweeps and ejections can be clearly recognized from the results of the measurements of the conductivity probes at a level between 24.2 and 84.2 mm above the bottom of the measurement section. At the moment the erosion front reached the level of the conductivity probe the density decreased suddenly, but within a short moment the density increased again. Sometimes this behavior repeated itself more than once. This behavior is caused by a sequence of ejections and sweeps causing consecutive pick-up and re-sedimentation.



### 8.2.2. Behavior of the sand bed

A phenomenon observed during several erosion experiments was that the top of the sand bed moved downward and upward before the sand bed was eroded. This effect can be recognized clearly from the measurements during the experiments on the finest sand type (Silverbond $d_{50}$ = 51 $\mu$m), especially at very low relative densities ($R_n$ between -0.3 and -0.1). In this case the sedimentation process, in order to create a sand bed in the measurement section, led to a higher porosity than the value of $n_{max}$, which was determined in dry conditions.

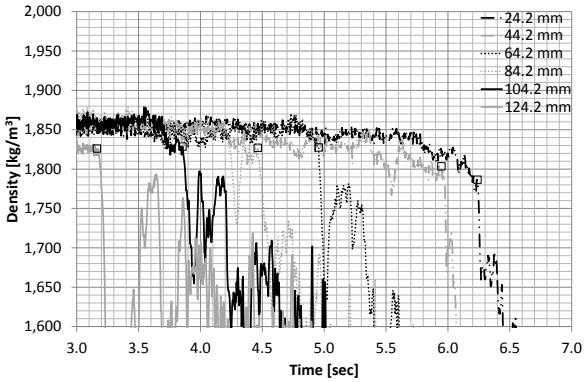


Figure 8.4: Change of density at selected levels in the measurement section, as measured by the conductivity probes, during experiment 28: $d_{50} = 262$ $\mu$m, $R_n = 0.0$ - 0.2, $h_f = 0.12$ m, $v_s = 3.5$ - 4.1 m/s, $\rho_m = 1180$ kg/m$^3$

Figure 8.5a shows the results of experiment 77 on Silverbond sand with a relative density of the sand bed of -0.2. This figure shows that at the level of the different conductivity probes the density changes between the density of the sand bed (top of sand bed moved in upward direction) and the density of the eroding flow (top of sand bed moved in downward direction) as a result of the undulating behavior of the sand bed. Effectively the sand bed moved in upward and downward direction until the erosion front reached the level of the conductivity probes. Figure 8.5a shows also that at a level 44.4 and 66.2 mm above the bottom of the measurement section the density of the sand bed increased just before the sand bed eroded at this level. This is caused by the effect of turbulent wall stresses resulting in (temporarily) contractant behavior (compaction) of loose sand.

8

Figure 8.5b shows the density at different levels in the measurement section during erosion experiment 88. During this experiment the depth-averaged flow velocity varied between 3.8 and 4.1 m/s, while the relative density varied over the height between 0.1 and 0.9. The top of the sand bed did have an initial relative density of approximately 0.1, while the lowest part of the the sand bed did have a initial relative density of up to 0.7. Figure 8.5b shows a relative constant density of the sand bed before the sand bed eroded and a constant decrease of the density after the erosion front passed the corresponding conductivity probe

More specifically the undulating behavior of the sand bed can be recognized from the measurements of the conductivity probe at a level of 54.2 mm above the bottom of the measurement section during experiment 77 as depicted in Figure 8.6. During experiment 77 the density of the sand bed decreased at $t = 19.5$ s and increased at $t = 19.6$ s. This behavior is repeated several times until the sand bed is totally eroded at $t = 22.5$ s. This figure shows also clearly the constant density at the same level during experiment 88 with a higher relative density of the sand bed. The undulating behavior of the sand bed made it also difficult to define the exact moment of erosion during the experiments on this type of sand and relative density of less than 0.

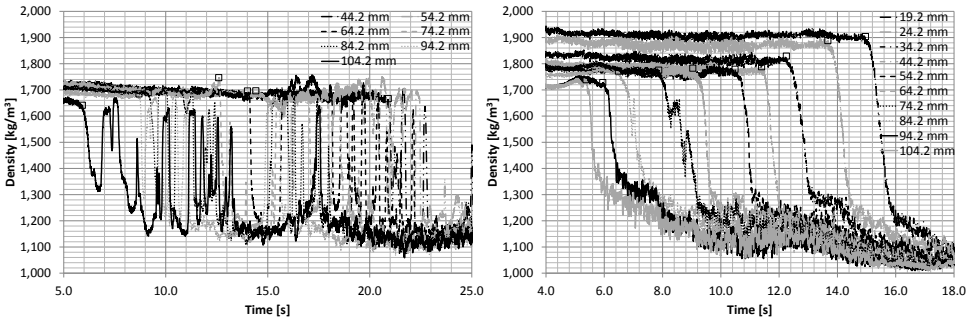


(a) (b)

Figure 8.5: Measured density at different levels above the bottom of the measurement section before and during the actual erosion front reaches the corresponding conductivity probe during erosion experiment 77 (a) and 88 (b). Operational conditions experiment 77: $d_{50}$ = 51 $\mu$m, $R_n$ = -0.2, $v_s$ = 1.3 - 1.4 m/s, $\rho_m$ = 1050 kg/m$^3$ and operational conditions experiment 88: $d_{50}$ = 51 $\mu$m, $R_n$ = 0.1 - 0.7, $v_s$ = 3.8 - 4.1 m/s, $\rho_m$ = 1060 kg/m$^3$

This behavior can be explained by the effect of liquefaction. Liquefaction can be the result of static or cyclic loading (Lunne et al., 1997). At a very low relative density of a sand bed a static load can result in liquefaction, while a cyclic load can result in liquefaction at a higher relative density. The permeability of the sand plays also a major role during liquefaction in case of cyclic loading. In case the loading results in contractant behavior of the sand bed the volume of the voids in between the grains decreases. This effect generates temporarily excess pore water pressures, which will decrease by the flow of water out of the sand bed. The value of the excess pore water pressure depends on the thickness of the liquefied layer, permeability of the sand and rate of the cyclic loading. These excess pore water pressures decrease the effective vertical stress ($\sigma'_z$), see Equation (2.14), because the total vertical stress ($\sigma_z$) remains constant. This results in a decrease of the strength of the sand bed, see Equation (2.13). The presence of excess pore pressures resulting in liquefaction has been investigated by Bezuijen and Mastbergen (1988). They measured excess pore pressure during the construction of a sand dam by means of a hydraulic fill. During the decrease of the excess pore pressures the density of the sand increased as a result of contractant behavior.

In case of erosion, sweeps have caused (temporarily) liquefaction. Due to alternating sweeps the sand bed is subjected to cyclic loading. The sweeps result in contractant behavior (Section 2.3.3), especially in case of sand with a low relative density. As a result excess pore water pressures are generated, resulting in a decrease of the strength of the sand bed and a highly deformable sand bed. Due to this decrease of strength, outflow of water and consecutive sweeps and ejections traveling in horizontal direction the top of the sand bed starts undulating. The thickness of the liquefied zone depends on the relative density ($R_n$) and permeability ($k$) of the sand bed and magnitude and rate of cyclic loading, as a result of the impact of consecutive sweeps.

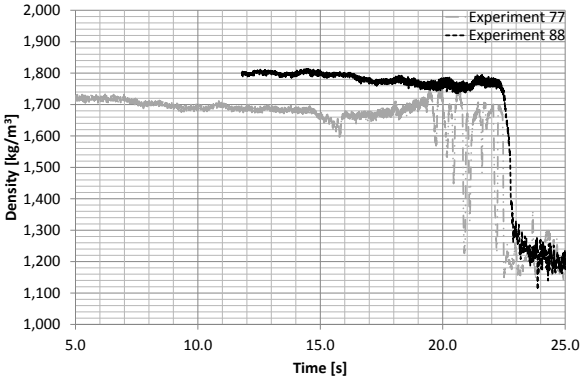


Figure 8.6: Measured density at a level of 54.2 mm above the bottom of the measurement during experiment 77 and 88. Note: the time-scale of experiment 88 has been changed to compare both measurements

The effect of the relative density on the thickness of the liquefied zone can be explained by the difference in behavior during the erosion experiments executed on sand with a $d_{50}$ of 125 and 262 $\mu$m (Geba and Zilverzand). Visual observations during these experiments on both sand types showed that liquefaction took place over a thickness of 5 to 20 mm from the top of the sand bed in case of a high relative density ($R_n$ between 0.6 and 1.0) of the sand bed. Visual observation of the experiments, with a lower relative density ($R_n$ between 0.0 and 0.5), showed liquefaction of a larger part of the sand bed (up to a depth of 50 to 100 mm below the top of the sand bed). This shows that a lower density of a sand bed leads to more compaction, resulting in a relative thick liquefied zone. This behavior is not the same as the behavior during sheet flow, because the liquefied layer exhibits none or almost none displacement in horizontal direction. During sheet flow the sheet flow layer moves also in horizontal direction.

The experiments on the coarsest sand type (Dorsilit: $d_{50}$ = 562 $\mu$m) showed only temporarily liquefaction of the top of the sand bed (5 to 20 mm). Liquefaction occurred only in small zones with a diameter of 10 to 20 mm just below the top of the sand bed. These liquefied zones disappeared before the next sweep reached the bottom. This local liquefaction is caused by turbulent normal wall stresses, as a result of sweeps hitting the top of the sand bed. The resulting excess pore water pressures decrease relative quickly as a result of the relative high permeability of this type of sand in comparison with the permeability of the other sand types. As a consecutive sweep hits the top of the sand bed again, the excess pore water pressures will be reduced significantly, resulting in smaller dimensions of the liquefied zone.

The decrease of the excess pore water pressures can be determined using the consolidation theory of Terzaghi (Lambe and Whitman, 1969). The average time between two sweeps during the experiments was between 0.02 and 0.1 s. Based on a permeability of 1.5 *cdot* $10^{-3}$ m/s, the consolidation ratio of a layer of 0.1 m is 100 %. This means that the excess pore pressure decreased to zero before the

next sweep hits the top of the sand bed, resulting in hardly any liquefaction of the sand bed. This agrees with the visual observations during the erosion experiments on this type of sand. The consolidation rate of the finest sand type (Silverbond) is approximately 10 %. The excess pore pressure hardly decreased between two consecutive sweeps, leading to liquefaction of the whole sand bed during the erosion experiments on this sand type as observed.

### 8.2.3. Influence of the concentration of the eroding flow

Figure 8.7 shows the effect of the eroded grains on the concentration profile above the bed. At the start of the erosion process ($t = 2.5$ s) the grains were suspended in vertical direction over almost the whole flow height above the sand bed in the measurement section. Figure 8.7 shows that at $t = 3$ s the density of the eroding flow at a height of approximately 0.05 m above the eroding bed increased to between 1500 kg/m$^3$ and 1600 kg/m$^3$. During this experiment the level, at which the density of the eroding flow is between 1500 kg/m$^3$ and 1600 kg/m$^3$, dropped to a level of approximately 0.01 m above the erosion front. The flow is more stratified. This is the result of the increase of the density of the eroding flow during the first moments of the erosion experiment. At the start of the erosion process the density of the flow is relative low. The eroded grains are not or almost not hindered by grains in the eroding flow. However, during the experiment the density of the eroding flow increased and grains in suspension hindered eroded grains moving upward in the flow, hence reducing the entrainment of grains in the suspension zone of the main flow.

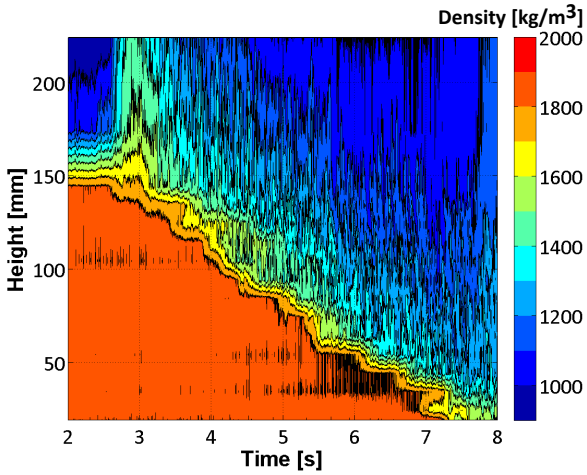


Figure 8.7: Measured density profile during experiment 50: $d_{50} = 125$ $\mu$m, $R_n = 0.2$ - 0.4, $v_s = 4.1$ - 4.9 m/s, $\rho_m = 1178$ kg/m$^3$

### 8.2.4. Erosion regime

The physics of the erosion process is further investigated on the basis of the following characteristic values: quotient erosion velocity and permeability, theoretical sheared layer thickness and the Péclet number, determining whether drained or undrained conditions occurred during the erosion experiments. It should be noted that the value of these characteristic values is based on the assumption that the erosion process is dominated by the shearing of layers of sand over the whole surface of the sand bed, while the present experimental study shows that erosion is dominated by sweeps hitting the top of the sand bed at different locations, causing local erosion of the surface. Despite this difference, these characteristic values give an indication of the average conditions of the sand bed during erosion.

#### Influence of quotient erosion velocity and permeability

As the erosion process is influenced by the soil bulk properties of the sand bed, like dilatancy as a result of shearing, the ratio $v_e/k$ should fulfill the criterion for dilatancy reduced erosion: $v_e/k > 50$ to 100 (see Figure 8.8a). The conditions during the erosion experiments on the three sand types with the smallest grain size ($d_{50} = 51$, 125 and 262 $\mu$m) fulfilled this criterion. Another condition, to determine if the erosion process is influenced by the soil bulk properties of the sand bed, is the value of the Shields parameter ($\theta_b$). In case $\theta_b > 0.5$ to 1.0 it is considered that the bulk properties of the sand start to influence the pick-up of grains. This criterion is comparable to the criterion for sheet flow, during which multiple layers of sand are sheared along the top of the sand bed (see Section 3.5). All experiments fulfilled this criterion (see Figure 8.8b), showing that the erosion process should be influenced by the behavior of multiple layers of sand. This confirms that the soil bulk properties have influenced the erosion process during the erosion experiments on the three sand types with the smallest grain size.

However, during the erosion experiments on the coarsest sand type ($d_{50} = 562$ $\mu$m) the value for $v_e/k$ varied between 5 and 70, mainly below or just fulfilling the criterion for the dilatancy reduced erosion regime (see Figure 8.8a). On the other hand, the value of the Shields parameter was during these experiments far above 1.0. This shows that the conditions during the experiments enabled the shearing of layers of sand (sheet flow conditions), but that the resulting dilatancy will not have led to a significant inward hydraulic gradient into the sand bed, due to the relative high permeability of this type of sand.



#### Layer thickness

Figure 8.8b shows that during all experiments the Shields parameter was far above 1.0, considering that the erosion process is influenced by the soil bulk properties of the sand bed. An indication of the thickness of the bulk influenced by the flow conditions can be derived using the theoretical approach for dilatancy reduced erosion and the results of the erosion experiments. Assuming the criterion for dilantancy reduced erosion is met and the erosion process is dominated by the shearing of layers of sand, the thickness of the sheared layer ($h_s$) can be derived on the basis of Equation (4.29):

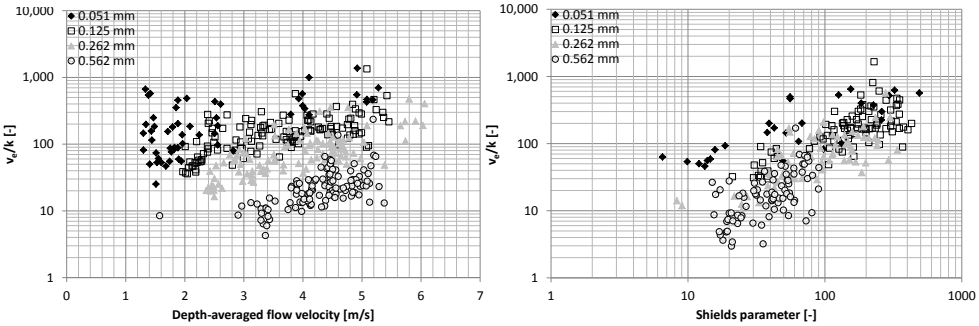


(a) (b)

Figure 8.8: Criterion for dilatancy reduced erosion during all experiments: $v_e/k$ as function of the flow velocity (a) and as function of the Shields parameter (b). Value for the erosion velocity ($v_e$) is based on the pick-up flux as based on the average concentration of the eroding flow

$$h_s = \frac{\tau_b}{g \cdot tan\phi \cdot \left[(1 - n_{max}) \cdot (\rho_s - \rho_w) + \frac{v_e}{k} \cdot \frac{n_{max} - n_i}{1 - n_{max}} \cdot \rho_w\right]} \tag{8.1}$$

The angle of internal friction ($\phi$) of the different types of sand is determined on the basis of Equation (2.16), an empirical relation between the angle of friction and the relative density and coefficient of uniformity. Figure 8.9 shows the thickness and relative thickness of the sheared layer ($h_s/d_{50}$) as function of the bed shear stress. Considering that the erosion process is determined by mobile layers of multiple sheared layers of sand, the thickness of this layer is between $10 \cdot d_{50}$ and $500 \cdot d_{50}$. This means that the behavior of the sand bed is determined by the soil bulk properties of the sand bed, because sand can be described as a soil bulk at a layer thickness of at least 10 times the average grain size (Section 3.5.6).



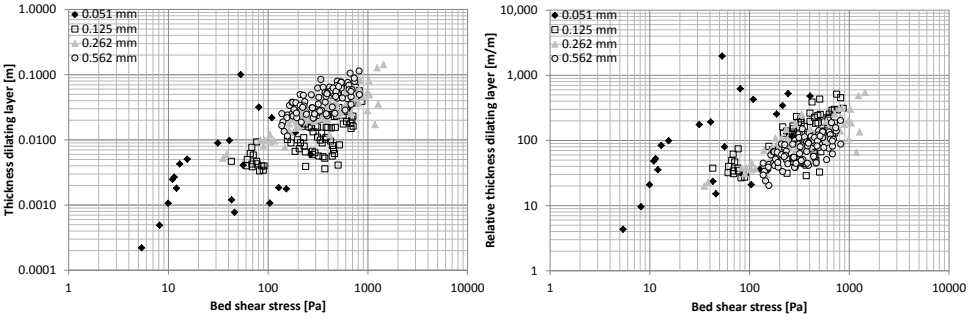


(a) (b)

Figure 8.9: Thickness of the sheared layer ($d_{dil}$) and relative thickness of sheared layer ($d_{dil}/d_{50}$) according to the theoretical approach of dilatancy reduced erosion using the results of the experiments as function of the bed shear stress

Drained or undrained conditions

In case shearing leads to dilatancy, this results in a volume increase of the pores. Pore water under pressures are generated in the top of the sand bed, resulting in an inward hydraulic gradient. Depending on the relative density, the sand bed could also show contractant behavior as a result of the turbulent normal wall stresses due to the sweeps. Whether during both types of behavior drained or undrained conditions occur depends on the Péclet number ($Pe_w$):

$$Pe_w = \frac{v \cdot l}{c_i} \tag{8.2}$$

in which $v$ is a velocity scale, $l$ is a length scale and $c_i$ is the isotropic consolidation coefficient (Bisschop and van Kesteren, 1994). Fully drained conditions occur at $Pe_w < 1$, while at $Pe_w > 10$ almost fully undrained conditions occur (Winterwerp and van Kesteren, 2004).

It should be noted that the theory of dilatancy reduced erosion assumes drained conditions, because erosion occurs when the pore water under pressures are compensated by the inflow of water. As a measure for the velocity scale ($v$) the average erosion velocity, neglecting the sedimentation flux: $v_e = \frac{E}{\rho_s \cdot (1-n_i)}$, can be used. Another measure for the velocity scale could be the local downward flow velocity ($\hat{w}$) in the vortices causing ejections and sweeps close to the top of the sand bed. Because these ejections and sweeps are considered as the cause of erosion, the local velocity scale will be rather of the order of the local downward velocity than the average erosion velocity. The average erosion velocity is a measure for the velocity scale ($v$), but the local velocity scale of the bursts, resulting in erosion, is higher. For the determination of the Péclet number the local downward flow velocity in the vortices is assumed to be of the order of the depth-averaged flow velocity ($U$).

The length scale is based on the theoretical thickness of the dilating layer, while the consolidation coefficient is determined on the basis of (Lambe and Whitman, 1969):

$$c_i = \frac{k}{\rho_i \cdot g \cdot m_v} \tag{8.3}$$

in which $m_v$ is the coefficient of volume compressibility. Assuming $1/m_v \approx E_{oed}$ and:

$$E_{oed} = C^{'} \cdot \sigma^{'} \tag{8.4}$$

in which $E_{oed}$ is the oedometer loading stiffness of the sand bed as function of the constant of compressibility ($C^{'}$) and the effective stress ($\sigma^{'}$). In case of loose sand $C'$ is approximately 1000.

Figure 8.10a shows the Péclet number based on the erosion velocity, while Figure 8.10b shows the Péclet number based on the depth-averaged flow velocity. Figure 8.10a shows that the Péclet number during the experiments should have been less than 1, meaning that the erosion process should have been dominated by fully drained conditions in the eroding sand bed. The resulting excess pore water pressures should have been dissipated fully by pore water flow, enabling erosion.

However, during the experiments on Silverbond sand liquefaction of the whole sand bed took place during the experiments with a relative density $< 0$. The experiments executed with a relative density $> 0$, showed liquefaction at the top of the sand bed (0.02 to 0.05 m). The initiation of liquefaction is an undrained process. A static or cyclic load in combination with sand with a low relative density leads to contraction and excess pore water pressures. The excess pore water pressures result in a decrease of the effective stress and hence lower resisting shear strength, leading to liquefaction.

The occurrence of liquefaction during the experiments on the sand types Silverbond, Geba and Zilverzand can be explained by the findings of Figure 8.10b. In this case the velocity scale of the Péclet number is based on the depth-averaged flow velocity, because the occurrence of liquefaction depends on the flow velocity in the sweeps. This determines the normal stress on the sand bed and hence the excess pore water pressures. The value of the Péclet number during the experiments on the sand types Silverbond, Geba and Zilverzand is mainly above 10, confirming the occurrence of undrained behavior, resulting in liquefaction. The Péclet number during the experiments on Dorsilit sand is between 1 than 10, meaning that the sand will have exhibited partly undrained and drained behavior. This is confirmed by the visual observations during the experiments. It should be noted that the Péclet number is not the only parameter determining whether liquefaction occurs. The relative density plays also a large role.

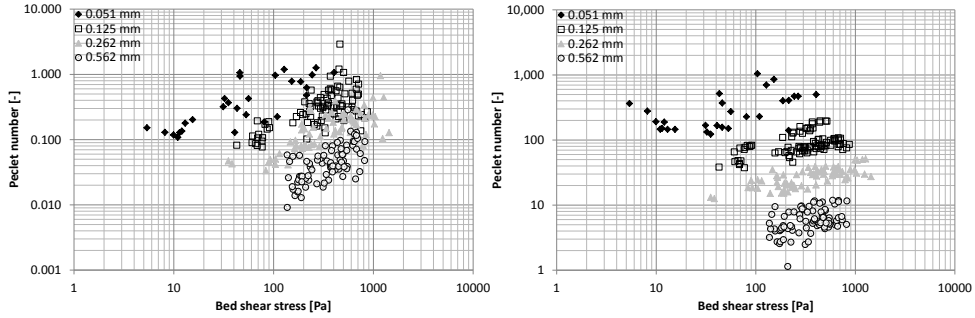


(a) (b)

Figure 8.10: Péclet number ($Pe_w$) being a measure for the occurrence of drained or undrained conditions, as based on the erosion velocity (a) and depth-averaged flow velocity (b) as function of the bed shear stress

## 8.3. Determination pick-up flux: near-bed concentration

The determination of the net pick-up flux ($E$) from the results of the experiments needs an estimate for the sedimentation flux ($S$) during the experiments:

$$E = v_e \cdot (1 - n_i - c_{nb}) \cdot \rho_s + S \tag{8.5}$$

in which $S$ can be determined with:

$$S = c_{nb} \cdot \rho_s \cdot w_{hs} \tag{8.6}$$

The main unknown in Equation 8.6 is the near-bed concentration ($c_{nb}$). Section 8.3.1 describes the different assumptions in order to determine the sedimentation flux during erosion. Based on the results of the experiments the best approach for the determination of the sedimentation flux is chosen for the determination of the pick-up flux. This analysis is described in Section 8.3.2.

### 8.3.1. Near-bed concentration and sedimentation flux

The near-bed concentration influences the volume of grains moving through a downward moving (eroding) interface and volume of grains eroding from the sand bed. A first guess for the near-bed concentration is the average concentration of the eroding flow ($c_{av}$). However, close to the top of the eroding sand bed the concentration of the eroding flow increases as a result of sedimentation and pick-up. Besides, the flow conditions and movement of the grains close to the top of the sand bed are influenced by vortices close to the bed. This means that a better approach for the representative concentration for the sedimentation flux is the concentration close to the top of the sand bed: the near-bed concentration. The height over which the near-bed concentration should be determined depends on the size of the turbulent vortices close to the top of the sand bed. Based on the visual observations of the erosion process (Figure 8.1), it is estimated that these vortices have an average height of approximately 0.03 m. This means that the best guess for the near-bed concentration is the average concentration of the eroding flow over a height of 0.03 m above the top of the eroding sand bed.



The sedimentation flux can be considered as being determined by the average settling velocity of the grains in the eroding flow, including the effect of hindered settling, using the average concentration of the eroding flow or the near-bed concentration. However, a second approach could be the assumption that the sweeps of the turbulent bursts transport the grains from the main flow to the top of the sand bed and determine the sedimentation flux. In this case the vertical downward velocity of the sweeps and area which is influenced by these sweeps determine the sedimentation flux, in combination with the near-bed concentration.

In order to determine the effect of the near-bed concentration and the mechanism determining the sedimentation flux, a sensitivity analysis was carried out to determine the effect of different approaches on the determination of the sedimentation flux and resulting net pick-up flux. The first two assumptions, (1a) and (1b) are based on the assumption that the sedimentation flux is determined by the average settling velocity of the grains over the whole surface of the sand bed, including the effect of hindered settling. The effect of hindered settling on the settling velocity is determined according to Richardson and Zaki (1954). The third assumption (2) is based on sweeps transporting grains to the top of the sand bed with the rotational

flow velocity in these sweeps. The main starting points of these three approaches are:

- approach (1a): the sedimentation flux is determined by the individual settling velocity of the grains as based on Equation (8.6), including the effect of hindered settling as based on the depth-averaged concentration of the flow above the sand bed. The depth-averaged concentration of the eroding flow, see Equation (6.6), is considered to be the representative concentration for the sedimentation flux;
- approach (1b): this approach is also based on the individual settling velocity of the grains including the effect of hindered settling. The representative concentration for the determination of the the sedimentation flux is considered to be the average concentration of the eroding flow just above the eroding sand bed: the near-bed concentration. Visual observations of the erosion process showed that the sedimentation flux is influenced by the vortices close to the bed (turbulent bursts). These bursts have a height of approximately 0.03 m. This height is taken as representative for the level over which the near-bed concentration is determined;
- approach (2): the sedimentation flux is determined by the size of and flow velocity in the sweeps of the turbulent bursts, while the near-bed concentration is considered as the concentration in these sweeps.

The sedimentation flux as determined by the turbulent bursts, approach (2), depends on the size of and flow velocity in the sweeps of these bursts. The bursts leading to pick-up are considered to cover approximately 2% of the area (Cao, 1997) of the eroding sand bed. It should be considered that these bursts cover a larger relative area, but only the most energetic and bursts of suffucient size will lead to significant pick-up. The sweeps are assumed to cover half of the area of the bursts. The local vertical flow velocity ($\hat{w}$) in the sweeps depends on the shape of the vortices. Visual observations of the vortices (see Section 8.2.1) show that the length of the vortices is approximately twice the height of the vortices. Considering that the local flow velocity at the top of the vortices is approximately the depth-averaged flow velocity ($U$) and the vortices have a length twice the height in the direction perpendicular to the flow, the average local vertical flow velocity in the sweeps is approximately $0.5 \cdot U$.

This assumption for the local vertical flow velocity of the sweeps agrees globally with the findings of Nezu and Nakagawa (1993). They have presented results of several experiments regarding the vertical flow velocity of grains moved downwards by sweeps. According to these experiments the maximum vertical velocity ($\hat{w}$) of the grains equals the shear velocity.

This is in accordance with the findings of Mohajeri et al. (2016). They measured the local vertical flow velocity over a gravel bed at depth-averaged low velocities of approximately 0.35 m/s. According to these measurements the local vertical flow velocity close to the bed varied between 0.8 and 1.2 $\cdot u_*$. Figure 8.11 shows that the quotient between the horizontal depth-averaged flow velocity and the shear velocity

$(U/u_*)$ is related to the shear velocity. At a shear velocity of more than 1.0 m/s this quotient is approximately 4. Considering that $\hat{w} \approx 1.0 \cdot u_*$, the average vertical flow velocity in the sweeps $(\hat{w})$ is approximately $0.25 \cdot U$.

Using $\tau_b = f_b/8 \cdot \rho \cdot U^2$, the quotient $U/u_*$ can be rewritten as: $\sqrt{8/f_b}$. Using this relation, Figure 8.11 shows that the bed friction coefficient increases at in creasing shear velocity, as was also concluded in Section 7.5.

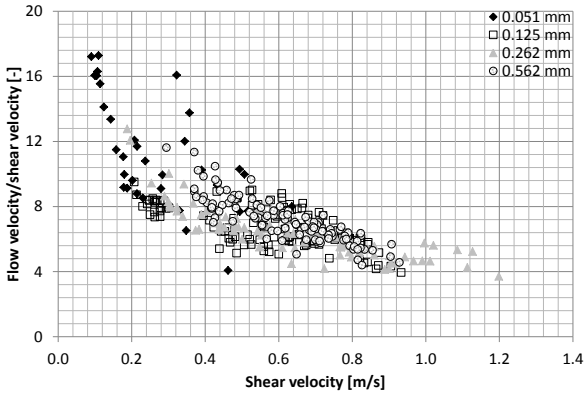


Figure 8.11: The quotient of the measured depth-averaged flow velocity and shear velocity as function of the shear velocity as derived from the results from all experiments. It should be noted that the quotient $U/u_*$ can be rewritten as: $\sqrt{8/f_b}$

Assuming that the sedimentation flux is determined mainly by the turbulent bursts, neglects the sedimentation in between these bursts. The sedimentation in between the bursts will be influenced by smaller vortices and sedimentation as a result of the individual settling velocity of the grains.

8

### 8.3.2. Near-bed concentration during experiments

Figure 8.12 shows the relation between the average near-bed concentration during an experiment and the depth-averaged concentration of the eroding flow for all experiments. This figure shows that at a depth-averaged concentration of 0.3 the near-bed concentration approaches the average concentration of the eroding flow for the three coarsest sand types. However, at a lower average concentration of the eroding flow the near-bed concentration of the coarsest sand type ($d_{50}$ = 562 $\mu$m) is higher than the near-bed concentration during the experiments on the sand types with a $d_{50}$ of 262 and 125 $\mu$m. This is the result of the higher settling velocity of the coarsest sand type in comparison with the finer sand types. The grains of the coarsest sand type, which are entrained into the flow, stay closer to the top of the eroding sand bed. This leads to a relative high near-bed concentration. The near-bed concentration of the finest sand type ($d_{50}$ = 51 $\mu$m) is relative low. This is the result of the lower pick-up flux of this material and the relative low settling velocity of the grains.

The influence of the pick-up flux and sedimentation flux as derived according to

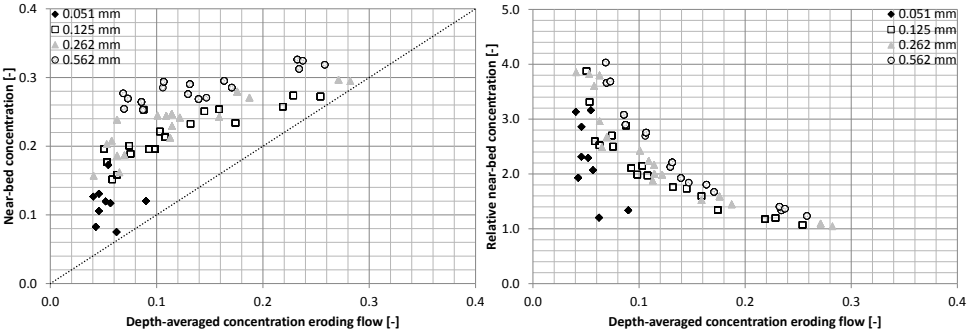


(a) (b)

Figure 8.12: Near-bed concentration (a) and relative near-bed concentration: $c_{nb}/c_{av}$ (b) as function of the depth-averaged concentration of the eroding flow: $c_{av}$

approach (1b) on the near-bed concentration is shown in Figure 8.13. This figure shows clearly an increasing near-bed concentration as a result of an increasing pick-up and sedimentation flux.

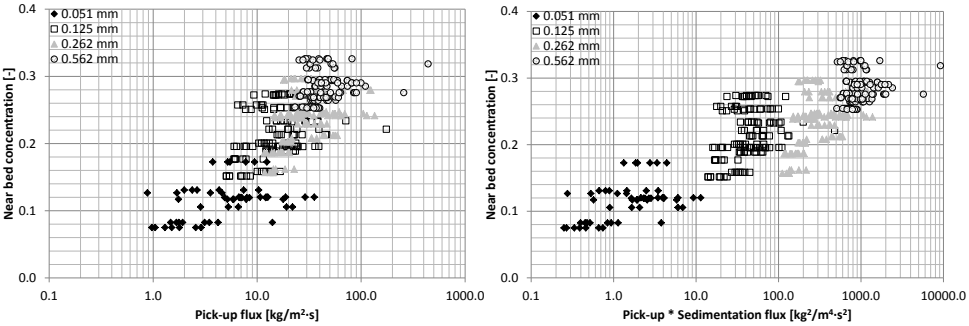


(a) (b)

Figure 8.13: Average near-bed concentration over a height of 0.03 m above the top of the eroding sand bed, as determined during all experiments, as function of the pick-up flux (a) and product of pick-up and sedimentation flux (b), as derived with the help of approach (1b)

### 8.3.3. Differences in sedimentation flux and effect on pick-up flux

Figure 8.14 shows the effect of the concentration on the sedimentation flux near the top of the sand bed, using Equations (8.5) and (8.6). The depth-averaged concentration of the eroding flow during the experiments varied between 0.05 and 0.3. This means that the calculated sedimentation flux varies between $0.5 \cdot S_{max}$ and $S_{max}$, when the representative concentration is based on the depth-averaged concentration of the eroding flow.

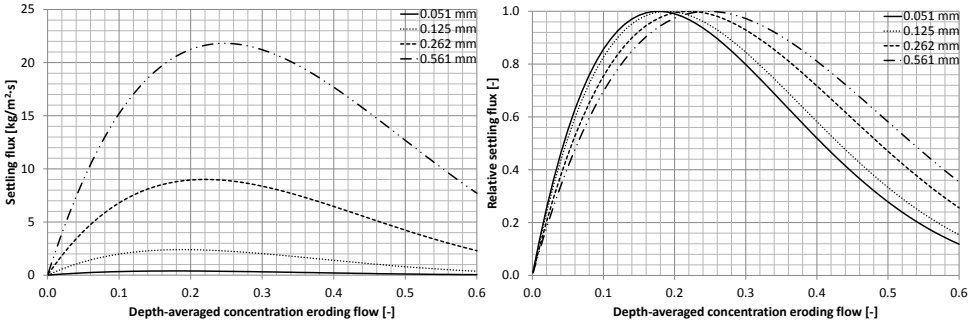


(a) (b)

Figure 8.14: Relation between sedimentation flux ($S$) and relative sedimentation flux ($S/S_{max}$) as function of the depth-averaged concentration of the eroding flow as based on Equation (4.15)

The near-bed concentration varied between 0.15 and 0.3 for the three coarsest sand types and between 0.05 and 0.1 for Silverbond sand (the finest sand type). In case the near-bed concentration is considered as being representative for the sedimentation flux, this flux varies between $0.9 \cdot S_{max}$ and $S_{max}$. This means that in case the near-bed concentration is representative for the sedimentation flux near the top of the sand bed, deviations of the near-bed concentration does not have a significant influence on the resulting sedimentation flux. For the finest sand type the near-bed concentration varied between 0.08 and 0.17. In this case the sedimentation flux varies between $0.75 \cdot S_{max}$ and $S_{max}$. Deviations of the sedimentation flux seem to have a larger influence on the pick-up flux for this sand type, but it should be considered that in this case the sedimentation flux is negligible in comparison with the pick-up flux.

8

Figure 8.15 shows the pick-up flux as derived from the experiments on the basis of three approaches in determining the sedimentation flux: (1a), (1b) and (2) as function of the depth-averaged flow velocity. This figure shows that these approaches show the same trend between the pick-up flux and depth-averaged flow velocity, only the absolute value of the pick-up flux differs between these approaches. However, the relative difference of the pick-up flux, determined according to these approaches, is not significant.

Figure 8.16 shows the relative sedimentation flux (ratio between sedimentation and pick-up flux: $S/E$) as function of the depth-averaged flow velocity. This figure shows when using approach (1a) and (1b) the relative sedimentation flux increases as function of the grain size. At a grain size of 51 $\mu$m the relative sedimentation flux varies between 0.0 and 0.2. For the coarsest sand type this ratio varies between 0.05 and 0.95. Using approach (1a) and (1b) shows also that this ratio decreases as function of the depth-averaged flow velocity. The pick-up flux increases as function of the depth-averaged flow velocity, while the sedimentation flux stays more or less constant at an increasing depth-averaged flow velocity. However, the near-bed concentration increases at increasing depth-averaged flow velocity, the sedimentation

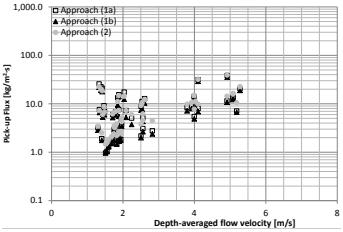


(a) Silverbond: 1070 - 1150 kg/m$^3$

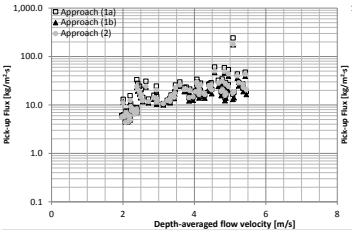


(b) Geba: 1080 - 1180 kg/m$^3$

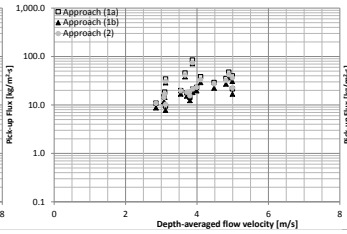


(c) 1235 - 1290 kg/m$^3$

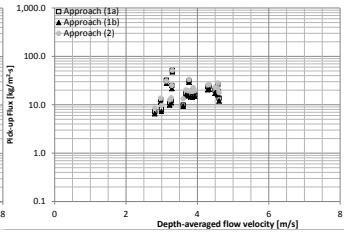


(d) 1360 - 1420 kg/m$^3$

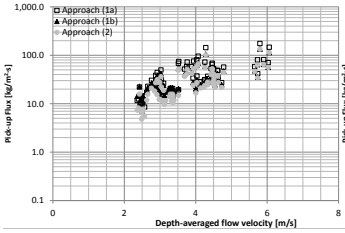


(e) Zilverzand: 1060 - 1205 kg/m$^3$

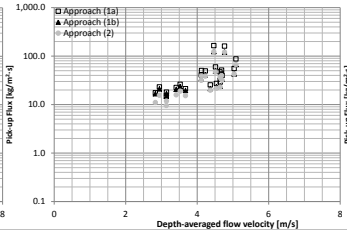


(f) 1260 - 1310 kg/m$^3$

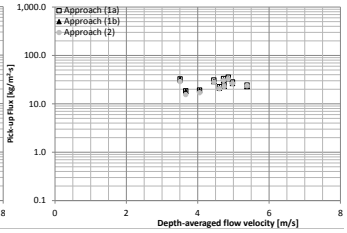


(g) 1440 - 1470 kg/m$^3$

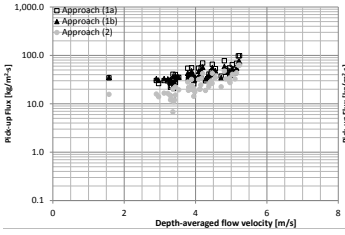


(h) Dorsilit: 1110 - 1180 kg/m$^3$

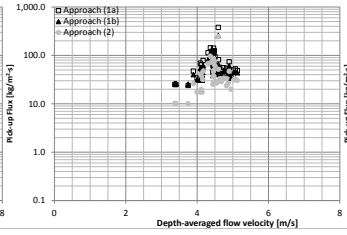


(i) 1210 - 1285 kg/m$^3$

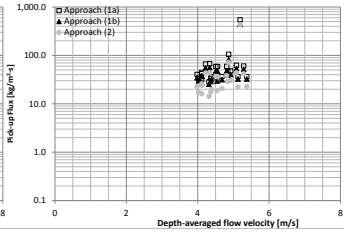


(j) 1380 - 1430 kg/m$^3$

Figure 8.15: Pick-up flux as derived from the experiments on the basis of three approaches in determining the sedimentation flux: (1a), (1b) and (2) as function of the depth-averaged flow velocity

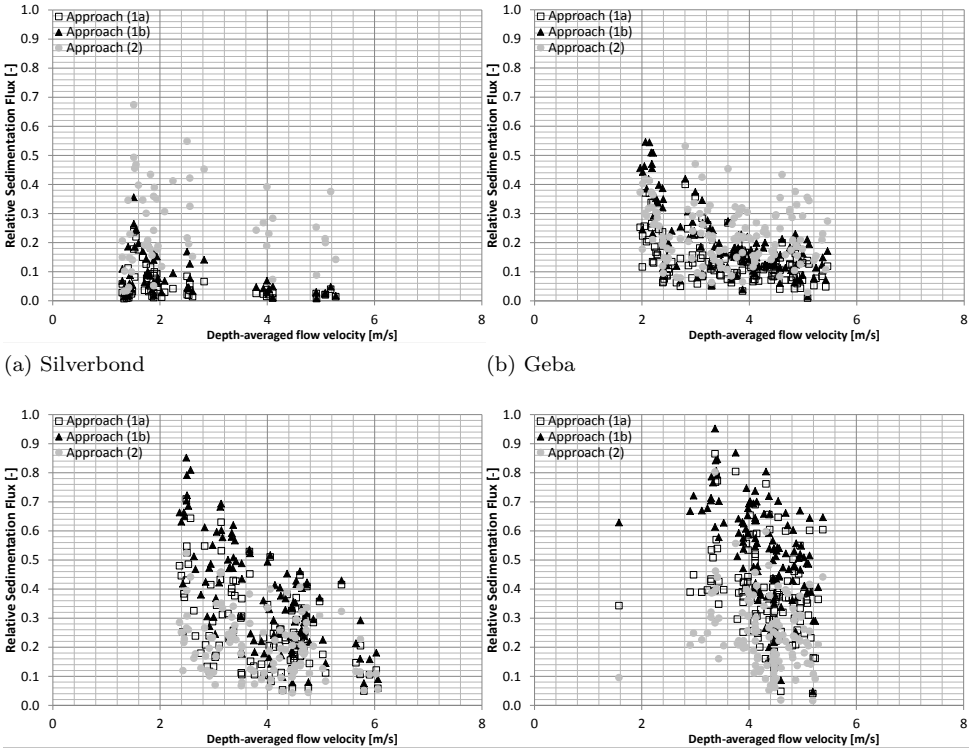


(a) Silverbond (b) Geba

(c) Zilverzand (d) Dorsilit

Figure 8.16: Relative Sedimentation flux ($S/E$) on the basis of three approaches in determining the sedimentation flux: (1a), (1b) and (2) as function of the depth-averaged flow velocity for all experiments and sand types



flux stays more or less constant. This is the result of the effect of hindered settling, reducing the effective settling velocity at increasing concentrations.

Using approach (2) leads to a relative sedimentation flux varying between 0.05 and 0.50 for all sand types, while this ratio hardly increases as function of the depth-averaged flow velocity. This is caused by the fact that the both pick-up and sedimentation increase as function of the depth-averaged flow velocity.

Because erosion and sedimentation both are influenced by vortices close to the bed and influence the near-bed concentration, approach (1b) is considered as the most reliable method to derive the pick-flux from the results of the erosion experiments. Approach (1a) does not take the effect of the near-bed concentration into account. Approach (2) takes also the effect of the flow velocity in the turbulent bursts into account. However, this approach is not used in the further analysis of the experimental data, because this approach does not take into account the sedimentation in between these turbulent bursts. The effect of this influence on the sedimentation flux is unknown. Both are reasons that the analysis of all experi-

ments in the following sections is based on the pick-up flux, as derived according to approach (1b). However, it should be noted that the difference between all three approaches is not significant, because, all three approaches exhibit comparable trends of the relation between the pick-up flux and depth-averaged flow velocity (Figure 8.15).

## 8.4. Influence flow conditions

This section describes the influence of the depth-averaged flow velocity, bed shear stress and density of the eroding flow on the erosion velocity and pick-up flux, as derived on the basis of approach (1b) (Section 8.3).

### 8.4.1. Depth-averaged flow velocity

Figure 8.17 shows the influence of the depth-averaged flow velocity on the erosion velocity and pick-up flux for all sand types for a density of the eroding flow between 1060 and 1205 kg/m$^3$. The erosion velocity, the vertical velocity with which the erosion front moves down, has been derived from the measurements with the conductivity probes (see Section 6.3.2). The effective pick-up flux is based on the erosion velocity and estimated settling flux during erosion (see Section 8.3). Figure 8.17 shows that the pick-up flux increases at an increasing depth-averaged flow velocity. Apparently the pick-up flux increases more than the sedimentation flux at increasing depth-averaged flow velocity, because the results of the experiments show that the erosion velocity increases at increasing depth-averaged flow velocity. The increase of the pick-up flux at an increasing depth-averaged flow velocity is caused by the increasing velocity in the vortices close to the top of the sand bed, resulting in higher turbulent normal stresses on top of the sand bed.

### 8.4.2. Bed shear stress

Figures F.1a, F.1c, F.1e and F.1g show an influence of the relative density of the sand bed on the pick-up flux for all sand types. This effect, however, is not visible when the pick-up flux is compared to the bed shear stress. This effect can be explained by the effect of the pick-up flux on the concentration gradient (Figure 8.18) and resulting influence on the bed friction coefficient as depicted in Figure 8.19 and Figure E.2 (Appendix E).

Figure 8.18 shows the influence of the pick-up flux on the concentration gradient just above the top of the sand bed. An increasing pick-up flux causes a decrease of the concentration gradient, hence an increase of the density just above the eroding bed. In accordance with Figure 7.8 an upper envelope of the relation between the concentration gradient and pick-up flux is visible. This envelope represents the resulting minimum concentration above the eroding front as a result of the pick-up flux, turbulence intensity (flow velocity), density eroding flow and settling velocity of the grains. The irregular character of the erosion process causes a highly variable concentration gradient above the erosion front and hence temporarily increasing the concentration above the eroding front, corresponding to a decreasing concentration gradient.

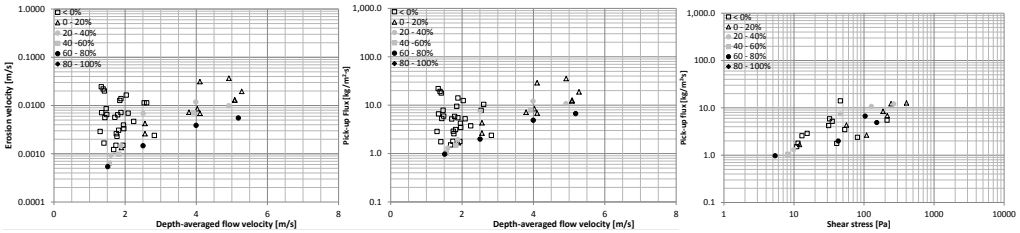


(a) Silverbond (b) (c)

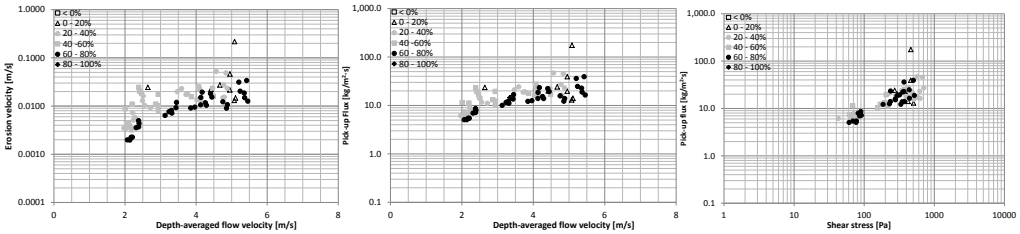


(d) Geba (e) (f)

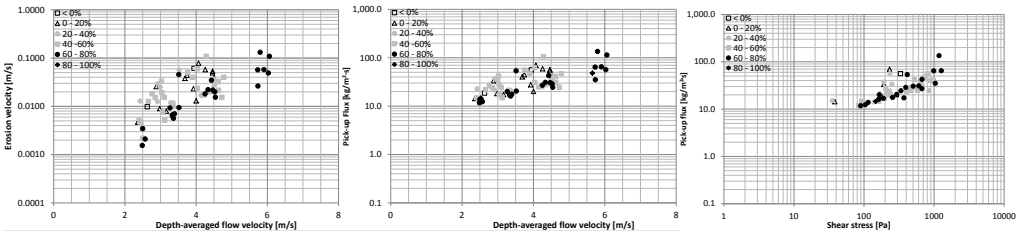


(g) Zilverzand (h) (i)

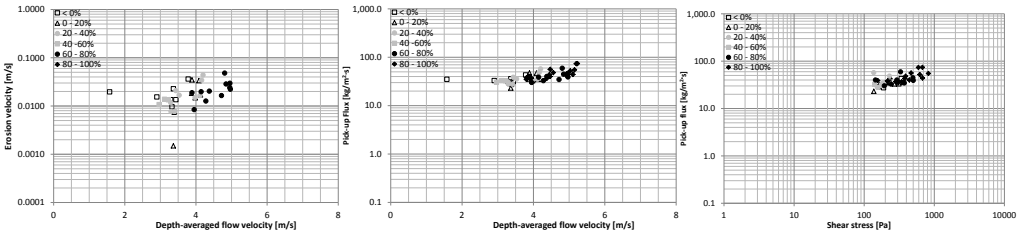


(j) Dorsilit (k) (l)

Figure 8.17: Erosion velocity and pick-up flux as function of the depth-averaged flow velocity, bed shear stress and relative density (density eroding flow between 1060 and 1205 kg/m$^3$). These figures are also presented on a larger scale in Appendix F

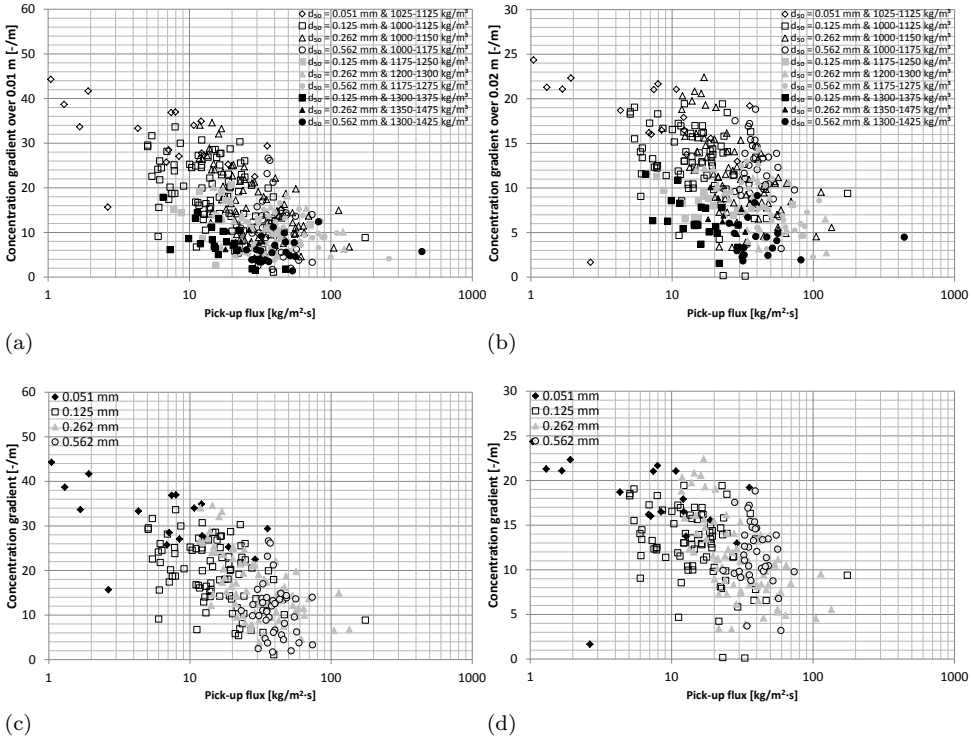


Figure 8.18: Concentration gradient over 0.01 m and 0.02 m above erosion front as function of the pick-up flux for all experiments: (a) and (b) and concentration gradient above erosion front for all experiments with an average density of the eroding flow of less than 1205 kg/m$^3$: (c) and (d). All figures are based on experiments with a relative density of the sand bed larger than 0%: Note negative values for the concentration gradient are not shown and the scale of the vertical-axes of the left and right figures are not equal



Figures 8.18a and 8.18b show the influence of the density of the eroding flow on the concentration gradient. A higher density of the eroding flow leads to a lower concentration gradient, because the vertical transport of the eroded grains is influenced and hindered by the density of the eroding flow. This results in a relative high density and thus a relative low concentration gradient of the eroding flow close to the eroding bed in comparison with erosion with an eroding flow of low density.

An increasing pick-up flux causes a decrease of the concentration gradient just above the non-eroded sand bed (see Figure 8.18), hence leading to a larger density of the eroding fluid just above the non-eroded sand bed. This effect causes an increase of the bed friction coefficient (Figure 7.8) and resulting bed shear stress. The increase of the bed friction coefficient as a result of an increasing pick-up flux is confirmed by Figure 8.19, showing the bed friction coefficient as function of the pick-up flux.

Besides the effect of the concentration just above the non-eroded sand bed on

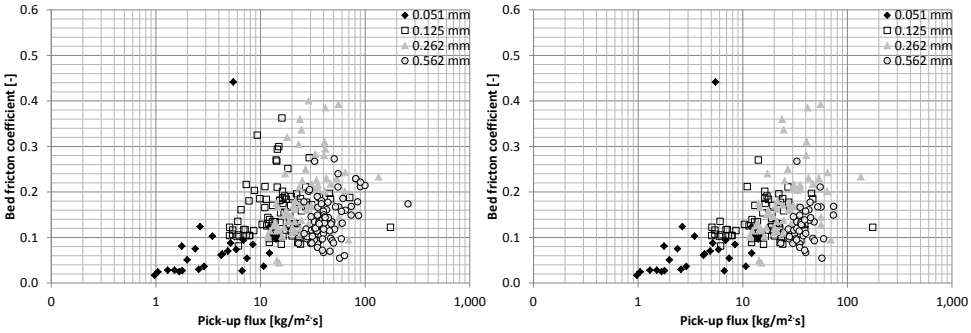


(a) (b)

Figure 8.19: Relation between bed friction and pick-up flux as derived from the experimental results for all experiments (a) and for the experiments with a density of the eroding flow between 1050 and 1205 kg/m$^3$ (b)

the bed friction, an increasing pick-up flux causes an increase of the energy loss due to the larger bulk of eroded sand which must be accelerated. This second effect causes an extra increase of the bed friction at constant flow velocity.

The effect of the pick-up flux on the bed shear stress can also be derived from Figure 8.17. The relation between the pick-up flux and depth-averaged flow velocity shows an influence of the relative density on the pick-up flux. However, this effect disappears when the pick-up flux is compared to the bed shear stress. Obviously the effect of a lower relative density, leading to a higher pick-up flux and higher bed friction, is compensated by the increase of the bed shear stress as a result of the higher pick-up flux. This underlines the mutual effect of the depth-averaged flow velocity and pick-up flux on the effective bed shear stress or friction loss along the eroding bed. Both flow velocity and resulting pick-up flux influence bed friction and hence the effective bed shear stress. This means that the effective bed shear stress does not determine the pick-up flux, as assumed in numerous models, but it is determined by the depth-averaged flow velocity and resulting pick-up flux.



### 8.4.3. Influence depth-averaged density eroding flow

Figure 8.20 shows that the effect of the depth-averaged density of the eroding fluid on the erosion velocity and pick-up flux is negligible. However, the relation between the pick-up flux and bed shear stress shows a small influence of the density of the eroding flow on the pick-up flux. This is the result of the same effect as described in the relation between the pick-up flux, depth-averaged flow velocity and bed shear stress (see Section 8.4.2). The absence of the effect of the depth-averaged density of the eroding fluid on the pick-up flux deviates from the concept of hindered erosion, as described in Section 4.8. This could be explained by the fact that the pick-up flux is determined on the basis of the erosion velocity and the sedimentation flux, determined by the near-bed concentration instead of the depth-averaged concentration of the flow. However, the approach to determine the pick-up flux on the sedimentation

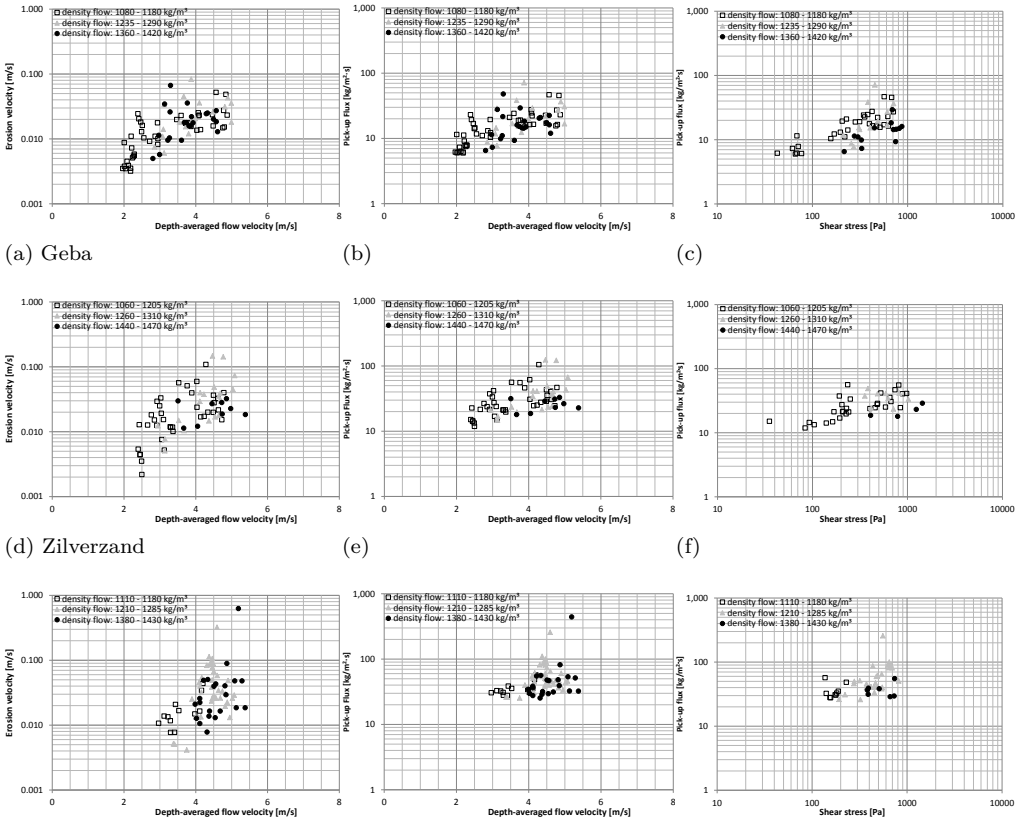


(a) Geba (b) (c)

(d) Zilverzand (e) (f)

(g) Dorsilit (h) (i)

Figure 8.20: Erosion velocity and pick-up flux as function of the flow velocity (relative density sand bed between 20 and 60%) and density of the eroding flow



flux, based on the depth-averaged concentration, also does not show any influence of the density of the eroding flow. This shows that according to the results of these experiments the effect of hindered erosion, seems not to exist.

## 8.5. Influence of properties sand bed

It was expected that bulk properties as relative density and permeability influence the pick-up flux at flow velocities of more than 1 m/s. This section describes the influence of these bulk properties of the sand bed on the pick-up flux on the basis of the results of the experiments.

### 8.5.1. Relative density of sand bed

Figures F.1a, F.1c, F.1e and F.1g show the influence of the relative density on the pick-up flux for all sand types. This gives an indication that the erosion process

at these flow conditions is influenced by the bulk properties of the sand bed. The pick-up flux at a relative density of more than 60% is lower than the pick-up flux at a relative density lower than 60%. The strongest effect of the relative density of the sand bed on the pick-up flux is shown by the finest sand type (Silverbond: $d_{50} = 52$ $\mu$m), while the effect of the relative density on the pick-up flux for the coarsest sand type (Dorsilit: $d_{50} = 561$ $\mu$m) is negligible. This is an indication that not only the relative density affects the pick-up flux but also the permeability (see Section 8.5.2).

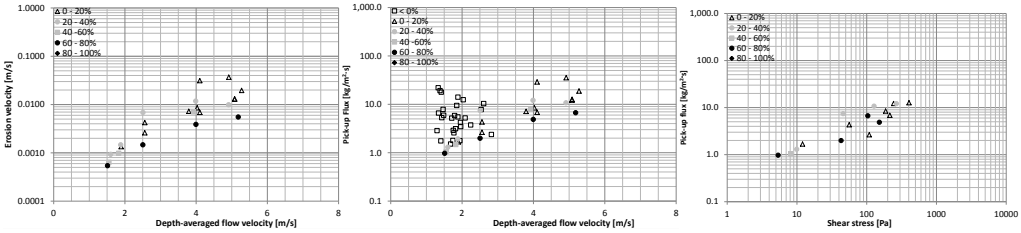


(a) (b) (c)

Figure 8.21: Erosion velocity and pick-up flux as function of the depth-averaged flow velocity, bed shear stress and relative density for Silverbond sand with a relative density higher than 0% (density eroding flow between 1070 and 1150 kg/m$^3$)

The experiments on Silverbond sand ($d_{50} = 51$ $\mu$m) were also executed with a relative density of the sand bed of just below 0%. The figure shows that at this condition ($R_n < 0\%$), the pick-up flux is relative high and highly variable, influencing the overall relation between the erosion velocity, pick-up flux and depth-averaged flow velocity. Due to the effect of the relative density, which was lower than the minimum density, no or almost none dilatancy will have taken place during erosion, causing almost none or no inflow of water into the sand bed during erosion and no or almost no influence of the bulk behavior. The grain by grain erosion regime will have prevailed in case of these low relative densities. Also due the extremely low density the angle of internal friction between the grains will have been very low and the susceptibility for liquefaction is larger, reducing the shear resistance of the sand bed. Both effects result in a relative high pick-up flux. When the results of the experiments with a relative density of less than 0% are omitted (Figure 8.21) from the results the reduction of the pick-up flux at a higher relative density ($> 60\%$) is also recognized in case of Silverbond sand.



### 8.5.2. Permeability

Figure 8.22 shows the influence of the grain size on the relation between the erosion velocity, pick-up flux and the depth-averaged flow velocity. The finest sand shows lower erosion rates and pick-up fluxes than the coarser sand types. The three coarsest sand types show a comparable relation between the erosion velocity, pick-up flux and depth-averaged flow velocity. Only at depth-averaged flow velocities of more than 4 m/s there is tendency that the coarsest sand type has a higher pick-up

flux than Geba and Zilverzand sand. The effect of the grain size shows implicitly the influence of the permeability on the pick-up flux. The finest sand type has the lowest permeability, leading to larger pore water under pressures and hence a larger reduction of the depth of the shear plane in comparison with the three coarsest sand types.

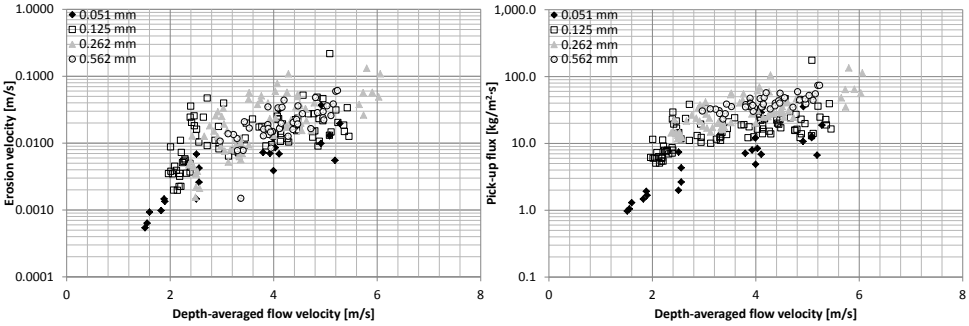


(a) (b)

Figure 8.22: Erosion velocity and pick-up flux as function of the depth-averaged flow velocity for all sand types with a relative density of the sand bed larger than 0 and a density of the eroding flow of less than 1205 kg/m$^3$

The above mentioned effect is also confirmed by Figure 8.23, showing the influence of the relative density and grain size on the relation between the pick-up flux and depth-averaged flow velocity for Silverbond sand ($d_{50} = 52$ $\mu$m).

## 8.6. Model pick-up flux

This Section describes the characteristics of the erosion process in order to develop an analytical pick-up function (Section 8.6.1). Section 8.6.2 describes the basic approach of the developed pick-up function. This analytical function incorporates the influence of turbulent normal wall stresses and the resistance of a sand bed to a normal stress including the effect of dilatancy and effect of inertia (Section 8.6.3 and 8.6.4. The final model is summarized in Section 8.6.5 and validated with the results of the erosion experiment in Section 8.6.6.



### 8.6.1. Physics erosion process

Figure 8.1 shows that the erosion process is determined by ejections and sweeps of vortices hitting the top of the sand bed ('bursting') as a result of the turbulent behavior of a flow. These bursts cover part of the sand bed and cause erosion. This process of pick-up is divided in two phases:

- sweeps locally inducing turbulent normal wall stresses on the top of the sand, resulting in the shearing of lumps of sand;
- ejections causing entrainment of grains into the main flow.

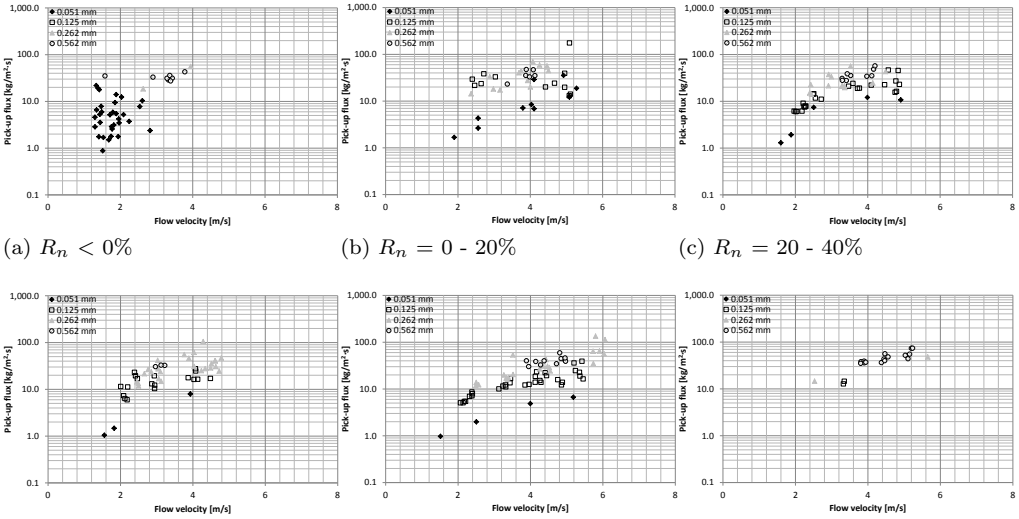


(a) $R_n < 0\%$ (b) $R_n = 0$ - $20\%$ (c) $R_n = 20$ - $40\%$

(d) $R_n = 40$ - $60\%$ (e) $R_n = 60$ - $80\%$ (f) $R_n = 80$ - $100\%$

Figure 8.23: Pick-up flux as function of the depth-averaged flow velocity and grain size at a different relative density ($R_n$) for all experiments with a density of the eroding flow of between 1060 and 1205 kg/m$^3$. These figures are also presented on a larger scale in Appendix G

The existence of sweeps endorses the fact that erosion is not caused by the shearing of layers of sand over the whole surface, but is dominated by local shearing of lumps of sand. As a result of the sweeps a zone of the sand bed is locally subjected to turbulent normal wall stresses causing contraction of part of the sand bed resulting in excess pore water pressures and liquefaction. This zone is relative small at a high relative density (Figure 8.24a) in comparison with sand with a low relative density (Figure 8.24b), because sand with a low relative density has a larger tendency for contraction in comparison with sand with a larger relative density. From this contractive zone a lump of sand is sheared, causing dilatancy.

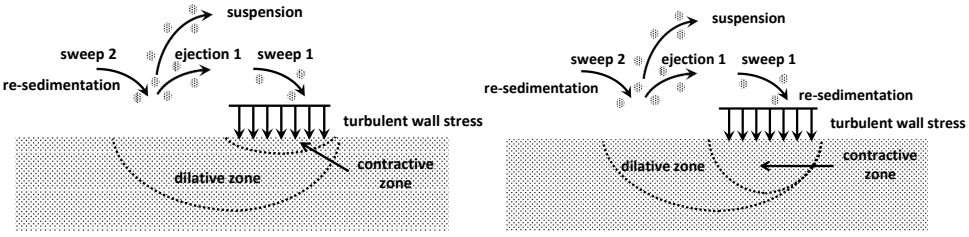


Figure 8.24: Erosion process as determined by ejections and sweeps in case of sand with a high relative density (a) and low relative density (b)

The results of the experiments underline these visual observations. The results show that an increase of the relative density leads to a decrease of the pick-up flux. This influence can be explained by two effects of the relative density on:

- the effect on the resistance to shear: an increase of the relative density leads to a decrease of the pick-up flux, because an increasing relative density leads to an increase of the angle of friction and thus increasing resistance to shear. This results in smaller sheared lumps of sand and thus a lower pick-up flux;
- the effect on dilatancy: a higher relative density increases dilatancy. As a result of dilatancy during shearing the porosity of the sand bed in the sheared zone increases from the in-situ porosity ($n_i$) to at least the critical porosity ($n_{crit}$), causing pore water under pressures. The critical porosity is lower than the maximum porosity and depends on the effective stress. A larger difference between the in-situ porosity and the critical porosity leads to a larger volume increase and hence larger pore water under pressures. This results in a larger effective stress and increase of the resistance to shear and thus a lower pick-up flux.

The existence of contraction and dilatancy endorses also the effect of the permeability of the sand bed on the erosion process. Sand with a relative high permeability shows relative small zones of liquefaction, because the permeability will enhance the decrease of excess pore water pressures, resulting in lower excess pore water pressures and a smaller liquefied zone. In the dilative zone the permeability plays also a role. Dilatancy results in pore water under pressures, increasing the resistance to shear. A relative low permeability induces relative large pore water under pressures giving a relative large increase of the resistance to shear and smaller lumps of sand which can be sheared, resulting in a lower pick-up flux. The effect of the permeability is shown in Figure 8.22b. The sand type with the smallest grain size and thus the lowest permeability, has a lower pick-up flux than the coarser sand types at a corresponding depth-averaged flow velocity.



Part of the flow in the sweeps moves in opposite direction of the main flow along the bed, causing ejections. These ejections entrain part of the grains into suspension (see Figure 8.2), while part of the grains is re-sedimented by sweeps of consecutive vortices hitting the top of the sand bed. When the pick-up flux exceeds the re-sedimentation flux net erosion takes place. The results of the experiments are corrected for this effect. Using this correction for the determination of the pick-up flux shows that the depth-averaged density of the eroding flow does not significantly influence the relation between the pick-up flux and depth-averaged flow velocity. The effect of hindered erosion is not visible. The concentration or density of the flow close to the bed influences the erosion velocity and thus the determination of the pick-up flux from the erosion experiments. The concentration of the grains in the main flow hardly influences the pick-up flux.

### 8.6.2. Basic approach

The erosion process is determined by the shearing of lumps of sand as a result of normal wall stresses cause by turbulent fluctuations. The first attempt to describe

the resistance to shear as a result of a normal stress by a strip load was based on the classical earth pressure theory of Rankine. Pauker (1889) was the first describing the resistance to shear as a result of a normal stress by a strip load and assumed that the failure zone is determined by the resistance of two separate wedges (see Figure 2.8a). This model underestimates the actual resisting shear, because the actual failure zone is considered to be bounded by curves instead of two straight surfaces, introducing a shorter failure zone. Besides it neglects the shear stress acting between wedge I and wedge II (Lambe and Whitman, 1969). Other solutions following a more curved shape, like the solution of Prandtl (Prandtl, 1921), give a better description of the actual resisting shear resistance against a normal stress (see Figure 2.8b). However the solution of Rankine was used in order to determine the pick-up flux, because the shape of the shear planes during erosion show a better agreement with the wedges of Rankine than the spiral shear planes according to Prandtl. These shear planes have a more prolongated shape than the actual shear planes. Both models do not have the same solution, but the influence of the internal angle of friction on the resistance to a normal stress is comparable.

As long as the relative density is larger than 0, shearing causes dilatancy, resulting in pore water under pressures. This increases the effective stress and thus the shear resistance. This effect has been incorporated in the model according to the approach of van Rhee (2010). The third effect taken into account is the effect of inertia. The eroded mass of grains needs to be accelerated to the flow velocity above the bed during the time between two consecutive sweeps.

Summarizing, in order to determine the pick-up flux at high flow velocities, the following sub-models are used:

- Driving mechanism: turbulent normal wall stress on the sand bed as a result of turbulent bursts;
- Resisting mechanism:
  - shear resistance of a shear plane to a vertical stress on a sand bed;
  - effect of pore water pressure in the dilating shear plane on the shear resistance;
  - effect of inertia: accelerating the bulk of eroded grains;
- Resulting pick-up flux: based on the time between turbulent bursts and area covered by these bursts.

The effect of liquefaction is neglected in the model.

### 8.6.3. Driving mechanism: turbulent normal wall stress

The turbulent normal wall stress on the sand bed ($p'$) as a result of the turbulent bursts is determined by the vertical velocity in the sweeps ($\hat{w}$) close to the sand bed. As described in Section 8.3.1 the average vertical velocity in sweeps is approximately $0.5 \cdot U$. As already mentioned, failure of lumps of sand will not take place over the whole area of the sweeps. Only part of the sand bed below a sweep fails. The most

probable location in the sweeps is the location with the maximum vertical velocity, causing the highest turbulent normal wall stress. In determining the turbulent normal wall stress, it is considered that the maximum vertical velocity in the sweeps causing erosion is of the same order of magnitude of the depth-averaged flow velocity. The turbulent normal wall stress on the sand bed, causing erosion, is considered to be equal to:

$$p' = 0.5 \cdot \rho_w \cdot \hat{w}^2 \tag{8.7}$$

Figure 8.25 shows the turbulent normal wall stress on the sand bed as determined with Equation (8.7), compared to the result of Equation (3.13) as determined by Blake (1970) on the basis of experiments. Because these measurements are based on the average turbulent normal wall stress below a sweep, the turbulent normal wall stress calculated with Equation (8.7) is based on $0.5 \cdot U$ instead of $U$. The experiments of Blake (1970) were executed at depth-averaged flow velocities up to 50 m/s along smooth and rough walls. Comparison of Equation (8.7) and (3.13) shows that the approach according to Equation (8.7) gives higher values for the turbulent normal wall stress than the approach of Blake (1970). In order to receive a comparable turbulent normal wall stress, the average vertical velocity in the sweeps should be lowered to $0.35 \cdot U$. Regarding the experiments of Blake (1970), it should be noted that these experiments were based on much higher depth-averaged flow velocities than during the present erosion experiments, while the experiments of Blake (1970) were also based on a non-eroding smooth or rough surface.

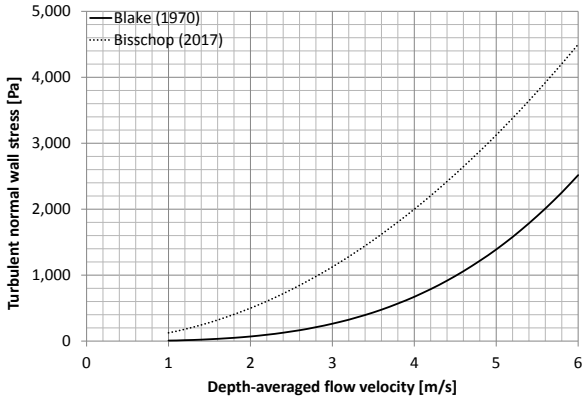


Figure 8.25: Comparison of turbulent normal wall stress as derived according to Blake (1970) and Equation (8.7)

### 8.6.4. Resisting mechanism

#### Shear resistance

It is considered that the turbulent normal wall stresses cause shearing of wedges of sand. The resisting force of these wedges is based on the classical earth pressure

theory of Rankine. Considering sand has no cohesion the vertical resistance of a cohesion less material (Lambe and Whitman, 1969) is, see Figure 8.26:

$$\sigma_p = 0.5 \cdot g \cdot (\rho_i - \rho_w) \cdot B \cdot N_\gamma \tag{8.8}$$

in which $\frac{B}{2}$ is the width of the top of wedge I shearing as a result of the vertical stress $\sigma_p$ and $N_\gamma$ is defined as:

$$N_\gamma = 0.5 \cdot \left[ \left( \frac{1 + sin\phi}{1 - sin\phi} \right)^{5/2} - \left( \frac{1 + sin\phi}{1 - sin\phi} \right)^{1/2} \right] \tag{8.9}$$

The depth of the shear plane ($h_s$) is (Lambe and Whitman, 1969):

$$h_s = \frac{B}{2} \cdot tan\,(\pi/4 + \phi/2) \tag{8.10}$$

The angle of friction is based on (see also Equation (2.16):

$$\phi = 33 - \frac{3}{C_u} + \left( 15 - \frac{4}{C_u} \right) \cdot R_e \tag{8.11}$$

This empirical equation relates the relative density ($R_e$) and uniformity coefficient ($C_u = d_{60}/d_{10}$) to the internal angle of friction.

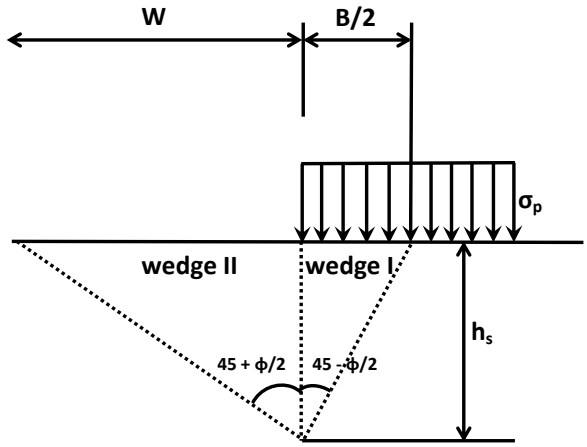


Figure 8.26: Depth and width of wedges as based on the classical earth pressure theory of Rankine (Lambe and Whitman, 1969)

The width (W) of wedge II can be derived from Figure 8.26:

$$W = h_s \cdot tan\,(\pi/4 + \phi/2) \tag{8.12}$$

Assuming a 2-dimensional shape of the wedge, the volume of the total wedge ($m^3/m$) is:

$$A_w = 0.5 \cdot \left( \frac{1}{2} \cdot B \cdot h_s + W \cdot h_s \right) \tag{8.13}$$

Effect dilatancy

In case the in-situ porosity exceeds the critical porosity, shearing will induce dilatancy. The porosity of the sheared zone increases to the critical porosity ($n_{crit}$). The critical porosity depends on the effective stress and type of sand. van Rhee (2010) has used $n_{max}$ as the best estimate $n_{crit}$. van Rhee (2010) has assumed this as reasonable, because the porosity has to increase to a porosity above the critical porosity in order to make it possible for the flow to pick-up the grains.

The increase of the pore volume results in an inward hydraulic gradient, hence increasing the effective stress. This increases the shear resistance and decreases the depth of the sheared wedge of sand ($h_s$). The hydraulic gradient during erosion matches (van Os and van Leussen, 1987), (van Rhee, 2010) [1]:

$$i = \frac{v_e}{k_{max}} \cdot \frac{n_{max} - n_i}{1 - n_{max}} \tag{8.14}$$

Equation (8.14) assumes that the deformation in the sheared zone, as a result of dilatancy, is continuous. The theory of Rankine is based on shearing along a distinctive dilating failure zone of the wedges. However, the wedge above this failure zone will also dilate in order to be picked up by the flow, resulting in continuous deformation. The vertical velocity ($v_e$) can be compared with the horizontal or active wall velocity, propagation velocity of a vertical wall of sand, in dredging practice (Section 4.5). A measure for this vertical velocity is: $h_s/T_B$. A measure for the mean bursting period for open channel flow is (Nezu and Nakagawa, 1993):

$$\frac{T_B \cdot U}{h_f} = (1.5 - 3.0) \tag{8.15}$$

The effect of the inward hydraulic gradient on the increase of the shearing resistance can be incorporated in Equation (8.8):

$$\sigma_p = 0.5 \cdot [g \cdot (\rho_i - \rho_w) + i \cdot \rho_w \cdot g] \cdot B \cdot N_\gamma \tag{8.16}$$

The depth of the wedge ($h_s$) can be determined combining Equations (8.16) and (8.10):

$$h_s = \frac{p' \cdot tan\,(\pi/4 + \phi/2)}{N_\gamma \cdot g \cdot (\rho_i - \rho_w + i \cdot \rho_w)} \tag{8.17}$$

[1] Equation (8.14) can be rewritten as function of $k_i$. Using the adapted Kozeny-Carman equation, see Equation (2.9), for the quotient between the in-situ permeability and the permeability at the maximum porosity, leads to:

$$\frac{k_i}{k_{max}} = \frac{n_i^3 \cdot (1 - n_{max})^2}{(1 - n_i)^2 \cdot n_{max}^3}$$

Using this expression and assuming $n_i = 0.4$ and $n_{max} = 0.5$, changes the expression for $i$ in $i = v_e / (14 \cdot k_i)$.

It should be noted this is an implicit equation because the inward gradient ($i$) depends on the depth of the wedge ($h_s$). Equations (8.14), (8.15) and (8.17) can be solved iteratively.

Effect of inertia

Inertia influences the pick-up flux, because the sheared grains need to be accelerated to the depth-averaged flow velocity above the bed (van Rhee, 2010), assuming the grains will be fully suspended after pick-up. The extra stress ($\sigma_a$) to be exerted by a sweep on the sheared mass ($m$) in order to accelerate this mass to the depth-averaged flow velocity above the bed can be determined by:

$$\sigma_a = \frac{m \cdot a}{A_{sw}} \tag{8.18}$$

in which $a$ is the acceleration of the shear mass and $A_{sw}$ is equal to the surface area of the sweep leading to shearing of a lump of sand. The total mass ($m$) of the lump of sand per unit of bed area to be accelerated is equal to:

$$\frac{m}{A_{sw}} = \frac{A_w \cdot L}{A_{sw}} \cdot \rho_s \cdot (1 - n_i) = \frac{0.5 \cdot (B/2 \cdot h_s + W \cdot h_s) \cdot L}{(B/2 + W) \cdot L} \cdot \rho_s \cdot (1 - n_i) = \frac{h_s}{2} \cdot \rho_s \cdot (1 - n_i) \tag{8.19}$$

in which $L$ is the length of the sheared mass perpendicular to the direction of the flow. The acceleration of the sheared mass depends on the depth-averaged flow velocity and the mean bursting period:

$$a = \frac{U}{T_B} \tag{8.20}$$

### 8.6.5. Resulting pick-up flux

Sections 8.6.3 and 8.6.4 show the description of the main steps in the determination of the pick-up flux, considering that the turbulent normal wall stress ($p'$) should exceed the shear resistance of a lump of sand ($\sigma_p$) and the extra stress to accelerate the grains of the sheared mass ($\sigma_a$). These steps are combined in order to determine the pick-up flux as function of the depth-averaged flow velocity. This gives the following expression for the pick-up flux ($E$):

$$E = \frac{\frac{A_w}{B/2+W} \cdot \lambda_b \cdot (1 - n_i) \cdot \rho_s}{T_B} \tag{8.21}$$

Using Equation (8.13) this equation can be rewritten as:

$$E = \frac{0.5 \cdot h_s \cdot \lambda_s \cdot (1 - n_i) \cdot \rho_s}{T_B} \tag{8.22}$$

in which $\lambda_s$ is the averaged area of all sweeps per unit of bed area. This area is considered as $0.5 \cdot \lambda_b$. The mean bursting period is based on Equation (8.15). Because $p' = \sigma_p + \sigma_a$ the depth of the shear plane ($h_s$) is:

$$h_s = \frac{(p' - \sigma_a) \cdot tan\,(\pi/4 + \phi/2)}{N_\gamma \cdot g \cdot (\rho_i - \rho_w + i \cdot \rho_w)} \tag{8.23}$$

This is an implicit equation, because the inward gradient ($i$) and extra stress to accelerate the eroded mass ($\sigma_a$) depend on the depth of the shear plane ($h_s$). However, this equation can be solved iteratively.

### 8.6.6. Validation of model

The model to determine the pick-up flux needs an estimate of the vertical flow velocity in the sweeps ($\hat{w}$), the area of all sweeps per unit of bed area ($\lambda_s$) and the constant in Equation (8.15) determining the mean bursting period. Comparison of the model with the data of the experiments as presented in Figure 8.28 shows that the model has the best correlation with the data in case of:

- a vertical flow velocity in the sweeps equal to the depth-averaged flow velocity ($\hat{w} = 1.0 \cdot U$);
- turbulent bursts hitting the top of the sand bed over the whole bed area ($\lambda_b = 1.0$);
- a dimensionless mean bursting period ($T_B \cdot U/h_f$) of 1.5.

The value used for the factor $\lambda_b$ means that the top of the sand bed is totally covered by turbulent bursts, in which the sweeps cause a vertical load on the sand bed, while the ejections transport the grains in vertical direction. It is considered that a sweep causes shearing of consecutive lumps of sand, while the sweeps travel in horizontal direction over the top of the sand bed. This explains why the width of the shear planes (0.001 m to 0.020 m) as determined by Equations (8.8) and (8.12) is much smaller than the dimensions of the sweeps and ejections (length of the bursts is 0.05 m to 0.10 m). as described in Section 8.2. Considering the sweeps cover half of the surface of the bursts, the calculated width of consecutive wedges, sheared as a result of the turbulent normal wall stresses, is a factor 10 to 20 smaller than the total length of the bursts.

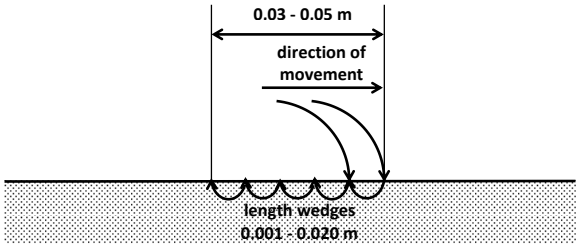


Figure 8.27: Sweeps causing the shearing of multiple separate wedges

(Nezu and Nakagawa, 1993) have considered that the average vertical velocity ($w$) in a sweep is approximately $0.25 \cdot U$. However, due to vorticity the vertical

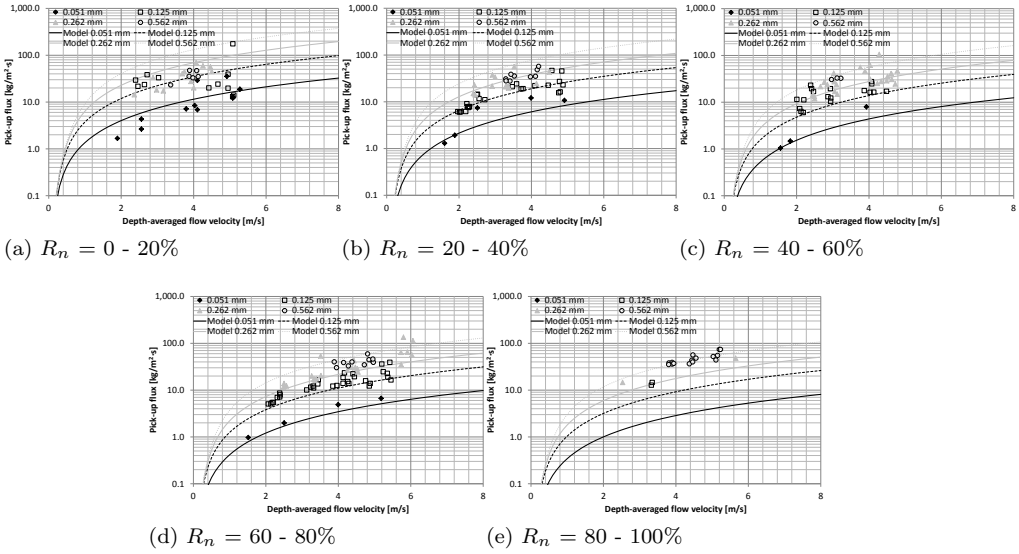


(a) $R_n$ = 0 - 20% (b) $R_n$ = 20 - 40% (c) $R_n$ = 40 - 60%

(d) $R_n$ = 60 - 80% (e) $R_n$ = 80 - 100%

Figure 8.28: Pick-up flux as function of the depth-averaged flow velocity for different sand types and relative density for all experiments with a density of the eroding flow of between 1060 and 1205 kg/m$^3$ compared to the pick-up flux model. These figures are also presented on a larger scale in Appendix H

flow velocity in the sweep will not be constant over its surface. It is considered that the eddies roll over the top of the sand bed and that the wedges are sheared at the location with the highest flow velocity in the sweep and moves in horizontal direction over the top of the sand bed (see Figure 8.27). The depth-averaged flow velocity in horizontal direction is chosen as a measure for the time-averaged maximum vertical flow velocity in the sweep.

Figure 8.28 shows a comparison between the calculated pick-up flux with the model developed and the results of measurements of the pick-up flux as function of the depth-averaged flow velocity and the relative density. The soil parameters of the different sand types are based on the properties as presented in Section 5.4. The angle of internal friction is based on an empirical relation between the relative density and the angle of internal friction, see Equation (8.11). The effect of the relative density on the permeability is determined with the help of Equation (5.7). The results of the permeability experiments are used to determine the value of $C_k$ (Table 5.2). The calculated pick-up flux for each range of the relative density is based on the average relative density of this range.

At a relative density of 0 to 20 % the model overestimates the pick-up flux for the two coarsest sand types (262 and 562 $\mu$m). At a relative density of more than 20 % the model gives a rather accurate prediction of the pick-up flux.

Figure 8.29 shows the influence of the relative density on the pick-up flux per sand type compared to the results of the model as described above. Despite the variation of the results of the erosion experiments, the data show a rather adequate

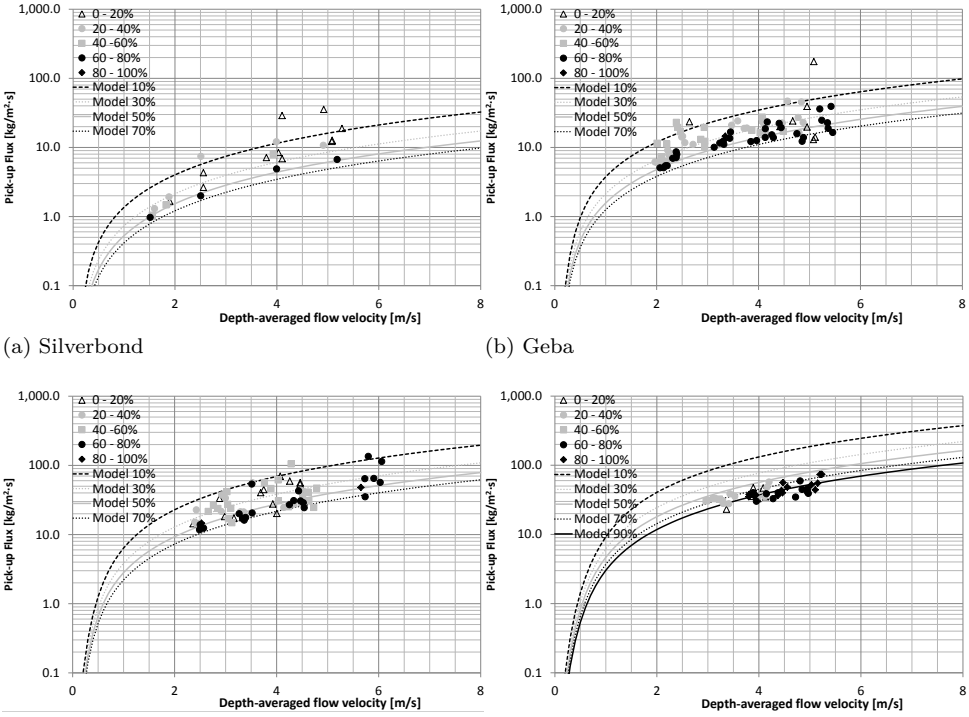


(a) Silverbond (b) Geba

(c) Zilverzand (d) Dorsilit

Figure 8.29: Pick-flux as function of the depth-averaged flow velocity per sand type at varying relative density for all experiments with a density of the eroding flow of between 1060 and 1205 kg/m$^3$ compared to the pick-up flux model



correspondence with the results of the erosion experiments.

The model does not take into account the effect of liquefaction as described in Section 8.2.2. This effect will lead to excess pore water pressures in the sand bed, resulting in a decreasing resistance against shear. Especially sand with a low permeability and low relative density is susceptible for liquefaction.

The applicability of the model is based on Figure 8.30. This figure shows the quotient of the thickness of the sheared wedges, as calculated by the pick-up flux model, and the grain size as function of the depth-averaged flow velocity. Considering, that sand can be described by its bulk properties, when the thickness is more than 10 times the average grain size, the model developed is applicable from a depth-averaged flow velocity of 1 to 2 m/s, depending on the relative density and permeability of the sand.

Bisschop et al. (2016) concluded that the pick-up function of van Rhee (2010) is consistent with the results of the experiments of Bisschop (1993) and the results of the first series of experiments of this study. This pick-up function gives the best prediction of the pick-up flux in comparison with the other existing models in the

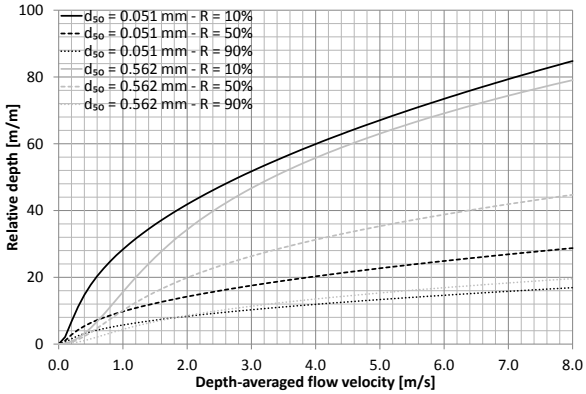


Figure 8.30: Relative thickness of sheared wedges ($h_s/d_{50}$) as function of the depth-averaged flow velocity

dilatancy reduced erosion regime, as described in Section 4.5.1. Figure 8.31 gives a comparison of the pick-up function of van Rhee (2010) with the developed pick-up function and the data of the second series of experiments. The pick-up function of van Rhee (2010) needs an estimate of the bed shear stress. The bed shear stress was determined on the basis of Equation (7.10). Figure 8.31 shows that the pick-up function of van Rhee (2010) gives a rather accurate prediction of the pick-up flux for the two finest sand types (Silverbond and Geba), while this function overestimates the pick-flux for the two coarsest sand types (Zilverzand and Dorsilit). As mentioned the pick-up function of van Rhee (2010) needs an estimate of the bed shear stress and is therefore sensitive for the method on which the bed shear stress is determined. The present developed pick-up function misses this disadvantage.

8

### 8.6.7. Practical application: erosion during breaching of sand dikes or embankments

This section describes the practical application of the knowledge developed, to give more understanding into the relevance of the erosion process in case of breaching of a sand dike. Dikes have failed in the past all over the world and will continue to do so in the future (Lemmens et al., 2016). Failure of a dike happens mainly during high river or sea levels. In most cases sand dikes are protected by a cover of clay and grass or revetment. In case this cover fails, a dike starts to breach. A major breach can form within a few hours after the failure of the protective cover (Visser, 1998). Water enters the polder and the area will be inundated. This flooding causes casualties and economic damage. The amount of casualties depends on the inundation rate of the polder (Jonkman, 2007). This inundation rate depends on the rate of the growth of the dimensions of the breach, the water level difference between the sea and/or river and the polder and the size of the polder.

Bisschop et al. (2010) compared the pick-up function of van Rhee (2010), valid in the dilatancy reduced erosion regime, with the measurements of the development

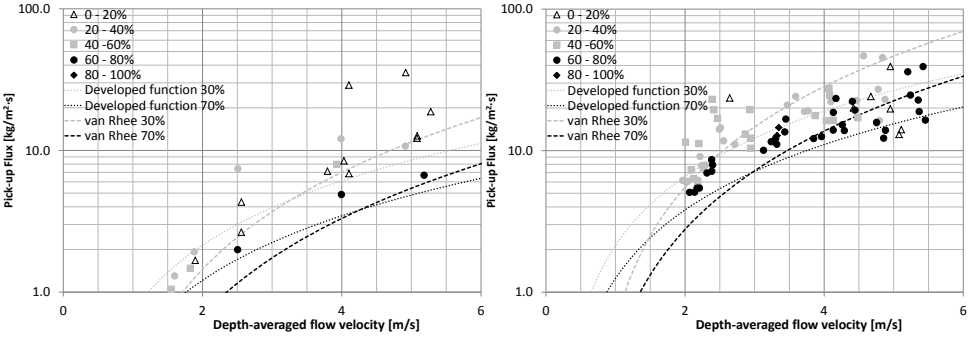


(a) Silverbond (b) Geba

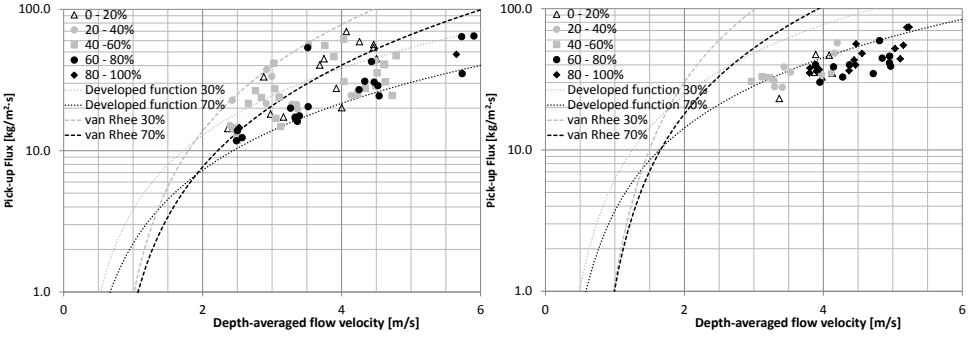


(c) Zilverzand (d) Dorsilit

Figure 8.31: Comparison of the developed pick-up function and pick-up function of van Rhee (2010) per sand type at varying relative density for all experiments with a density of the eroding flow of between 1060 and 1205 kg/m$^3$

of the breach width during the Zwin'94 experiment (Visser, 1998). The Zwin'94 experiment was executed in 1994 in the Zwin channel, a tidal inlet at the Dutch-Belgian border connecting the nature-reserve 'Het Zwin' with the North Sea. The data of this experiment have been used to calibrate a model for breach development (Visser, 1998). Use of the pick-up function of van Rhee (2010), including the effect of dilatancy reduced erosion and thus the effect of the porosity and permeability, improved the prediction of the development of the breach width in time.

Reduction of the inundation rate can be achieved by retarding the breaching process. This reduces the number of casualties, resulting in an increasing safety for the inhabitants. Lemmens et al. (2016) have studied the effect of adding bentonite to sand on the pick-up flux and retardation of breaching. Adding bentonite to sand leads to a reduction of the permeability, while the strength characteristics of the material remains constant. Adding a mass percentage of 2.4% bentonite reduces the permeability with a factor 6 in comparison with the same sand without bentonite. As a result the pick-up flux showed a reduction with a factor 10 in comparsion with sand without bentonite. Calculations with the breach model, as developed by Visser (1998), has shown that in case of adding 2.4 % bentonite to sand, the inundation velocity reduces with a factor 2. This results in a decreased mortality rate.

Foortse (2016) has extended the range of the erosion experiments as executed by Lemmens et al. (2016). The erosion experiments of Lemmens et al. (2016) were executed on sand with a maximum mass percentage of added bentonite of 2.4% and a maximum depth-averaged flow velocity of 1.1 m/s. The experiments of Foortse (2016) were executed up to a depth-averaged flow velocity of 2.2 m/s, while the maximum percentage of bentonite was 6.0%. Direct shear tests have revealed that up to a bentonite percentage of 6% the strength characteristics (angle of internal friction and cohesion) of the sand remains unaltered. This effect has been supported by the results of the determination of the Atterberg limits. Up to a mass percentage of 6% bentonite, the plastic limit could not be determined. This has confirmed that the material at this amount of added bentonite still can be described as non plastic, behaving as a granular material.



While the shear tests have shown no influence on the strength characteristics, the added bentonite influenced the permeability. A percentage of 6% bentonite reduces the permeability with a factor of 100 in comparison with sand without bentonite (Figure 2.4). This effect has leaded to a reduction of the pick-up flux with a factor 10 to 20 in comparison with sand without bentonite (Figure 4.16). A case study has shown that an increase of the safety level by a factor of 10 can be achieved using sand-bentonite mixtures in the core of the dike. However, it should be noted that the amount of bentonite in order to achieve such a reduction depends on the size of the polder (Foortse, 2016).

This means that when a new dike is build with sand the height and dimensions of the dike can be reduced, in comparison with a dike build of 'normal' sand, when the permeability of the sand is reduced by an additive like bentonite. The results of the experiments and calculations of Lemmens et al. (2016) and Foortse (2016) have shown that a higher safety level can be reached in comparison with a dike of the same dimensions build with sand without additives. It should be considered there

is a maximum mass percentage of the bentonite or other clay-type additive in order to remain the strength characteristics of the sand in the dike. Reduction of the amount of space necessary for the construction of a dike can be reached when a dike is build with sand and additive in comparison with a dike build of 'normal' sand. This could be an option when the space available for the construction of a dike is limited due to existing buildings and/or other constructions. In case a present sand dike should be improved and space is limited for increasing the height and/or width of the dike, improving the dike by reducing the permeability is an option to improve the dike.

## 8.7. Discussion

Initiation of motion of sand grains takes place when the critical Shields parameter is exceeded by the flow conditions. At this condition grains start to move along the sand bed by saltation, rolling or shearing. The level of the sand bed does not change. The grains are not entrained into the main flow. Pick-up starts at the moment when grains are entrained into the main flow and the top of the sand bed moves down. Pick-up starts as grain by grain erosion and will develop in dilatancy reduced erosion as the flow velocity and resulting bed shear stress increase. During dilatancy reduced erosion, it is considered thin layers of sand are sheared in horizontal direction before they are eroded. In this regime the turbulent bursts are considered not to be strong enough to shear lumps of sand. However, it could be the case that at these flow velocities, turbulent bursts already influence the erosion process.

At depth-averaged flow velocities of more than 1 to 2 m/s, the impact of turbulent bursts increases and causes shearing of lumps of sand: turbulence induced erosion. These bursts consist of vortices traveling close to the top of the sand bed. The sweeps of these vortices hit the top of the sand bed, causing shearing of lumps of sand. These lumps are disintegrated and (partly) transported to the main flow by ejections. However, not all grains reach the main flow, part of the eroded grains are re-sedimented by sweeps of the next vortices. This behavior forms the basis of the new developed model in determining the pick-up flux. The model incorporates the effect of shearing of lumps of sand by turbulent bursts, the effect of dilatancy resulting in pore water under pressures in the sand bed and the effect of inertia.



However, the model does not take into account the effect of liquefaction, as a result of the impact of consecutive turbulent bursts. The relative density of the sand bed influences this effect. In case of loosely packed sand, contractive behavior was experienced during the experiments on the finer sand types, increasing the sensitivity for liquefaction. The effect was larger in fine sand in comparison with coarse sand. The impact of the turbulent bursts, cause temporarily excess pore water pressures. In case of a low permeability, consecutive turbulent bursts will lead to liquefaction of (part) of the sand bed. Due to the low permeability the excess pore water pressures decrease hardly between consecutive turbulent bursts. In case of sand with a high permeability, the temporarily excess pore water pressures will be dissipated between consecutive bursts, leading to a small and local liquefied zone of sand. This effect had not yet been incorporated in the pick-up flux model. In practice this effect will be less strong, because normally sand has a rather high relative density, reducing

the sensitivity for liquefaction significant.

Liquefaction will reduce the resistance against shear. The present pick-up flux model is calibrated on the data of the experiments mainly on the basis of a fit of the factor $\lambda_B$. The results of the present calibration of the model developed, have showed that the factor $\lambda_B$ is equal to 1.0. It is expected that if the effect of liquefaction is taken into account in the pick-up flux model, the value of this factor will be lower and more realistic.

Besides the effect of liquefaction, the present model does not take into account the effect of the water pressure at the top of the sand bed. In case of drained behavior this water pressure will cause a flow in the sand bed dragging the grains in the direction of the ejections.

The description of the erosion process have made it possible to improve the determination of the pick-up flux from the erosion experiments. In order to determine the pick-up flux from the results of the experiments, the sedimentation flux should be known. The sedimentation flux influencing the effective pick-up flux depends on the near-bed concentration. However, the level at which the near-bed concentration is determined, should be known. Sweeps, following directly behind a preceding ejection, influence re-sedimentation. Consequently the resulting sedimentation flux is determined by the average concentration of grains over the height of the vortices close to the top of the sand bed. Visual observations during the erosion experiments showed that these vortices have a height of 0.02 to 0.03 m and a length of 0.05 to 0.10 m. On the basis of these observations it was decided to determine the sedimentation flux on an average near-bed concentration over a height of 0.03 m above the sand bed.

The results of the experiments show the influence of the relative density and permeability of the sand bed on the pick-up flux. This substantiates the fact that the erosion process is influenced by the bulk properties of the sand bed. Besides the results of the experiments showed no influence of the average density of the eroding flow on the pick-up flux. This is caused by the fact that during erosion the effective pick-up is reduced by the effect of sedimentation of the grains in the layer just above the top of the sand bed (near-bed concentration). The results of the erosion experiments are corrected for this process, resulting in the determination of the pick-up flux ($E$). The grains which are transported through this are kept in suspension and as long as the transport capacity of the flow is not reached the average density of the concentration above this layer does not influence the pick-up flux.

The pick-up flux depends also on the depth-averaged flow velocity and bed shear stress. The relation of the pick-up flux with the depth-averaged flow velocity showed the influence of the mentioned bulk properties of the sand bed. However the influence of these bulk properties vanished partly when the pick-up flux was compared to the bed shear stress. This is the result of the influence of the near-bed concentration on the bed shear stress. An increasing bed concentration leads to an increase of the bed friction coefficient. The near-bed concentration however, depends on the pick-up and sedimentation flux. This means that an increasing pick-up flux, as a result of for instance a low relative density, leads to an increase of the bed shear

stress. The effect causes that the effect of the bulk properties on the pick-up flux is compensated by an extra increase or decrease of the bed shear stress, causing a vanishing influence of the bulk properties on the relation between the pick-up flux and bed shear stress. This emphasizes that the bed shear stress is not the driving mechanism for the pick-up of grains, but the bed shear stress is the result of the flow velocity, pick-up and sedimentation flux.

Pick-up functions in the grain by grain and dilatancy reduced erosion regime use the average bed shear stress as driving mechanism for the determination of the pick-up flux. The approach in the turbulence induced erosion regime is different. It is considered that the bed shear stress actually does not exist in this regime, but the bed shear stress is a measure for the energy losses as a result of grain-grain, grain-fluid interaction and acceleration of the eroded grains. The bed shear stress is the result of pick-up and simultaneous sedimentation at a certain flow velocity, instead of the driving mechanism. The driving mechanism in the turbulence induced erosion regime is the normal stress as a result of the sweeps in turbulent bursts hitting the top of the sand bed. This is also the reason that the pick-up flux in the turbulent induced erosion regime is related to the depth-averaged flow velocity instead of the bed shear stress.

# 9

# Conclusions and recommendations

## 9.1. Conclusions

The conclusions are described on the basis of the goals of this research program as described in Chapter 1.

- to observe and to get understanding of the process of erosion of sand at flow velocities of 2 to 6 m/s and to gather experimental data of the erosion process with varying bulk properties of the sand bed;
- to develop a pick-up flux function applicable at these flow velocities.

This leads to a subdivision of the conclusions according to the following subjects:

- attained experimental data set;
- physics of the erosion process;
- influence of operational parameters and properties sand bed;
- experimental procedure;
- pick-up function.

Furthermore conclusions are given regarding the energy loss along an eroding sand bed, often represented by the bed shear stress.

### Attained experimental data set

This experimental study comprises the data of several experiments influencing the pick-up flux of sand at flow velocities of more than 1 m/s. The operational conditions of the test program are depicted in Table 5.4. Parameters varied during the experiments are the depth-averaged flow velocity, density of the eroding flow, relative density of the sand bed, grain size and thus the influence of the permeability. Appendix A gives an overview of the operational conditions during each experiment. The results of the experiments are summarized in Appendix B, C and D.

### Physics of the erosion process

Based on the visual observations during the erosion experiments and the analysis of the results of the erosion experiments, the physical process during erosion, at depth-averaged flow velocities between 2 and 6 m/s, have been determined and described. From this description the following conclusions can be drawn:

- the turbulent behavior of the flow influences the erosion process. Turbulent bursts, consisting of vortices hitting the top of the sand bed, determine the intensity of the erosion process. The sweeps of the turbulent bursts cause a normal stress on the top of the sand bed, resulting in shearing of lumps of sand. These lumps are disintegrated and the grains are (partly) transported to the main flow by ejections. Not all grains reach the main flow. Part of the eroded grains are re-sedimented by consecutive sweeps;

- considering above, the near-bed concentration, necessary to determine the sedimentation and hence the pick-up flux, has been based on the vertical height of the sweeps and ejections. These sweeps and ejections determine the erosion process and influence the pick-up flux by re-sedimentation of grains picked up by ejections;

- the analysis of the results of the experiments shows the influence of the relative density and permeability on the relation between the pick-up flux and depth-averaged flow velocity. The relative density of a sand bed determines the angle of internal friction and effect on dilatancy, while the permeability determines the (decreased) pore water pressures during dilatancy. This underlines that the erosion process is influenced by the shearing of lumps of sand including the effect of dilatancy;

- the influence of the bulk properties of the sand bed, like relative density and permeability, vanishes when the pick-up flux is related to the bed shear stress. In case of an increasing pick-up flux, due to for instance a low relative density of the sand bed, this leads to an increase of the near-bed concentration, hence increasing the bed shear stress as described in the conclusions regarding the bed shear stress (see further). The effects of the bulk properties on the pick-up flux are compensated by an extra increase or decrease of the bed shear stress, causing a vanishing influence of the bulk properties on the relation between the pick-up flux and bed shear stress;

- the impact of consecutive turbulent bursts on the sand bed causes local liquefaction of the sand bed. The turbulent bursts cause a vertical stress on top of the sand bed resulting in temporarily excess pore water pressures. The dimensions of the liquefied zone depend on the relative density and permeability of the sand bed. A sand bed with a low relative density shows a larger liquefied zone, in comparison with sand with a high relative density. A high permeability enables a rather rapid decrease of the excess pore water pressures, decreasing the dimensions of the liquefied zone in comparison with sand with a lower permeability;
- the results of the experiments show no influence of the depth-averaged density of the flow on the pick-up flux. However, the near-bed concentration influences the erosion velocity because this increases the sedimentation flux.

### Influence of operational parameters and properties sand bed

The influence of the parameters varied during the experiments are described below:

- depth-averaged flow velocity: the pick-up flux increases at increasing depth-averaged flow velocity. An increase of the depth-averaged flow velocity results in higher normal stresses on the top of the sand bed, hence resulting in larger wedges of sheared sand and resulting increase of the pick-up flux (Section 8.4.1);
- density eroding flow: it was expected that the density of the eroding flow should influence the pick-up flux (hindered erosion). However, the data of the experiments did not show any influence of the depth-averaged concentration of the eroding flow on the pick-up flux (Section 8.4.3);
- relative density sand bed: an increase of the relative density leads to a decrease of the pick-up flux. This underlines the conclusion that the erosion process is determined by shearing of sand. A high relative density increases the resistance to shear and hence causing a reduction of the pick-up flux (Section 8.5.1);
- grain size (influence of permeability): at depth-averaged flow velocities of more than 4 m/s the experimental results show for the three coarsest sand types an influence of the grain size, and thus the permeability of the sand, on the pick-up flux. The relative low permeability of the finest sand type, results in already an influence of the grain size on the pick-up flux from depth-averaged flow velocities of 1.5 m/s. An increase of the grain size, and thus the permeability, causes an increase of the pick-up flux. A low permeability will lead to relative high pore water under pressures during shearing, increasing the resistance the shear and hence causing a reduction of the pick-up flux in comparison to sand with a high permeability (Section 8.5.2).



### Experimental procedure

The conclusions regarding the experimental procedure are:

- the acceleration of the flow during the experiments has made it difficult to derive the energy loss along the eroding sand bed. This effect has complicated an accurate determination of the effective bed shear stress and bed friction from the pressure gradient measurements. As a result of the experimental errors, in order to the determine the bed shear stress, the experimental error of the bed shear stress varies within a range of between 30% and 80% above and below the calculated value of the bed shear stress at depth-averaged flow velocities up to 4 m/s. At higher flow velocities the range of the experimental error decreases to between 5% and 30%;
- the frictional properties of the walls of the measurement section changed during the experimental program, due to wear as a result of the impact of sand grains on the walls. Therefore it was not only necessary to calibrate the pressure gauges during the experimental program, but it was also necessary to check the measurements of the pressure gradient in the measurement section during the experimental program on a regular basis;
- besides the influence of the temperature and the composition of the water in the slurry-circuit, the type of sand influences the relation between the results of the measurements with the (electrical) conductivity probes and the density measurements with the radio-active density meter. The sand types used, have a varying relation (curved or linear) between the measured potential difference and the density as measured with the radio-active density meter;
- based on the findings during the erosion experiments a cooling system for the slurry circuit is developed, to keep the temperature of the slurry in the circuit constant during the experiments. This will improve and simplify the calibration procedure of the conductivity probes and keeps physical parameters like the viscosity of the fluid and resulting settling velocity of grains constant.

### Pick-up function

A semi-empirical pick-up function has been derived on the basis of the results of the experiments and visual observations during the experiments. This function is based on the shearing of lumps of sand as a result of turbulent normal wall stresses. The thickness of the sheared lumps is determined on the basis of the resisting force of a wedge to a normal force according to the solution of Rankine. The effect of dilantancy is incorporated in this approach by including the effect of the inward hydraulic gradient into the sand bed on the increased vertical effective stress. The main conclusions regarding this function are:

- using the depth-averaged flow velocity for the modeling of the normal stress on top of the sand bed and modeling the failure mechanism during the shearing of lumps of sand according to the description of the resistance of a sand bed to a vertical strip load, gives a good description of the influence of the relative density and the angle of internal friction on the pick-up flux;
- the effect of dilatancy and resulting decreased pore water pressures explains the difference in pick-up flux between sand with a low and high permeability;

- as described sweeps cause normal stresses on top of the sand bed, resulting in sheared lumps of sand. The bed shear stress is not the driving mechanism for the pick-up of grains.

### Bed shear stress

The shear stress at the surface of an eroding sand bed is a widely studied subject. The results of the analysis of this experimental program show that:

- in case of an eroding sand bed, using the widely used approach to relate the bed friction, via for instance the Colebrook equation, to a relation between the relative bed roughness ($k_s/d_{50}$) and the Shields parameter, leads to an apparent roughness ($k_s$) of larger dimensions than the grain size. However, using this approach for the analysis of the erosion experiments at depth-averaged flow velocities of more than 4 to 5 m/s, the fictitious roughness exceeds the height of the measurement section, which is physically impossible. Based on these findings it should be noted that the effective roughness during erosion has no physical meaning. It is only a measure for the energy loss, in case of erosion or sheet flow;

- the Darcy-Weisbach bed friction coefficient, in case of an eroding sand bed, is considered as an equivalent bed friction coefficient. It does not represents the friction between two layers, but it represents the energy loss in a layer along an eroding sand bed. This friction coefficient can be used in order to determine the hydraulic pressure gradient of a flow along an eroding sand bed;

- the results of the experiments show no significant influence of the average density of the flow on the bed friction coefficient. However, the results of the erosion experiments show that the bed friction coefficient is influenced by the concentration gradient (and thus the concentration or density) of the sand-water mixture close to the top of the eroding sand bed (near-bed concentration). This shows that the bed friction coefficient is determined by the energy loss in a relative small zone above the top of the sand bed consisting of a relative highly concentrated sand-water mixture. It should be considered that this height will be dependent on the flow conditions (height and velocity of the flow). During the erosion experiments this height was between 0.01 and 0.03 m.

- the concentration of the sand-water mixture close to the top of the sand bed depends on the pick-up flux and sedimentation flux. Considering the above mentioned conclusion that the bed friction coefficient is influenced by the concentration of the sand-water mixture close to the top of the sand bed, this effect shows that the energy loss along an eroding sand bed is influenced by the pick-up flux and sedimentation flux;

Summarizing, the energy loss of a flow along an eroding sand bed is influenced by:

- the energy necessary to accelerate the grains, which are picked-up by the flow;
- the influence of the concentration of the grains, just above the top of the sand bed, introducing an increase of the effective viscosity of the sand-water mixture;
- energy losses as a result of collisions between the grains just above the top of the sand bed;
- turbulence of the flow, which is determined by the depth-averaged flow velocity and bed associated hydraulic diameter. An increase of the depth-averaged flow velocity and bed associated hydraulic diameter causes an increase of turbulence.

## 9.2. Recommendations

This section describes the recommendations regarding the experimental procedure, developed pick-up function, determination of the bed shear stress as a measure for the energy loss along an eroding sand bed and practical implications for the design or improvement of dikes and dredging sand with a trailing suction hopper dredger.

### Execution experiments

The analysis of the results of the experiments shows that:

- an experimental set-up should be developed in which the depth-averaged flow velocity can be kept constant during a significant period of the erosion process, in order to improve the determination of the pick-up flux and energy loss along an eroding sand bed;
- the visual observations demonstrate the presence of excess pore water pressures and the description of the erosion process assumes the presence of pore water under pressures during erosion. However, during the erosion experiments the pressure gauges did not show significant changes of the pore water pressures during the erosion process. Improvement of the experimental set-up is necessary to measure the pore water pressures during erosion.
- a more constant relative density over the height of the sand bed before erosion should be achieved by preparing the sand bed by compaction in a dry state and by hammering. In combination with measuring the density of the prepared sand bed at more locations in horizontal direction, this enables the preparation of a sand bed with a constant density in vertical as well as in horizontal direction and check of this density. It should be considered that when using this procedure thorough attention is necessary to saturate the sand bed.



### Improvement pick-up function

Investigate if improvement of the developed pick-up function is possible by a better fundamental description of the erosion process:

- adjust the description of the described failure mechanism during erosion by improving the description of the failure mechanism of sand as a result of the flow of water through the sand bed in the direction of the ejections;
- by including the effect of liquefaction on the excess pore water pressures and resulting decrease of the resistance to a normal stress on the sand bed;
- measuring the vertical velocity in the sweeps close to the sand bed in order to determine the normal stresses on the sand bed during erosion;
- executing erosion experiments with small pressure gauges in the sand bed, in order to determine the vertical stresses on the sand bed during erosion.

### Determination bed shear stress

Improvement of the developed empirical relation for the determination of the bed friction coefficient is possible by:

- developing an empirical relation by including the effect of the pick-up and sedimentation flux on the influence on the bed friction coefficient;
- developing a more theoretical approach for the energy loss along an eroding sand bed on a micro-scale by including the effect of the acceleration of the eroded grains, influence of the concentration of the grains on the effective viscosity, energy losses as a result of collisions between grains and turbulence.

### Practical implications

The recommendations regarding the practical implications of this experimental study are:

- in case of limited space for the improvement of a present dike or construction of a new dike, improve the safety against inundation of a polder by retarding the breaching process. The breaching process can be retarded by reducing the permeability of the sand (to be used) in the dike;
- typical jet flow velocities during dredging are around 30 to 60 m/s, which is higher than the maximum depth-averaged flow velocity (6 m/s) during the erosion experiments as described. Erosion experiments at higher depth-averaged flow velocities are necessary in order to check if the physical process during water jetting at flow velocities of 30 to 60 m/s is comparable to the erosion process as described;
- improve the production rate of a trailing suction hopper dredger by constructing extra rows of water jets on the drag head and improve the discharge through the suction pipe by water jets constructed on the visor of the drag head.

# A

# Operational conditions experiments

Table A.1 gives an overview of the operational conditions during all experiments which gave useful results. The variables are: grain size, depth-averaged flow velocity above the sand bed, density of the eroding inflow and relative density of the sand bed.

Begin of Table A.1 Operational conditions experiments

| Experiment | Grain size | Depth-averaged flow velocity | Density inflow | Relative density |
|---|---|---|---|---|
| - | $mm$ | $m/s$ | $kg/m^3$ | - |
| 1 | 0.125 | 2.4 - 2.5 | 1070 | 0.6 - 0.7 |
| 2 | 0.125 | 3.4 - 4.2 | 1090 | 0.4 - 0.8 |
| 3 | 0.125 | 5.1 - 5.7 | 1090 | 0.3 - 0.9 |
| 4 | 0.125 | 6.0 - 6.3 | 1040 | 0.5 - 1.0 |
| 6 | 0.125 | 2.7 - 2.9 | 1090 | 0.8 |
| 7 | 0.125 | 2.8 - 3.4 | 1080 | 0.2 - 0.4 |
| 8 | 0.125 | 3.7 - 4.5 | 1080 | 0.3 - 0.4 |
| 9 | 0.125 | 4.3 - 5.4 | 1050 | 0.4 - 0.5 |
| 10 | 0.125 | 4.6 - 5.9 | 1060 | 0.4 |
| 12 | 0.562 | 3.3 - 3.7 | 1130 | -0.03 - 0.41 |
| 13 | 0.562 | 3.2 - 4.5 | 1070 | -0.02 - 0.22 |
| 14 | 0.562 | 3.1 - 3.9 | 1100 | 0.04 - 0.16 |
| 25 | 0.262 | 3.0 - 3.4 | 1060 | 0.1 - 0.3 |
| 26 | 0.262 | 2.4 - 2.6 | 1070 | 0.2 |
| 27 | 0.262 | 2.9 - 3.0 | 1070 | 0.2 - 0.3 |

Continued on next page

Table A.1 continued from previous page

| Experiment | Grain size | Depth-averaged flow velocity | Density inflow | Relative density |
|---|---|---|---|---|
| - | $mm$ | $m/s$ | $kg/m^3$ | - |
| 28 | 0.262 | 3.5 - 4.1 | 1060 | 0.0 - 0.2 |
| 29 | 0.262 | 4.3 - 4.5 | 1090 | 0.0 - 0.2 |
| 30 | 0.262 | 2.5 - 2.6 | 1090 | 0.8 - 1.1 |
| 31 | 0.262 | 3.3 - 3.5 | 1100 | 0.6 - 0.8 |
| 32 | 0.262 | 3.9 - 4.5 | 1120 | 0.4 - 0.7 |
| 33 | 0.262 | 5.7 - 6.1 | 1110 | 0.7 - 0.9 |
| 34 | 0.262 | 2.4 - 2.5 | 1070 | 0.4 - 0.5 |
| 35 | 0.262 | 2.7 - 3.1 | 1100 | 0.5 |
| 36 | 0.262 | 3.5 - 4.3 | 1100 | 0.4 - 0.7 |
| 37 | 0.262 | 3.0 - 4.8 | 1100 | 0.4 - 0.6 |
| 38 | 0.262 | 2.8 - 3.7 | 1240 | 0.4 - 0.9 |
| 39 | 0.262 | 4.1 - 4.7 | 1260 | 0.4 - 0.5 |
| 40 | 0.262 | 4.4 - 5.1 | 1220 | 0.3 - 0.5 |
| 41 | 0.262 | 3.5 - 4.1 | 1445 | 0.4 - 0.5 |
| 42 | 0.262 | 4.6 - 5.4 | 1450 | 0.3 - 0.6 |
| 43 | 0.125 | 2.0 - 2.3 | 1070 | 0.3 - 0.4 |
| 44 | 0.125 | 2.2 - 2.5 | 1040 | 0.3 - 0.6 |
| 45 | 0.125 | 2.4 - 3.0 | 1090 | 0.1 - 0.2 |
| 46 | 0.125 | 4.4 - 5.1 | 1120 | 0.1 - 0.2 |
| 47 | 0.125 | 2.0 - 2.2 | 1070 | 0.3 - 0.4 |
| 48 | 0.125 | 2.5 - 3.0 | 1060 | 0.2 - 0.4 |
| 49 | 0.125 | 3.5 - 4.1 | 1080 | 0.3 - 0.6 |
| 50 | 0.125 | 4.1 - 4.9 | 1100 | 0.2 - 0.4 |
| 51 | 0.125 | 2.1 - 2.4 | 1080 | 0.7 - 0.8 |
| 52 | 0.125 | 3.1 - 3.5 | 1070 | 0.7 - 0.9 |
| 53 | 0.125 | 3.9 - 4.5 | 1070 | 0.6 - 0.8 |
| 54 | 0.125 | 4.8 - 5.5 | 1110 | 0.7 - 0.8 |
| 55 | 0.125 | 2.9 - 3.1 | 1200 | 0.5 |
| 56 | 0.125 | 3.1 - 4.0 | 1230 | 0.2 - 0.4 |
| 57 | 0.125 | 4.1 - 5.0 | 1190 | 0.3 - 0.4 |
| 58 | 0.125 | 2.8 - 3.3 | 1330 | 0.3 - 0.5 |
| 59 | 0.125 | 3.3 - 3.9 | 1370 | 0.3 - 0.5 |
| 60 | 0.125 | 3.1 - 4.6 | 1330 | 0.4 |
| 61 | 0.562 | 1.6 - 3.4 | 1090 | -0.2 - 0.1 |
| 62 | 0.562 | 3.4 - 3.8 | 1110 | -0.2 - -0.1 |
| 63 | 0.562 | 4.1 - 5.1 | 1160 | 0.2 - 0.6 |
| 64 | 0.562 | 3.0 - 3.4 | 1080 | 0.3 - 0.5 |
| 65 | 0.562 | 3.4 - 4.2 | 1070 | 0.1 - 0.4 |

Continued on next page

Table A.1 continued from previous page

| Experiment | Grain size | Depth-averaged flow velocity | Density inflow | Relative density |
|---|---|---|---|---|
| - | $mm$ | $m/s$ | $kg/m^3$ | - |
| 66 | 0.562 | 4.2 - 4.5 | 1130 | 0.1 - 0.3 |
| 67 | 0.562 | 3.8 - 4.0 | 1120 | 0.7 - 1.0 |
| 68 | 0.562 | 4.2 - 4.6 | 1070 | 0.7 - 1.0 |
| 69 | 0.562 | 4.7 - 5.2 | 1090 | 0.6 - 0.9 |
| 70 | 0.562 | 3.4 - 3.8 | 1230 | 0.4 |
| 71 | 0.562 | 3.9 - 4.5 | 1230 | 0.3 - 0.5 |
| 72 | 0.562 | 4.4 - 4.8 | 1220 | 0.4 - 0.5 |
| 74 | 0.562 | 4.0 - 4.4 | 1370 | 0.3 - 0.5 |
| 75 | 0.562 | 5.1 - 5.4 | 1390 | 0.2 - 0.5 |
| 76 | 0.051 | 1.4 - 1.8 | 1060 | -0.2 - -0.1 |
| 77 | 0.051 | 1.3 - 1.4 | 1050 | -0.2 |
| 78 | 0.051 | 1.9 - 2.5 | 1050 | -0.3 - -0.1 |
| 79 | 0.051 | 1.5 - 1.8 | 1100 | -0.1 - 0.7 |
| 80 | 0.051 | 1.8 - 2.0 | 1060 | -0.2 - 0.5 |
| 81 | 0.051 | 2.5 - 2.8 | 1060 | -0.1 - 0.6 |
| 82 | 0.562 | 4.3 - 4.7 | 1120 | 0.3 - 0.5 |
| 83 | 0.562 | 4.4 - 4.9 | 1340 | 0.2 - 0.6 |
| 85 | 0.562 | 4.0 - 4.9 | 1380 | 0.4 - 0.7 |
| 87 | 0.051 | 1.3 - 1.5 | 1050 | -0.2 - -0.1 |
| 88 | 0.051 | 3.8 - 4.1 | 1060 | 0.1 - 0.7 |
| 89 | 0.051 | 4.1 - 5.2 | 1120 | 0.0 - 0.6 |

Table A.1: Operational Conditions Experiments

# B

# Results experiments pick-up flux versus flow velocity

The data of the experiments giving reliable results for the pick-up flux and depth-averaged flow velocity are presented per sand type in Tables B.1, B.2, B.3 and B.4. The following data are presented:

- Exp. no.: number of experiment;
- Relative density: average density of the sand bed between two conductivity probes;
- Flow velocity: depth-averaged flow velocity;
- Density flow: average density of the eroding flow during the whole erosion experiment at the location of the conductivity probes based on the average density of the eroding inflow of water and effect of the average pick-up flux on the density of the eroding flow;
- Erosion velocity: rate with which the erosion front moves down between two consecutive conductivity probes;
- Pick-up flux: calculated pick-up flux between two erosion moments;
- Flow height: height of the flow above the top of the eroding bed.

Begin of Table B.1 Results experiments on Zilverzand

| Exp. no. - | Relative density - | Flow velocity $m/s$ | Density flow $kg/m^3$ | Erosion velocity $m/s$ | Pick-up flux $kg/m^2 \cdot s$ | Flow height $m$ |
|---|---|---|---|---|---|---|
| 25 | 0.20 | 3.16 | 1088 | 0.0079 | 17.30 | 0.249 |
| | 0.28 | 3.29 | | 0.0119 | 21.21 | 0.229 |
| | 0.32 | 3.36 | | 0.0118 | 21.20 | 0.219 |
| | 0.34 | 3.37 | | 0.0101 | 19.66 | 0.209 |
| | 0.32 | 3.30 | | 0.0116 | 21.08 | 0.199 |
| | 0.14 | 2.98 | | 0.0090 | 18.15 | 0.179 |
| 26 | 0.18 | 2.36 | 1107 | 0.0047 | 14.34 | 0.219 |
| | 0.21 | 2.40 | | 0.0054 | 15.07 | 0.209 |
| | 0.21 | 2.43 | | 0.0128 | 22.73 | 0.199 |
| | -0.20 | 2.63 | | 0.0098 | 18.57 | 0.179 |
| 27 | 0.18 | 2.88 | 1095 | 0.0256 | 33.29 | 0.229 |
| | 0.27 | 2.92 | | 0.0294 | 37.41 | 0.219 |
| | 0.30 | 3.00 | | 0.0250 | 33.52 | 0.209 |
| | 0.21 | 2.92 | | 0.0125 | 21.54 | 0.199 |
| 28 | 0.02 | 3.93 | 1180 | 0.0231 | 27.59 | 0.266 |
| | -0.01 | 3.94 | | 0.0610 | 56.04 | 0.259 |
| | 0.02 | 4.07 | | 0.0781 | 69.65 | 0.249 |
| | 0.10 | 4.00 | | 0.0130 | 20.15 | 0.229 |
| | 0.13 | 3.75 | | 0.0439 | 44.66 | 0.219 |
| | 0.17 | 3.69 | | 0.0379 | 40.34 | 0.209 |
| | 0.21 | 3.53 | | 0.0568 | 56.20 | 0.199 |
| 29 | 0.03 | 4.26 | 1186 | 0.0575 | 59.08 | 0.249 |
| | 0.10 | 4.46 | | 0.0532 | 56.36 | 0.229 |
| | 0.14 | 4.46 | | 0.0495 | 53.67 | 0.219 |
| | 0.20 | 4.50 | | 0.0388 | 44.83 | 0.209 |
| | 0.23 | 4.49 | | 0.0365 | 43.17 | 0.199 |
| 30 | 0.79 | 2.49 | 1104 | 0.0016 | 11.73 | 0.179 |
| | 0.78 | 2.57 | | 0.0021 | 12.35 | 0.169 |
| | 0.77 | 2.50 | | 0.0034 | 13.84 | 0.159 |
| | 1.14 | 2.53 | | 0.0038 | 14.57 | 0.149 |
| 31 | 0.62 | 3.27 | 1115 | 0.0093 | 19.94 | 0.229 |
| | 0.65 | 3.36 | | 0.0056 | 16.11 | 0.219 |
| | 0.69 | 3.34 | | 0.0063 | 16.86 | 0.209 |
| | 0.68 | 3.39 | | 0.0070 | 17.61 | 0.199 |
| | 0.75 | 3.52 | | 0.0094 | 20.45 | 0.179 |
| | 0.70 | 3.33 | | 0.0066 | 17.24 | 0.169 |
| 32 | 0.65 | 4.54 | 1189 | 0.0154 | 24.39 | 0.229 |
| | 0.68 | 4.52 | | 0.0200 | 28.80 | 0.219 |

Continued on next page

Table B.1 continued from previous page

| Exp. no. - | Relative density - | Flow velocity $m/s$ | Density flow $kg/m^3$ | Erosion velocity $m/s$ | Pick-up flux $kg/m^2 \cdot s$ | Flow height $m$ |
|---|---|---|---|---|---|---|
| | 0.70 | 4.47 | | 0.0217 | 30.54 | 0.209 |
| | 0.71 | 4.34 | | 0.0221 | 30.93 | 0.199 |
| | 0.70 | 4.43 | | 0.0347 | 42.62 | 0.179 |
| | 0.67 | 4.25 | | 0.0181 | 26.96 | 0.169 |
| | 0.59 | 3.89 | | 0.0397 | 46.18 | 0.159 |
| | 0.43 | 4.03 | | 0.0595 | 61.53 | 0.149 |
| 33 | 0.67 | 5.74 | 1201 | 0.0263 | 35.04 | 0.229 |
| | 0.68 | 5.73 | | 0.0568 | 64.00 | 0.219 |
| | 0.69 | 5.80 | | 0.1316 | 134.79 | 0.209 |
| | 0.69 | 5.91 | | 0.0575 | 64.65 | 0.199 |
| | 0.70 | 6.06 | | 0.1087 | 113.60 | 0.179 |
| | 0.68 | 6.03 | | 0.0490 | 56.59 | 0.169 |
| | 0.88 | 5.65 | | 0.0379 | 47.99 | 0.159 |
| 34 | 0.53 | 2.50 | 1067 | 0.0022 | 11.85 | 0.179 |
| | 0.54 | 2.45 | | 0.0045 | 14.44 | 0.169 |
| | 0.51 | 2.49 | | 0.0035 | 13.32 | 0.159 |
| | 0.34 | 2.44 | | 0.0044 | 14.14 | 0.149 |
| 35 | 0.48 | 3.12 | 1104 | 0.0052 | 14.79 | 0.229 |
| | 0.48 | 3.06 | | 0.0076 | 16.92 | 0.219 |
| | 0.48 | 3.04 | | 0.0192 | 27.40 | 0.209 |
| | 0.47 | 3.10 | | 0.0154 | 23.93 | 0.199 |
| | 0.49 | 2.85 | | 0.0152 | 23.77 | 0.179 |
| | 0.50 | 2.66 | | 0.0127 | 21.57 | 0.169 |
| | 0.50 | 2.76 | | 0.0182 | 26.54 | 0.159 |
| 36 | 0.45 | 4.34 | 1166 | 0.0200 | 27.68 | 0.229 |
| | 0.42 | 4.23 | | 0.0172 | 25.14 | 0.219 |
| | 0.42 | 4.04 | | 0.0238 | 30.82 | 0.209 |
| | 0.43 | 4.28 | | 0.1087 | 104.87 | 0.199 |
| | 0.36 | 4.14 | | 0.0169 | 24.59 | 0.179 |
| | 0.49 | 3.76 | | 0.0510 | 55.46 | 0.169 |
| | 0.74 | 3.51 | | 0.0455 | 53.54 | 0.159 |
| 37 | 0.51 | 4.49 | 1189 | 0.0198 | 28.71 | 0.249 |
| | 0.53 | 4.73 | | 0.0153 | 24.56 | 0.229 |
| | 0.55 | 4.63 | | 0.0216 | 30.64 | 0.219 |
| | 0.56 | 4.62 | | 0.0321 | 40.52 | 0.209 |
| | 0.54 | 4.61 | | 0.0327 | 40.94 | 0.199 |
| | 0.44 | 4.78 | | 0.0400 | 46.81 | 0.179 |
| | 0.41 | 4.51 | | 0.0279 | 35.48 | 0.169 |

Continued on next page

Table B.1 continued from previous page

| Exp. no. - | Relative density - | Flow velocity $m/s$ | Density flow $kg/m^3$ | Erosion velocity $m/s$ | Pick-up flux $kg/m^2 \cdot s$ | Flow height $m$ |
|---|---|---|---|---|---|---|
| | 0.57 | 3.03 | | 0.0331 | 41.62 | 0.149 |
| 38 | 0.48 | 3.14 | 1262 | 0.0051 | 14.75 | 0.219 |
| | 0.44 | 3.14 | | 0.0077 | 16.99 | 0.209 |
| | 0.43 | 2.95 | | 0.0123 | 21.04 | 0.199 |
| | 0.50 | 3.67 | | 0.0104 | 19.57 | 0.179 |
| | 0.48 | 3.53 | | 0.0149 | 23.50 | 0.169 |
| | 0.61 | 3.42 | | 0.0112 | 20.62 | 0.159 |
| | 0.86 | 2.83 | | 0.0065 | 16.71 | 0.149 |
| 39 | 0.51 | 4.23 | 1309 | 0.0377 | 41.08 | 0.229 |
| | 0.42 | 4.51 | | 0.0488 | 49.01 | 0.209 |
| | 0.39 | 4.54 | | 0.0169 | 23.48 | 0.199 |
| | 0.41 | 4.70 | | 0.0294 | 33.45 | 0.179 |
| | 0.37 | 4.12 | | 0.0400 | 41.52 | 0.169 |
| | 0.52 | 4.11 | | 0.0294 | 34.30 | 0.159 |
| 40 | 0.50 | 4.37 | 1290 | 0.0147 | 21.42 | 0.266 |
| | 0.51 | 4.64 | | 0.0180 | 24.08 | 0.229 |
| | 0.48 | 4.68 | | 0.0391 | 40.67 | 0.219 |
| | 0.45 | 4.64 | | 0.0355 | 37.48 | 0.209 |
| | 0.42 | 4.68 | | 0.0314 | 34.09 | 0.199 |
| | 0.43 | 4.47 | | 0.1471 | 124.12 | 0.179 |
| | 0.45 | 4.77 | | 0.1429 | 121.76 | 0.169 |
| | 0.43 | 5.09 | | 0.0735 | 67.04 | 0.159 |
| | 0.29 | 5.03 | | 0.0450 | 43.10 | 0.149 |
| 41 | 0.45 | 4.05 | 1466 | 0.0121 | 18.66 | 0.219 |
| | 0.42 | 3.67 | | 0.0114 | 18.00 | 0.209 |
| | 0.41 | 3.51 | | 0.0299 | 31.54 | 0.199 |
| 42 | 0.60 | 4.61 | 1447 | 0.0147 | 21.22 | 0.249 |
| | 0.51 | 4.73 | | 0.0282 | 30.99 | 0.229 |
| | 0.43 | 4.97 | | 0.0227 | 26.41 | 0.219 |
| | 0.36 | 4.74 | | 0.0187 | 23.13 | 0.209 |
| | 0.33 | 4.45 | | 0.0270 | 28.89 | 0.199 |
| | 0.38 | 4.86 | | 0.0323 | 32.97 | 0.179 |
| | 0.34 | 5.38 | | 0.0183 | 22.77 | 0.169 |

Table B.1: Results experiments on Zilverzand

Begin of Table B.2 Results experiments on Geba

| Exp. no. - | Relative density - | Flow velocity $m/s$ | Density flow $kg/m^3$ | Erosion velocity $m/s$ | Pick-up flux $kg/m^2 \cdot s$ | Flow height $m$ |
|---|---|---|---|---|---|---|
| 43 | 0.26 | 2.01 | 1083 | 0.0038 | 6.01 | 0.249 |
| | 0.27 | 2.22 | | 0.0072 | 9.09 | 0.229 |
| | 0.30 | 2.29 | | 0.0058 | 7.89 | 0.219 |
| | 0.34 | 2.26 | | 0.0053 | 7.52 | 0.209 |
| | 0.37 | 2.29 | | 0.0056 | 7.80 | 0.199 |
| | 0.42 | 2.12 | | 0.0039 | 6.34 | 0.179 |
| 44 | 0.27 | 2.51 | 1145 | 0.0161 | 14.49 | 0.229 |
| | 0.41 | 2.47 | | 0.0182 | 16.89 | 0.219 |
| | 0.52 | 2.42 | | 0.0204 | 19.43 | 0.209 |
| | 0.55 | 2.39 | | 0.0244 | 23.04 | 0.199 |
| | 0.40 | 2.20 | | 0.0110 | 11.21 | 0.179 |
| 45 | 0.14 | 2.46 | 1218 | 0.0255 | 21.62 | 0.229 |
| | 0.15 | 2.40 | | 0.0357 | 29.38 | 0.219 |
| | 0.17 | 2.72 | | 0.0472 | 38.29 | 0.209 |
| | 0.19 | 3.03 | | 0.0397 | 32.98 | 0.199 |
| 46 | 0.14 | 5.11 | 1170 | 0.0147 | 14.07 | 0.229 |
| | 0.17 | 5.08 | | 0.0131 | 13.00 | 0.219 |
| | 0.18 | 4.95 | | 0.0463 | 39.32 | 0.209 |
| | 0.19 | 5.08 | | 0.2174 | 174.92 | 0.199 |
| | 0.18 | 4.95 | | 0.0216 | 19.73 | 0.179 |
| | 0.16 | 4.67 | | 0.0273 | 24.13 | 0.169 |
| | 0.13 | 4.42 | | 0.0224 | 20.04 | 0.159 |
| 47 | 0.32 | 1.97 | 1088 | 0.0035 | 6.16 | 0.249 |
| | 0.41 | 2.01 | | 0.0088 | 11.47 | 0.229 |
| | 0.43 | 2.09 | | 0.0045 | 7.29 | 0.219 |
| | 0.42 | 2.18 | | 0.0032 | 5.98 | 0.209 |
| | 0.40 | 2.24 | | 0.0051 | 7.83 | 0.199 |
| | 0.31 | 2.19 | | 0.0035 | 6.17 | 0.179 |
| | 0.27 | 2.04 | | 0.0035 | 6.07 | 0.169 |
| 48 | 0.40 | 2.94 | 1123 | 0.0082 | 10.39 | 0.229 |
| | 0.43 | 2.95 | | 0.0101 | 12.26 | 0.219 |
| | 0.45 | 2.93 | | 0.0177 | 19.44 | 0.209 |
| | 0.43 | 2.87 | | 0.0110 | 13.08 | 0.199 |
| | 0.33 | 2.72 | | 0.0092 | 11.06 | 0.179 |
| | 0.27 | 2.49 | | 0.0129 | 14.12 | 0.169 |
| | 0.22 | 2.55 | | 0.0104 | 11.71 | 0.159 |
| | 0.20 | 2.64 | | 0.0244 | 23.55 | 0.149 |
| 49 | 0.36 | 3.72 | 1153 | 0.0174 | 18.87 | 0.259 |

Continued on next page

Table B.2 continued from previous page

| Exp. no. - | Relative density - | Flow velocity $m/s$ | Density flow $kg/m^3$ | Erosion velocity $m/s$ | Pick-up flux $kg/m^2 \cdot s$ | Flow height $m$ |
|---|---|---|---|---|---|---|
| | 0.34 | 3.77 | | 0.0177 | 19.08 | 0.249 |
| | 0.46 | 4.08 | | 0.0227 | 24.62 | 0.219 |
| | 0.51 | 4.13 | | 0.0139 | 16.41 | 0.209 |
| | 0.55 | 4.03 | | 0.0136 | 16.27 | 0.199 |
| | 0.51 | 4.07 | | 0.0253 | 27.50 | 0.179 |
| | 0.45 | 3.87 | | 0.0155 | 17.66 | 0.169 |
| | 0.38 | 3.59 | | 0.0229 | 24.15 | 0.159 |
| | 0.33 | 3.47 | | 0.0198 | 20.94 | 0.149 |
| 50 | 0.42 | 4.49 | 1178 | 0.0158 | 17.07 | 0.266 |
| | 0.32 | 4.76 | | 0.0148 | 15.58 | 0.249 |
| | 0.37 | 4.80 | | 0.0152 | 16.28 | 0.229 |
| | 0.38 | 4.78 | | 0.0275 | 27.12 | 0.219 |
| | 0.37 | 4.84 | | 0.0485 | 45.44 | 0.209 |
| | 0.33 | 4.88 | | 0.0233 | 22.98 | 0.199 |
| | 0.27 | 4.57 | | 0.0521 | 46.70 | 0.179 |
| | 0.25 | 4.47 | | 0.0236 | 22.57 | 0.169 |
| | 0.23 | 4.10 | | 0.0233 | 22.16 | 0.159 |
| 51 | 0.70 | 2.07 | 1096 | 0.0020 | 5.06 | 0.229 |
| | 0.74 | 2.14 | | 0.0020 | 5.08 | 0.219 |
| | 0.76 | 2.17 | | 0.0022 | 5.42 | 0.209 |
| | 0.77 | 2.21 | | 0.0023 | 5.43 | 0.199 |
| | 0.76 | 2.32 | | 0.0035 | 6.94 | 0.179 |
| | 0.75 | 2.38 | | 0.0050 | 8.63 | 0.169 |
| | 0.76 | 2.40 | | 0.0044 | 7.92 | 0.159 |
| | 0.77 | 2.38 | | 0.0037 | 7.14 | 0.149 |
| 52 | 0.73 | 3.13 | 1104 | 0.0064 | 10.05 | 0.229 |
| | 0.76 | 3.24 | | 0.0076 | 11.55 | 0.219 |
| | 0.78 | 3.30 | | 0.0081 | 12.2 | 0.209 |
| | 0.79 | 3.32 | | 0.0071 | 11.08 | 0.199 |
| | 0.79 | 3.44 | | 0.0093 | 13.55 | 0.179 |
| | 0.80 | 3.45 | | 0.0119 | 16.7 | 0.169 |
| | 0.84 | 3.35 | | 0.0099 | 14.55 | 0.159 |
| | 0.94 | 3.32 | | 0.0082 | 12.77 | 0.149 |
| 53 | 0.62 | 3.85 | 1125 | 0.0091 | 12.15 | 0.259 |
| | 0.62 | 3.96 | | 0.0095 | 12.54 | 0.249 |
| | 0.68 | 4.13 | | 0.0106 | 13.94 | 0.229 |
| | 0.70 | 4.17 | | 0.0194 | 23.33 | 0.219 |
| | 0.71 | 4.26 | | 0.0117 | 15.20 | 0.209 |

Continued on next page

Table B.2 continued from previous page

| Exp. no. - | Relative density - | Flow velocity $m/s$ | Density flow $kg/m^3$ | Erosion velocity $m/s$ | Pick-up flux $kg/m^2 \cdot s$ | Flow height $m$ |
|---|---|---|---|---|---|---|
| | 0.72 | 4.29 | | 0.0104 | 13.84 | 0.199 |
| | 0.75 | 4.45 | | 0.0153 | 19.31 | 0.179 |
| | 0.74 | 4.41 | | 0.0181 | 22.28 | 0.169 |
| | 0.67 | 4.13 | | 0.0151 | 18.62 | 0.159 |
| 54 | 0.75 | 4.75 | 1162 | 0.0123 | 15.81 | 0.266 |
| | 0.70 | 4.86 | | 0.009 | 12.23 | 0.259 |
| | 0.69 | 4.88 | | 0.0107 | 13.9 | 0.249 |
| | 0.75 | 5.20 | | 0.0313 | 36.02 | 0.229 |
| | 0.78 | 5.35 | | 0.0186 | 22.75 | 0.219 |
| | 0.80 | 5.46 | | 0.0126 | 16.42 | 0.209 |
| | 0.80 | 5.37 | | 0.0149 | 18.87 | 0.199 |
| | 0.79 | 5.42 | | 0.0338 | 39.21 | 0.179 |
| | 0.79 | 5.24 | | 0.0203 | 24.67 | 0.169 |
| 55 | 0.52 | 3.08 | 1239 | 0.0109 | 11.78 | 0.219 |
| | 0.54 | 3.12 | | 0.0061 | 7.77 | 0.209 |
| | 0.53 | 3.10 | | 0.0140 | 14.45 | 0.199 |
| | 0.45 | 2.85 | | 0.0075 | 8.76 | 0.169 |
| 56 | 0.34 | 3.72 | 1287 | 0.0154 | 15.33 | 0.249 |
| | 0.37 | 3.87 | | 0.0833 | 71.34 | 0.229 |
| | 0.36 | 3.99 | | 0.0207 | 19.72 | 0.219 |
| | 0.33 | 3.88 | | 0.0189 | 18.13 | 0.209 |
| | 0.30 | 3.80 | | 0.0120 | 12.38 | 0.199 |
| | 0.25 | 3.79 | | 0.0161 | 15.40 | 0.179 |
| | 0.26 | 3.67 | | 0.0455 | 38.36 | 0.169 |
| | 0.26 | 3.55 | | 0.0180 | 16.88 | 0.159 |
| | 0.22 | 3.12 | | 0.0338 | 28.84 | 0.149 |
| 57 | 0.39 | 4.81 | 1262 | 0.0313 | 27.09 | 0.229 |
| | 0.41 | 4.89 | | 0.0431 | 36.59 | 0.219 |
| | 0.41 | 4.99 | | 0.0357 | 30.76 | 0.209 |
| | 0.39 | 4.99 | | 0.0181 | 16.82 | 0.199 |
| | 0.31 | 4.48 | | 0.0262 | 22.36 | 0.179 |
| | 0.27 | 4.10 | | 0.0360 | 29.12 | 0.169 |
| 58 | 0.37 | 2.81 | 1361 | 0.0050 | 6.52 | 0.259 |
| | 0.37 | 2.97 | | 0.0114 | 11.38 | 0.249 |
| | 0.47 | 2.99 | | 0.0057 | 7.30 | 0.229 |
| | 0.48 | 3.27 | | 0.0103 | 11.02 | 0.209 |
| | 0.33 | 3.22 | | 0.0096 | 9.87 | 0.169 |
| 59 | 0.34 | 3.74 | 1419 | 0.0179 | 15.27 | 0.259 |

Continued on next page

Table B.2 continued from previous page

| Exp. no. - | Relative density - | Flow velocity $m/s$ | Density flow $kg/m^3$ | Erosion velocity $m/s$ | Pick-up flux $kg/m^2 \cdot s$ | Flow height $m$ |
|---|---|---|---|---|---|---|
| | 0.34 | 3.60 | | 0.0095 | 9.31 | 0.249 |
| | 0.43 | 3.86 | | 0.0159 | 14.34 | 0.229 |
| | 0.46 | 3.81 | | 0.0159 | 14.52 | 0.219 |
| | 0.46 | 3.68 | | 0.0179 | 16.04 | 0.209 |
| | 0.44 | 3.77 | | 0.0357 | 29.25 | 0.199 |
| | 0.36 | 3.88 | | 0.0220 | 18.31 | 0.179 |
| | 0.32 | 3.93 | | 0.0177 | 14.97 | 0.169 |
| | 0.26 | 3.30 | | 0.0667 | 47.97 | 0.149 |
| 60 | 0.42 | 4.57 | 1377 | 0.0184 | 16.12 | 0.259 |
| | 0.41 | 4.61 | | 0.0129 | 11.97 | 0.249 |
| | 0.41 | 4.57 | | 0.0272 | 22.49 | 0.229 |
| | 0.41 | 4.50 | | 0.0202 | 17.32 | 0.219 |
| | 0.41 | 4.29 | | 0.0244 | 20.42 | 0.209 |
| | 0.41 | 4.33 | | 0.0250 | 20.85 | 0.199 |
| | 0.41 | 3.28 | | 0.0260 | 21.59 | 0.179 |
| | 0.41 | 3.13 | | 0.0345 | 27.75 | 0.169 |

Table B.2: Results experiments on Geba

Begin of Table B.3 Results experiments on Dorsilit

| Exp. no. - | Relative density - | Flow velocity $m/s$ | Density flow $kg/m^3$ | Erosion velocity $m/s$ | Pick-up flux $kg/m^2 \cdot s$ | Flow height $m$ |
|---|---|---|---|---|---|---|
| 61 | 0.09 | 3.37 | 1115 | 0.0015 | 23.14 | 0.229 |
| | -0.06 | 3.33 | | 0.0096 | 28.76 | 0.219 |
| | -0.11 | 3.29 | | 0.0135 | 31.28 | 0.209 |
| | -0.09 | 3.44 | | 0.0135 | 31.36 | 0.199 |
| | 0.00 | 3.39 | | 0.0074 | 27.31 | 0.179 |
| | -0.02 | 2.9 | | 0.0154 | 32.98 | 0.169 |
| | -0.18 | 1.57 | | 0.0196 | 35.03 | 0.149 |
| 62 | -0.08 | 3.37 | 1175 | 0.0227 | 35.91 | 0.249 |
| | -0.19 | 3.78 | | 0.0362 | 42.99 | 0.229 |
| 63 | 0.40 | 4.88 | 1230 | 0.0225 | 40.41 | 0.266 |
| | 0.44 | 4.83 | | 0.0307 | 47.22 | 0.259 |
| | 0.54 | 5.02 | | 0.0260 | 44.25 | 0.249 |
| | 0.64 | 5.13 | | 0.0245 | 43.71 | 0.229 |
| | 0.58 | 4.95 | | 0.0131 | 33.64 | 0.219 |
| | 0.47 | 5.07 | | 0.0290 | 46.14 | 0.209 |
| | 0.35 | 4.90 | | 0.0488 | 60.50 | 0.199 |
| | 0.19 | 4.11 | | 0.0169 | 34.93 | 0.179 |
| 64 | 0.30 | 3.41 | 1113 | 0.0078 | 27.75 | 0.209 |
| | 0.34 | 3.29 | | 0.0117 | 30.83 | 0.199 |
| | 0.40 | 3.30 | | 0.0077 | 27.96 | 0.179 |
| | 0.42 | 3.23 | | 0.0134 | 32.45 | 0.169 |
| | 0.45 | 3.12 | | 0.0138 | 32.84 | 0.159 |
| | 0.48 | 2.97 | | 0.0107 | 30.49 | 0.149 |
| 65 | 0.11 | 3.89 | 1142 | 0.0347 | 47.36 | 0.266 |
| | 0.09 | 3.88 | | 0.0183 | 35.40 | 0.259 |
| | 0.08 | 3.98 | | 0.0148 | 32.88 | 0.249 |
| | 0.14 | 4.08 | | 0.0336 | 46.83 | 0.229 |
| | 0.19 | 4.13 | | 0.0171 | 35.08 | 0.219 |
| | 0.25 | 4.16 | | 0.0342 | 48.40 | 0.209 |
| | 0.30 | 4.11 | | 0.0164 | 35.07 | 0.199 |
| | 0.36 | 4.20 | | 0.0439 | 57.13 | 0.179 |
| | 0.36 | 3.97 | | 0.0149 | 34.13 | 0.169 |
| | 0.35 | 3.53 | | 0.0167 | 35.52 | 0.159 |
| | 0.32 | 3.44 | | 0.0208 | 38.59 | 0.149 |
| 66 | 0.13 | 4.47 | 1214 | 0.0592 | 63.54 | 0.229 |
| | 0.17 | 4.47 | | 0.0885 | 84.88 | 0.219 |
| | 0.20 | 4.53 | | 0.0260 | 40.93 | 0.209 |
| | 0.23 | 4.17 | | 0.0541 | 61.52 | 0.199 |

Continued on next page

Table B.3 continued from previous page

| Exp. no. - | Relative density - | Flow velocity $m/s$ | Density flow $kg/m^3$ | Erosion velocity $m/s$ | Pick-up flux $kg/m^2 \cdot s$ | Flow height $m$ |
|---|---|---|---|---|---|---|
| | 0.27 | 4.45 | | 0.0388 | 50.76 | 0.179 |
| | 0.27 | 4.40 | | 0.0877 | 86.82 | 0.169 |
| | 0.26 | 4.42 | | 0.0926 | 90.17 | 0.159 |
| | 0.24 | 4.59 | | 0.3226 | 257.41 | 0.149 |
| 67 | 0.65 | 3.95 | 1144 | 0.0084 | 30.12 | 0.219 |
| | 0.73 | 3.89 | | 0.0189 | 40.05 | 0.209 |
| | 0.82 | 3.81 | | 0.0161 | 37.94 | 0.199 |
| | 0.97 | 3.89 | | 0.0165 | 39.04 | 0.179 |
| | 0.99 | 3.90 | | 0.0134 | 36.01 | 0.169 |
| | 0.96 | 3.94 | | 0.0146 | 37.07 | 0.159 |
| | 0.89 | 3.80 | | 0.0128 | 35.04 | 0.149 |
| 68 | 0.65 | 4.15 | 1121 | 0.0198 | 38.70 | 0.229 |
| | 0.72 | 4.28 | | 0.0127 | 32.78 | 0.219 |
| | 0.80 | 4.38 | | 0.0203 | 40.03 | 0.209 |
| | 0.88 | 4.37 | | 0.0159 | 36.40 | 0.199 |
| | 0.99 | 4.47 | | 0.0360 | 56.25 | 0.179 |
| | 1.01 | 4.56 | | 0.0275 | 48.19 | 0.169 |
| | 0.99 | 4.44 | | 0.0225 | 43.30 | 0.159 |
| | 0.95 | 4.46 | | 0.0193 | 39.97 | 0.149 |
| 69 | 0.73 | 4.95 | 1176 | 0.0240 | 41.26 | 0.266 |
| | 0.66 | 4.72 | | 0.0164 | 34.67 | 0.259 |
| | 0.61 | 4.81 | | 0.0481 | 59.31 | 0.249 |
| | 0.63 | 4.97 | | 0.0222 | 39.10 | 0.229 |
| | 0.69 | 4.85 | | 0.0286 | 44.61 | 0.219 |
| | 0.75 | 4.96 | | 0.0296 | 46.02 | 0.209 |
| | 0.82 | 5.03 | | 0.0361 | 52.15 | 0.199 |
| | 0.91 | 5.20 | | 0.0595 | 73.61 | 0.179 |
| | 0.92 | 5.11 | | 0.0258 | 44.09 | 0.169 |
| | 0.90 | 5.15 | | 0.0385 | 55.01 | 0.159 |
| | 0.86 | 5.23 | | 0.0610 | 73.95 | 0.149 |
| 70 | 0.44 | 3.75 | 1242 | 0.0041 | 25.36 | 0.179 |
| | 0.44 | 3.38 | | 0.0052 | 26.17 | 0.169 |
| | 0.40 | 3.41 | | 0.0051 | 26.04 | 0.149 |
| 71 | 0.26 | 4.14 | 1270 | 0.0134 | 30.73 | 0.229 |
| | 0.33 | 4.00 | | 0.0134 | 31.00 | 0.219 |
| | 0.39 | 4.08 | | 0.0132 | 31.01 | 0.209 |
| | 0.43 | 3.90 | | 0.0253 | 40.01 | 0.199 |
| | 0.45 | 4.47 | | 0.0385 | 49.93 | 0.179 |

Continued on next page

Table B.3 continued from previous page

| Exp. no. - | Relative density - | Flow velocity $m/s$ | Density flow $kg/m^3$ | Erosion velocity $m/s$ | Pick-up flux $kg/m^2 \cdot s$ | Flow height $m$ |
|---|---|---|---|---|---|---|
| | 0.44 | 4.12 | | 0.0403 | 51.23 | 0.169 |
| | 0.43 | 4.16 | | 0.0321 | 45.02 | 0.159 |
| | 0.42 | 4.09 | | 0.0455 | 54.66 | 0.149 |
| 72 | 0.37 | 4.82 | 1282 | 0.0195 | 36.41 | 0.229 |
| | 0.35 | 4.46 | | 0.0258 | 40.92 | 0.219 |
| | 0.36 | 4.60 | | 0.0581 | 64.93 | 0.209 |
| | 0.40 | 4.74 | | 0.0333 | 46.91 | 0.199 |
| | 0.47 | 4.50 | | 0.0676 | 74.08 | 0.179 |
| | 0.49 | 4.37 | | 0.1136 | 110.01 | 0.169 |
| 74 | 0.34 | 4.39 | 1386 | 0.0164 | 31.81 | 0.209 |
| | 0.39 | 4.11 | | 0.0258 | 38.34 | 0.199 |
| | 0.46 | 4.34 | | 0.0505 | 56.06 | 0.179 |
| | 0.47 | 4.02 | | 0.0127 | 29.84 | 0.169 |
| | 0.47 | 4.22 | | 0.0490 | 55.19 | 0.159 |
| | 0.46 | 4.12 | | 0.0223 | 36.45 | 0.149 |
| 75 | 0.24 | 5.38 | 1426 | 0.0185 | 32.31 | 0.229 |
| | 0.27 | 5.13 | | 0.0185 | 32.45 | 0.219 |
| | 0.31 | 5.29 | | 0.0481 | 51.44 | 0.209 |
| | 0.44 | 5.19 | | 0.6250 | 441.01 | 0.179 |
| | 0.47 | 5.09 | | 0.0481 | 53.62 | 0.149 |
| 82 | 0.34 | 4.50 | 1217 | 0.0287 | 42.35 | 0.266 |
| | 0.31 | 4.51 | | 0.0270 | 40.83 | 0.259 |
| | 0.28 | 4.63 | | 0.0344 | 45.79 | 0.249 |
| | 0.28 | 4.56 | | 0.0263 | 40.15 | 0.229 |
| | 0.30 | 4.44 | | 0.0235 | 38.34 | 0.219 |
| | 0.34 | 4.31 | | 0.0833 | 81.74 | 0.209 |
| | 0.39 | 4.46 | | 0.1064 | 99.75 | 0.199 |
| | 0.47 | 4.69 | | 0.0262 | 41.53 | 0.179 |
| | 0.49 | 4.46 | | 0.0781 | 81.40 | 0.169 |
| | 0.50 | 4.46 | | 0.0495 | 59.60 | 0.159 |
| | 0.48 | 4.48 | | 0.0901 | 90.23 | 0.149 |
| 83 | 0.22 | 4.37 | 1383 | 0.0137 | 28.83 | 0.229 |
| | 0.28 | 4.56 | | 0.0431 | 46.87 | 0.219 |
| | 0.34 | 4.84 | | 0.0294 | 39.13 | 0.209 |
| | 0.41 | 4.68 | | 0.0164 | 31.33 | 0.199 |
| | 0.51 | 4.54 | | 0.0130 | 29.50 | 0.179 |
| | 0.54 | 4.51 | | 0.0397 | 47.78 | 0.169 |
| | 0.55 | 4.87 | | 0.0893 | 81.85 | 0.159 |

Continued on next page

Table B.3 continued from previous page

| Exp. no. - | Relative density - | Flow velocity $m/s$ | Density flow $kg/m^3$ | Erosion velocity $m/s$ | Pick-up flux $kg/m^2 \cdot s$ | Flow height $m$ |
|---|---|---|---|---|---|---|
| | 0.54 | 4.81 | | 0.0403 | 48.25 | 0.149 |
| 85 | 0.36 | 4.32 | 1392 | 0.0078 | 25.34 | 0.229 |
| | 0.47 | 3.98 | | 0.0210 | 34.40 | 0.209 |
| | 0.53 | 4.11 | | 0.0106 | 27.63 | 0.199 |
| | 0.66 | 4.93 | | 0.0275 | 40.19 | 0.159 |

Table B.3: Results experiments on Dorsilit

Begin of Table B.4 Results experiments on Silverbond

| Exp. no. - | Relative density - | Flow velocity $m/s$ | Density flow $kg/m^3$ | Erosion velocity $m/s$ | Pick-up flux $kg/m^2 \cdot s$ | Flow height $m$ |
|---|---|---|---|---|---|---|
| 76 | -0.14 | 1.79 | 1093 | 0.0064 | 5.86 | 0.259 |
| | -0.17 | 1.71 | | 0.0057 | 5.18 | 0.249 |
| | -0.14 | 1.49 | | 0.0065 | 5.95 | 0.229 |
| | -0.11 | 1.42 | | 0.0200 | 17.81 | 0.219 |
| | -0.12 | 1.47 | | 0.0086 | 7.84 | 0.209 |
| | -0.15 | 1.41 | | 0.0017 | 1.75 | 0.199 |
| 77 | -0.16 | 1.43 | 1075 | 0.0056 | 5.28 | 0.249 |
| | -0.16 | 1.33 | | 0.0244 | 21.91 | 0.229 |
| | -0.16 | 1.34 | | 0.0071 | 6.60 | 0.219 |
| | -0.18 | 1.30 | | 0.0029 | 2.86 | 0.209 |
| | -0.23 | 1.38 | | 0.0220 | 19.18 | 0.199 |
| 78 | -0.12 | 2.24 | 1090 | 0.0047 | 3.74 | 0.266 |
| | -0.18 | 2.09 | | 0.0069 | 5.22 | 0.259 |
| | -0.14 | 1.85 | | 0.0127 | 9.45 | 0.229 |
| | -0.13 | 1.88 | | 0.0071 | 5.48 | 0.219 |
| | -0.10 | 2.03 | | 0.0164 | 12.40 | 0.199 |
| | -0.30 | 2.54 | | 0.0114 | 7.77 | 0.179 |
| 79 | 0.72 | 1.51 | 1103 | 0.0005 | 0.97 | 0.266 |
| | 0.52 | 1.55 | | 0.0006 | 1.04 | 0.259 |
| | 0.22 | 1.60 | | 0.0009 | 1.30 | 0.249 |
| | -0.01 | 1.68 | | 0.0012 | 1.51 | 0.229 |
| | -0.02 | 1.74 | | 0.0015 | 1.79 | 0.219 |
| | -0.05 | 1.75 | | 0.0026 | 2.89 | 0.209 |
| | -0.06 | 1.77 | | 0.0023 | 2.57 | 0.199 |
| 80 | 0.54 | 1.83 | 1071 | 0.0010 | 1.47 | 0.266 |
| | 0.30 | 1.88 | | 0.0015 | 1.92 | 0.259 |
| | 0.09 | 1.90 | | 0.0013 | 1.67 | 0.249 |
| | -0.03 | 1.96 | | 0.0039 | 4.21 | 0.229 |
| | -0.03 | 1.94 | | 0.0015 | 1.77 | 0.219 |
| | -0.05 | 1.88 | | 0.0139 | 14.04 | 0.209 |
| | -0.11 | 1.96 | | 0.0033 | 3.47 | 0.199 |
| | -0.20 | 1.82 | | 0.0031 | 3.13 | 0.179 |
| 81 | 0.62 | 2.51 | 1076 | 0.0015 | 1.99 | 0.266 |
| | 0.38 | 2.51 | | 0.0068 | 7.42 | 0.259 |
| | 0.14 | 2.56 | | 0.0042 | 4.32 | 0.249 |
| | 0.00 | 2.61 | | 0.0114 | 10.35 | 0.229 |
| | 0.01 | 2.56 | | 0.0026 | 2.64 | 0.219 |
| | -0.07 | 2.82 | | 0.0024 | 2.38 | 0.199 |

Continued on next page

Table B.4 continued from previous page

| Exp. no. - | Relative density - | Flow velocity $m/s$ | Density flow $kg/m^3$ | Erosion velocity $m/s$ | Pick-up flux $kg/m^2 \cdot s$ | Flow height $m$ |
|---|---|---|---|---|---|---|
| 87 | -0.07 | 1.51 | 1067 | 0.0007 | 0.88 | 0.266 |
| | -0.10 | 1.53 | | 0.0016 | 1.69 | 0.259 |
| | -0.13 | 1.44 | | 0.0038 | 3.55 | 0.229 |
| | -0.16 | 1.30 | | 0.0052 | 4.59 | 0.199 |
| 88 | 0.65 | 4.00 | 1086 | 0.0039 | 4.88 | 0.266 |
| | 0.43 | 3.93 | | 0.0070 | 7.96 | 0.259 |
| | 0.21 | 3.99 | | 0.0118 | 12.08 | 0.249 |
| | 0.08 | 4.10 | | 0.0069 | 6.86 | 0.229 |
| | 0.08 | 4.03 | | 0.0085 | 8.43 | 0.219 |
| | 0.06 | 3.80 | | 0.0072 | 7.13 | 0.209 |
| 89 | 0.60 | 5.18 | 1148 | 0.0055 | 6.68 | 0.266 |
| | 0.35 | 4.91 | | 0.0099 | 10.72 | 0.259 |
| | 0.11 | 4.92 | | 0.0368 | 35.47 | 0.249 |
| | 0.03 | 5.08 | | 0.0129 | 12.19 | 0.229 |
| | 0.08 | 5.08 | | 0.0131 | 12.68 | 0.219 |
| | 0.08 | 5.28 | | 0.0196 | 18.79 | 0.209 |
| | 0.01 | 4.10 | | 0.0313 | 28.94 | 0.199 |

Table B.4: Results experiments on Silverbond

# C

# Results experiments bed shear stress versus flow velocity

The data of the experiments giving reliable results for the bed shear stress, bed friction coefficient and depth-averaged flow velocity are presented per sand type in Tables C.1, C.2, C.3 and C.4. The following data are presented:

- Exp. no.: number of experiment;
- Density flow: average density of the eroding flow during the whole erosion experiment at the location of the conductivity probes based on the average density of the eroding inflow of water and effect of the average pick-up flux on the density of the eroding flow;
- Relative density: average density of the sand bed between two conductivity probes;
- Flow velocity: depth-averaged flow velocity;
- Shear Stress: bed shear stress as derived from the hydraulic pressure gradient measurements;
- Friction coefficient: bed friction coefficient as derived from the bed shear stress and depth-averaged flow velocity;
- Flow height: height of the flow above the top of the eroding bed.

Begin of Table C.1 Results experiments on Zilverzand

| Exp. no. - | Density flow $kg/m^3$ | Flow velocity $m/s$ | Shear stress $Pa$ | Friction coefficient $-$ | Flow height $m$ |
|---|---|---|---|---|---|
| 25 | 1088 | 3.21 | 117.04 | 0.084 | 0.239 |
| | | 3.29 | 168.31 | 0.115 | 0.229 |
| | | 3.36 | 207.59 | 0.136 | 0.219 |
| | | 3.37 | 226.08 | 0.147 | 0.209 |
| | | 3.30 | 240.73 | 0.162 | 0.199 |
| | | 3.27 | 231.07 | 0.159 | 0.189 |
| | | 2.98 | 181.51 | 0.150 | 0.179 |
| 26 | 1107 | 2.36 | 38.35 | 0.050 | 0.219 |
| | | 2.40 | 35.22 | 0.044 | 0.209 |
| 27 | 1095 | 3.02 | 90.61 | 0.073 | 0.249 |
| | | 2.92 | 151.52 | 0.129 | 0.239 |
| | | 2.88 | 191.43 | 0.168 | 0.229 |
| | | 2.92 | 191.79 | 0.164 | 0.219 |
| | | 3.00 | 250.41 | 0.204 | 0.209 |
| 28 | 1180 | 3.94 | 331.60 | 0.145 | 0.259 |
| | | 4.07 | 231.65 | 0.095 | 0.249 |
| | | 4.13 | 306.21 | 0.122 | 0.239 |
| | | 4.00 | 287.88 | 0.122 | 0.229 |
| | | 3.53 | 235.10 | 0.128 | 0.199 |
| | | 3.33 | 184.73 | 0.113 | 0.189 |
| 30 | 1104 | 2.42 | 92.74 | 0.114 | 0.189 |
| | | 2.49 | 89.82 | 0.105 | 0.179 |
| | | 2.57 | 104.49 | 0.115 | 0.169 |
| | | 2.50 | 114.77 | 0.133 | 0.159 |
| | | 2.53 | 146.98 | 0.167 | 0.149 |
| 31 | 1115 | 3.01 | 135.12 | 0.107 | 0.239 |
| | | 3.36 | 162.47 | 0.103 | 0.219 |
| | | 3.34 | 189.17 | 0.122 | 0.209 |
| | | 3.39 | 256.45 | 0.160 | 0.199 |
| | | 3.45 | 306.25 | 0.184 | 0.189 |
| | | 3.52 | 294.12 | 0.170 | 0.179 |
| | | 3.33 | 371.98 | 0.240 | 0.169 |
| 32 | 1189 | 4.24 | 295.70 | 0.111 | 0.249 |
| | | 4.54 | 336.96 | 0.110 | 0.229 |
| | | 4.52 | 395.45 | 0.130 | 0.219 |
| | | 4.47 | 504.18 | 0.170 | 0.209 |
| | | 4.34 | 604.42 | 0.216 | 0.199 |
| | | 4.31 | 739.20 | 0.268 | 0.189 |

Continued on next page

Table C.1 continued from previous page

| Exp. no. - | Density flow $kg/m^3$ | Flow velocity $m/s$ | Shear stress $Pa$ | Friction coefficient $-$ | Flow height $m$ |
|---|---|---|---|---|---|
| | | 4.43 | 672.32 | 0.230 | 0.179 |
| | | 4.25 | 671.86 | 0.250 | 0.169 |
| | | 3.89 | 448.18 | 0.199 | 0.159 |
| 33 | 1201 | 5.74 | 1041.64 | 0.211 | 0.229 |
| | | 5.73 | 992.12 | 0.201 | 0.219 |
| | | 5.80 | 1178.91 | 0.234 | 0.209 |
| | | 5.91 | 1270.57 | 0.243 | 0.199 |
| 34 | 1067 | 2.39 | 64.29 | 0.084 | 0.189 |
| | | 2.50 | 83.63 | 0.100 | 0.179 |
| | | 2.45 | 92.52 | 0.115 | 0.169 |
| | | 2.49 | 104.41 | 0.126 | 0.159 |
| | | 2.44 | 139.74 | 0.175 | 0.149 |
| 35 | 1104 | 3.12 | 162.98 | 0.121 | 0.229 |
| | | 3.06 | 193.84 | 0.150 | 0.219 |
| | | 3.04 | 204.38 | 0.160 | 0.209 |
| | | 3.10 | 228.17 | 0.172 | 0.199 |
| | | 3.02 | 300.05 | 0.239 | 0.189 |
| | | 2.85 | 402.79 | 0.360 | 0.179 |
| 36 | 1166 | 4.25 | 318.30 | 0.121 | 0.249 |
| | | 4.31 | 432.29 | 0.159 | 0.239 |
| | | 4.34 | 480.38 | 0.175 | 0.229 |
| | | 4.23 | 587.35 | 0.225 | 0.219 |
| | | 4.48 | 811.31 | 0.277 | 0.189 |
| | | 4.14 | 841.89 | 0.337 | 0.179 |
| | | 3.76 | 810.44 | 0.393 | 0.169 |
| | | 3.51 | 414.59 | 0.230 | 0.159 |
| 37 | 1189 | 4.49 | 484.11 | 0.162 | 0.249 |
| | | 4.73 | 456.99 | 0.138 | 0.229 |
| | | 4.63 | 671.30 | 0.211 | 0.219 |
| | | 4.62 | 889.13 | 0.280 | 0.209 |
| | | 4.61 | 980.79 | 0.310 | 0.199 |
| | | 4.78 | 739.45 | 0.217 | 0.179 |
| | | 4.51 | 653.03 | 0.216 | 0.169 |
| | | 3.03 | 524.29 | 0.385 | 0.149 |
| 39 | 1309 | 3.97 | 389.63 | 0.151 | 0.249 |
| | | 3.90 | 635.90 | 0.255 | 0.239 |
| | | 4.23 | 591.34 | 0.202 | 0.229 |
| | | 4.51 | 383.25 | 0.115 | 0.209 |

Continued on next page

Table C.1 continued from previous page

| Exp. no. - | Density flow $kg/m^3$ | Flow velocity $m/s$ | Shear stress $Pa$ | Friction coefficient $-$ | Flow height $m$ |
|---|---|---|---|---|---|
| | | 4.54 | 711.57 | 0.211 | 0.199 |
| | | 4.50 | 934.19 | 0.282 | 0.189 |
| | | 4.70 | 1023.39 | 0.283 | 0.179 |
| | | 4.12 | 819.31 | 0.295 | 0.169 |
| | | 4.11 | 626.81 | 0.226 | 0.159 |
| 40 | 1290 | 4.64 | 415.88 | 0.120 | 0.229 |
| | | 4.68 | 483.92 | 0.137 | 0.219 |
| | | 4.64 | 356.26 | 0.103 | 0.209 |
| 41 | 1466 | 3.85 | 587.85 | 0.217 | 0.229 |
| | | 4.05 | 409.28 | 0.136 | 0.219 |
| | | 3.67 | 788.88 | 0.320 | 0.209 |
| 42 | 1447 | 4.61 | 641.41 | 0.167 | 0.249 |
| | | 4.61 | 569.58 | 0.148 | 0.239 |
| | | 4.74 | 1238.55 | 0.305 | 0.209 |
| | | 4.45 | 1436.81 | 0.400 | 0.199 |

Table C.1: Results experiments on Zilverzand

Begin of Table C.2 Results experiments on Geba

| Exp. no. - | Density flow $kg/m^3$ | Flow velocity $m/s$ | Shear stress $Pa$ | Friction coefficient $-$ | Flow height $m$ |
|---|---|---|---|---|---|
| 44 | 1145 | 2.37 | 192.49 | 0.239 | 0.259 |
| 46 | 1170 | 4.76 | 376.86 | 0.114 | 0.259 |
| | | 4.72 | 536.63 | 0.165 | 0.249 |
| | | 5.11 | 423.63 | 0.111 | 0.229 |
| | | 5.08 | 506.13 | 0.134 | 0.219 |
| | | 4.95 | 460.96 | 0.129 | 0.209 |
| | | 5.08 | 462.62 | 0.122 | 0.199 |
| | | 5.12 | 396.85 | 0.103 | 0.189 |
| | | 4.95 | 403.41 | 0.113 | 0.179 |
| | | 4.67 | 272.16 | 0.085 | 0.169 |
| | | 4.42 | 295.81 | 0.103 | 0.159 |
| 47 | 1088 | 1.86 | 45.53 | 0.097 | 0.266 |
| | | 1.97 | 42.79 | 0.081 | 0.249 |
| | | 1.98 | 58.74 | 0.110 | 0.239 |
| | | 2.01 | 68.74 | 0.125 | 0.229 |
| | | 2.09 | 61.74 | 0.104 | 0.219 |
| | | 2.18 | 66.31 | 0.102 | 0.209 |
| | | 2.24 | 71.01 | 0.104 | 0.199 |
| | | 2.25 | 72.67 | 0.105 | 0.189 |
| | | 2.19 | 68.59 | 0.106 | 0.179 |
| | | 2.04 | 76.95 | 0.135 | 0.169 |
| 48 | 1123 | 2.94 | 156.26 | 0.129 | 0.229 |
| | | 2.95 | 169.56 | 0.139 | 0.219 |
| | | 2.93 | 205.61 | 0.170 | 0.209 |
| | | 2.87 | 196.71 | 0.170 | 0.199 |
| | | 2.84 | 225.22 | 0.199 | 0.189 |
| | | 2.72 | 219.12 | 0.212 | 0.179 |
| | | 2.49 | 235.55 | 0.270 | 0.169 |
| 49 | 1153 | 3.72 | 282.24 | 0.142 | 0.259 |
| | | 3.77 | 313.56 | 0.153 | 0.249 |
| | | 3.80 | 391.02 | 0.188 | 0.239 |
| | | 4.08 | 380.62 | 0.159 | 0.219 |
| | | 4.13 | 430.09 | 0.175 | 0.209 |
| | | 4.03 | 471.79 | 0.201 | 0.199 |
| | | 4.02 | 503.52 | 0.216 | 0.189 |
| | | 4.07 | 423.69 | 0.177 | 0.179 |
| | | 3.87 | 396.99 | 0.184 | 0.169 |
| | | 3.59 | 344.95 | 0.185 | 0.159 |

Continued on next page

Table C.2 continued from previous page

| Exp. no. - | Density flow $kg/m^3$ | Flow velocity $m/s$ | Shear stress $Pa$ | Friction coefficient $-$ | Flow height $m$ |
|---|---|---|---|---|---|
| | | 3.47 | 227.88 | 0.131 | 0.149 |
| 50 | 1178 | 4.49 | 565.88 | 0.191 | 0.266 |
| | | 4.76 | 513.12 | 0.154 | 0.249 |
| | | 4.75 | 593.39 | 0.179 | 0.239 |
| | | 4.80 | 629.36 | 0.186 | 0.229 |
| | | 4.78 | 709.00 | 0.211 | 0.219 |
| | | 4.84 | 679.54 | 0.197 | 0.209 |
| | | 4.88 | 619.99 | 0.177 | 0.199 |
| | | 4.72 | 487.47 | 0.149 | 0.189 |
| | | 4.57 | 567.45 | 0.185 | 0.179 |
| | | 4.47 | 354.53 | 0.121 | 0.169 |
| | | 4.10 | 484.23 | 0.196 | 0.159 |
| 51 | 1096 | 1.84 | 52.80 | 0.114 | 0.266 |
| | | 1.87 | 62.49 | 0.130 | 0.259 |
| | | 1.93 | 69.17 | 0.135 | 0.249 |
| | | 2.07 | 60.96 | 0.104 | 0.229 |
| | | 2.14 | 76.68 | 0.122 | 0.219 |
| | | 2.17 | 69.30 | 0.107 | 0.209 |
| | | 2.21 | 77.60 | 0.116 | 0.199 |
| | | 2.28 | 77.05 | 0.108 | 0.189 |
| | | 2.32 | 86.39 | 0.117 | 0.179 |
| | | 2.38 | 89.56 | 0.115 | 0.169 |
| | | 2.40 | 82.16 | 0.104 | 0.159 |
| | | 2.38 | 91.00 | 0.117 | 0.149 |
| 53 | 1125 | 3.85 | 186.36 | 0.089 | 0.259 |
| | | 3.96 | 229.79 | 0.104 | 0.249 |
| | | 4.13 | 236.09 | 0.098 | 0.229 |
| | | 4.17 | 238.13 | 0.097 | 0.219 |
| | | 4.26 | 278.57 | 0.109 | 0.209 |
| | | 4.29 | 348.94 | 0.135 | 0.199 |
| | | 4.45 | 320.84 | 0.116 | 0.179 |
| | | 4.41 | 355.48 | 0.130 | 0.169 |
| | | 4.13 | 294.93 | 0.123 | 0.159 |
| 54 | 1162 | 4.75 | 278.18 | 0.085 | 0.266 |
| | | 4.86 | 334.00 | 0.097 | 0.259 |
| | | 4.88 | 376.65 | 0.109 | 0.249 |
| | | 5.20 | 370.57 | 0.094 | 0.229 |
| | | 5.35 | 369.83 | 0.089 | 0.219 |

Continued on next page

Table C.2 continued from previous page

| Exp. no. - | Density flow $kg/m^3$ | Flow velocity $m/s$ | Shear stress $Pa$ | Friction coefficient $-$ | Flow height $m$ |
|---|---|---|---|---|---|
| | | 5.46 | 442.65 | 0.102 | 0.209 |
| | | 5.37 | 519.24 | 0.124 | 0.199 |
| | | 5.35 | 559.72 | 0.135 | 0.189 |
| | | 5.42 | 503.85 | 0.118 | 0.179 |
| | | 5.24 | 439.56 | 0.110 | 0.169 |
| 55 | 1239 | 2.85 | 179.20 | 0.143 | 0.259 |
| | | 2.96 | 231.55 | 0.171 | 0.239 |
| | | 3.08 | 211.29 | 0.144 | 0.219 |
| | | 3.12 | 271.63 | 0.180 | 0.209 |
| | | 3.10 | 312.84 | 0.211 | 0.199 |
| | | 2.95 | 313.09 | 0.233 | 0.189 |
| | | 2.85 | 256.27 | 0.203 | 0.169 |
| 56 | 1287 | 3.70 | 394.42 | 0.179 | 0.259 |
| | | 3.72 | 404.50 | 0.182 | 0.249 |
| | | 3.80 | 455.56 | 0.196 | 0.239 |
| | | 3.87 | 453.13 | 0.188 | 0.229 |
| | | 3.99 | 486.45 | 0.190 | 0.219 |
| | | 3.79 | 308.16 | 0.133 | 0.179 |
| | | 3.67 | 382.78 | 0.177 | 0.169 |
| 57 | 1262 | 4.51 | 761.37 | 0.237 | 0.266 |
| | | 4.80 | 624.83 | 0.172 | 0.249 |
| | | 4.82 | 660.22 | 0.180 | 0.239 |
| | | 4.81 | 611.39 | 0.167 | 0.229 |
| | | 4.89 | 711.75 | 0.189 | 0.219 |
| | | 4.99 | 673.96 | 0.172 | 0.209 |
| | | 4.99 | 611.58 | 0.156 | 0.199 |
| | | 4.96 | 578.72 | 0.149 | 0.189 |
| 58 | 1361 | 2.81 | 215.62 | 0.161 | 0.259 |
| | | 2.97 | 275.88 | 0.184 | 0.249 |
| | | 3.04 | 360.24 | 0.229 | 0.239 |
| | | 2.99 | 329.72 | 0.216 | 0.229 |
| | | 3.27 | 300.86 | 0.165 | 0.209 |
| | | 3.22 | 265.22 | 0.150 | 0.189 |
| | | 3.22 | 327.05 | 0.185 | 0.169 |
| 59 | 1419 | 3.56 | 544.54 | 0.242 | 0.266 |
| | | 3.74 | 448.36 | 0.181 | 0.259 |
| | | 3.60 | 748.08 | 0.325 | 0.249 |
| | | 3.86 | 708.40 | 0.268 | 0.229 |

Continued on next page

Table C.2 continued from previous page

| Exp. no. - | Density flow $kg/m^3$ | Flow velocity $m/s$ | Shear stress $Pa$ | Friction coefficient $-$ | Flow height $m$ |
|---|---|---|---|---|---|
| | | 3.81 | 758.60 | 0.294 | 0.219 |
| | | 3.68 | 870.38 | 0.362 | 0.209 |
| | | 3.77 | 692.34 | 0.275 | 0.199 |
| | | 3.88 | 672.31 | 0.251 | 0.179 |
| | | 3.93 | 818.96 | 0.300 | 0.169 |

Table C.2: Results experiments on Geba

Begin of Table C.3 Results experiments on Dorsilit

| Exp. no. - | Density flow $kg/m^3$ | Flow velocity $m/s$ | Shear stress $Pa$ | Friction coefficient $-$ | Flow height $m$ |
|---|---|---|---|---|---|
| 61 | 1115 | 3.30 | 137.15 | 0.090 | 0.239 |
| | | 3.37 | 137.24 | 0.087 | 0.229 |
| | | 3.33 | 163.87 | 0.106 | 0.219 |
| | | 3.29 | 173.58 | 0.115 | 0.209 |
| | | 3.44 | 176.67 | 0.107 | 0.199 |
| | | 3.42 | 86.78 | 0.053 | 0.189 |
| | | 3.39 | 189.50 | 0.118 | 0.179 |
| 62 | 1175 | 3.83 | 234.11 | 0.109 | 0.259 |
| | | 3.37 | 225.71 | 0.136 | 0.249 |
| | | 3.78 | 337.95 | 0.161 | 0.229 |
| 63 | 1230 | 4.88 | 547.84 | 0.150 | 0.266 |
| | | 4.83 | 465.17 | 0.130 | 0.259 |
| | | 4.95 | 453.25 | 0.120 | 0.219 |
| | | 5.07 | 275.45 | 0.070 | 0.209 |
| | | 4.90 | 484.32 | 0.131 | 0.199 |
| | | 4.11 | 494.06 | 0.190 | 0.179 |
| 64 | 1113 | 3.41 | 156.70 | 0.097 | 0.209 |
| | | 3.29 | 174.82 | 0.116 | 0.199 |
| | | 3.32 | 174.72 | 0.114 | 0.189 |
| | | 3.30 | 154.24 | 0.102 | 0.179 |
| | | 3.23 | 141.03 | 0.097 | 0.169 |
| | | 3.12 | 182.00 | 0.134 | 0.159 |
| | | 2.97 | 178.29 | 0.146 | 0.149 |
| 65 | 1142 | 3.88 | 356.27 | 0.166 | 0.259 |
| | | 3.98 | 271.30 | 0.120 | 0.249 |
| | | 4.01 | 230.43 | 0.100 | 0.239 |
| | | 4.08 | 233.30 | 0.098 | 0.229 |
| | | 4.13 | 210.01 | 0.086 | 0.219 |
| | | 4.16 | 229.28 | 0.093 | 0.209 |
| | | 4.11 | 188.66 | 0.078 | 0.199 |
| | | 4.13 | 183.21 | 0.075 | 0.189 |
| | | 4.20 | 137.08 | 0.054 | 0.179 |
| 66 | 1214 | 4.54 | 343.79 | 0.110 | 0.249 |
| | | 4.64 | 491.43 | 0.150 | 0.239 |
| | | 4.47 | 182.18 | 0.060 | 0.229 |
| | | 4.47 | 540.20 | 0.178 | 0.219 |
| | | 4.53 | 414.21 | 0.133 | 0.209 |
| | | 4.17 | 489.45 | 0.186 | 0.199 |

Continued on next page

Table C.3 continued from previous page

| Exp. no. - | Density flow $kg/m^3$ | Flow velocity $m/s$ | Shear stress $Pa$ | Friction coefficient $-$ | Flow height $m$ |
|---|---|---|---|---|---|
| | | 4.24 | 861.87 | 0.316 | 0.189 |
| | | 4.45 | 817.49 | 0.273 | 0.179 |
| | | 4.40 | 436.17 | 0.148 | 0.169 |
| | | 4.42 | 628.71 | 0.212 | 0.159 |
| | | 4.59 | 556.44 | 0.174 | 0.149 |
| 67 | 1144 | 3.95 | 193.69 | 0.087 | 0.219 |
| | | 3.89 | 144.84 | 0.067 | 0.209 |
| | | 3.81 | 215.07 | 0.104 | 0.199 |
| | | 3.99 | 297.10 | 0.131 | 0.189 |
| | | 3.89 | 156.22 | 0.072 | 0.179 |
| | | 3.90 | 287.39 | 0.132 | 0.169 |
| | | 3.94 | 283.11 | 0.127 | 0.159 |
| | | 3.80 | 307.71 | 0.149 | 0.149 |
| | | 3.59 | 371.35 | 0.201 | 0.129 |
| 68 | 1121 | 4.28 | 242.04 | 0.094 | 0.219 |
| | | 4.38 | 292.31 | 0.109 | 0.209 |
| | | 4.37 | 343.35 | 0.128 | 0.199 |
| | | 4.37 | 304.41 | 0.114 | 0.189 |
| | | 4.47 | 467.17 | 0.167 | 0.179 |
| | | 4.56 | 390.02 | 0.134 | 0.169 |
| | | 4.44 | 381.10 | 0.138 | 0.159 |
| | | 4.46 | 440.22 | 0.158 | 0.149 |
| 69 | 1176 | 4.72 | 373.64 | 0.114 | 0.259 |
| | | 4.81 | 330.15 | 0.097 | 0.249 |
| | | 4.83 | 364.41 | 0.106 | 0.239 |
| | | 4.97 | 501.93 | 0.138 | 0.229 |
| | | 4.85 | 495.93 | 0.144 | 0.219 |
| | | 5.03 | 622.16 | 0.167 | 0.199 |
| | | 5.05 | 587.43 | 0.157 | 0.189 |
| | | 5.20 | 592.85 | 0.149 | 0.179 |
| | | 5.11 | 679.23 | 0.177 | 0.169 |
| | | 5.15 | 822.72 | 0.211 | 0.159 |
| | | 5.23 | 677.29 | 0.168 | 0.149 |
| 70 | 1242 | 3.61 | 199.21 | 0.099 | 0.189 |
| | | 3.38 | 192.10 | 0.108 | 0.169 |
| | | 3.41 | 322.18 | 0.178 | 0.149 |
| | | 3.29 | 420.78 | 0.251 | 0.129 |
| 71 | 1270 | 4.00 | 222.25 | 0.088 | 0.219 |

Continued on next page

Table C.3 continued from previous page

| Exp. no. - | Density flow $kg/m^3$ | Flow velocity $m/s$ | Shear stress $Pa$ | Friction coefficient $-$ | Flow height $m$ |
|---|---|---|---|---|---|
| | | 4.47 | 278.44 | 0.088 | 0.179 |
| | | 4.12 | 318.46 | 0.118 | 0.169 |
| 72 | 1282 | 4.83 | 608.26 | 0.163 | 0.266 |
| | | 4.72 | 553.10 | 0.155 | 0.259 |
| | | 4.78 | 661.69 | 0.181 | 0.239 |
| | | 4.46 | 420.07 | 0.132 | 0.219 |
| | | 4.60 | 541.31 | 0.160 | 0.209 |
| | | 5.39 | 520.21 | 0.112 | 0.189 |
| 74 | 1386 | 3.85 | 664.78 | 0.259 | 0.266 |
| | | 3.63 | 683.04 | 0.299 | 0.259 |
| | | 4.12 | 431.73 | 0.147 | 0.249 |
| | | 4.23 | 323.47 | 0.105 | 0.229 |
| | | 4.47 | 418.42 | 0.121 | 0.219 |
| | | 4.11 | 509.65 | 0.174 | 0.199 |
| | | 4.18 | 505.60 | 0.167 | 0.189 |
| | | 4.02 | 455.37 | 0.163 | 0.169 |
| | | 4.12 | 381.63 | 0.130 | 0.149 |
| | | 4.66 | 484.29 | 0.129 | 0.129 |
| 75 | 1426 | 4.70 | 614.39 | 0.156 | 0.249 |
| 82 | 1217 | 4.51 | 449.24 | 0.145 | 0.259 |
| | | 4.63 | 373.69 | 0.114 | 0.249 |
| | | 4.66 | 516.35 | 0.156 | 0.239 |
| | | 4.56 | 373.76 | 0.118 | 0.229 |
| | | 4.44 | 541.48 | 0.180 | 0.219 |
| | | 4.31 | 645.30 | 0.229 | 0.209 |
| | | 4.46 | 648.72 | 0.214 | 0.199 |
| | | 4.60 | 603.02 | 0.187 | 0.189 |
| | | 4.69 | 479.44 | 0.144 | 0.179 |
| | | 4.46 | 694.57 | 0.229 | 0.169 |
| | | 4.46 | 475.25 | 0.157 | 0.159 |
| | | 4.48 | 676.43 | 0.221 | 0.149 |
| 83 | 1383 | 4.37 | 663.69 | 0.201 | 0.229 |
| | | 4.84 | 391.89 | 0.097 | 0.209 |
| | | 4.68 | 389.36 | 0.103 | 0.199 |
| | | 4.54 | 731.66 | 0.205 | 0.179 |

Table C.3: Results experiments on Dorsilit

Begin of Table C.4 Results experiments on Silverbond

| Exp. no. - | Density flow $kg/m^3$ | Flow velocity $m/s$ | Shear stress $Pa$ | Friction coefficient $-$ | Flow height $m$ |
|---|---|---|---|---|---|
| 76 | 1093 | 1.81 | 24.87 | 0.055 | 0.266 |
| | | 1.79 | 32.30 | 0.074 | 0.259 |
| | | 1.71 | 35.21 | 0.088 | 0.249 |
| | | 1.64 | 31.85 | 0.087 | 0.239 |
| 78 | 1090 | 1.88 | 213.57 | 0.442 | 0.219 |
| | | 2.27 | 121.15 | 0.172 | 0.189 |
| 79 | 1103 | 1.55 | 8.16 | 0.024 | 0.259 |
| | | 1.60 | 9.93 | 0.028 | 0.249 |
| | | 1.63 | 10.32 | 0.028 | 0.239 |
| | | 1.68 | 10.97 | 0.028 | 0.229 |
| | | 1.74 | 11.44 | 0.027 | 0.219 |
| | | 1.75 | 15.44 | 0.036 | 0.209 |
| | | 1.77 | 13.01 | 0.030 | 0.199 |
| 80 | 1071 | 1.90 | 12.05 | 0.025 | 0.249 |
| | | 1.91 | 20.45 | 0.042 | 0.239 |
| | | 1.96 | 31.29 | 0.061 | 0.229 |
| | | 1.94 | 40.82 | 0.081 | 0.219 |
| | | 1.88 | 45.97 | 0.097 | 0.209 |
| | | 1.96 | 53.06 | 0.103 | 0.199 |
| 81 | 1076 | 2.51 | 43.00 | 0.051 | 0.266 |
| | | 2.51 | 46.01 | 0.054 | 0.259 |
| | | 2.56 | 56.14 | 0.064 | 0.249 |
| | | 2.55 | 78.20 | 0.090 | 0.239 |
| | | 2.56 | 108.88 | 0.124 | 0.219 |
| | | 2.82 | 80.59 | 0.075 | 0.199 |
| 88 | 1086 | 4.00 | 152.20 | 0.070 | 0.266 |
| | | 3.99 | 266.47 | 0.123 | 0.249 |
| | | 4.13 | 118.44 | 0.051 | 0.239 |
| | | 4.03 | 187.04 | 0.085 | 0.219 |
| | | 3.80 | 243.84 | 0.125 | 0.209 |
| 89 | 1148 | 5.18 | 103.95 | 0.027 | 0.266 |
| | | 4.91 | 127.59 | 0.037 | 0.259 |
| | | 5.06 | 256.51 | 0.070 | 0.239 |
| | | 5.08 | 243.38 | 0.066 | 0.229 |
| | | 5.08 | 404.14 | 0.109 | 0.219 |

Table C.4: Results experiments on Silverbond

# D

# Results experiments pick-up flux versus bed shear stress

The data of the experiments giving reliable results for the pick-up flux and bed shear stress are presented per sand type in Tables D.1, D.2, D.3 and D.4. The following data are presented:

- Exp. no.: number of experiment;
- Relative density: average density of the sand bed between two conductivity probes;
- Flow velocity: depth-averaged flow velocity;
- Density flow: average density of the eroding flow during the whole erosion experiment at the location of the conductivity probes based on the average density of the eroding inflow of water and effect of the average pick-up flux on the density of the eroding flow;
- Erosion velocity: rate with which the erosion front moves down between two consecutive conductivity probes;
- Pick-up flux: calculated pick-up flux between two erosion moments;
- Shear Stress: bed shear stress as derived from the hydraulic pressure gradient measurements.

Begin of Table D.1 Results experiments on Zilverzand

| Exp. no. - | Relative density - | Flow velocity $m/s$ | Density flow $kg/m^3$ | Erosion velocity $m/s$ | Pick-up flux $kg/m^2 \cdot s$ | Shear stress $Pa$ |
|---|---|---|---|---|---|---|
| 25 | 0.28 | 3.29 | 1088 | 0.0119 | 21.21 | 168.31 |
| | 0.32 | 3.36 | | 0.0118 | 21.20 | 207.59 |
| | 0.34 | 3.37 | | 0.0101 | 19.66 | 226.08 |
| | 0.32 | 3.30 | | 0.0116 | 21.08 | 240.73 |
| | 0.14 | 2.98 | | 0.0090 | 18.15 | 181.51 |
| 26 | 0.18 | 2.36 | 1107 | 0.0047 | 14.34 | 38.35 |
| | 0.21 | 2.40 | | 0.0054 | 15.07 | 35.22 |
| 27 | 0.18 | 2.88 | 1095 | 0.0256 | 33.29 | 191.43 |
| | 0.27 | 2.92 | | 0.0294 | 37.41 | 191.79 |
| | 0.30 | 3.00 | | 0.0250 | 33.52 | 250.41 |
| | 0.21 | 2.92 | | 0.0125 | 21.54 | 209.71 |
| 28 | -0.01 | 3.94 | 1180 | 0.0610 | 56.04 | 331.60 |
| | 0.02 | 4.07 | | 0.0781 | 69.65 | 231.65 |
| | 0.10 | 4.00 | | 0.0130 | 20.15 | 287.88 |
| | 0.21 | 3.53 | | 0.0568 | 56.20 | 235.10 |
| 30 | 0.79 | 2.49 | 1104 | 0.0016 | 11.73 | 89.82 |
| | 0.78 | 2.57 | | 0.0021 | 12.35 | 104.49 |
| | 0.77 | 2.50 | | 0.0034 | 13.84 | 114.77 |
| | 1.14 | 2.53 | | 0.0038 | 14.57 | 146.98 |
| 31 | 0.62 | 3.27 | 1115 | 0.0093 | 19.94 | 165.41 |
| | 0.65 | 3.36 | | 0.0056 | 16.11 | 162.47 |
| | 0.69 | 3.34 | | 0.0063 | 16.86 | 189.17 |
| | 0.68 | 3.39 | | 0.0070 | 17.61 | 256.45 |
| | 0.75 | 3.52 | | 0.0094 | 20.45 | 294.12 |
| | 0.70 | 3.33 | | 0.0066 | 17.24 | 371.98 |
| 32 | 0.65 | 4.54 | 1189 | 0.0154 | 24.39 | 336.96 |
| | 0.68 | 4.52 | | 0.0200 | 28.80 | 395.45 |
| | 0.70 | 4.47 | | 0.0217 | 30.54 | 504.18 |
| | 0.71 | 4.34 | | 0.0221 | 30.93 | 604.42 |
| | 0.70 | 4.43 | | 0.0347 | 42.62 | 672.32 |
| | 0.67 | 4.25 | | 0.0181 | 26.96 | 671.86 |
| 33 | 0.67 | 5.74 | 1201 | 0.0263 | 35.04 | 1041.64 |
| | 0.68 | 5.73 | | 0.0568 | 64.00 | 992.12 |
| | 0.69 | 5.80 | | 0.1316 | 134.79 | 1178.91 |
| | 0.69 | 5.91 | | 0.0575 | 64.65 | 1270.57 |
| 34 | 0.53 | 2.50 | 1067 | 0.0022 | 11.85 | 83.63 |
| | 0.54 | 2.45 | | 0.0045 | 14.44 | 92.52 |
| | 0.51 | 2.49 | | 0.0035 | 13.32 | 104.41 |

Continued on next page

Table D.1 continued from previous page

| Exp. no. - | Relative density - | Flow velocity $m/s$ | Density flow $kg/m^3$ | Erosion velocity $m/s$ | Pick-up flux $kg/m^2 \cdot s$ | Shear stress $Pa$ |
|---|---|---|---|---|---|---|
| | 0.34 | 2.44 | | 0.0044 | 14.14 | 139.74 |
| 35 | 0.48 | 3.12 | 1104 | 0.0052 | 14.79 | 162.98 |
| | 0.48 | 3.06 | | 0.0076 | 16.92 | 193.84 |
| | 0.48 | 3.04 | | 0.0192 | 27.40 | 204.38 |
| | 0.47 | 3.10 | | 0.0154 | 23.93 | 228.17 |
| | 0.49 | 2.85 | | 0.0152 | 23.77 | 402.79 |
| 36 | 0.45 | 4.34 | 1166 | 0.0200 | 27.68 | 480.38 |
| | 0.42 | 4.23 | | 0.0172 | 25.14 | 587.35 |
| | 0.36 | 4.14 | | 0.0169 | 24.59 | 841.89 |
| | 0.49 | 3.76 | | 0.0510 | 55.46 | 810.44 |
| | 0.74 | 3.51 | | 0.0455 | 53.54 | 414.59 |
| 37 | 0.51 | 4.49 | 1189 | 0.0198 | 28.71 | 484.11 |
| | 0.53 | 4.73 | | 0.0153 | 24.56 | 456.99 |
| | 0.55 | 4.63 | | 0.0216 | 30.64 | 671.3 |
| | 0.56 | 4.62 | | 0.0321 | 40.52 | 889.13 |
| | 0.54 | 4.61 | | 0.0327 | 40.94 | 980.79 |
| | 0.44 | 4.78 | | 0.0400 | 46.81 | 739.45 |
| | 0.41 | 4.51 | | 0.0279 | 35.48 | 653.03 |
| | 0.57 | 3.03 | | 0.0331 | 41.62 | 524.29 |
| 39 | 0.51 | 4.23 | 1309 | 0.0377 | 41.08 | 591.34 |
| | 0.42 | 4.51 | | 0.0488 | 49.01 | 383.25 |
| | 0.39 | 4.54 | | 0.0169 | 23.48 | 711.57 |
| | 0.41 | 4.70 | | 0.0294 | 33.45 | 1023.39 |
| | 0.37 | 4.12 | | 0.0400 | 41.52 | 819.31 |
| | 0.52 | 4.11 | | 0.0294 | 34.30 | 626.81 |
| 40 | 0.51 | 4.64 | 1290 | 0.0180 | 24.08 | 415.88 |
| | 0.48 | 4.68 | | 0.0391 | 40.67 | 483.92 |
| | 0.45 | 4.64 | | 0.0355 | 37.48 | 356.26 |
| 41 | 0.45 | 4.05 | 1466 | 0.0121 | 18.66 | 409.28 |
| | 0.42 | 3.67 | | 0.0114 | 18.00 | 788.88 |
| 42 | 0.60 | 4.61 | 1447 | 0.0147 | 21.22 | 641.41 |
| | 0.36 | 4.74 | | 0.0187 | 23.13 | 1238.55 |
| | 0.33 | 4.45 | | 0.0270 | 28.89 | 1436.81 |

Table D.1: Results experiments on Zilverzand

Begin of Table D.2 Results experiments on Geba

| Exp. no. - | Relative density - | Flow velocity $m/s$ | Density flow $kg/m^3$ | Erosion velocity $m/s$ | Pick-up flux $kg/m^2 \cdot s$ | Shear stress $Pa$ |
|---|---|---|---|---|---|---|
| 46 | 0.14 | 5.11 | 1170 | 0.0147 | 14.07 | 423.63 |
| | 0.17 | 5.08 | | 0.0131 | 13.00 | 506.13 |
| | 0.18 | 4.95 | | 0.0463 | 39.32 | 460.96 |
| | 0.19 | 5.08 | | 0.2174 | 174.92 | 462.62 |
| | 0.18 | 4.95 | | 0.0216 | 19.73 | 403.41 |
| | 0.16 | 4.67 | | 0.0273 | 24.13 | 272.16 |
| | 0.13 | 4.42 | | 0.0224 | 20.04 | 295.81 |
| 47 | 0.32 | 1.97 | 1088 | 0.0035 | 6.16 | 42.79 |
| | 0.41 | 2.01 | | 0.0088 | 11.47 | 68.74 |
| | 0.43 | 2.09 | | 0.0045 | 7.29 | 61.74 |
| | 0.42 | 2.18 | | 0.0032 | 5.98 | 66.31 |
| | 0.40 | 2.24 | | 0.0051 | 7.83 | 71.01 |
| | 0.31 | 2.19 | | 0.0035 | 6.17 | 68.59 |
| | 0.27 | 2.04 | | 0.0035 | 6.07 | 76.95 |
| 48 | 0.40 | 2.94 | 1123 | 0.0082 | 10.39 | 156.26 |
| | 0.43 | 2.95 | | 0.0101 | 12.26 | 169.56 |
| | 0.45 | 2.93 | | 0.0177 | 19.44 | 205.61 |
| | 0.43 | 2.87 | | 0.0110 | 13.08 | 196.71 |
| | 0.33 | 2.72 | | 0.0092 | 11.06 | 219.12 |
| | 0.27 | 2.49 | | 0.0129 | 14.12 | 235.55 |
| 49 | 0.36 | 3.72 | 1153 | 0.0174 | 18.87 | 282.24 |
| | 0.34 | 3.77 | | 0.0177 | 19.08 | 313.56 |
| | 0.46 | 4.08 | | 0.0227 | 24.62 | 380.62 |
| | 0.51 | 4.13 | | 0.0139 | 16.41 | 430.09 |
| | 0.55 | 4.03 | | 0.0136 | 16.27 | 471.79 |
| | 0.51 | 4.07 | | 0.0253 | 27.50 | 423.69 |
| | 0.45 | 3.87 | | 0.0155 | 17.66 | 396.99 |
| | 0.38 | 3.59 | | 0.0229 | 24.15 | 344.95 |
| | 0.33 | 3.47 | | 0.0198 | 20.94 | 227.88 |
| 50 | 0.42 | 4.49 | 1178 | 0.0158 | 17.07 | 565.88 |
| | 0.32 | 4.76 | | 0.0148 | 15.58 | 513.12 |
| | 0.37 | 4.80 | | 0.0152 | 16.28 | 629.36 |
| | 0.38 | 4.78 | | 0.0275 | 27.12 | 709 |
| | 0.37 | 4.84 | | 0.0485 | 45.44 | 679.54 |
| | 0.33 | 4.88 | | 0.0233 | 22.98 | 619.99 |
| | 0.27 | 4.57 | | 0.0521 | 46.70 | 567.45 |
| | 0.25 | 4.47 | | 0.0236 | 22.57 | 354.53 |
| | 0.23 | 4.10 | | 0.0233 | 22.16 | 484.23 |

Continued on next page

Table D.2 continued from previous page

| Exp. no. - | Relative density - | Flow velocity $m/s$ | Density flow $kg/m^3$ | Erosion velocity $m/s$ | Pick-up flux $kg/m^2 \cdot s$ | Shear stress $Pa$ |
|---|---|---|---|---|---|---|
| 51 | 0.70 | 2.07 | 1096 | 0.0020 | 5.06 | 60.96 |
| | 0.74 | 2.14 | | 0.0020 | 5.08 | 76.68 |
| | 0.76 | 2.17 | | 0.0022 | 5.42 | 69.3 |
| | 0.77 | 2.21 | | 0.0023 | 5.43 | 77.6 |
| | 0.76 | 2.32 | | 0.0035 | 6.94 | 86.39 |
| | 0.75 | 2.38 | | 0.0050 | 8.63 | 89.56 |
| | 0.76 | 2.40 | | 0.0044 | 7.92 | 82.16 |
| | 0.77 | 2.38 | | 0.0037 | 7.14 | 91.00 |
| 53 | 0.62 | 3.85 | 1125 | 0.0091 | 12.15 | 186.36 |
| | 0.62 | 3.96 | | 0.0095 | 12.54 | 229.79 |
| | 0.68 | 4.13 | | 0.0106 | 13.94 | 236.09 |
| | 0.70 | 4.17 | | 0.0194 | 23.33 | 238.13 |
| | 0.71 | 4.26 | | 0.0117 | 15.20 | 278.57 |
| | 0.72 | 4.29 | | 0.0104 | 13.84 | 348.94 |
| | 0.75 | 4.45 | | 0.0153 | 19.31 | 320.84 |
| | 0.74 | 4.41 | | 0.0181 | 22.28 | 355.48 |
| | 0.67 | 4.13 | | 0.0151 | 18.62 | 294.93 |
| 54 | 0.75 | 4.75 | 1162 | 0.0123 | 15.81 | 278.18 |
| | 0.70 | 4.86 | | 0.0090 | 12.23 | 334.00 |
| | 0.69 | 4.88 | | 0.0107 | 13.90 | 376.65 |
| | 0.75 | 5.20 | | 0.0313 | 36.02 | 370.57 |
| | 0.78 | 5.35 | | 0.0186 | 22.75 | 369.83 |
| | 0.80 | 5.46 | | 0.0126 | 16.42 | 442.65 |
| | 0.80 | 5.37 | | 0.0149 | 18.87 | 519.24 |
| | 0.79 | 5.42 | | 0.0338 | 39.21 | 503.85 |
| | 0.79 | 5.24 | | 0.0203 | 24.67 | 439.56 |
| 55 | 0.52 | 3.08 | 1239 | 0.0109 | 11.78 | 211.29 |
| | 0.54 | 3.12 | | 0.0061 | 7.77 | 271.63 |
| | 0.53 | 3.10 | | 0.0140 | 14.45 | 312.84 |
| | 0.45 | 2.85 | | 0.0075 | 8.76 | 256.27 |
| 56 | 0.34 | 3.72 | 1287 | 0.0154 | 15.33 | 404.5 |
| | 0.37 | 3.87 | | 0.0833 | 71.34 | 453.13 |
| | 0.36 | 3.99 | | 0.0207 | 19.72 | 486.45 |
| | 0.25 | 3.79 | | 0.0161 | 15.4 | 308.16 |
| | 0.26 | 3.67 | | 0.0455 | 38.36 | 382.78 |
| 57 | 0.39 | 4.81 | 1262 | 0.0313 | 27.09 | 611.39 |
| | 0.41 | 4.89 | | 0.0431 | 36.59 | 711.75 |
| | 0.41 | 4.99 | | 0.0357 | 30.76 | 673.96 |

Continued on next page

Table D.2 continued from previous page

| Exp. no. - | Relative density - | Flow velocity $m/s$ | Density flow $kg/m^3$ | Erosion velocity $m/s$ | Pick-up flux $kg/m^2 \cdot s$ | Shear stress $Pa$ |
|---|---|---|---|---|---|---|
| | 0.39 | 4.99 | | 0.0181 | 16.82 | 611.58 |
| 58 | 0.37 | 2.81 | 1361 | 0.0050 | 6.52 | 215.62 |
| | 0.37 | 2.97 | | 0.0114 | 11.38 | 275.88 |
| | 0.47 | 2.99 | | 0.0057 | 7.3 | 329.72 |
| | 0.48 | 3.27 | | 0.0103 | 11.02 | 300.86 |
| | 0.33 | 3.22 | | 0.0096 | 9.87 | 327.05 |
| 59 | 0.34 | 3.74 | 1419 | 0.0179 | 15.27 | 448.36 |
| | 0.34 | 3.60 | | 0.0095 | 9.31 | 748.08 |
| | 0.43 | 3.86 | | 0.0159 | 14.34 | 708.4 |
| | 0.46 | 3.81 | | 0.0159 | 14.52 | 758.6 |
| | 0.46 | 3.68 | | 0.0179 | 16.04 | 870.38 |
| | 0.44 | 3.77 | | 0.0357 | 29.25 | 692.34 |
| | 0.36 | 3.88 | | 0.0220 | 18.31 | 672.31 |
| | 0.32 | 3.93 | | 0.0177 | 14.97 | 818.96 |

Table D.2: Results experiments on Geba

Begin of Table D.3 Results experiments on Dorsilit

| Exp. no. - | Relative density - | Flow velocity $m/s$ | Density flow $kg/m^3$ | Erosion velocity $m/s$ | Pick-up flux $kg/m^2 \cdot s$ | Shear stress $Pa$ |
|---|---|---|---|---|---|---|
| 61 | 0.09 | 3.37 | 1115 | 0.0015 | 23.14 | 137.24 |
| | -0.06 | 3.33 | | 0.0096 | 28.76 | 163.87 |
| | -0.11 | 3.29 | | 0.0135 | 31.28 | 173.58 |
| | -0.09 | 3.44 | | 0.0135 | 31.36 | 176.67 |
| | 0.00 | 3.39 | | 0.0074 | 27.31 | 189.50 |
| | -0.02 | 2.90 | | 0.0154 | 32.98 | 313.83 |
| | -0.18 | 1.57 | | 0.0196 | 35.03 | 209.72 |
| 62 | -0.08 | 3.37 | 1175 | 0.0227 | 35.91 | 225.71 |
| | -0.19 | 3.78 | | 0.0362 | 42.99 | 337.95 |
| 63 | 0.40 | 4.88 | 1230 | 0.0225 | 40.41 | 547.84 |
| | 0.44 | 4.83 | | 0.0307 | 47.22 | 465.17 |
| | 0.58 | 4.95 | | 0.0131 | 33.64 | 453.25 |
| | 0.47 | 5.07 | | 0.0290 | 46.14 | 275.45 |
| | 0.35 | 4.90 | | 0.0488 | 60.50 | 484.32 |
| | 0.19 | 4.11 | | 0.0169 | 34.93 | 494.06 |
| 64 | 0.30 | 3.41 | 1113 | 0.0078 | 27.75 | 156.70 |
| | 0.34 | 3.29 | | 0.0117 | 30.83 | 174.82 |
| | 0.40 | 3.30 | | 0.0077 | 27.96 | 154.24 |
| | 0.42 | 3.23 | | 0.0134 | 32.45 | 141.03 |
| | 0.45 | 3.12 | | 0.0138 | 32.84 | 182.00 |
| | 0.48 | 2.97 | | 0.0107 | 30.49 | 178.29 |
| 65 | 0.09 | 3.88 | 1142 | 0.0183 | 35.40 | 356.27 |
| | 0.08 | 3.98 | | 0.0148 | 32.88 | 271.30 |
| | 0.14 | 4.08 | | 0.0336 | 46.83 | 233.30 |
| | 0.19 | 4.13 | | 0.0171 | 35.08 | 210.01 |
| | 0.25 | 4.16 | | 0.0342 | 48.40 | 229.28 |
| | 0.30 | 4.11 | | 0.0164 | 35.07 | 188.66 |
| | 0.36 | 4.20 | | 0.0439 | 57.13 | 137.08 |
| 66 | 0.13 | 4.47 | 1214 | 0.0592 | 63.54 | 182.18 |
| | 0.17 | 4.47 | | 0.0885 | 84.88 | 540.20 |
| | 0.20 | 4.53 | | 0.0260 | 40.93 | 414.21 |
| | 0.23 | 4.17 | | 0.0541 | 61.52 | 489.45 |
| | 0.27 | 4.45 | | 0.0388 | 50.76 | 817.49 |
| | 0.27 | 4.40 | | 0.0877 | 86.82 | 436.17 |
| | 0.26 | 4.42 | | 0.0926 | 90.17 | 628.71 |
| | 0.24 | 4.59 | | 0.3226 | 257.41 | 556.44 |
| 67 | 0.65 | 3.95 | 1144 | 0.0084 | 30.12 | 193.69 |
| | 0.73 | 3.89 | | 0.0189 | 40.05 | 144.84 |

Continued on next page

Table D.3 continued from previous page

| Exp. no. - | Relative density - | Flow velocity $m/s$ | Density flow $kg/m^3$ | Erosion velocity $m/s$ | Pick-up flux $kg/m^2 \cdot s$ | Shear stress $Pa$ |
|---|---|---|---|---|---|---|
| | 0.82 | 3.81 | | 0.0161 | 37.94 | 215.07 |
| | 0.97 | 3.89 | | 0.0165 | 39.04 | 156.22 |
| | 0.99 | 3.90 | | 0.0134 | 36.01 | 287.39 |
| | 0.96 | 3.94 | | 0.0146 | 37.07 | 283.11 |
| | 0.89 | 3.80 | | 0.0128 | 35.04 | 307.71 |
| 68 | 0.72 | 4.28 | 1121 | 0.0127 | 32.78 | 242.04 |
| | 0.80 | 4.38 | | 0.0203 | 40.03 | 292.31 |
| | 0.88 | 4.37 | | 0.0159 | 36.40 | 343.35 |
| | 0.99 | 4.47 | | 0.0360 | 56.25 | 467.17 |
| | 1.01 | 4.56 | | 0.0275 | 48.19 | 390.02 |
| | 0.99 | 4.44 | | 0.0225 | 43.30 | 381.10 |
| | 0.95 | 4.46 | | 0.0193 | 39.97 | 440.22 |
| 69 | 0.66 | 4.72 | 1176 | 0.0164 | 34.67 | 373.64 |
| | 0.61 | 4.81 | | 0.0481 | 59.31 | 330.15 |
| | 0.63 | 4.97 | | 0.0222 | 39.10 | 501.93 |
| | 0.69 | 4.85 | | 0.0286 | 44.61 | 495.93 |
| | 0.82 | 5.03 | | 0.0361 | 52.15 | 622.16 |
| | 0.91 | 5.20 | | 0.0595 | 73.61 | 592.85 |
| | 0.92 | 5.11 | | 0.0258 | 44.09 | 679.23 |
| | 0.90 | 5.15 | | 0.0385 | 55.01 | 822.72 |
| | 0.86 | 5.23 | | 0.0610 | 73.95 | 677.29 |
| 70 | 0.44 | 3.38 | 1242 | 0.0052 | 26.17 | 192.10 |
| | 0.40 | 3.41 | | 0.0051 | 26.04 | 322.18 |
| 71 | 0.33 | 4.00 | 1270 | 0.0134 | 31.00 | 222.25 |
| | 0.45 | 4.47 | | 0.0385 | 49.93 | 278.44 |
| | 0.44 | 4.12 | | 0.0403 | 51.23 | 318.46 |
| 72 | 0.35 | 4.46 | 1282 | 0.0258 | 40.92 | 420.07 |
| | 0.36 | 4.60 | | 0.0581 | 64.93 | 541.31 |
| 74 | 0.39 | 4.11 | 1386 | 0.0258 | 38.34 | 509.65 |
| | 0.47 | 4.22 | | 0.0490 | 55.19 | 740.54 |
| | 0.46 | 4.12 | | 0.0223 | 36.45 | 381.63 |
| 82 | 0.31 | 4.51 | 1217 | 0.0270 | 40.83 | 449.24 |
| | 0.28 | 4.63 | | 0.0344 | 45.79 | 373.69 |
| | 0.28 | 4.56 | | 0.0263 | 40.15 | 373.76 |
| | 0.30 | 4.44 | | 0.0235 | 38.34 | 541.48 |
| | 0.34 | 4.31 | | 0.0833 | 81.74 | 645.30 |
| | 0.39 | 4.46 | | 0.1064 | 99.75 | 648.72 |
| | 0.47 | 4.69 | | 0.0262 | 41.53 | 479.44 |

Continued on next page

Table D.3 continued from previous page

| Exp. no. - | Relative density - | Flow velocity $m/s$ | Density flow $kg/m^3$ | Erosion velocity $m/s$ | Pick-up flux $kg/m^2 \cdot s$ | Shear stress $Pa$ |
|---|---|---|---|---|---|---|
| | 0.49 | 4.46 | | 0.0781 | 81.40 | 694.57 |
| | 0.50 | 4.46 | | 0.0495 | 59.60 | 475.25 |
| | 0.48 | 4.48 | | 0.0901 | 90.23 | 676.43 |
| 83 | 0.22 | 4.37 | 1383 | 0.0137 | 28.83 | 663.69 |
| | 0.34 | 4.84 | | 0.0294 | 39.13 | 391.89 |
| | 0.41 | 4.68 | | 0.0164 | 31.33 | 389.36 |
| | 0.51 | 4.54 | | 0.0130 | 29.50 | 731.66 |

Table D.3: Results experiments on Dorsilit

Begin of Table D.4 Results experiments on Silverbond

| Exp. no. - | Relative density - | Flow velocity $m/s$ | Density flow $kg/m^3$ | Erosion velocity $m/s$ | Pick-up flux $kg/m^2 \cdot s$ | Shear stress $Pa$ |
|---|---|---|---|---|---|---|
| 76 | -0.14 | 1.79 | 1093 | 0.0064 | 5.86 | 32.30 |
| | -0.17 | 1.71 | | 0.0057 | 5.18 | 35.21 |
| 78 | -0.13 | 1.88 | 1090 | 0.0071 | 5.48 | 213.57 |
| 79 | 0.72 | 1.51 | 1103 | 0.0005 | 0.97 | 5.38 |
| | 0.52 | 1.55 | | 0.0006 | 1.04 | 8.16 |
| | 0.22 | 1.60 | | 0.0009 | 1.30 | 9.93 |
| | -0.01 | 1.68 | | 0.0012 | 1.51 | 10.97 |
| | -0.02 | 1.74 | | 0.0015 | 1.79 | 11.44 |
| | -0.05 | 1.75 | | 0.0026 | 2.89 | 15.44 |
| | -0.06 | 1.77 | | 0.0023 | 2.57 | 13.01 |
| 80 | 0.09 | 1.90 | 1071 | 0.0013 | 1.67 | 12.05 |
| | -0.03 | 1.96 | | 0.0039 | 4.21 | 31.29 |
| | -0.03 | 1.94 | | 0.0015 | 1.77 | 40.82 |
| | -0.05 | 1.88 | | 0.0139 | 14.04 | 45.97 |
| | -0.11 | 1.96 | | 0.0033 | 3.47 | 53.06 |
| 81 | 0.62 | 2.51 | 1076 | 0.0015 | 1.99 | 43.00 |
| | 0.38 | 2.51 | | 0.0068 | 7.42 | 46.01 |
| | 0.14 | 2.56 | | 0.0042 | 4.32 | 56.14 |
| | 0.01 | 2.56 | | 0.0026 | 2.64 | 108.88 |
| | -0.07 | 2.82 | | 0.0024 | 2.38 | 80.59 |
| 88 | 0.65 | 4.00 | 1086 | 0.0039 | 4.88 | 152.2 |
| | 0.21 | 3.99 | | 0.0118 | 12.08 | 266.47 |
| | 0.08 | 4.10 | | 0.0069 | 6.86 | 214.7 |
| | 0.08 | 4.03 | | 0.0085 | 8.43 | 187.04 |
| 89 | 0.60 | 5.18 | 1148 | 0.0055 | 6.68 | 103.95 |
| | 0.35 | 4.91 | | 0.0099 | 10.72 | 127.59 |
| | 0.03 | 5.08 | | 0.0129 | 12.19 | 243.38 |
| | 0.08 | 5.08 | | 0.0131 | 12.68 | 404.14 |

Table D.4: Results experiments on Silverbond

# E

# Relation between concentration gradient, pick-up flux and apparent bed friction

This appendix shows several results of the erosion experiments as discussed in 8. Figure E.1 shows the relation between the concentration gradient over 0.01 and 0.02 meter above the erosion front and the pick-up flux for all sand types and at different densities of the eroding fluid.

Figure E.2 shows the relation between the apparent bed friction and pick-up flux for all sand types and different densities of the eroding fluid.

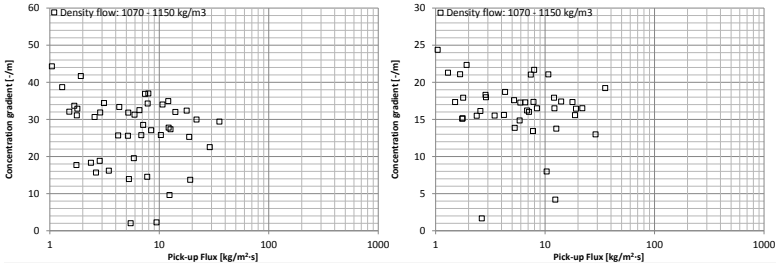


(a) Silverbond (b)

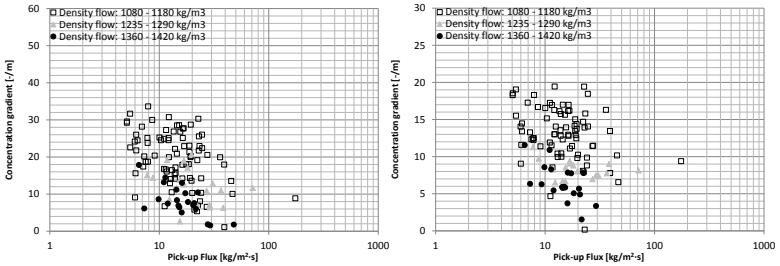


(c) Geba (d)

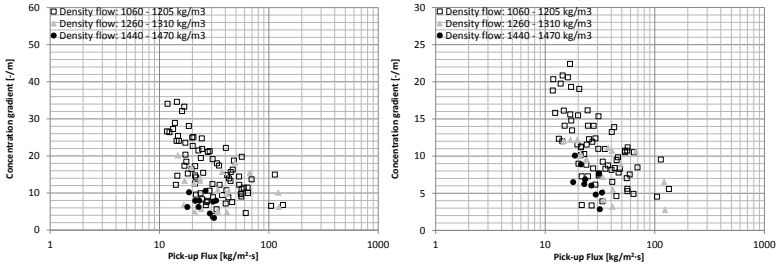


(e) Zilverzand (f)

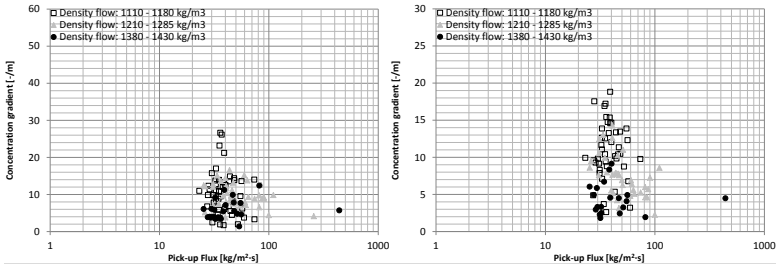


(g) Dorsilit (h)

Figure E.1: Concentration gradient over 0.01 and 0.02 meter above erosion front as function of the pick-up flux. Note negative values for the concentration gradient are not shown and the maximum concentration gradient at the y-axes of the left and right figures are not equal

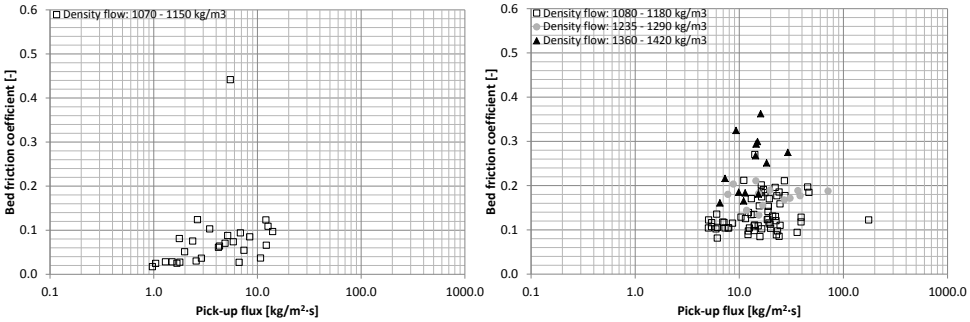


(a) Silverbond




(b) Geba

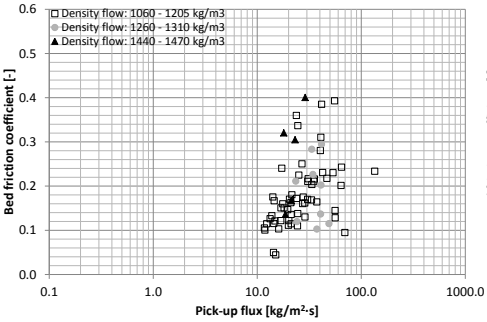


(c) Zilverzand

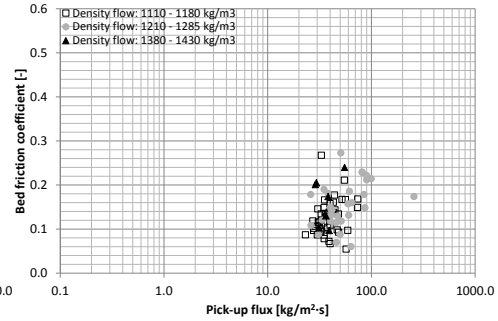


(d) Dorsilit

Figure E.2: Relation between bed friction and pick-up flux

# F

# Influence relative density on pick-up flux

Figure F.1 shows the pick-up flux as function of the depth-averaged flow velocity, bed shear stress and relative density for different sand types at a larger scale than presented in Figure 8.17.

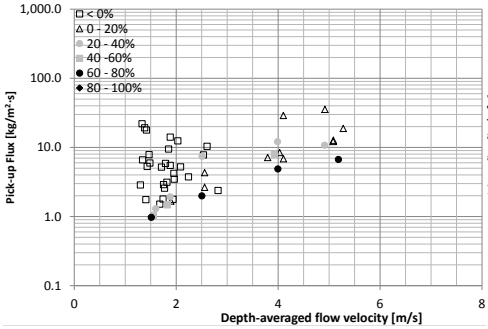


(a) Silverbond

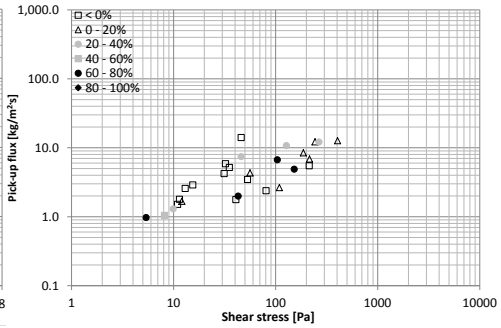


(b)

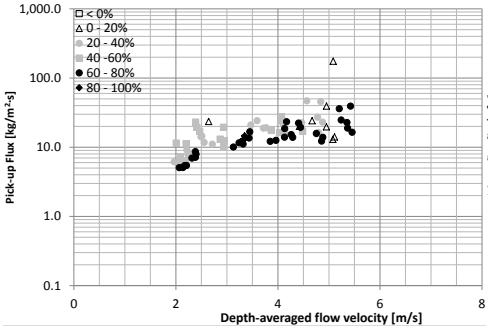


(c) Geba

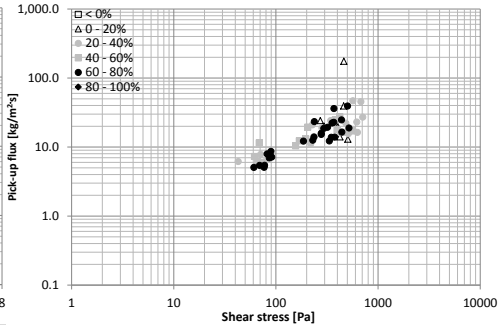


(d)

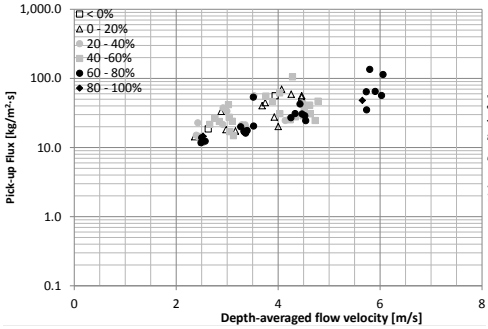


(e) Zilverzand

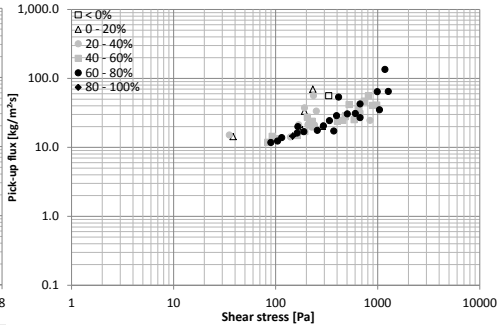


(f)

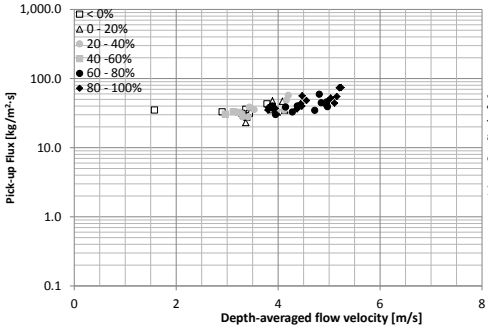


(g) Dorsilit

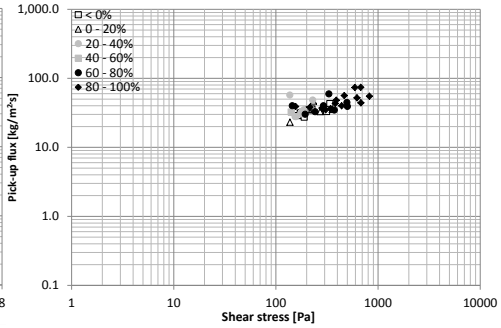


(h)

Figure F.1: Pick-up flux as function of the depth-averaged flow velocity, bed shear stress and relative density for different sand types (density eroding flow between 1060 and 1205 kg/m$^3$)

# G

# Influence grain size on pick-up flux

Figure G.1 shows the pick-up flux as function of the depth-averaged flow velocity and grain size at a larger scale than presented in Figure 8.23.

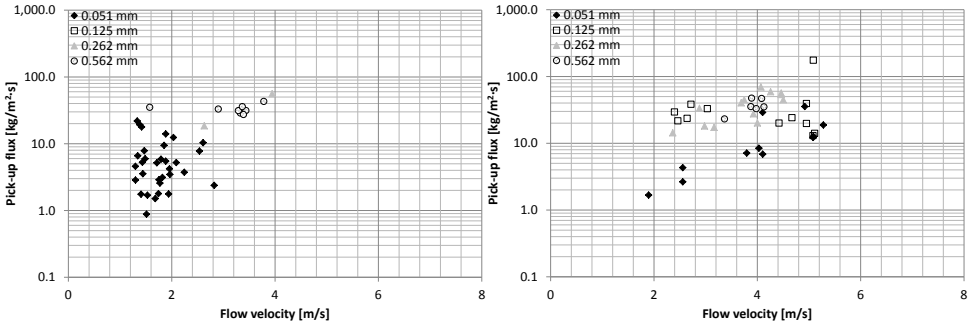


(a) $R_n < 0\%$ (b) $R_n = 0$ - $20\%$

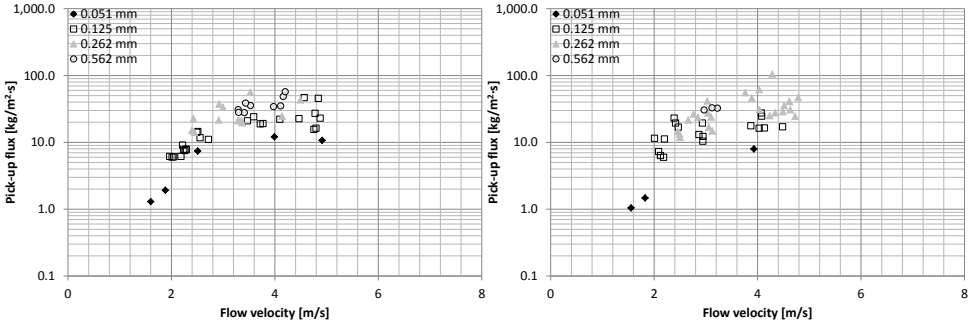


(c) $R_n = 20$ - $40\%$ (d) $R_n = 40$ - $60\%$

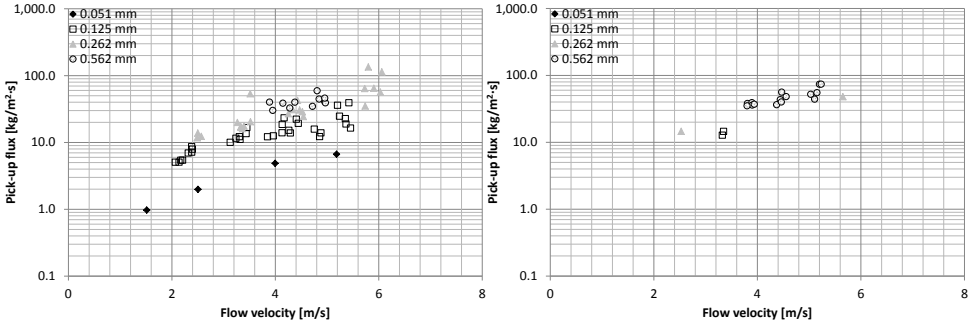


(e) $R_n = 60$ - $80\%$ (f) $R_n = 80$ - $100\%$

Figure G.1: Pick-up flux as function of the depth-averaged flow velocity and grain size at a different relative density ($R_n$) for all experiments with a density of the eroding flow of between 1060 and 1205 kg/m$^3$

# H

# Comparison results experiments and model pick-up flux

Figure H.1 shows a comparison between the model and the results of the experiments at different relative densities at a larger scale than presented in Figure 8.28.

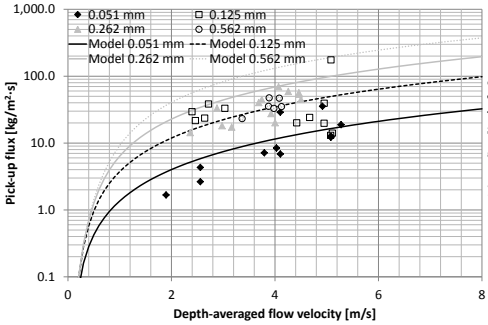


(a) $R_n$ = 0 - 20%

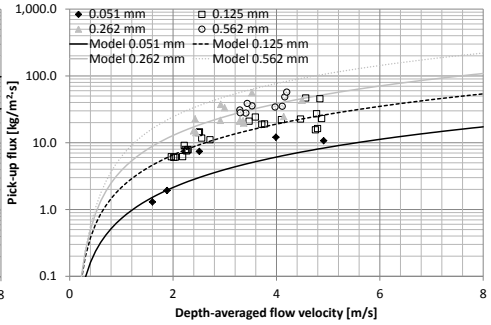


(b) $R_n$ = 20 - 40%

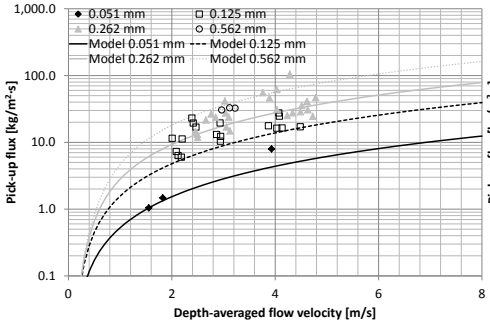


(c) $R_n$ = 40 - 60%

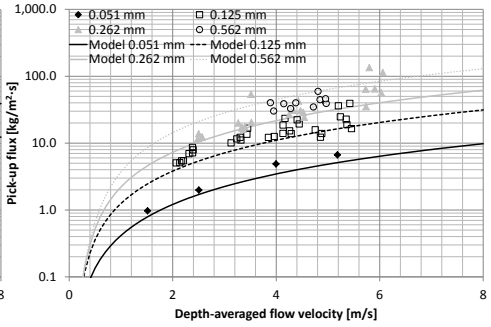


(d) $R_n$ = 60 - 80%

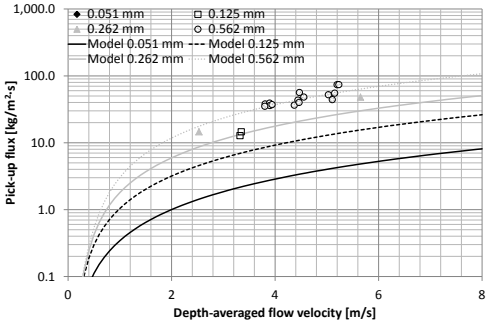


(e) $R_n$ = 80 - 100%

Figure H.1: Pick-up flux as function of the depth-averaged flow velocity for different sand types and relative density for all experiments with a density of the eroding flow of between 1060 and 1205 kg/m$^3$ compared to the pick-up flux model

# Bibliography


Alshibli, K. A. and Sture, S. (1999). Sand shear band thickness measurements by digital imaging techniques. *Journal of Computing in Civil Engineering*, 13(2):103–109.

Amer, A. M. and Awad, A. A. (1999). Permeability of cohesionless soils. *Journal of Geotechnical and Geoenvironmental Engineering*, 100(12):1309–1316.

Annandale, G. W. (2006). *Scour Technology: Mechanics and Engineering Practice*. McGraw-Hill, New York, NY, USA.

Aseada, T., Nakai, M., Manandhar, S. K., and Tamai, N. (1989). Sediment entrainment in channel with rippled bed. *Journal of Hydraulic Engineering*, 115(3):327–339.

Bagnold, R. A. (1954). Experiments on a gravity-free dispersion of large solid spheres in a newtonian fluid under shear. *Proceedings of the Royal Society*, 225(1160):49–63.

Bagnold, R. A. (1956). The flow of cohesionless grains in fluids. *Philosophical Transactions of the Royal Society*, 249:235–297.

Batu, V. (1998). *Aquifer Hydraulics; A Comprehensive Guide to Hydrogeologic Data Analysis*. John Wiley and Sons, New York, NY, USA.

Bear, J. (1972). *Dynamics of Fluids in Porous Media*. American Elsevier, New York, NY, USA.

Bezuijen, A. and Mastbergen, D. R. (1988). On the construction of sand fill dams - part 2 - soil mechanical aspects. In *Proceedings of the International Symposium on Modelling Soil-Water-Structure Interactions*, pages 363–371, Delft, the Netherlands. Balkema.

Bisschop, F. (1993). Bagt 510: Erosieproeven op zand met variatie in doorlatendheid. Technical report, Delft Hydraulics, Delft, the Netherlands.

Bisschop, F. (2009). *Materialen in (constructieve) ophogingen en aanvullingen: Richtlijn ter beoordeling van alternatieven voor zand*. CROW, Ede, the Netherlands (in Dutch).

Bisschop, F., Miedema, S. A., Visser, P. J., Keetels, G. H., and van Rhee, C. (2016). Experiments on the pickup flux of sand at high flow velocities. *Journal of Hydraulic Engineering*, 142(7):04016013.

Bisschop, F. and van Kesteren, W. G. M. (1994). Vastlegging bestaande kennis squeezingproces. Technical report, Delft Hydraulics, Delft, the Netherlands (in Dutch).

Bisschop, F., Visser, P. J., van Rhee, C., and Verhagen, H. J. (2010). Erosion due to high flow velocities: a description of relevant processes. In *Proceedings $32^{nd}$ International Conference on Coastal Engineering*, Shanghai, China. ASCE, Texas Digital Library.

Blake, W. K. (1970). Turbulent boundary-layer wall-pressure fluctuations on smooth and rough walls. *Journal of Fluid Mechanics*, 12(44(04)):637 – 660.

Breusers, H. N. C. (1977). Hydraulic excavation of sand. In *Proceedings International Course on Modern Dredging*, The Hague, the Netherlands. Post Graduate courses in Civil Engineering.

Brink, W. E. and Oldenziel, D. M. (1974). Influence of suction and blowing on entrainment of sand particles. *Journal of the Hydraulics Division*, 100(7):935–949.

Bruggeman, D. A. G. (1935). Berechnung verschiedener physikalischer konstanten von heterogenen substanzen i. dielektrizitätskonstanten und leitfähigkeiten der mischkörper aus isotropen substanzen. *Annalen der Physik*, 24(5):636–664.

Buffin-Bélanger, T., Roy, A. G., and Kirkbride, A. D. (2000). On large-scale flow structures in a gravel-bed river. *Geomorphology*, 32:417–435.

Camenen, B. and Larson, M. (2013). Accuracy of equivalent roughness height formulas in practical applications. *Journal of Hydraulic Engineering*, 139(3):331–335.

Cao, D. and Chiew, Y.-M. (2013). Suction effects on sediment transport in closed-conduit flows. *Journal of Hydraulic Engineering*, 140(5):04014008.

Cao, Z. (1997). Turbulent bursting-based sediment entrainment function. *Journal of Hydraulic Engineering*, 123(3):233–236.

Carrier, W. D. (2003). Goodbye, Hazen; Hello, Kozeny-Carman. *Journal of Geotechnical and Geoenvironmental Engineering*, 129(11):1054–1056.

Chen, X. and Chiew, Y.-M. (2004). Velocity distribution of turbulent open-channel flow with bed suction. *Journal of Hydraulic Engineering*, 130(2):140–148.

Cheng, N. and Chiew, Y.-M. (1999). Incipient sediment motion with seepage. *Journal Hydraulic Research*, 37(5):665–681.

Colebrook, C. F. (1939). Turbulent flow in pipes, with particular reference to the transition region between the smooth and rough pipe laws. *Journal of the Institution of Civil Engineers*, 11(4):133–156.

Coleman, N. L. (1967). A theoretical and experimental study of drag and lift forces acting on sphere resting on a hypothetical streambed. In *Proceedings12$^{th}$ Congress IAHR 3*, pages 185 – 192, Fort Collins, Colorado, USA. IAHR.

De La Rue, R. E. and Tobias, C. W. (1959). On the conductivity of dispersions. *Journal of the Electrochemical Society*, 106(9):827–833.

Delft Hydraulics (1972). Systematic investigation of two dimensional scour. Technical Report Report M648/M863, Delft Hydraulics Laboratory, Delft, the Netherlands.

Dohmen-Janssen, C. M. (1999). *Grain size influence on sediment transport in oscillatory sheet flow: phase lags and mobile-bed effects*. PhD thesis, Delft University of Technology, Delft, the Netherlands.

Dohmen-Janssen, C. M. and Hanes, D. M. (2002). Sheet flow dynamics under monochromatic nonbreaking waves. *Journal of Geophysical Research*, 107(C10):1301–1321.

Doligalski, T. L., Smith, C. R., and Walker, J. D. A. (1994). Vortex interactions with walls. *Annual Review of Fluid Mechanics*, 26(1):573–616.

Einstein, A. (1906). Eine neue bestimmung der molekuldimensionen. *Annalen der Physik*, 324(2):289–306.

Einstein, A. (1911). Berichtigung zu meiner arbeit: Eine neue bestimmung der molekuldimensionen. *Annalen der Physik*, 339(3):591–592.

Farabee, T. M. and Casaralla, M. J. (1991). Spectral features of wall pressure fluctuations beneath turbulent boundary layers. *Physics of Fluids*, 3:2410–2420.

Fernandez Luque, R. (1974). *Erosion and Transport of Bed-Load Sediment*. PhD thesis, Delft University of Technology, Delft, the Netherlands.

Foortse, B. (2016). Retardation of breach growth under high flow velocities - applicability of a bentonite-additive. Master's thesis, Delft University of Technology, Delft, the Netherlands.

Galappatti, R. (1983). A depth-integrated model for suspended transport. Technical Report Communications on Hydraulics, Report 83-7, Department of Civil Engineering, Delft University of Technology, Delft, the Netherlands.

Gao, P. (2008). Transition between two bed-load transport regimes: Saltation and sheet flow. *Journal of Hydraulic Engineering*, 134(3):340–349.

Graf, W. H. and Pazis, G. C. (1977). Les phenomenes de deposition et d'erosion dans un canal alluvionnaire. *Journal of Hydraulic Research*, 15(2):151–166.

Grass, A. J. and Mansour-Tehrani, M. (1996). Generalized scaling of coherent structures in the near-wall region of turbulent flow over smooth and rough boundaries. *Coherent flow structures in open channels*, pages 41–61.

Greimann, B. P. and Holly, F. M. (2001). Two-phase flow analysis of concentration profiles. *Journal of Hydraulic Engineering*, 127(9):753–762.

Hjulström, F. (1935). Studies of the morphological activity of rivers as illustrated by the river fyris. *Bulletin of the Geological Institute*, 25:221–527.

Hjulström, F. (1939). Transportation of debris by moving water. In *Recent Marine Sediments: A symposium*, pages 5–31, Tulsa, Oklahoma, USA. American Association of Petroleum Geologists.

Hofland, B. (2005). *Rock & Roll: Turbulence-induced damage to granular bed protections*. PhD thesis, Delft University of Technology, Delft, the Netherlands.

Hunt, M. L., Zenit, R., Campbell, C. S., and Brennen, C. E. (2002). Revisiting the 1954 suspension experiments of R. A. Bagnold. *Journal of Fluid Mechanics*, 452:1 – 24.

Ishii, M. and Mishima, K. (1984). Two-fluid model and hydrodynamic constitutive relations. *Nuclear Engineering and Design*, 82(2–3):107 – 126.

Iverson, R. M. and Vallance, J. W. (2001). New views of granular mass flows. *Geology*, 29(2):115–118.

Jacobsen, H. M. and Magda, W. (1988). Erosion and pore pressure gradients. In *NGM-88, $10^{th}$ Nordiske Geoteknikermøte*, volume 10, pages 49–53, Oslo, Norway.

Jahan, M. (2014). Effect of suction on local scour around circular bridge piers. Master's thesis, University of Windsor, Windsor, Ontario, Canada.

Jongeling, T. H. G., Blom, A., Stolker, H. R. A., and Verheij, H. J. (2003). Design method granular protections. Technical Report Q2933/Q3018, Delft Hydraulics, Delft, the Netherlands.

Jonkman, S. N. (2007). *Loss of Life Estimation in Flood Risk Management*. PhD thesis, Delft University of Technology, Delft, the Netherlands.

Kavcar, P. C. and Wright, S. J. (2009). Experimental results on the stability of non-cohesive sediment beds subject to vertical pore water flux. In *World Environmental and Water Resources Congress 2009*, pages 1–10.

Kim, J.-M. and Parizek, R. R. (1999). A mathematical model for the hydraulic properties of deforming porous media. *Groundwater*, 37(4):546–554.

Kline, S. J., Reynolds, W. C., Schraub, F. A., and Runstadler, P. W. (1967). The structure of turbulent boundary layers. *Journal of Fluid Mechanics*, 30(4):741–773.

Lambe, T. W. and Whitman, R. V. (1969). *Soil Mechanics*. John Wiley and Sons, New York, NY, USA.

Lee, H.-Y. and Hsu, I.-S. (1994). Investigation of saltating particle motions. *Journal of Hydraulic Engineering*, 120(7):831–845.

Lemmens, D. D. M. M., Bisschop, F., Visser, P. J., and van Rhee, C. (2016). Retarding the breaching process of dikes. *Proceeding of ICE Maritime Engineering*, 169(3):99–115.

Liefferink, D. (2012). Conductivity of the transition zone between an eroding submerged sand bed and water. Technical report, Delft University of Technology, Delft, the Netherlands.

Ling, C.-H. (1995). Criteria for incipient motion of spherical sediment particles. *Journal of Hydraulic Engineering*, 121(6):472–478.

Liu, X. X. and Chiew, Y.-M. (2012). Effect of seepage on initiation of cohesionless sediment transport. *Acta Geophysica*, 60(6):1778 – 1796.

Lu, S. (2012). Comparison of erosion data with a theoretical erosion model at high flow velocity. Technical report, Delft University of Technology, Delft, the Netherlands.

Lubking, P. (2004). *Handboek Zandboek*. CROW, Ede, the Netherlands (in Dutch).

Luchik, T. S. and Tiederman, W. G. (1987). Timescale and structure of ejections and bursts in turbulent channel flows. *Journal of Fluid Mechanics*, 174:529–552.

Luckner, T. (2002). *Zum Bewegungsbeginn von Sedimenten*, volume 124. Technical University Darmstadt, Darmstadt, Germany.

Lunne, T., Robertson, P. K., and Powell, J. J. M. (1997). *Cone Penetration Testing in Geotechnical Practice*. Spon Press, London, Great Britain.

Marsh, N. A., Western, A. W., and Grayson, R. B. (2004). Comparison of methods for predicting incipient motion for sand beds. *Journal of Hydraulic Engineering*, 130(7):616–621.

Mastbergen, D. R. (2006). Oeverstabiliteit in zandwinputten: Rekenmodel hmbreach. Technical report, Delft Hydraulics, Delft, the Netherlands.

Mastbergen, D. R. and van den Berg, J. H. (2003). Breaching in fine sands and the generation of sustained turbidity currents in submarine canyons. *Sedimentology*, 50(4):625–637.

Matousek, V. (2007). Interaction of slurry pipe flow with a stationary bed. *Journal of the South African Institute of Mining and Metallurgy*, 107(6):365–372.

Maxwell, J. C. (1881). *A Treatise on Electricity and Magnetism*. Clarendon Press.

Meyer-Peter, E. and Müller, R. (1948). Formulas for bed-load transport. In *Proceedings of the 2nd Meeting of the International Association for Hydraulic Structures Research*, page 39–64, Stockholm, Sweden.

Miedema, S. A. (2010). Constructing the Shields curve, a new theoretical approach and its applications. In *WODCON XIX*, Beijing, China. WODA.

Miedema, S. A. (2012a). Constructing the Shields curve part A: Fundamentals of the sliding, rolling and lifting mechanisms for the entrainment of particles. *Journal of Dredging Engineering*, 12(1):1–49.

Miedema, S. A. (2012b). Constructing the Shields curve part B: Sensitivity analysis, exposure & protrusion levels, settling velocity, shear stress & friction velocity, erosion flux and laminar main flow. *Journal of Dredging Engineering*, 12(1):50–92.

Miedema, S. A. (2013). Constructing the Shields curve part C: Cohesion by silt. In *WODCON XX*, Brussels, Belgium.

Miedema, S. A. and Matousek, V. (2014). An explicit formulation of bed friction factor for sheet flow. In *15th Internation Freight Pipeline Society Symposium 2014*, Praha, Czech Republik. International Freight Pipeline Society.

Miedema, S. A. and Ramsdell, R. C. (2016). *Slurry Transport Fundamentals, A Historical Overview & The Delft Head Loss & Limit Deposit Velocity Framework*. IOS Press, Amsterdam, the Netherlands.

Mohajeri, S. H., Righetti, M., Wharton, G., and Romano, G. P. (2016). On the structure of turbulent gravel bed flow: Implications for sediment transport. *Advances in Water Resources*, 92:90–104.

Nagakawa, H. and Tsujimoto, T. (1980). Sand bed instability due to bed load motion. *Journal of the Hydraulics Division*, 106(12):2029–2051.

NEN (2016). *NEN-EN-ISO 14688-1 +A1+C11 Geotechnisch onderzoek en beproeving - Identificatie en classificatie van grond - Deel 1: Identificatie en beschrijving (ISO 14688-1:2002)*.

Nezu, I. and Nakagawa, H. (1993). *Turbulence in Open Channel Flows*. Balkema, Rotterdam, the Netherlands.

Nnadi, F. N. and Wilson, K. C. (1992). Motion of contact-load particles at high shear stress. *Journal of Hydraulic Engineering*, 118(12):1670–1684.

Pauker, H. E. (1889). An explanatory report on the project of a sea-battery. *Journal Ministry of Ways and Communications (in Russian)*.

Powers, M. C. (1953). A new roundness scale for sedimentary particles. *Journal of Sedimentary Petrology*, 23(2):117–119.

Prandtl, L. (1921). Uber die Eindringungsfestigkeit (Härte) plasticher Baustoffe und die Festigkeit von Schneiden. *Zeitschrift für Angewandte Mathematik und Mechanik*, 1(1):15–20.

Pugh, F. J. and Wilson, K. C. (1999). Velocity and concentration distributions in sheet flow above plane beds. *Journal of Hydraulic Engineering*, 125(2):117–125.

Rao, A. R. and Sitaram, N. (1999). Stability and mobility of sand-bed channels affected by seepage. *Journal of Irrigation and Drainage Engineering*, 125(6):370–379.

Richardson, J. F. and Zaki, W. N. (1954). Sedimentation and fluidisation: Part I. *Trans. Inst. Chem. Eng.*, 32:35–53.

Roberts, J., Jepsen, R., Gotthard, D., and Lick, W. (1998). Effects of particle size and bulk density on erosion of quartz particles. *Journal of Hydraulic Engineering*, 124(12):1261–1267.

Rouse, H. (1937). Modern conceptions of the mechanics of fluid turbulence. *Trans. ASCE*, 102(1):463–505.

Schlichting, H. and Gersten, K. (1999). *Boundary Layer theory*. McGraw-Hill Book Co. Inc., New York, NY, USA.

Sellgren, A. and Wilson, K. C. (2007). Validation of a four-component pipeline friction-loss model. In *Proceedings 17$^{th}$ International Conference on the Hydraulic Transportation of Solids in Pipes*, pages 193–204. South African Institute of Mining and Metallurgy, South Africa.

Shields, A. (1936). Anwendung der Aenlichkeitsmechanik und der Turbulenzforschung auf die Geschiebebewegung. *Mitteilungen der Preussischen Versuchsanstalt fur Wasserbau und Schiffbau*, 26.

Smith, J. D. and McLean, S. R. (1977). Spatially averaged flow over a wavy surface. *Journal of Geophysical Research*, 82(12):1735–1746.

Soltani-Gerdefaramarzi, S., Afzalimehr, H., Chiew, Y.-M., and Gallichand, J. (2014). Reduction of pier scour using bed suction and jet injection. *Proceedings of the ICE - Water Management*, 167(2):105–114.

Soulsby, R. L. and Whitehouse, R. J. S. (1997). Threshold of sediment motion in coastal environments. In *Pacific Coasts and Ports '97: Proceedings of the 13$^{th}$ Australasian Coastal and Ocean Engineering Conference and the 6th Australasian Port and Harbour Conference; Volume 1*, pages 145–150, Christchurch, New Zealand. Center for Advanced Engineering, University of Canterbury.

Sumer, B. M., Kozakiewicz, A., Fredsøe, J., and Deigaard, R. (1996). Velocity and concentration profiles in sheet-flow layer of movable bed. *Journal of Hydraulic Engineering*, 122(10):549–558.

Swamee, P. K. and Jain, A. K. (1976). Explicit equations for pipe-flow problems. *Journal of the Hydraulics Division*, 102(5):657–664.

Swamee, P. K. and Ojha, C. S. P. (1991). Drag coefficient and fall velocity of nonspherical particles. *Journal of Hydraulic Engineering*, 117(5):660–667.

Terzaghi, K. and Peck, R. (1964). *Soil mechanics in engineering practice*. John Wiley and Sons, New York, NY, USA.

Thomas, D. G. (1965). Transport characteristics of suspension: Viii. a note on the viscosity of newtonian suspensions of uniform spherical particles. *Journal of Colloid Science*, 20(3):267 – 277.

Tomkins, C. D. (2001). *The structure of turbulence over smooth and rough walls*. PhD thesis, University of Illinois, Urbana, Illinois, USA.

van Os, A. G. (1977). *Behavior of Soil when Excavated Underwater - International Course Modern Dredging*. The Hague, the Netherlands.

van Os, A. G. and van Leussen, W. (1987). Basic research on cutting forces in saturated sand. *Journal of Geotechnical Engineering*, 113(12):1501–1516.

van Rhee, C. (2002). *On the sedimentation process in a trailing suction hopper dredger*. PhD thesis, Delft University of Technology, Delft, the Netherlands.

van Rhee, C. (2010). Sediment entrainment at high flow velocity. *Journal of Hydraulic Engineering*, 136(9):572–582.

van Rhee, C. and Bisschop, F. (2015). Numerical simulation of high-speed sediment entrainment. In *Proceedings 17$^{th}$ International Conference Transport and Sedimentation of Solid Particles*, Delft, the Netherlands.

van Rhee, C. and Talmon, A. M. (2010). Sedimentation and erosion of sediment at high solids concentration. In *Proceedings 18$^{th}$ International Conference on Hydrotransport*, Bedfordshire, U.K. BHR Group Limited.

van Rijn, L. C. (1984a). Sediment pick-up functions. *Journal of Hydraulic Engineering*, 110(10):1494–1502.

van Rijn, L. C. (1984b). Sediment transport, part ii: Suspended load transport. *Journal of Hydraulic Engineering*, 110(10):1613–1641.

van Rijn, L. C. (1993). *Principles of Sediment Transport in Rivers, Estuaries and Coastal Seas*. Aqua Publications, Amsterdam, the Netherlands.

van Rijn, L. C. (2008). *Principle of Fluid Flow and Surface Waves in Rivers, Estuaries, Seas and Oceans*. Aqua Publications, Amsterdam, the Netherlands.

Vanoni, V. A. and Brooks, N. H. (1957). Laboratory studies of the roughness and suspended load of alluvial streams. Technical report, Sedimentation Laboratory, California Institute of Technology, Pasadena, California, USA.

Verruijt, A. (2001). *Grondmechanica*. Delft Unversity of Technology, Delft, the Netherlands (in Dutch).

Visser, P. J. (1998). *Breach Growth in Sand-Dikes*. PhD thesis, Delft University of Technology, Delft, the Netherlands.

Vollmer, S. and Kleinhans, M. G. (2007). Predicting incipient motion, including the effect of turbulent pressure fluctuations in the bed. *Water Resources Research*, 43(5).

Voogt, L., van Rijn, L. C., and van den Berg, J. H. (1991). Sediment transport of fine sands at high velocities. *Journal of Hydraulic Engineering*, 117(7):869–890.

Wang, Y.-H. and Yu, G.-H. (2007). Velocity and concentration profiles of particle movement in sheet flows. *Advances in Water Resources*, 30(5):1355 – 1359.

White, F. M. (2009). *Fluid Mechanics*. McGraw-Hill, New York, NY, USA.

Wilson, K. C. (1988). Evaluation of interfacial friction for pipeline transport models. In *Proceedings $11^{th}$ International Conference on the Hydraulic Transport of Solids in Pipes*, pages 107–116, Stratford-upon-Avon, U.K. BHRA.

Wilson, K. C. (1989). Mobile bed friction at high shear stres. *Journal of Hydraulic Engineering*, 115(6):825–830.

Wilson, K. C. (2005). Rapid increase in suspended load at high bed shear. *Journal of Hydraulic Engineering*, 131(1):46–51.

Winterwerp, J. C., Bakker, W. T., Mastbergen, D. R., and van Rossum, H. (1992). Hyperconcentrated sand-water mixture flows over erodible bed. *Journal of Hydraulic Engineering*, 118(11):1508–1525.

Winterwerp, J. C., de Groot, M. B., Mastbergen, D. R., and Verwoert, H. (1990). Hyperconcentrated sand-water mixture flows over a flat bed. *Journal of Hydraulic Engineering*, 116(1):36–54.

Winterwerp, J. C. and van Kesteren, W. G. M. (2004). *Developments in Sedimentology: Introduction to the Physics of Cohesive Sediment Dynamics in the Marine Environment*. Elsevier, Amsterdam, the Netherlands.

Wu, W. and Wang, S. S. A. (2006). Formulas for sediment porosity and settling velocity. *Journal of Hydraulic Engineering*, 132(8):858–862.

Xie, Z.-T. and Castro, I. P. (2008). Efficient generation of inflow conditions for large eddy simulation of street-scale flows. *Flow, Turbulence and Combustion*, 81(3):449–470.

Yue, W., Meneveau, C., Parlange, M. B., Zhu, W., van Hout, R., and Katz, J. (2007). A comparative quadrant analysis of turbulence in a plant canopy. *Water Resources Research*, 43(5). W05422.

Zanke, U. (1977). Berechnung der sinkgeschwindigkeiten von sedimenten. *Mitt. des Franzius-Instituts fur Wasserbau*, 46.

# Curriculum Vitæ

## Frederik BISSCHOP

| | |
|---|---|
| 25-04-1967 | Born in Heerde, the Netherlands. |

## Education

| | |
|---|---|
| 1979-1985 | Secondary School<br>Ichtus College, Driehuis |
| 1985-1991 | MSc, Faculty of Mining and Petroleum Engineering<br>Delft University of Technology<br>Track: Engineering Geology |
| 2009-2017 | PhD, Offshore and Dredging Engineering<br>Delft University of Technology |
| *Thesis* | Erosion of Sand at High Flow Velocities - An Experimental Study |
| *Promotor* | Prof. dr. ir. C. van Rhee |
| *Co-promotor* | Dr. ir. S. A. Miedema |
| *Co-promotor* | Dr. ir. P. J. Visser |

## Work Experience

| | |
|---|---|
| 1991-1995 | Research Engineer, Waterloopkundig Laboratorium<br>(now Deltares) |
| 1995-1996 | Project Engineer, Delft Dredging Consultants |
| 1996-1998 | Production Calculator, HAM Dredging<br>(now van Oord Dredging and Marine Contractors) |
| 1998-2002 | Project Engineer, HAM VOW<br>(now van Oord Dredging and Marine Contractors) |
| 2002-present | Senior Geotechnical Specialist, Arcadis |

# List of Publications

## Journal Papers

2. **F. Bisschop, P. J. Visser, S. A. M. Miedema, G. Keetels, and C. van Rhee**, *Pick-up flux of sand at high flow velocities*, Journal of Hydraulic Engineering **142**, 04016013, (2016).

1. **D. D. M. M. Lemmens, F. Bisschop, P. J. Visser, and C. van Rhee**, *Retarding the breaching process of dikes*, Maritime Engineering Journal **169**, 99-115, (2016).

## Conference Papers

4. **C. van Rhee, F. Bisschop**, *Numerical Simulation of High-Speed Sediment Entrainment*, $17^{th}$ International Conference Transport & Sedimentation of Solid Particles, 2015, Delft, the Netherlands.

3. **F. Bisschop, P. J. Visser, C. van Rhee, and H. J. Verhagen**, *Erosion due to high flow velocities: a description of relevant processes*, $32^{nd}$ International Conference on Coastal Engineering, 2010, Shanghai, China.

2. **W. G. M. van Kesteren, F. Bisschop and C. Kuyper**, *Verification of the Delft erosion formula for cohesive sediments*, $4^{th}$ Nearshore and Estuarine Cohesive Sediments Transport Conference, 1994, Wallingford, England.

1. **W. G. M. van Kesteren, and F. Bisschop**, *The excavation of soils in Trenchless Tunnelling Techniques*, International Conference No-Dig, 1992, Paris, France.

## Magazines

9. **F. Bisschop, L. Kwakman, and M. Ursem**, *Geotechnische Aspecten Versterking Hondsbossche en Pettemer Zeewering*, Land + Water, 2010.

8. **K.J. van der Burg, F. Bisschop, M. Ursem, and F. de Haan**, *Praktijkproef fluïderen bij drukken damwandplanken*, Land + Water, 2008.

7. **L. Kwakman, F. Bisschop, R. J. Bruin, and G. Jonkers**, *Probabilistische aanpak maakt risico's ondergrond expliciet*, Land + Water, 2007.

6. **F. Bisschop, and R. H. Dolfsma**, *Beperken van restzetting betaalt zich op termijn terug*, Land + Water, 2005.

5. **F. Bisschop, C. van Rhee, and C. Nieuwenhuizen**, *Beheersing Restzetting*, Geotechniek, 2003.

4. **G. A. M. Kruse, F. Bisschop, and R. G. Smits**, *Gebaggerde klei als constructief ophoogmateriaal: een economisch en duurzaam alternatief voor zand*, Wegbouwkundige Werkdagen, 2002.

3. **F. Bisschop, and D. R. Mastbergen**, *Gedrag boorvloeistof bepalend voor effectiviteit*, Land + Water, 1995.

2. **F. Bisschop, and D. R. Mastbergen**, *Eigenschappen boorvloeistof afhankelijk van functie*, Land + Water, 1995.

1. **F. Bisschop**, *Pile foundations on Rock in the Netherlands*, Vakblad Ingeokring, 1989.

## Publication

1. **F. Bisschop**, *Materialen in (constructieve) ophogingen en aanvullingen - Richtlijn ter bevordering van alternatieven voor zand*, CROW-publicatie 281, 2009.

# Acknowledgements

In 2007 begon er iets te knagen. Ik kreeg behoefte om mijzelf weer eens echt te verdiepen in een nieuw onderwerp. Op mijn veertigste had ik ook een motor kunnen kopen, maar een promotie-onderzoek leek mij uitdagender. Na een aantal verkennende gesprekken kwam ik in contact met een oud opdrachtgever en oud-collega: Cees van Rhee. Hij zag kansen om een promotie-onderzoek op te zetten naar de erosie van zand bij het baggeren met een sleephopperzuiger. Cees organiseerde financiële ondersteuning vanuit de baggerbedrijven Boskalis, van Oord en MTI Holland (nu IHC MTI). Ook zorgde Rijkswaterstaat voor een financiële bijdrage via de Dr. Ir. Cornelis Lely Stichting en kon ik in 2009 beginnen met mijn promotie-onderzoek. Mijn leidinggevende, Jos van Kerckhoven, ondersteunde het idee gedurende de afgelopen jaren. Hij maakte het mogelijk dat ik enige jaren in deeltijd aan mijn promotie kon werken en de vrijheid had mijn werk rondom mijn promotie in te plannen.

Het onderwerp was niet nieuw voor mij. In 1993 en 1994 heb ik experimenten uitgevoerd naar de invloed van het gedrag van zand tijdens erosie bij relatief hoge stroomsnelheden. Helaas was er toen geen budget beschikbaar voor een verdere verdieping. Het onderwerp boeide mij en boeit mij nog steeds vanwege het feit dat voor dit onderwerp zowel kennis van vloeistofmechanica als grondmechanica noodzakelijk is.

Veel dank gaat uit naar mijn begeleiders Cees van Rhee, Sape Miedema en Paul Visser. Bij jullie kon ik aankloppen als ik behoefte had aan terugkoppeling of ergens in vastliep. Cees heeft mij scherp gehouden tijdens de uitvoering van de experimenten door het overbrengen van zijn ervaring met experimenten tijdens zijn promotie-onderzoek. Daarnaast had hij altijd goede suggesties als ik ergens in vast liep. Sape zijn deur stond altijd open voor discussies. Hier heb ik veel aan gehad. Zeker in de tijd dat ik bezig was met de analyse van de proeven. Wij hebben toen veel interessante gesprekken gehad op het raakvlak tussen de onderzoeken waar wij beiden mee bezig waren.

Paul was vanaf de eerste dag nauw betrokken bij het onderzoek. Paul en ik hebben twee studenten (Dennis Lemmens en Björn Foortse) begeleid, die experimentele studies hebben uitgevoerd naar de invloed van de doorlatendheid van zand op het bressen van een dijk. Dit heb ik ervaren als een leuke periode. De experimenten gaven interessante resultaten te zien in relatie tot mogelijkheden om de veiligheid van een dijk te vergroten, zonder deze te moeten ophogen. Paul en Sape, ik heb genoten van de sessies die wij hadden om mijn proefschrift door te nemen. Mooie discussies, die mij de mogelijkheid gaven om mijn proefschrift te verbeteren.

Het experimentele onderdeel van mijn onderzoek was een intensieve periode, waar ik met veel enthousiasme aan terugdenk. In het laboratorium heb ik veel ondersteuning gehad van Freek Brakel en Ed Stok. Zij stonden altijd klaar met goede

alternatieven als iets in de praktijk niet goed uitvoerbaar bleek. Jullie praktische insteek en oplossingsgerichtheid hebben mij veel geholpen. Bij de analyse van de experimenten heb ik veel hulp gehad van Marthijn Sunder. Hij ondersteunde mij bij de verwerking van de meetgegevens. Binnen korte tijd was hij beter in programmeren dan ik en heeft hij veel handige functies ontwikkeld voor de verwerking van de vele meetgegevens. Natuurlijk moet ik de hulp van een aantal studenten niet vergeten. Deze hebben, deels als afstudeerder en deels als student-assistent, onderdelen van de experimenten uitgevoerd. David van Diepen en Peter de Jong hebben de bestaande experimentele opstelling aangepast en opnieuw laten opbouwen. De opstelling voldeed volledig aan de verwachtingen. Juneed Sethi, Saad Wahid, Daniël Liefferink, Max van het Hooft en Jord Wiegerink hebben vele experimenten uitgevoerd en moesten lange dagen maken. Hun flexibiliteit en enthousiaste inzet heb ik zeer gewaardeerd.

De laatste jaren van mijn promotie heb ik vooral onderdeel uitgemaakt van de onderzoeksgroep van Cees bij 3ME. Vele leuke en (on)zinnige discussies hebben wij gehad bij de koffie-automaat. De scherpte en het (jeugdige) enthousiasme van deze groep spreken mij nog steeds aan. Bas, Dave, Frans, Geert, Thijs, Rudy, Xiuhan en Joep bedankt voor het plezier en de vele interessante (inhoudelijke) discussies. In het bijzonder wil ik de discussies met Geert, Joep en Lynyrd (enige jaren geleden gepromoveerd) over hardlopen en wielrennen nog noemen. Het was leuk mijn enthousiasme voor deze sporten met jullie te kunnen delen. Jullie vragen op dit gebied, hebben mij weer aan het denken gezet wat betreft het trainen van wielrenners, veldrijders en mountainbikers.

Rini, jou wil ik het meest bedanken voor alle steun tijdens deze jaren. Jij bent in staat geweest mij altijd te motiveren of als klankbord te fungeren als het wat moeizaam liep met mijn onderzoek. Daarnaast heb jij enige jaren geleden zelf ook een studie opgepakt en volbracht. Hiermee heb jij jezelf in 2 jaar omgeschoold tot verpleegkundig specialist. Een knappe prestatie, ik ben nog steeds onder de indruk. Femke en Tomas, jullie hebben tijdens de experimenten ook een bijdrage geleverd door het maken van de briefjes met de proefinstellingen. Jullie enthousiasme tijdens deze werkzaamheden gaf mij veel plezier. Of mijn promotie-onderzoek daaraan bij gedragen heeft weet ik niet, maar Femke, het is erg leuk om te zien dat jij nu Civiele Techniek studeert aan de TU in Delft: een mooie keuze. Ik weet nu zeker, een promotie-onderzoek is onmogelijk zonder een stabiele en enthousiaste thuis-basis.

*Frederik Bisschop*
*Delft, January 2018*